MECHANISMS OF RIBOTOXIC STRESS RESPONSE AND DOWNSTREAM SEQUELAE

By

Kaiyu He

A DISSERTATION

Submitted to
Michigan State University
in partial fulfillment of the requirements
for the degree of

DOCTOR OF PHILOSOPHY

Microbiology - Environmental Toxicology

2012

ABSTRAC

MECHANISMS OF RIBOTOXIC STRESS RESPONSE
AND DOWNSTREAM SEQUELAE

By

Kaiyu He

Translational inhibitors and other translation-interfering toxicants, termed ribotoxins, activate MAPKs via a process termed ribotoxic stress response (RSR). Deoxynivalenol (DON), a trichothecene mycotoxin produced by *Fusarium spp.*, is a ribotoxin and commonly contaminates cereal-based foods and has the potential to adversely affect humans and animals. At low doses, DON induces immunostimulatory effects by upregulating expression of proinflammatory genes in macrophages, IL-8 in monocytes and IL-2 in T cells. In contrast, high doses of DON cause immunosuppression by inducing apoptosis and rRNA cleavage.

While it is recognized that DON induces transcription and stability of inflammation-associated mRNAs in the macrophage, it is not known whether this toxin can selectively modulate translation of these mRNAs. DON-induced changes in profiles of polysome-associated mRNA transcripts (translatome) was compared to total cellular mRNA transcripts (transcriptome) in the RAW 264.7 murine macrophage model. DON induced robust expression changes in inflammatory response genes including cytokines, cytokine receptors, chemokines, chemokine receptors, and transcription factors, which were remarkably similar in the translatome and transcriptome. Over 70 percent of DON-regulated genes in the translatome and transcriptome overlapped and most expression

ratios in these pools are <2. Taken together, DON's capacity to alter translation expression of inflammation-associated genes is likely to be driven predominantly by selective transcription, however, a small subset of these genes might further be regulated at the translational level.

The complete cleavage profile and exact signaling mechanism of DON-induced rRNA cleavage are unknown. PKR, Hck and p38 were found to be required for rRNA cleavage. Furthermore, rRNA fragmentation was suppressed by the p53 inhibitors pifithrin-α and pifithrin-μ as well as the pan caspase inhibitor Z-VAD-FMK. DON activated caspases 3, 8 and 9 thus suggesting the possible co-involvement of both extrinsic and intrinsic apoptotic pathways in rRNA cleavage. Notably, pan inhibitor for cathepsins also suppressed anisomycin-, SG-, ricin- and DON-induced rRNA cleavage. Accordingly, all four ribotoxins induced apoptosis-associated rRNA cleavage via activation of cathepsins and p53→caspase 8/9→caspase 3, the activation of which by DON and anisomycin involved PKR-and Hck-activated p38 whereas SG and ricin activated p53 by an alternative mechanism.

Taken together, at low doses, DON selectively upregulates translation of inflammation-associated genes, which is likely to be driven predominantly by selective transcription of these genes. However, a small subset of these genes might further be regulated at the translational level. At high doses, DON induces apoptosis-associated rRNA cleavage via activation of cathepsins and PKR/Hck/p38/p53→caspase 8/9→caspase 3. Interestingly, DON and anisomycin share the same signaling pathways, whereas SG and ricin activate p53 by an alternative mechanism, indicating the downstream signalings are conserved for ribotoxins.

ACKNOWLEDGEMENTS

I would like to express my deepest gratitude to my advisor, Dr. James Pestka, for his excellent guidance, patience, and providing an excellent atmosphere for doing research at Michigan State. He helped me to develop various skills, such as independent thinking and scientific writing, from which I will benefit not only for my future researches but also my whole life.

I am grateful to my Committee members: Dr. Robert Britton, Dr. Kathleen Gallo and Dr. John Linz for their invaluable suggestions, assistance and guidance. I am also thankful to all the members in Dr. Pestka and Dr. Linz's laboratories, especially Dr. Hui-Ren Zhou, who, as a good friend and scientific mentor, was always willing to help me and give me best suggestions.

I would also like to thank my parents, younger brother and wife, Qi Wang. They were always supporting me and encouraging me with their best wishes.

TABLE OF CONTENTS

LIST OF TABLES

LIST OF FIGURES

LIST OF ABBREVIATIONS

2-AP	2-aminopurine
AP-1	activator protein-1
Apaf-1	apoptotic protease activating factor 1
ASK1	apoptosis signal kinase 1
ATF6	activating transcription factor 6
BiP	immunoglobulin binding protein
caspases	cysteine-dependent aspartate-directed proteases
COX-2	cyclooxygenase-2
DON	deoxynivalenol
DRBD	double-stranded RNA binding domains
eIF	eukaryotic initation factor
ER	Endoplasmic reticulum
ERK	extracellular signal-regulated kinases
Hck	hematopoietic cell kinase
IL	interleukine
IRE1	inositol requiring enzyme 1
IRES	internal ribosome entry site
JNK	c-Jun N-terminal kinase
LMP	lysosomal membrane permeabilization

MAPK	mitogen-activated protein kinase
MIP-2	macrophage-inflammatory protein 2
NF-κB	nuclear factor-kappa B
PEB	polysome extraction buffer
PERK	PKR-like endoplasmic reticulum kinase
PKR	double-stranded protein kinase R
PTC	peptidyl transferase center
RIP	RNA immunoprecipitation
RIPs	ribosome-inactivating proteins
RPL	ribosomal protein large subunit
RPS	ribosomal protein small subunit
rRNA	ribosomal RNA
RSR	ribotoxic stress response
SG	Satratoxin G
TNF-α	tumor necrosis factor-α
uORF	upstream open reading frame
UPR	unfolded protein response
ZAK	zipper sterile-alpha-motif kinase

INTRODUCTION

The trichothecenes, a group of sesquiterpenoid mycotoxins produced by *Fusarium* that contaminate wheat, barley and corn globally (Pestka, 2010a), are problematic because of their resistance to degradation during processing and potential to adversely affect human and animal health. Among the over 200 trichothecenes discovered to date, deoxynivalenol (DON) is most frequently encountered in food(Desjardins and Proctor, 2007). One of the principal targets of DON is the innate immune system, with low doses causing immunostimulatory effects, and high doses causing immunosuppression (Pestka, 2010b). DON has been shown *in vivo* and *in vitro* to activate mitogen-activated protein kinases (MAPKs), including p38, JNK and ERK (Shifrin and Anderson, 1999; Zhou *et al.*, 2003a), which mediate upregulation of proinflammatory cytokine and chemokine expression as well as apoptosis (Moon and Pestka, 2002; Chung *et al.*, 2003b; Islam *et al.*, 2006). Notably, DON concentration-dependently induces competing survival (ERK/AKT/p90Rsk/Bad) and apoptotic (p38/p53/Bax/mitochondria/caspase-3) pathways in the macrophage (Zhou *et al.*, 2005a).

DON-induced phosphorylation of MAPKs mediate upregulation of expression of mRNAs for inflammation-related genes such as the cytokines, chemokines and cyclooxygenase-2 (COX-2) (Shifrin and Anderson, 1999; Moon and Pestka, 2002; Chung *et al.*, 2003b; Zhou *et al.*, 2003a; Islam *et al.*, 2006). DON-induced increases in cellular pools of inflammation-associated mRNAs have been linked to both transcriptional activation and stabilization of mRNA through an AUUUA motif in the 3'-untranslated region (Moon and Pestka, 2002; Chung *et al.*, 2003b). It is expected that

translation of these mRNAs might be regulated at global and individual levels, respectively. The general translation rate can be upregulated by controlling the availability of the cap-binding protein eIF4E (Gebauer and Hentze, 2004; Ma and Blenis, 2009) and downregulated by phosphorylation of eIF2α at Ser51(Gebauer and Hentze, 2004). Besides global regulation, translation of specific messages could be controlled by specific RNA-binding proteins (RBPs) (Gebauer and Hentze, 2004) and microRNAs, a family of small non-coding RNAs about 22 nucleotides in length, can also precisely regulate specific gene expression by imperfectly binding to the 3'-UTR of target mRNA. Considering the complex multiple translation regulatory mechanisms, whether the total mRNA pool is fully translated in DON-exposed macrophage is unknown. The comparison of the translatome and transcriptome will illustrate the coordination between transcription and translation, thereby improving our understanding of how DON affects the immune system. These studies will be further compared to other ribotoxins to reveal the general mechanisms.

A prominent consequence of DON exposure is the induction of rRNA cleavage, which has been suggested to result from upregulated RNase expression, most notably RNase L (Li and Pestka, 2008). Interestingly, DON, as well as the ribosome-inactivating protein (RIP) ricin that specifically cleaves rRNA via a highly specific mechanism involving N-glycosidase-mediated adenine depurination at sarcin/ricin (S/R) loop, both induce rRNA cleavage at two cleavage sites (A3560 and A4045) on 28S rRNA in macrophage (Li and Pestka, 2008). To date, induction of rRNA cleavage by chemicals or viruses has been linked to either RNase L-dependent or apoptosis-associated mechanisms (Banerjee *et al.*, 2000; Naito *et al.*, 2009). RNase L is a latent

endonuclease with a broad range of functions including inhibition of protein synthesis, apoptosis induction and antiviral activity(Stark *et al.*, 1998). It can inhibit protein synthesis via the degradation of mRNA and rRNA, resulting in cellular stress response and activation of the JNK pathway in DON-exposed macrophage(Clemens and Vaquero, 1978; Wreschner *et al.*, 1981; Iordanov *et al.*, 2000; Li *et al.*, 2004). However, the role of RNase L in ribotoxin-induced rRNA cleavage, as well as the complete profile of rRNA cleavage and the intracellular signaling pathways, has not yet been fully elucidated. Thus, elucidation of the signaling pathway leading to rRNA cleavage will deepen our understanding of ribotoxin-induced RSR and potentially help to prevent or provide therapy for their adverse effects.

This dissertation addresses the aforementioned knowledge gaps. Chapter I is a literature review of trichothecenes, deoxynivalenol (DON), ribotoxic stress response, translational regulation and apoptosis. Chapter II is a comparison of DON-induced transcriptome and translatome of inflammatory genes. Chapter III includes studies on the mechanisms by which DON induced rRNA cleavage. Chapter IV contains the investigation of anisomycin-, SG- and ricin-induced rRNA cleavage. Chapter V is a summary and conclusion for this dissertation.

CHAPTER 1

Literature Review

A.Trichothecenes

Trichothecenes are the secondary sesquiterpenoid mycotoxin metabolites of various fungal genera, including *Fusarium, Stachybotrys*, *Myrothecium*, *Spicellum*, *Cephalosporium*, *Trichoderma*, and *Trichothecium* (Kimura *et al.*, 2007; McCormick *et al.*, 2011). Trichothecene mycotoxins impact humans because of their worldwide contamination in corn, wheat and barley, difficulty to be degraded in processing, adverse effects on health and the potential to be chemical warfare reagents(Peraica *et al.*, 1999; Anderson, 2012). To date, over 200 trichothecenes have been identified, all of which have a conserved sesquiterpene backbone with a 9,10-double bond and a 12,13-epoxide(Kimura *et al.*, 2007). According to chemical structure differences, they are divided into four types: A, B, C and D(Ueno, 1984; Ueno, 1985). Type A have hydroxyl or acyl group at four modification sites; Type B have a keto group at C-8, while Type C have a C-7,8 epoxide. Of all the trichothecenes, representatives of Type A, T-2 and diacetoxyscirpenol, and Type B, nivalenol and deoxynivalenol, are the most prevalent trichothecenes in cereal grains(Desjardins and Proctor, 2007). In contrast to the group substitution for Type A, B and C, Type D trichothecene contains a macrocyclic ring between C-4 and C-15 such as satratoxin G, which is detected in indoor environments contaminated with *Stachybotrys* mycotoxin; it is associated with damp building-related illnesses (DBRI)(Pestka *et al.*, 2008b).

Trichothecenes are low molecular weight translational inhibitors that can passively diffuse through cell membranes, bind to ribosome and potently inhibit eukaryotic translation by either inhibiting polypeptide chain initiation or elongation-termination (Ueno, 1985). They are also easily absorbed by gastrointestinal systems and cause

nausea, vomiting, feed refusal, growth retardation, immunotoxicity, hemorrhagic lesions and reproductive disorders(Rousseaux et al., 1986; Peraica et al., 1999; McCormick et al., 2011). Trichothecenes primarily target leukocytes(Ueno, 1985), including macrophages, monocytes, B and T cells, in the toxicity order of Type D > Type A> Type B(Bondy and Pestka, 2000), and induce either immunostimulatory or immunosuppressive effects depending on the dose and duration of exposure (Pestka *et al.*, 2004).

B. Deoxynivalenol (DON)

B.1. Introduction

Deoxynivalenol (DON), also known as vomitoxin, was first isolated in Japan (Yoshizaw.T and Morooka, 1973). It is a Type B trichothecene primarily produced by *Fusarium spp*. growing on wheat, barley and corn(Hope *et al.*, 2005). DON not only causes great annual economic losses (hundreds of millions in dollars) but also adversely affects human health. *Fusarium*-contaminated food has been linked to the outbreaks of human gastroenteritis with typical syndrome of vomiting in Japan and Korea in the middle of 20^{th} century and later in China, in which DON was detected in some wheat samples (Peraica *et al.*, 1999; Pestka, 2010b). Because DON is chemically stable and resistant to normal food processing such as cleaning, milling and baking (Abbas *et al.*, 1985; Trigo-Stockli, 2002), it still contaminates cereal-based foods in many countries(Pestka, 2010b). For example, beers, which were fermentated from cereal grains in Holland and Germany, were found to contain up to 200 ng/ml of DON(Sobrova *et al.*, 2010). Studies in United Kingdom showed that urinary DON was detected in over 98% of the adults consuming cereal foods, revealing a positive

correlation between cereal intake and urinary DON(Turner *et al.*, 2008b; Turner *et al.*, 2008c) and indicating that the morning urinary DON is a biomarker for human exposure(Turner *et al.*, 2010). For the sake of safety, the U.S. Food and Drug Administration has established an advisory limit of 1 part per million (ppm) of DON for human, 10 ppm for cattle and poultry and 5 ppm for other animals.

DON can cause acute and chronic toxic effects in animals. In animal acute toxicity tests, swine are most sensitive to low doses of DON exposure with the order swine>rodent>dog>cat>poultry>ruminants with as low as 0.05-1 mg/kg body weight DON rapidly induces vomiting in swine(Prelusky and Trenholm, 1992). In mouse models, intraperitoneal injection has similar LD50 to that of oral administration, ranging from 40 to 70 mg/kg body weight (Yoshizawa *et al.*, 1983; Forsell *et al.*, 1987). DON doses higher than LD50 induce intestinal hemorrhage, necrosis of bone marrow, depletion of lymphoid tissues and organ lesions. In B6C3F1 male mice, orally administered DON (25 mg/kg body weight), is detectable from 5 min to 24 h in plasma, liver, spleen and brain and from 5 min to 8 h in heart and kidney(Pestka *et al.*, 2008a). Chronic DON consumption in mice causes reduced food intake, decreased weight gain, anorexia, altered nutritional efficiency and increased serum immunoglobulin A (IgA)(Rotter *et al.*, 1996; Sobrova *et al.*, 2010).

B.2. DON-induced immunostimulation and immunosuppression

DON has been proposed to bind to the peptidyl transferase region of the ribosome thus interfering with initiation and elongation of ribosome(Pestka, 2010a). The primary targets of DON are leukocytes in immune system including macrophages, monocytes, T cells and B cells with the former two as most sensitive cell populations(Pestka *et al.*,

2004). Depending on the dose and exposure frequency, DON induces either immunostimulatory or immunosuppressive effects by upregulating gene expression and apoptosis, respectively.

Regarding immunosuppression, mice fed DON at concentrations greater than 10 ppm, exhibit reduction in thymus weight, antibody production and stimulation of B and T cells by mitogens (Robbana-Barnat *et al.*, 1988). Mice exposed acutely to DON (25 mg/kg body weight) exhibit apoptosis in bone marrow, thymus, spleen and Peyer's patches (Zhou *et al.*, 2000). In in vitro cell cultures, rapid apoptosis of immune cells induced by high concentrations of DON, including macrophages, monocytes, T and B cells, has also been reported(Pestka *et al.*, 1994; Uzarski and Pestka, 2003). Similarly, DON exposure within 250 to 500 ng/ml induces apoptosis in thymus, spleen and bone marrow cultures (Uzarski *et al.*, 2003).

In contrast, low doses of DON stimulate the immune system primarily by upregulating the transcription and expression of inflammatory response genes, including TNF-α, IL-6, MIP-2 and COX-2 in macrophages(Moon and Pestka, 2002; Chung *et al.*, 2003a; Chung *et al.*, 2003b; Jia *et al.*, 2004), IL-8 in monocytes(Gray and Pestka, 2007; Gray *et al.*, 2008) and IL-2 in T cells(Li *et al.*, 1997). In an in vivo mouse model, DON exposure induces robust upregulation of proinflammatory genes in spleen at 3 h, including TNF-α, IL-1β and IL-6(Zhou *et al.*, 2003a). Further studies employing microarrays to profile gene expression in spleen of DON-exposed mice found marked upregualtion of various cytokines (IL-1α, IL-1β, IL-6, IL-11) and chemokines (MIP-2, CINC-1, MCP-1, MCP-3) at 2 h(Kinser *et al.*, 2004; Kinser *et al.*, 2005).

DON upregulates the mRNA expression of proinflammatory genes at both the

transcriptional and post-transcriptional levels by elevating transcription rate and improving mRNA stability. The expression of transcription factors, including c-fos, Fra-2, c-jun and JunB, were found upregulated in response to DON treatment (Kinser *et al.*, 2004; Kinser *et al.*, 2005) and the activation of transcription factors, such as NF-κB and AP-1 were also confirmed by EMSA and promoter reporter gene assays (Ouyang *et al.*, 1996; Li *et al.*, 2000; Wong *et al.*, 2002; Gray and Pestka, 2007). DON as low as 100 ng/mL elevates the binding of AP-1 and C/EBP after 2 hours and NF-κB after 8 hours(Wong *et al.*, 2002). Furthermore, DON-induced elevation of AP-1 binding activity is concentration- and time-dependent in primary macrophages (Jia *et al.*, 2006). To enhance the mRNA stability is an alternative way to increase protein expression. DON is reported to enhance COX-2 mRNA stability via AU rich elements in the 3'-UTR of mRNA, which promotes rapid degradation of mRNA, but this only applies to Type B trichothecenes, not Type A and Type D(Moon *et al.*, 2003). Similarly, DON also induces elevated stabilization of TNF-α (Chung *et al.*, 2003b) and IL-6 (Jia *et al.*, 2006) mRNAs in macrophages and IL-2 mRNA in T cells(Li *et al.*, 1997). Additionally, HuR/Elav-like RNA binding protein 1 (ELAVL1) is involved in DON-induced stabilization of IL-8 mRNA by translocation from nucleus to cytosol and binding to the 3'-UTR of IL-8 transcript (Choi *et al.*, 2009).

C. Mitogen-activated Protein Kinases (MAPKs)

C.1. Introduction

DON-induced transcriptional and post-transcriptional regulation of inflammatory response genes is mediated by the mitogen-activated protein kinases (MAPKs). MAPKs are evolutionarilly conserved pathways to respond to diverse stimuli, such as growth

factors, stress, and cytokines, and coordinate many cellular activities like proliferation, apoptosis, differentiation, and development(Cobb, 1999). The MAPKs reported in mammals include p38, c-Jun N-terminal kinase (JNK) 1/2/3 and extracellular regulated kinases (ERK)1/2, 7/8, 3/4 and 5. Only p38, JNK1/2 and ERK1/2 have been extensively studied(Krishna and Narang, 2008). MAPKs are phosphorylated by MAPK kinases (MAPKK), which are the downstream substrates of MAPK kinase kinase (MAPKKK). Although there are conserved modules for MAPKKK, MAPKK and MAPK sequential activations, MAPKKKs are a heterogenous group kinases while MAPKK and MAPK are highly homologous families(Goh *et al.*, 2000). ERK1/2, JNK1/2 and p38 are phosphorylated by MEK1/2, MEK4/7 and MEK 3/6, respectively, and activate various transcription factors to regulate downstream gene transcription(Keshet and Seger, 2010).

C.2. Role of MAPKs in DON exposure

MAPKs play cirtical roles in DON-induced upregulation of proinflammatory cytokine and chemokine expression. DON has been shown to activate p38, JNK and ERK1/2 in Jurkat T-cell line by triggering “ribotoxic stress response” (RSR) (Shifrin and Anderson, 1999; Pestka *et al.*, 2005). However, only ERKs and p38, but not JNKs, were found to mediate DON-induced COX-2 gene expression in macrophages (Moon and Pestka, 2002). In addition, DON treatment could activate p38 to upregulate IL-8 (Islam *et al.*, 2006) and TNF-α expression by elevating both transcription and mRNA stability (Chung *et al.*, 2003b). Consistent with the in vitro studies, in vivo studies on the activation of MAPKs and transcription factors in mouse spleen confirm that rapid phosphorylation of MAPKs precedes the activation of transcription factors including AP-

1, CREB and NF-κB and proinflammatory cytokine mRNA expression(Zhou *et al.*, 2003a).

DON-induced phosphorylation of p38, JNK1/2 and ERK1/2 is correlated with and precedes apoptosis(Yang *et al.*, 2000). DON rapidly induces activation of p38 and ERK1/2 within 15 min in RAW 264.7 macrophages and the inhibitors for p38 and ERK1/2 markedly suppressed DON-evoked caspase 3-dependent DNA fragmentation, respectively, suggesting they play opposite roles in apoptosis(Zhou *et al.*, 2005a). DON is proposed to induce competing apoptotic (p38/p53/Bax/mitochondria/caspase-3) and survival (ERK/AKT/p90Rsk/Bad) pathways in the macrophages (Zhou *et al.*, 2005a).

D. Ribotoxic stress response

D.1. Introduction

MAPKs are proposed to be activated by translational inhibitors and other translation-interfering toxicants, termed ribotoxins, via a process named ‘ribotoxic stress response’, which was first defined by Irodanov in 1997(Iordanov *et al.*, 1997). In this process, binding or damage to the 28S rRNA perturb the 3′-end of the 28S ribosomal RNA, which functions in aminoacyl-tRNA binding, peptidyltransferase activity, and ribosomal translocation(Uptain *et al.*, 1997), resulting in activation of p38, JNK1/2 and ERK1/2 and subsequent regulation of gene expression (Iordanov *et al.*, 1997; Laskin *et al.*, 2002). Thus the 28S rRNA has been proposed to be the sensor for ribotoxic stress (Iordanov *et al.*, 1997).

Some ribotoxins are of low-molecular-weight, such as the trichothecenes, which directly bind to ribosome and inhibit protein synthesis. A variety of trichothecenes including T-2 toxin, nivalenol and DON have been proposed to bind to the 28S rRNA

petidyltransferase center(PTC), have been found to trigger “ribotoxic stress response”, and activated JNK and p38 kinase (Shifrin and Anderson, 1999). Consistent with the notion that these inhibitors sharing common binding sites and initiate identical signaling, another PTC-binding antibiotic anisomycin also strongly activate JNK and p38 (Iordanov *et al.*, 1997; Xiong *et al.*, 2006).

Ribosome-inactivating proteins (RIPs) are a different type of ribotoxins, and contain an RNA N-glycosidase domain that specifically cleaves a conserved adenine off the eukaryotic 28S rRNA. RIPs have been isolated from various organisms, including plants (e.g. ricin from castor bean)(Woo *et al.*, 1998), fungi (e.g. α-sarcin from *Aspergillus giganteus*)(Endo *et al.*, 1983) and bacteria (e.g., Shiga toxin from *Shigella dysenteriae*)(Gyles, 2007), and they are divided into three types based on composition of peptide chain. Type 1 RIPs consist of a single enzymatically active A-chain such as Pokeweed antiviral protein (PAP). Type 2 RIPs, like ricin, are composed of two peptides with A-chain disulfide-linked to a B-chain, which can bind to the cell surface and mediate the entrance of whole RIP into the cell by endocytosis (Hartley and Lord, 2004a). Type 3 RIPs, represented by maize RIP, contain a single chain and become active only after the removal of a short internal peptide(Walsh *et al.*, 1991). Since the Type 2 RIPs are much more toxic and potentially could be used as agents of bioterrorism, they have been extensively studied.

Ricin, isolated from castor beans, has been studied as a prototypical representative of Type 2 RIP. After entering the cells by endocytosis, ricin undergoes vesicular retrograde transport from early endosomes to the trans-Golgi network (TGN) and reaches the lumen of the ER, where the A-chain is released and translocated into

the cytosol to depurinate 28S rRNA(Olsnes, 2004). The target nucleoside residue of ricin is A4324, close to the α-sarcin sites in 28S rRNA(Endo and Tsurugi, 1986), therefore the region containing 12 nucleotides is termed the ricin/α-sarcin loop. Specific activities on the ricin/α-sarcin loop are also exhibited by other RIPs including abrin, modeccin, Vero and Shiga toxin, suggesting that there is a conserved mechanism for RIPs to inactivate the ribosome (Endo *et al.*, 1987; Endo *et al.*, 1988).

RIPs are proposed to depurinate 28S rRNA in the cytosol, subsequently activate MAPKs and mediate gene expression during the ribotoxic stress response. Ricin and α-sarcin potently activate JNKs and its activator MEK4, and induce the expression of the immediate-early genes c-fos and c-jun(Iordanov *et al.*, 1997). Ricin induces robust activation of NF-κB at 6 h, knockdown of which by siRNA results in decreased mRNA level of various pro-inflammatory genes including CXCL1, CCL2, IL-8, IL-1b and TNF- α. These findings suggest that ricin-induced expression of these genes are downstream events of the ribotoxic stress response (Wong *et al.*, 2007b). In addition, ricin-induced traslocation of NF-κB to nucleus is detected in mouse lung tissue(Wong *et al.*, 2007a). Ricin induces expression of IL-1β by sequentially activating MAPKs and NF-κB, which upregulate expression of pro-IL-1β that is converted to mature IL-1β via Nalp3 inflammasome(Jandhyala *et al.*, 2012).

Besides translational inhibitors and RIPs, the RSR can also be triggered by ultraviolet light radiation and palytoxin (Iordanov and Magun, 1998; Iordanov and Magun, 1999; Iordanov *et al.*, 2002). Instead of directly associating with the ribosome, palytoxin binds to the Na/K ATPase in the plasma membrane and elevates potassium efflux from cells. The lowered intracellular cation concentration perturbs the 3'-end of

the 28S ribosomal RNA, which is proposed to possess a potassium-sensitive site(Iordanov and Magun, 1998). This process mimics the ribosome-binding agents such as trichothecеces and is capable of inducing a ribotoxic stress response to stimulate the JNKs and p38. Additionally, ultraviolet C (200–290 nm) and B (290–320 nm) rapidly activate JNK and p38 kinase by nucleotide and site-specific damage to the 3’-end of 28S rRNA, which impairs PTC activity and inhibits protein synthesis (Iordanov et al., 2002).

D.2 Upstream transducers of MAPKs

In the ribotoxic stress response model, MAPKs are the central signaling molecules that connect rRNA perturbation and downstream regulation of gene expression. Studies to identify the upstream mediators of DON-induced MAPK activation identified two kinases, the double-stranded RNA-(dsRNA)-activated protein kinase (PKR) and hematopoietic cell kinase (Hck)(Zhou *et al.*, 2003b; Zhou *et al.*, 2005b). They are activated earlier than MAPKs and specific inhibitors for them blocks MAPK activation in macrophage, respectively. Another mitogen-activated protein kinase kinase kinase (MAP3K), zipper sterile-alpha-motif kinase (ZAK), is also proposed to be the upstream mediator for RSR(Jandhyala *et al.*, 2012).

PKR is a widely-distributed, constitutively-expressed serine/threonine protein kinase that can be activated by dsRNA, interferon, proinflammatory stimuli, cytokines and oxidative stress(Williams, 2001; Garcia *et al.*, 2006) and has diverse functions including control of cell growth, tumor suppression, apoptosis, and antiviral infection(Koromilas *et al.*, 1992; Lengyel, 1993; Chu *et al.*, 1999). PKR contains two double-stranded RNA binding domains (DSBDs) and one kinase domain whose activity

is autoinhibited by DSBD in an intramolecular manner. After binding to dsRNA, PKR is activated by dimerization and autophosphorylation and phosphorylates serine 51 on the alpha subunit of eukaryotic initiation factor 2 (eIF-2α) (Fig.1.1), which leads to the higher affinity to the GTP exchange factor eIF-2β and results in global translation inhibition(Sudhakar *et al.*, 2000). Additionally, PKR activates various factors including signal transducers and activator of transcription (STAT), interferon regulatory factor1 (IRF-1), p53, JNK, p38 and NF-κB(Verma *et al.*, 1995; Williams, 1999; Williams, 2001) and regulates the expression of proinflammatory genes. In RAW 264.7 macrophages, DON rapidly activates PKR within 5 minutes. However, the phosphorylation of MAPKs are suppressed by pretreating PKR inhibitor 2-aminopurine (2AP) or adenine(Zhou *et al.*, 2003b), indicating that PKR mediates the activation of MAPKs. Human U-937 monocyte cell line transfected with stable PKR antisense RNA vector also showed significantly reduced MAPK activation upon DON exposure(Gray and Pestka, 2007). In addition, PKR inhibition also suppresses the DON-induced cytokine and chemokine expression, including TNF-a, MIP-2 and IL-8.

Hemopoietic cell kinase (Hck) is a member of the Src family of tyrosine kinases, which share two conserved Src homology (SH) domains SH2 and SH3. These domains bind on the surface of the catalytic domain in an intramolecular manner and inactivate

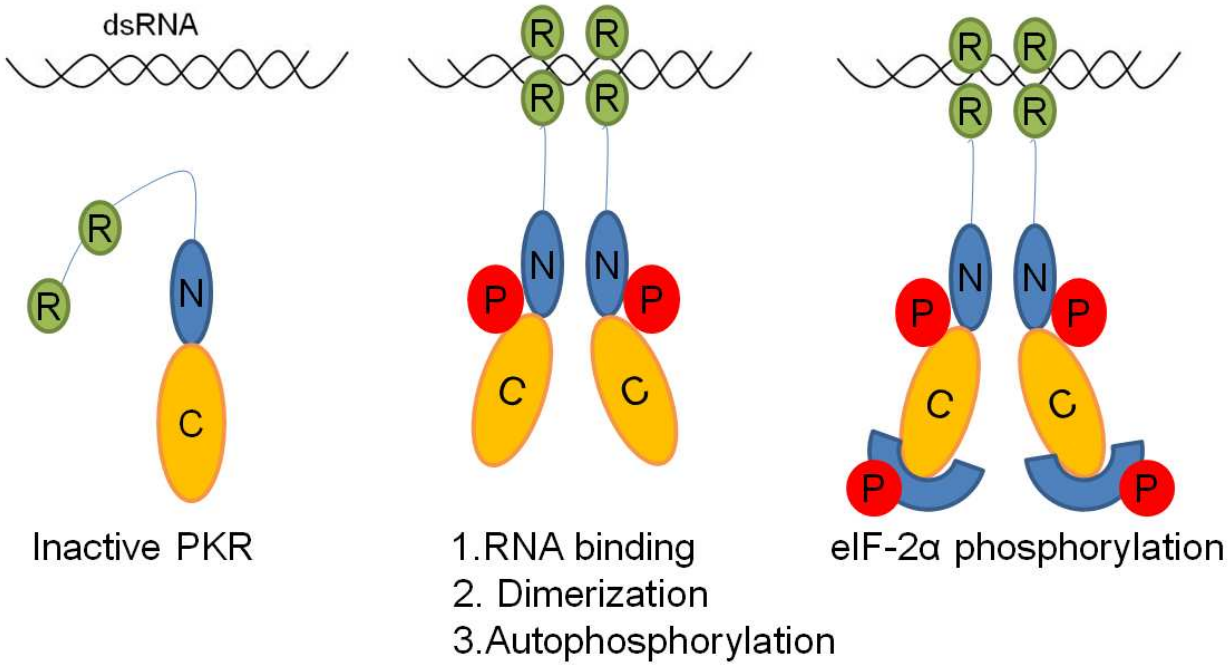

Figure 1.1 PKR activation by dsRNA. dsRNA binding domains (DRBDs) inactive PKR by interacting with kinase domain. When they bind to dsRNA, the kinase domain is released, dimerized and autophosphorylated to phosphorylate eIF2α. R, dsRNA binding domain. N and C, N-terminal and C-terminal lobes of kinase domain. For interpretation of the references to color in this and all other figures, the reader is referred to the electronic version of this dissertation.

the kinase. When phosphorylated at Tyrosine 416, Src kinases undergo a conformational change to be fully activated and its SH2 and SH3 domains can target proteins containing Pro-X-X-Pro motifs (Schindler *et al.*, 1999). Hck is expressed specifically in myelomonocytic cell lineages(Tsygankov, 2003) and transduces extracellular signals that regulate proliferation, differentiation and migration(Ernst *et al.*, 2002). DON exposure induces rapid phosphorylation of Hck at 1 min and MAPK at 5 min in RAW 264.7 macrophage. Notably, the Hck inhibitor, PP1, dose-dependently impairs the DON-induced MAPK activation, suggesting that Hck is an upstream mediator of MAPKs. Pretreatment of specific Hck inhibitor also suppresses the phosphorylation of MAPK substrates c-jun, ATF-2 and p90Rsk as well as the DON-induced activation of NF-kB, AP-1 and C/EBP(Zhou *et al.*, 2005b). Similarly, Hck siRNA also suppresses DON-induced TNF-α production and caspase activation. Consistent with these data, an Hck inhibitor suppresses p38 activation and p38-driven interleukin 8 (IL-8) expression (Bae et al., 2010) in the U937 human monocyte. Hck, as well as PKR, are important transducers of ribotoxic stress-induced apoptosis, the inhibition of which suppresses DON-induced p53 binding activity thus blocking the p38/p53/Bax/mitochondria/caspase-3 apoptosis pathway(Pestka, 2008).

ZAK contains an N-terminal kinase catalytic domain, a leucine zipper motif and a sterile-alpha motif(Liu et al., 2000). It has been found to activate both p38 and JNK(Jandhyala et al., 2008), and be involved in cell cycle arrest(Yang, 2002). In lipopolysaccharide (LPS) primed murine macrophages, ZAK inhibition decreases ricin-induced p38 and JNK activation(Lindauer et al., 2010). Classic RSR activators including anisomycin, ricin and UV, induced activation of JNK and p38 in cell lines and mouse

tissue, and are inhibited by a ZAK specific inhibitor (Wang *et al.*, 2005a; Jandhyala *et al.*, 2008). Notably, inhibition of ZAK does not suppress IL-1β and TNF-α induced JNK and p38 activation, suggesting that ZAK mediates activation of MAPKs in a RSR-specific manner(Jandhyala *et al.*, 2012). Additionally, the ZAK inhibitor also blocks anisomycin and UV-induced apoptosis and ricin-induced caspase 3 activation.

D.3. Initiating events in the ribotoxic stress response

Although the mechanisms for the RSR are still unclear, two hypotheses have been proposed: direct activation of ribosome-associated kinases and indirect activation via endoplasmic reticulum (ER) stress response(Pestka, 2010a).

D.3.1. Direct activation of ribosome-associated kinases

D.3.1.1. Ribosome is scaffold to signaling molecules

Within the mammalian cells, PKR associates with 60S ribosomal subunits via its two double-stranded RNA binding domains (DRBDs) and kinase domain(Wu *et al.*, 1998; Kumar *et al.*, 1999). Overexpression of the ribosomal large subunit protein L18 (RPL18) interacts with DRBDs of PKR, apparently inhibiting autophosphorylation of PKR and PKR-mediated eIF2α in vitro by competing with dsRNA and reversing dsRNA binding to PKR (Kumar et al., 1999). Deletions or residue substitutions in the DRBD sequences block its interaction with both dsRNA and RPL18.

PKR has also been found to have a novel role of forming a functional complex by direct binding to p38 and/or Akt, which permits PKR to effectively regulate their inhibition/activation (Alisi et al., 2008). Rapid ribosomal association and/or activation of PKR, Hck, p38 and ERK have also been observed in DON-treated macrophages (Fig. 1.2)(Bae *et al.*, 2010). Our lab has further found that DON recruits p38 to the ribosome

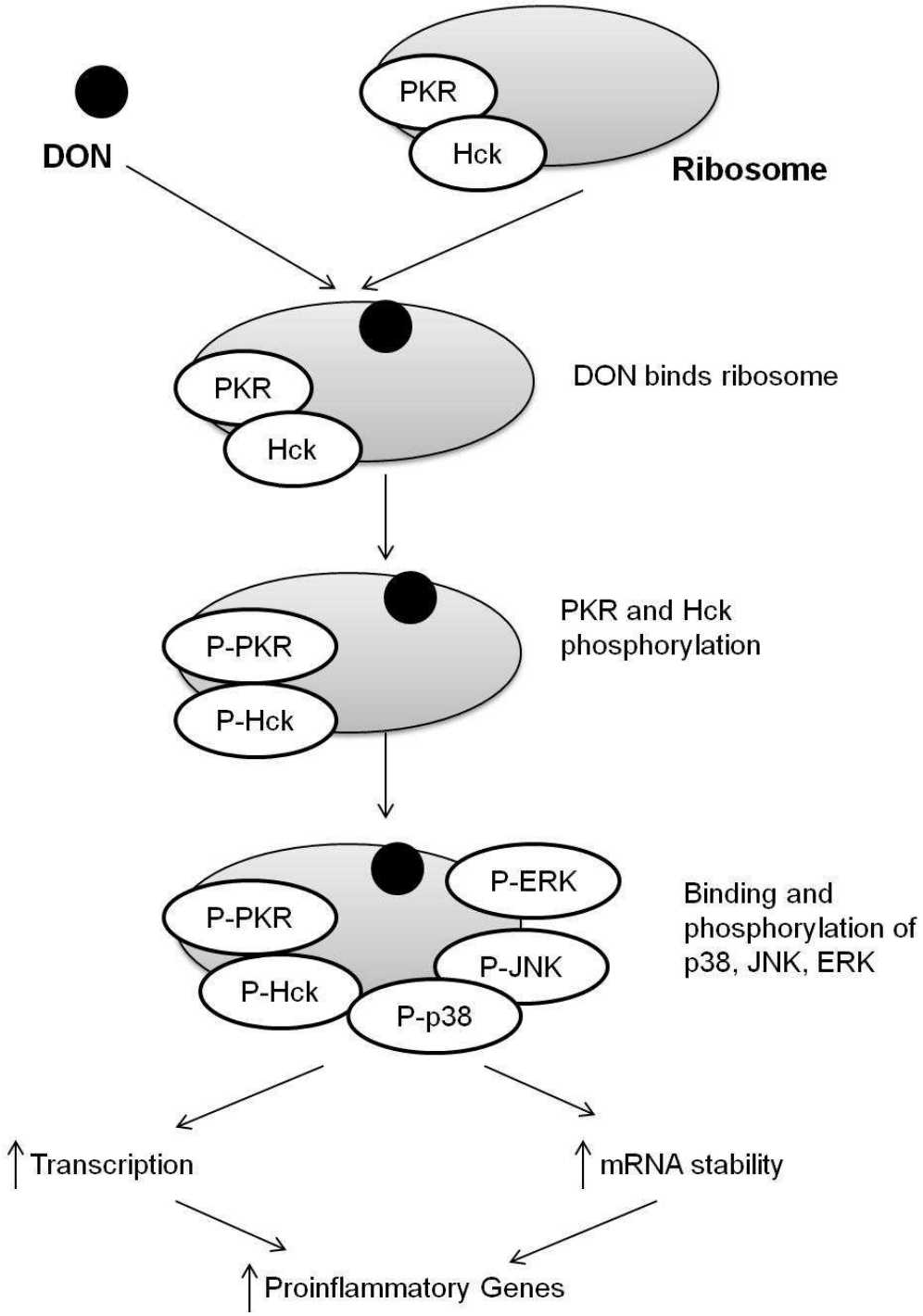

Figure 1. 2. Ribosome functions as scaffold for PKR, Hck and MAPKs in DON-induced ribotoxic stress response. DON-induced ribotoxic is proposed to involve: (1) rapid DON uptake and binding to ribosome (2) activation of ribosome-associated PKR and Hck (3) interaction and activation of p38, JNK and ERK (4) upregulation of proinflammatory genes by enhenncing transcription and mRNA stability.

in normal but not in PKR-deficient macrophages, suggesting that PKR might be required for DON-induced p38 activation(Bae *et al.*, 2010). PKR appears to sense ribotoxins and/or translational inhibition and be activated to trigger downstream signaling pathways. The ribosome might function as a scaffold for various signaling molecules, which mobilize to the ribosome upon ribotoxin exposure. This key step may promote their phosphorylation or activation, and the rapid activation of related signaling pathways to regulate the downstream gene transcription and post-transcriptional expression in response to translational stresses.

D.3.1.2. Role of RPL3 in RSR

It is believed that trichothecenes can diffuse rapidly into cells and interact with the eukaryotic ribosome to block translation because of their low molecular weight (approximately 200–500 Da)(Carter and Cannon, 1977; Ueno, 1984). However, certain mutation on the ribosomal protein L3 (RPL3) confers resistance to specific trichothecenes in yeast and plants (Fried and Warner, 1981; Harris and Gleddie, 2001; Afshar *et al.*, 2007). Investigation of trichodermin-resistant yeast identified the resistant gene *tcm1*, which encodes a mutated form RPL3 with one amino acid residue transition from 255 tryptophan (W) to cysteine (C)(Fried and Warner, 1981; Schultz and Friesen, 1983). Meskauskas constructed a RPL3 saturation mutagenesis library by error-prone PCR, 31 mutated amino acid transitions were found in RPL3 but only W255C showed maximum resistance to anisomycin, a peptidyltransferase center inhibitor(Meskauskas *et al.*, 2005). Kobayashi substituted the W255 with the other 19 amino acids in *S. cerevisiae,* respectively, but only the W255C transition showed the same growth rates under anisomycin treatment to the wild-type yeast control(Kobayashi *et al.*, 2006).

Notably, mutated RPL3 is also resistent to RIPs, such as the Type 1 RIP Pokeweed antiviral protein (PAP), which binds to RPL3 in wild-type yeasts and subsequently depurinates the α-sarcin/ricin loop of rRNA(Hudak *et al.*, 1999).

Co-expression of an N-terminal fragment of yeast RPL3 encoding the first 99 amino acids (L3Δ) together with the wild-type PAP in transgenic tobacco plants suppressed the toxicity of PAP to depurinate ribosomes(Di and Tumer, 2005). Although PAP is still associated with the ribosome in L3Δ expressing yeast, the cells are markedly resist to PAP and to the trichothecene mycotoxin DON, implying that L3 might be primarily targeted by trichothecenes and RIPs as a common mechanism.

D.3.1.3. rRNA cleavage

To date, induction of rRNA cleavage by chemicals or viruses has been linked to either RNase L-dependent or apoptosis-associated mechanisms (Banerjee *et al.*, 2000; Naito *et al.*, 2009). RNase L is a latent endonuclease with a broad range of functions including inhibition of protein synthesis, apoptosis induction and antiviral activity(Stark *et al.*, 1998). It can inhibit protein synthesis via the degradation of mRNA and rRNA(Clemens and Vaquero, 1978; Wreschner *et al.*, 1981). Activation of RNase L is able to cause cleavage of 28S rRNA, resulting in cellular stress response and activation of the JNK pathway(Iordanov *et al.*, 2000; Li *et al.*, 2004). However, specific 28S rRNA cleavage also is induced in murine Coronavirus-infected RNase L knockout cells, suggesting the existence of RNase L-independent pathway. In contrast, the majority of rRNA cleavage occurs concurrently with apoptosis(Houge *et al.*, 1993; Houge *et al.*, 1995; Samali *et al.*, 1997; King *et al.*, 2000; Nadano and Sato, 2000; Johnson *et al.*, 2003). Except for one cleavage site identified on 18S rRNA (Lafarga *et al.*, 1997), most

rRNA cleavage was evoked on 28S rRNA and thus was specifically located in the evolutionarily conserved domain 2 and 8(Houge and Doskeland, 1996; Degen *et al.*, 2000).

Trichothecenes have been further found to promote ribosomal RNA cleavage possibly by employing endogenous RNases(Li and Pestka, 2008). Ribosomal inactivating proteins (RIPs) possess N-glycosidase activity to depurinate adenine in the highly conserved sarcin/ricin (S/R) loop and result in rRNA cleavage(Endo *et al.*, 1987). Interestingly, trichothecenes and ricin could promote cleavage in the peptidyltransferase center but outside the S/R loop, specifically at A3560 and A4045 on 28S rRNA. This suggests that rRNA cleavage is a general event in ribotoxin exposure.

DON and T-2 enhance mRNA and protein level of RNase L, suggesting that this enzyme might play a role in toxin-induced specific rRNA cleavage. The only known direct activator of RNase L, 2'-5'-oligoadenylate (2-5A), is the product of oligoadenylate synthetase (OAS) (Liang *et al.*, 2006). In human, OAS is associated with different subcellular fractions, among which only OAS3 is mainly associated with the ribosomal fraction(Chebath *et al.*, 1987).

Taken together, binding of DON to ribosome may change the confirmation of rRNA, in which RPL3 may be a critical protein, and evoke 28S rRNA cleavage possibly by upregulation and activation of endogenous RNase L. It might be speculated that pertubation or damage of 28S rRNA might produce double-stranded ribosomal RNAs, which could be sensed by ribosome-associated PKR, and initiate the RSR(Pestka, 2010a).

D.3.2. Indirect activation via endoplasmic reticulum (ER) stress response

D.3.2.1. Introduction of ER stress and UPR

The lumen of the endoplasmic reticulum (ER) is specialized for the synthesis, folding and modification of secretory and membrane proteins with the aid of various molecular chaperones. Perturbations in the ER environment, termed ER stress, such as alterations in redox state, calcium levels, or failure to posttranslationally modify secretory proteins can change ER homeostasis and subsequently lead to accumulation of unfolded or misfolded proteins in the ER lumen(Lai *et al.*, 2007). To deal with this problem, ER activates stress response signaling pathways called the “unfolded protein response” (UPR) (Fig.1.3), which includes transient attenuation of protein translation, ER-associated degradation of misfolded proteins, induction of molecular chaperones and folding of enzymes to adaptively elevate the ER’s capability to fold and degrade proteins.

The UPR is mediated by three ER-resident transmembrane proteins, PKR-like endoplasmic reticulum kinase (PERK), inositol requiring kinase 1 (IRE1) and activating transcription factor 6 (ATF6), which are inactivated under physiological states by binding to the ER chaperone immunoglobulin protein (BiP)/glucose-regulated protein 78 (GRP78)(Bertolotti *et al.*, 2000). During ER stress, BiP preferentially binds to the accumulated unfolded proteins and dissociates from three ER-transmembrane transducers leading to their activation. Activated PERK, IRE1 and ATF6, phosphorylate eIF2α, splice XBP1 mRNA and transcribe ER stress response genes, respectively, (Malhi and Kaufman, 2011).

D.3.2.2. Trichocecene- and RIP-induced ER stress

RIPs and trichothecenes have been shown to induce ER stress (Lee *et al.*, 2008;

Shi *et al.*, 2009; Horrix *et al.*, 2011). Ricin induces phosphorylation of eIF2α and activation of ATF-6 in human adenocarcinoma cells, as markers of the induction of ER stress (Horrix et al., 2011). Shiga toxin also induces ER stress with activation of all three UPR effectors PERK, IRE-1, and ATF-6 in a monocyte-like cell line (Lee et al., 2008). Although devoid of enzymatic activity, DON increases the expression of IRE1, ATF6 and XBP1 mRNA and proteolytical degradation of BiP, which is generally upregulated during ER-stress, in murine peritoneal macrophages(Shi *et al.*, 2009). Interestingly, trichothecenes (DON, satratoxin G, roridin, T-2 toxin) and ricin all shown to induce BiP degradation during ER stress, suggesting it is a conserved signaling pathway for ribotoxins to evoke ER stress (Shi et al., 2009). Although the exact mechanism by which BiP is degraded is not completely understood, it is possible that ribotoxin exposure inhibits translation of secreted proteins at the cytosolic surface of the ER with ribosomes still attached to the ER and the incomplete nascent peptide inside ER(Jandhyala et al., 2012). BiP binds to the partially translated unfolded proteins in ER lumen and form a complex, which possibly degraded by autophagy, leading to the degradation of BiP(Pestka, 2010a).

ER stress may indirectly contribute to the RSR. IRE1 is found to activate apoptosis signal regulating kinase 1 (ASK1) and JNK (Urano et al., 2000; Yang et al., 2009) (Fig. 1.3), both of which are also activated by DON (Bae et al., 2010). Similar to DON-induced degradation of BiP, knockdown of BiP by siRNA results in increased IL-6 gene expression (Shi et al., 2009). In addition, knockdown of ATF6 partially inhibits DON-induced IL-6 expression in macrophages, suggesting that ER stress promotes the

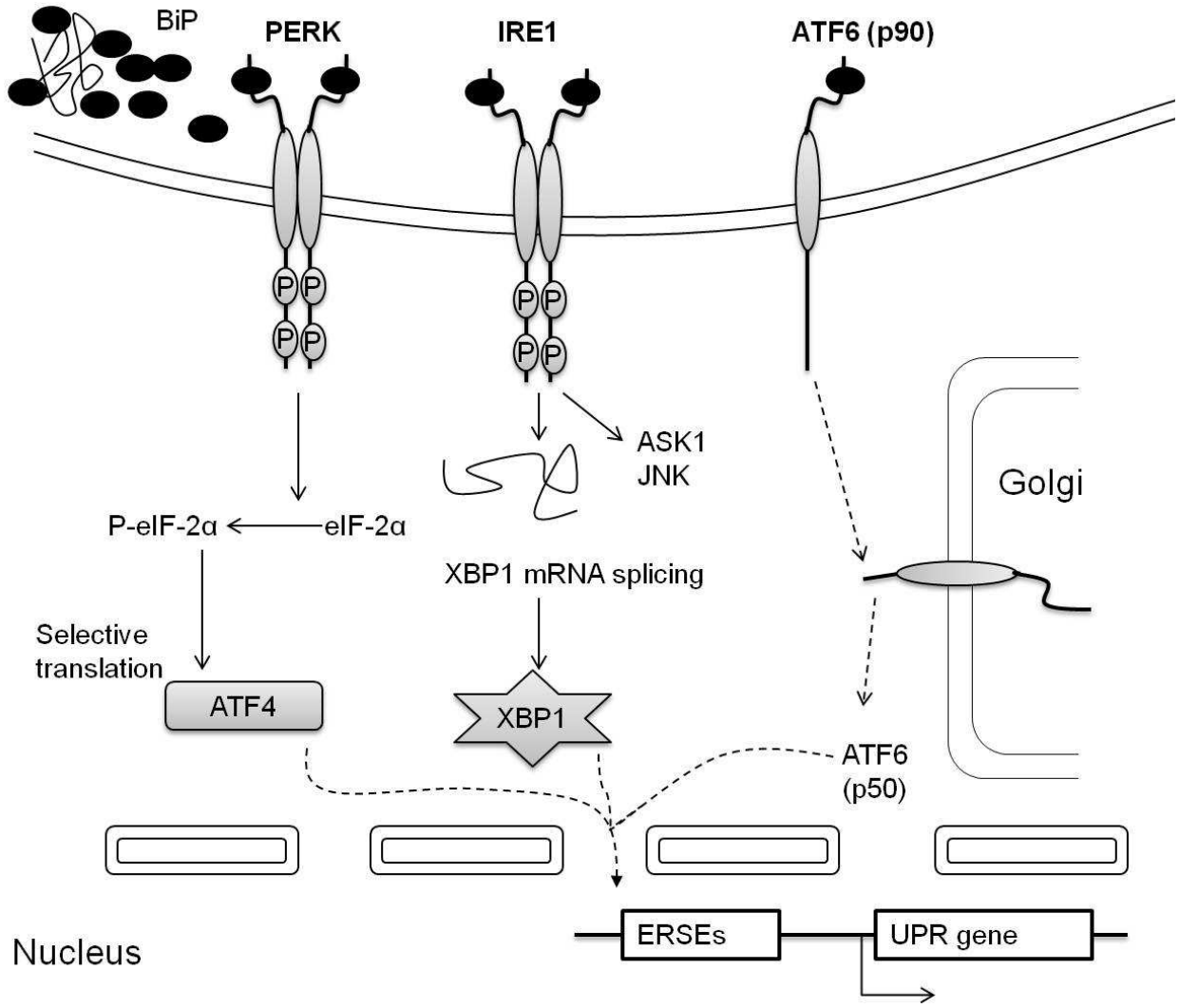

Figure 1.3. UPR signaling pathways in mammalian cells. The UPR is mediated by three ER-resident transmembrane proteins, PERK, IRE1 and ATF-6, which are inactivated by binding to BiP via their respecitve lumenal domains. The accumulated unfolded proteins sequester and dissocciate BiP from the three UPR mediators leading to their activation. The phosphorylated PERK kinase phosphorylates eIF2α, resulting in translation attenuation. Phosphorylated eIF2α selectively enhances translation of the ATF4 transcription factor that induces expression of UPR target genes. Activation of IRE1 by dimerization and phosphorylation causes JNK activation and IRE1-mediated splicing of XBP1 mRNA. Translation of spliced XBP1 mRNA produces a transcriptio factor that upregulates target genes via the ERSE promoter. ATF6 activation involves regulated intramembrane proteolysis. The protein translocates from the ER to the Golgi where it is proteolytically processed to release a 50-kDa transcription factor that translocates to the nucleus and binds the ERSEs of UPR target genes (Lai *et al.*, 2007).

expression of proinflammatory response genes upon DON exposure.

E. Apoptosis

E.1. Introduction

Apoptosis is the process of programmed cell death, generally characterized by distinct morphological characteristics including blebbing, cell shrinkage, nuclear fragmentation, chromatin condensation, and chromosomal DNA fragmentation(Elmore, 2007). Apoptosis occurs normally during development and aging as a homeostatic mechanism to maintain cell populations in tissues as well as bing part of a defense mechanism in immune reactions to eliminate damaged cells (Norbury and Hickson, 2001).

E.2. Caspase-dependent apoptotic pathways

Cysteine-dependent aspartate-directed proteases (caspases), are a family of cysteine proteases that play essential roles in apoptosis. These proteases are synthesized as inactive zymogens known as procaspases consisting of the highly diverse N-terminal prodomain and the C-terminal protease domain that can be further cleaved into the large (20 kDa α subunit/p18) and small (12 kDa β subunit/p10) subunits. These subunits subsequently assemble into an active α2β2 heterotetramer shared by all active caspases(Wang *et al.*, 2005b; Kumar, 2007). At least 14 mammalian caspases (caspase 1 to 14) have been identified and these can be divided into three functional groups: initiator caspases (2, 8, 9 and 10), effector caspases (3, 6 and 7) and the inflammatory caspases (1, 4, 5, 11, 12, 13 and 14)(Fan *et al.*, 2005). The executive caspases (3, 6 and 7) cleave and activate various substrates, such as cytokeratins, poly ADP ribose polymerase(PARP), the plasma membrane cytoskeletal protein and nuclear

proteins, leading to the ultimate morphological and biochemical changes in apoptotic cells(Slee *et al.*, 2001). To date, two conserved apoptotic pathways have been identified to activate caspases: the extrinsic and intrinsic pathways (Fig.1.4).

The intrinsic apoptotic pathway is mediated by mitochondria. Mitochondrial membrane permeability is a critical event in induction of apoptosis, which is precisely controlled by the Bcl-2 family of proteins(Cory and Adams, 2002). Bcl-2 family proteins can be either pro-apoptotic (Bcl-10, Bax, Bak, Bid, Bad, Bim, Bik, Mcl-2 and Blk) or anti-apoptotic (Bcl-2, Bcl-x, Bcl-XL, Bcl-XS, Bcl-w, BAG), and they coordinatingly determine the fate of cell, apoptosis or survival(Elmore, 2007). Cellular stresses change the mitochondrial transmembrane potential and membrane permeability resulting in the release of cytochrome c from mitochondria to the cytosol. In the presence of ATP, apoptotic protease activating factor 1 (Apaf-1) binds to cytosolic cytochrome c and oligomerizes to form a complex, termed an apoptosome, which recruits procaspase 9 via a caspase recruitment domain (CARD) (Bao and Shi, 2007). After activation, caspase-9 activates the effectors caspase 7 and 3 to initiate apoptosis. In the late stage of programmed cell death, apoptosis inducing factor (AIF), endonuclease G and caspase-activated DNase (CAD) are released from mitochondria and cause condensation of chromatin, DNA fragmentation and degradation(Elmore, 2007).

The extrinsic apoptotic pathway is characterized by activation of caspase 8 via death receptors, such as Fas and TNF receptors(Zhao *et al.*, 2010). After ligand binding, the receptors recruit cytoplasmic adapter proteins containing death effector domain (DED). The aggregation of these proteins exposes their DEDs to interact with the DEDs in the prodomain of procaspase-8 resulting in the oligomerization of procaspase 8. This

complex is known as death-inducing signal complex (DISC) and causes the subsequent auto-catalytic activation of procaspase 8. Activated caspase 8 directly activates the downstream procaspases (e.g. procaspase-3) to initiate apoptosis. Notably, there is crosstalk between the intrinsic and extrinsic pathways by which death receptor activated caspase 8 cleaves the pro-apoptotic Bcl-2 family member Bid into an active truncated form (tBid) (Fig.1.4), which translocates to mitochondrial membrane, binds to Bax, induces conformational change of Bax resulting in much more efficiently release of cytochrome c to trigger the activation of the mitochondrion pathway (Desagher *et al.*, 1999; Fan *et al.*, 2005).

E.3. Role of lysosome in apoptosis

. Lysosomes are acidic (pH ≤5), highly dynamic single-membrane bound organelles that contain hydrolytic enzymes that are capable of degrading intracellular macromolecules. Cathepsins are the best characterized proteases in lysosome and mainly include cysteine cathepsins as well as a few serine (A and G) and aspartic (D and E) cathespins (Johansson et al., 2010). In response to a variety of stress stimuli, the lysosomal membrane permeabilizes (LMP) releasing cathepsins into the cytosol. Notably, cathepsin B, L and D released from the cytosol remain active at neutral cytosolic pH, promote apoptosis (Boya and Kroemer, 2008).

The lysosomal apoptotic pathway, either cathepsin-dependent or -independent, is believed to proceed through mitochondria(Repnik and Turk, 2010) (Fig.1.4). LMP is suggested to be upstream of mitochondrial membrane permeabilization (MMP)(Terman et al., 2006; Droga-Mazovec et al., 2008). Active cathepsins (B, K, L and S) released upon LMP cleave various protein substrates involved in the intrinsic and extrinsic

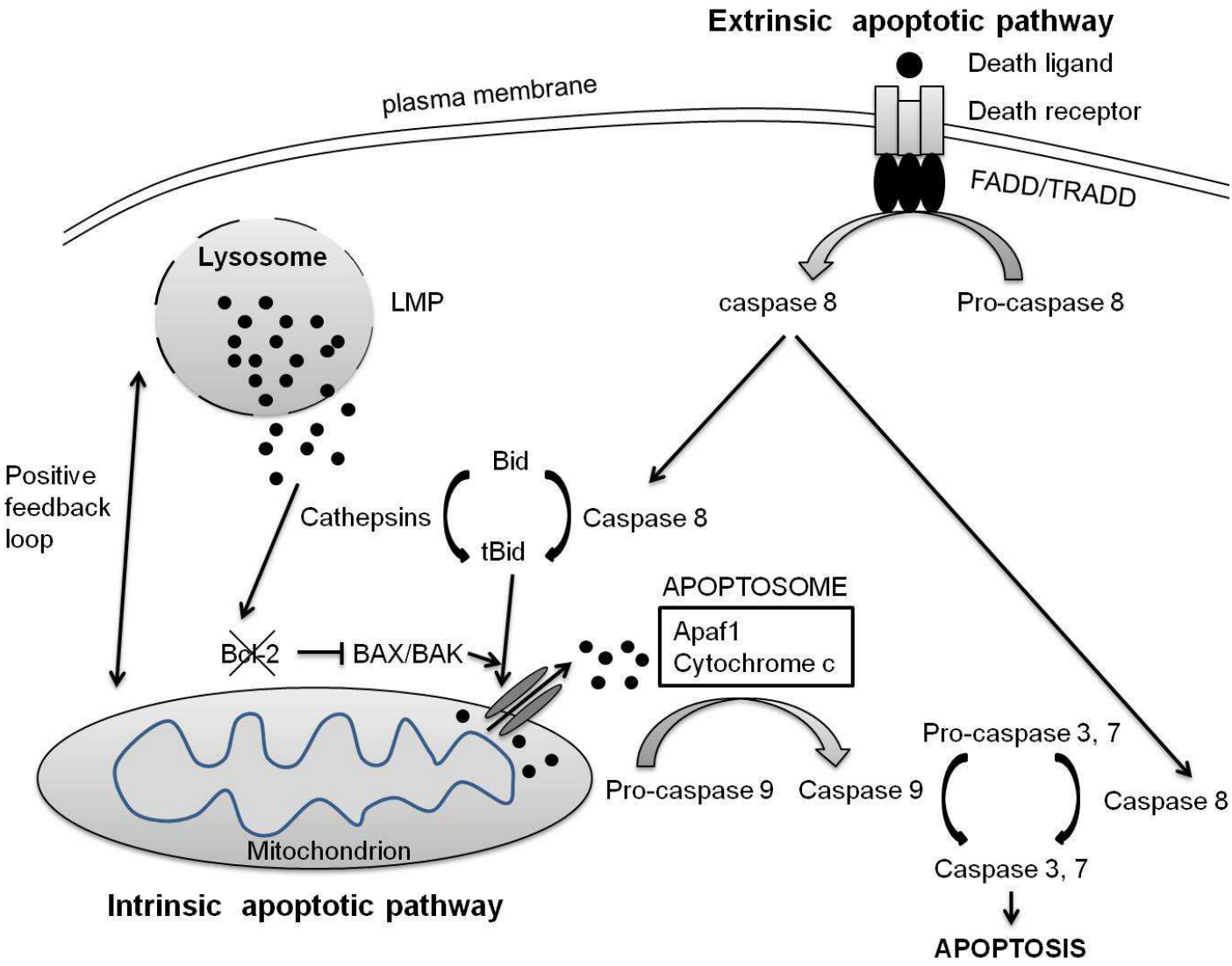

Figure 1.4. Crosstalk between lysosomes and apoptotic pathways. Cathepsins are released to process BID to the pro-apoptotic t-BID form and degrade anti-apoptotic BCL-2 proteins. Thereby BAX/BAK are activated to permeabilize the mitochondrial outermembrane, leading to the initiation of the intrinsic apoptotic pathway. Cytochrome c released from mitochondria and apoptotic peptidase activating factor 1 (Apaf1) form an oligomeric caspase-9-activating complex, called apoptosome. Activated caspase-9 then activates executioner caspases-3 and -7. The extrinsic pathway is triggered by the binding of death receptor (TNF-α, FasL or TRAIL) to their specific death receptors at the plasma membrane. Upon the recruitment of adaptor proteins (TRADD and FADD) to the receptor, caspase-8 is activated, which can directly cleave executioner caspases or amplify the signal through the intrinsic apoptotic pathway with via BID cleavage.

pathways including pro-apoptotic BID and anti-apoptotic BCL-2 molecules (BCL-2, BCL-XL and MCL-1) leading to MMP, the central event in the intrinsic apoptotic pathway regulating the release of cytochrome c(Repnik and Turk, 2010). In addition, it also degrades anti-apoptotic molecules downstream of mitochondria such as X-linked inhibitor of apoptosis protein (XIAP), the intracellular inhibitor of caspase 9, 7 and 3, to promote executioner caspase activation (Droga-Mazovec et al., 2008). In lysosome-induced caspase-independent apoptosis, cathepsin D triggers activation of Bax leading to selective release of AIF from the mitochondria, which initiates apoptosis by DNA fragmentation (Bidere et al., 2003). LMP-induced MMP is also proposed to contribute to LMP in an amplifying loop(Terman et al., 2006), suggesting that crosstalk between lysosomes and mitochondria is critical in determining the fate of cells.

E.4. DON-induced apoptotic pathways

DON rapidly induces activation of p38 and ERK1/2 within 15 min in RAW 264.7 macrophages and inhibitors of p38 and ERK1/2 markedly suppress and attenuate DON-evoked caspase 3-dependent DNA fragmentation, respectively, suggesting they play opposite roles in apoptosis(Zhou *et al.*, 2005a). In addition, p38 was found upstream of p53 activation, which positively promotes caspase 3 activation and DNA fragmentation. Concurrent with p53 activation, DON activates two anti-apoptotic survival mediators, ERK-dependent p90 Rsk and AKT. Accordingly, DON is proposed to induce competing intrinsic apoptotic (p38/p53/Bax/mitochondria/caspase-3) and survival (ERK/AKT/p90Rsk/Bad) pathways in the macrophages (Zhou *et al.*, 2005a).

F. Translational regulation

F.1. Introduction

Translation is the process of decoding mRNA into a specific amino acid chain by cellular protein synthesis via the ribosome. In response to environmental stress, organisms rapidly change their cellular protein synthesis by precise regulation of translation to adaptively cope with these stimuli. Translation can be divided into four stages: initiation, elongation, termination, and recycling(Kapp and Lorsch, 2004). In classic cap-dependent translation, translation initiation starts with the recruitment of the cap-binding protein complex, also known as eIF4F (eukaryotic initiation factor 4F), which consists of eIF4E (cap-binding protein), eIF4A (helicase) and eIF4G (scaffold protein), to the 5'-end of the mRNA(Gebauer and Hentze, 2004), which is the most frequently regulated process. To date, multiple mechanisms for both global translation and translation on individual mRNAs have been reported.

F.2. Global regulation

In the regulation of global translation, mammalian target of rapamycin complex 1 (mTORC1) can be activated by PI3K or ERK1/2 to enhance translation. It activates p70 S6 kinase (p70S6K) that phosphorylates the small ribosomal subunit protein S6 (RPS6) to promote translation (Ma and Blenis, 2009). Alternatively, p90 ribosomal S6 kinases (p90RSKs), activated by ERK1/2, phosphorylates eIF4B and eEF2K to facilitate translation (Ma and Blenis, 2009). In addition, the general translation rate can be regulated by controlling the availability of the cap-binding protein eIF4E. the PI3K-Akt pathway phosphorylates eIF4E-binding protein 1 to release eIF4E, which binds to the 7-methyl GTP cap of mRNAs and increase the rate of initiation (Gebauer and Hentze, 2004; Ma and Blenis, 2009). In contrast, a number of kinases including PKR and PERK are activated under different stresses to suppress global translation by coordinating the

phosphorylation of eIF2α at Ser51(Gebauer and Hentze, 2004).

Some featured regulatory sequences within the 5'-UTR of mRNA are also involved in global translation(Calvo *et al.*, 2009; Komar and Hatzoglou, 2011). The internal ribosome entry site (IRES), a unique nucleotide sequence, allows recruitment of the translation initiation complex downstream of the 5' cap and translates IRES-containing mRNAs in a cap-independent manner(Komar et al., 2012). This mode of initiation is frequently used during stress conditions in which the cap-dependent translation is impaired. Another example of a regulatory sequence as a common mechanism is the upstream open reading frame (uORF), which are mRNA elements defined by a start codon in the 5'-UTR that is out-of-frame with the main ORF and coding sequence(Calvo et al., 2009). uORFs typically interfere with expression of the downstream primary ORF by increasing translation initiation(Medenbach et al., 2011).

F.3. Individual regulation

Besides global regulation, translation of specific messages could be modulated at the individual level. For example, translation of specific messages can be controlled by specific RNA-binding proteins (RBPs) (Gebauer and Hentze, 2004), many of which interact with functionally related groups of mRNAs, illustrating the elaborate regulation at level of translation. Alternatively, microRNAs, a family of small non-coding RNAs about 22 nucleotides in length, can also precisely regulate specific gene expression by imperfectly binding to the 3'-UTR of target mRNA. The stalled translation complex could be degraded or relocalized to stress granules for future use (Leung and Sharp, 2010).

F.4 DON-induced translational regulation

DON is known to directly bind to ribosomes to inhibit translation and activate PKR to phosphorylate eIF2α resulting in global translation suppression(Zhou et al., 2003b). In contrast, DON also activates the translation-promoting pathway members Akt, ERK1/2 and p90RSK at the same time (Zhou *et al.*, 2005a). In addition, DON can modulate the profile of miRNAs in macrophage at 3 and 6 h, thus suggesting a possible regulation of inflammatory response genes (He and Pestka, 2010).

G. Summary

Low-molecular-weight (e.g. DON, anisomycin) and protein (e.g. ricin) ribotoxins are proposed to bind to or damage the 3'-end of 28S rRNA, respectively, to trigger the ribotoxic stress response. DON is a ribotoxin that commonly contaminates cereal-based foods and has the potential to adversely affect humans and animals. At low doses, DON partially inhibits translation, induces PKR-mediated MAPK activation and upregulates mRNA stability of proinflammatory genes. However, the relationship between DON-modulated transcription and translation of inflammatory genes is unclear. In contrast, high doses of DON cause immunosuppression by evoking apoptosis and rRNA cleavage. DON and ricin both induce common ribosomal RNA cleavage at A3560 and A4045 on 28S rRNA in RAW 264.7 macrophages. However, mechanisms of rRNA cleavage are not understood.

This dissertation aims to fill the aforementioned knowledge gaps. Chapter II will compare DON-induced transcriptome and translatome of inflammatory genes to elucidate how DON coordinates the transcription and translation of these genes. Chapter III will focus on the intracellular signaling pathways and targets of DON to induce rRNA cleavage. Chapters IV will investigate whether anisomycin, SG and ricin

share the identical mechanism as DON to induced rRNA cleavage.

CHAPTER 2

Modulation of Inflammatory Gene Expression by the Ribotoxin Deoxynivalenol Involves Coordinate Regulation of the Transcriptome and Translatome

This chapter has been accepted by Toxicological Sciences (2012).

ABSTRACT

The trichothecene deoxynivalenol (DON), a common contaminant of cereal-based foods, is a ribotoxic mycotoxin known to activate innate immune cells in vivo and in vitro. While it is recognized that DON induces transcription and stability of inflammation-associated mRNAs in the macrophage, it is not known whether the toxin can selectively modulate translation of these mRNAs. To address this question, we employed a focused inflammation/autoimmunity PCR array to compare DON-induced changes in profiles of polysome-associated mRNA transcripts (translatome) to total cellular mRNA transcripts (transcriptome) in the RAW 264.7 murine macrophage model. Exposure to DON at 250 ng/ml for 6 h induced robust expression changes in inflammatory response genes including cytokines, cytokine receptors, chemokines, chemokine receptors, and transcription factors, with over 70% of the changes being comparable in the two populations. Average fold up- and down-regulation per gene were 5.9 and 0.25 in the translatome, respectively, and 5.6 and 0.26 in the transcriptome, respectively. When expression changes of a total of 17 selected cytokine, chemokine, receptor, transcription factor and inflammatory response genes in the polysome and cellular mRNA pools were confirmed by real-time PCR in a follow-up study, coordinate regulation of the translatome and transcriptome was evident, however, modest differences in expression of some genes were again detectable. Taken together, DON's capacity to alter translation expression of inflammation-associated genes is likely to be driven predominantly by selective transcription, however, a small subset of these genes appear to be regulated at the translational level.

INTRODUCTION

Deoxynivalenol (DON), a trichothecene mycotoxin produced by toxigenic *Fusaria* that commonly contaminate cereal-based foods, has the potential to adversely affect humans and animals and therefore represents a major public health concern (Amuzie and Pestka, 2010). Primary targets of this ribotoxic mycotoxin are monocytes and macrophages of the innate immune system. Both in vitro and in vivo studies have demonstrated that DON induces phosphorylation of mitogen-activated protein kinases (MAPKs) which drives upregulated expression of mRNAs and proteins for inflammation-related genes such as the cytokines, chemokines and cyclooxygenase-2 (COX-2) (Shifrin and Anderson, 1999; Moon and Pestka, 2002; Chung *et al.*, 2003b; Zhou *et al.*, 2003a; Islam *et al.*, 2006). DON-induced increases in cellular pools of inflammation-associated mRNAs have been linked to both transcriptional activation and stabilization of mRNA through AUUUA motif in the 3'-untranslated region(Moon and Pestka, 2002; Chung *et al.*, 2003b) suggesting that these two mechanisms contribute to upregulated gene expression.

While the increased expression of selected proteins could directly result from the increased cellular pool of specific mRNAs induced by DON, it could also be caused by differential mRNA recruitment to translating ribosomes. The overall rate of translation is further dependent on the capacity for and efficiency of translation (Proud, 2007; Sonenberg and Hinnebusch, 2009). Capacity relates to the availability and abundance of ribosomal subunits and other translational components, while efficiency is regulated by the rate of translational initiation and peptide chain elongation. Individual mRNAs are subject to additional levels of translational regulation, and elements in their 5' and 3'

untranslated regions (UTRs) may interact with regulatory RNAs (e.g. antisense sequences, microRNAs) or RNA binding proteins to modulate ribosomal association (Sonenberg and Hinnebusch, 2009). It is not yet known whether ribotoxins such as DON selectively modulate translation through such mechanisms. This question is particularly intriguing because DON is capable of inhibiting translation at high concentrations(Zhou *et al.*, 2003b).

One strategy for monitoring changes in protein expression in stressed cells is proteomic analysis, however, this approaches is time-consuming, expensive and relatively insensitive when compared to transcriptomic approaches employing highly sensitive PCR(Cheeseman *et al.*, 2011; Kuny *et al.*, 2012). An alternative approach for identifying and quantitating genes being translated in cells under a specific set of conditions is to first isolate their polysomes and then profile the associated mRNAs. This “translatome” strategy has successfully been used in fungal, plant and animal cells (Preiss *et al.*, 2003; Shenton *et al.*, 2006; Halbeisen and Gerber, 2009; Markou *et al.*, 2010; Mustroph and Bailey-Serres, 2010). For example, yeast exposed to different stresses, such as amino acid depletion and fusel alcohol addition, shows distinct translational profiles (Smirnova *et al.*, 2005), suggesting the fundamental role of translational regulation in quick response to environmental stress. Further study employing additional high-throughput array analysis of the transcriptome indicated that the translatome correlates with the transcriptome under severe stresses such as amino acid depletion but not under mild stresses(Halbeisen and Gerber, 2009), suggesting coordination of the translatome and transcriptome is stress-dependent. Similar correlation and uncoupling of the transcriptome and translatome has also been

documented in human cells(Mikulits *et al.*, 2000; Grolleau *et al.*, 2002; Tebaldi *et al.*, 2012).

The purpose of this study was to test the hypothesis that DON selectively modulates translation of inflammation-associated genes in the macrophage. Specifically, we employed a focused inflammation/autoimmune PCR array to compare the DON-induced inflammation-associated translatome and transcriptome in the RAW 264.7 murine macrophage cell model. The results revealed that DON's capacity to modulate translation of most inflammation-associated genes is predominantly driven by selective transcription, however, a small subset of these genes appears to be regulated, in part, by selective translation.

MATERIALS AND METHODS

Chemicals. DON, acid-phenol (pH 4.3), trichloromethane, isoamyl alcohol, lithium cloride, sucrose, heparin, cycloheximide and Triton X-100 were purchased from Sigma-Aldrich (St. Louis, MO). TRIZOL was obtained from Invitrogen (Carlsbad, CA). RNase-free water was supplied by Ambion (Austin, Texas).

Macrophage cell culture. RAW 264.7 (ATCC, Rockville, MD), a mouse macrophage cell line, was cultured in Dulbecco's modified Eagle's medium (DMEM) supplemented with 10% (v/v) heat-inactivated fetal bovine serum (Atlanta Biologicals, Lawrenceville, GA), streptomycin (100 μg/ml) and penicillin (100 U/ml) at 37 ^{o}C in a humidified atmosphere with 5% CO_2. Macrophage cell number and viability were assessed by trypan blue dye exclusion using a hematocytometer. Prior to exposure of DON, cells (2.5 x 10^6/plate) were seeded and cultured in 100-mm tissue culture plates for 24 h to achieve approximately 80% confluency. Cells were treated with vehicle or 250 ng/ml DON for 6 h and subjected to polysomal and total RNA isolation. This concentration has been previously found in RAW 264.7 cells and partially inhibits translation but is optimal for inducing inflammatory gene expression(Moon and Pestka, 2002; Yang and Pestka, 2002).

Sucrose density gradient fractionation. For polysome isolation, cells were washed twice with ice-cold phosphate-buffered saline (PBS) and lysed in 500 μl ice-cold polysome extraction buffer (PEB) (50 mM KCl, 10 mM $MgCl_2$, 15 mM Tris–HCl [(pH 7.4), 1% (v/v) Triton X-100, 0.1 mg/ml cycloheximide and 0.5 mg/ml heparin)(Bae *et al.*, 2009). Sucrose solutions (10% and 50%, w/v) were prepared prior to use by dissolving sucrose into RNase-free water with 50 mM KCl, 15 mM Tris–HCl (pH 7.4), 10 mM

$MgCl_2$, 0.1 mg/ml cycloheximide and protease inhibitor. Cell lysates were centrifuged at 16,000 × g, 4 ℃, for 15 min to remove nuclei, mitoc hondria and cell debris. The resultant clear supernatant (1.8 ml) was layered on a 9 ml linear sucrose gradient solution (10–50%) prepared using an ISCO 160 Gradient Former and held at 4 ℃ in an 11.5 ml Sorvall centrifuge tube and centrifuged at 200,000 × g, 4 ℃ for 3 h in Sorvall TH-641 rotor. Polysomal fractions were isolated by fractionating gradient at a rate of 0.5 ml per min into 2 ml tube by upward displacement using an ISCO Density Gradient Fraction Collector, consisting of a needle-piercing device with a syringe pump connected to an EM-1 UV monitor for continuous measurement of the absorbance at 254 nm (Teledyne ISCO, Lincoln, NE).

Total and polysomal RNA purification*.* Briefly, the approach employed was a modification of previously described procedure (Zong *et al.*, 1999) for comparing transcription and translatome. For transcriptome analysis, total RNAs were extracted by TRIZOL (Invitrogen, Carlsbad, CA) following manufacturer's protocol. For translatome analysis, polysomal fractions (500 µl) were diluted with RNase-free water to a volume of 1000 µl and subsequently combined with equal volume of phenol: chloroform: isoamyl alcohol (25:24:1). Tubes were mixed, held at 25℃ for 5 min, and centrifuged at 16000 × g, 4 ℃ for 15 min. Supernatants were pooled and t ransferred to a 50 ml cornical centrifuge tube and RNA was precipitated with LiCl at final concentration of 2 M at -20 ℃ overnight. After centrifugation at 12,000 × g, 4 ℃ for 15 min, pellets were washed three times with 70% ethanol, air-dried, and resuspended in RNase-free water. RNA concentrations were also measured with a Nanodrop reader (Thermo Fisher, Wilmington, DE) and integrity verified using Agilent 2100 Bioanalyzer Nanochip

capillary electrophoresis unit. RNA integrity number (RIN) values were ≥ 9.9 for all samples, suggesting the RNA was of high purity with minimal degradation and suitable for cDNA synthesis. Both total and polysomal RNAs were stored at -80℃.

PCR array and data analysis. RNA (2 µg) samples were reverse transcribed using high capacity RNA-to-cDNA kit (Applied Biosystems, Foster City, CA) and the newly synthesized cDNA purified using a Qiagen PCR purification kit (Valencia, CA). Resultant cDNAs (8 ng/well) were applied to 384-well mouse Inflammatory Response and Autoimmunity (PAMM-077A) PCR array plates from SABiosciences (Valencia, CA) according to manufacturer's instructions. Plates were run in duplicate in an Applied Biosystems 7900 Real-Time PCR System. Mean Ct values of five house-keeping genes on the PCR array plate (β-glucuronidase, hypoxanthine guanine phosphoribosyl transferase, heat shock protein 90 α, glyceraldehyde-3-phosphate dehydrogenase (GAPDH), β-actin) were 17.4 (control-total cDNA), 17.6 (DON-total cDNA), 17.8 (control-polysomal cDNA) and 17.9 (DON-polysomal cDNA) verifying the quantity of mRNA recovered as well as the efficacy of PCR array protocol for all four experimental groups. Data were interpreted using SABiosciences' web-based PCR array data analysis tool.

Real-time PCR. Three independent biological replicates of control and DON-treated total and polysomal RNAs were purified, analyzed and synthesized into cDNA, respectively, as described above. Quantitative PCR using duplicate technical replicates of each cDNA was performed on a 7500 Fast Real-Time PCR System (Applied Biosystems) using Taqman gene expression assay probes (Applied Biosystems) of mouse target genes, IL-1β (Mm01336189_m1), IL-6 (Mm00446190_m1), IL-10

(Mm00439614_m1), IL-18 (Mm00434225_m1), TNF-α (Mm00443258_m1), CCL2 (Mm00441242_m1), CCL4 (Mm00443111_m1), CCL5 (Mm01302427_m1), CCL7 (Mm00443113_m1), CCR1 (Mm00438260_s1), CCR2 (Mm01216173_m1), CXCL2 (Mm00436450_m1), BCL6 (Mm00477633_m1), Fos (Mm00487425_m1), CXCR1 (Mm00731329_s1), TLR5 (Mm00546288_s1), ITGB2 (Mm00434513_m1) or an endogenous control GAPDH (Mm99999915_g1) and TaqMan Universal PCR Master Mix (Applied Biosystems). The expression levels of individual gene were normalized with GAPDH in the same sample by calculation of Delta-cycle threshold (ΔCt) value. Relative expression levels of respective genes in DON-treated samples were compared with corresponding control and calculated by relative quantification (ΔΔCt) (Takeda *et al.*, 2008). Data were represented as the mean ± SE of three biological replicates.

Statistical Analysis. Data were analyzed using Sigma Plot 11 (Jandel Scientific, San Rafael, CA). Data sets were considered significantly different when $p<0.05$.

RESULTS

Although it has been recognized that DON induces transcription and enhances stability of inflammation-associated mRNAs in the macrophage, the toxin's effects on translation of these mRNAs are not yet understood. DON-induced translational and transcriptional profiles of inflammation-related mRNAs were therefore measured in RAW 264.7 macrophage treated with 250 ng/ml of the toxin for 6 h using a focused PCR array containing 84 inflammation related genes. The percentages of up-regulated, down-regulated and unaffected genes were similar in the transcriptome (45%, 7% and 48%, respectively) (Fig. 2.1A), and the translatome (48%, 10%, and 42%, respectively) (Fig. 2.1B). Overall, the transcriptome and translatome shared 33 up-regulated genes (89% and 83%, respectively) (Fig. 2.3A) and 5 down-regulated genes (80% and 56%, respectively) (Fig. 2.3B). Scatter plots of the transcriptome and translatome revealed a remarkably similar gene distribution pattern (DON vs control) (Fig. 2.2A, B). The upregulated genes clustered similarly in the transcriptome and translatome. There were also a smaller number of downregulated genes which showed comparable distribution in the translatome and transcriptome.

Genes up- and down-regulated by DON at the transcriptome and translatome level were categorized as chemokines, chemokine receptors, cytokines, cytokine receptors or inflammatory response genes (Table 2.1). Quantitative changes in inflammatory response gene expression are summarized in Table 2 (up-regulation) and Table 2.3 (down-regulation). Notably, all CCL family chemokines and receptors within the array were upregulated. In addition, the average fold up- and down-regulation level

Table 2.1. Functional gene grouping of DON-induced up- and down-regulated genes in transcriptome and tranlatome.

Functional Gene Grouping	Translatome & Transcriptome	Translatome-specific	Transcriptome-specific
Chemokines	↑Ccl1, Ccl11, Ccl12, Ccl17, Ccl2, Ccl22, Ccl24, Ccl3, Ccl4, Ccl5, Ccl7, Cxcl2, Cxcl3 ↓Cxcl10	↑Cxcl1 ↓Ccl25, Cxcl11	↑Cxcl9
Chemokine Receptors	↑Ccr1, Ccr2, Ccr3, Ccr7,Cxcr2	↑Cxcr1	
Cytokines	↑Il1b, Il10, Il1f10, Tnf, Fasl, Il23a, Il6 ↓Il18, Il7, Ltb	↑Ifng	↑Tnfsf14, Lta
Cytokine Receptors	↑Il1r1, Il1rn	↑Il22ra2, ↓Il18rap	↑Il10rb
Inflammatory Response	↑Bcl6, Fos, C3ar1, C4b, Crp, Ripk2 ↓Cd40	↑C3, Itgb2, Tlr5 ↓Tlr3	↓Tlr2

Table 2.2. DON-induced up-regulation of inflammatory response genes in translatome (TLM) and transcriptome (TCM).

Symbol	Fold Change*			Gene Bank	Gene Description
	TLM/ TCM	TLM	TCM		
Cxcl1	11.6	6.1	0.5	NM_008176	Chemokine (C-X-C motif) ligand 1
Ifng	8.5	11.5	1.4	NM_008337	Interferon gamma
Tlr5	7.2	6.5	0.9	NM_016928	Toll-like receptor 5
Il1b	5.4	27.4	5.1	NM_008361	Interleukin 1 beta
Cxcr1	3.2	3.2	1	NM_178241	Chemokine (C-X-C motif) receptor 1
Il22ra2	2.1	3.9	1.9	NM_178258	Interleukin 22 receptor, alpha 2
Ccl7	2.0	12.2	6.2	NM_013654	Chemokine (C-C motif) ligand 7
Ccl12	1.9	5.4	2.9	NM_011331	Chemokine (C-C motif) ligand 12
Il10	1.9	3.9	2.1	NM_010548	Interleukin 10
Ccr1	1.8	32.9	18.2	NM_009912	Chemokine (C-C motif) receptor 1
Cxcl2	1.6	15.5	9.9	NM_009140	Chemokine (C-X-C motif) ligand 2
Itgb2	1.5	2.4	1.62	NM_008404	Integrin beta 2
Bcl6	1.5	3.8	2.6	NM_009744	B-cell leukemia/lymphoma 6
Ccl24	1.5	9.2	6.3	NM_019577	Chemokine (C-C motif) ligand 24
C3	1.4	2.6	1.8	NM_009778	Complement component 3
Ccr3	1.4	6.2	4.5	NM_009914	Chemokine (C-C motif) receptor 3
Il6	1.3	3.9	3.1	NM_031168	Interleukin 6
Fasl	1.2	3.3	2.7	NM_010177	Fas ligand (TNF superfamily, member 6)
Cxcr2	1.1	14.8	13.6	NM_009909	Chemokine (C-X-C motif) receptor 2
Ripk2	1.1	2.6	2.4	NM_138952	Receptor (TNFRSF)-interacting serine-threonine kinase 2
Ccl17	1.0	3	2.9	NM_011332	Chemokine (C-C motif) ligand 17
Ccl11	1.0	4.4	4.4	NM_011330	Chemokine (C-C motif) ligand 11
Ccr2	1.0	6.2	6.4	NM_009915	Chemokine (C-C motif) receptor 2
Fos	0.9	2	2.2	NM_010234	FBJ osteosarcoma oncogene
C3ar1	0.9	6.7	7.5	NM_009779	Complement component 3a receptor 1
Il1f10	0.9	2.4	2.8	NM_153077	Interleukin 1 family, member 10
Ccl4	0.9	6.6	7.7	NM_013652	Chemokine (C-C motif) ligand 4
Lta	0.8	1.9	2.3	NM_010735	Lymphotoxin A
Tnf	0.8	2.4	2.9	NM_013693	Tumor necrosis factor
Ccl2	0.8	3.8	4.6	NM_011333	Chemokine (C-C motif) ligand 2
Ccl3	0.8	8	10	NM_011337	Chemokine (C-C motif) ligand 3

Table 2.2. (cont'd)

Il23a	0.8	3.8	4.9	NM_031252	Interleukin 23, alpha subunit p19
Il1rn	0.7	7.7	10.6	NM_031167	Interleukin 1 receptor antagonist
Cxcl3	0.7	2.1	2.9	NM_203320	Chemokine (C-X-C motif) ligand 3
C4b	0.7	2.9	4.2	NM_009780	Complement component 4B
Ccl5	0.7	2.4	3.5	NM_013653	Chemokine (C-C motif) ligand 5
Il10rb	0.6	1.3	2.1	NM_008349	Interleukin 10 receptor, beta
Crp	0.6	2.1	3.5	NM_007768	C-reactive protein, pentraxin-related
Ccl1	0.5	3.9	8.4	NM_011329	Chemokine (C-C motif) ligand 1
Ccr7	0.4	3.1	7.7	NM_007719	Chemokine (C-C motif) receptor 7
Il1r1	0.4	4.2	10.9	NM_008362	Interleukin 1 receptor, type I
Cxcl9	0.3	1.12	3.8	NM_008599	Chemokine (C-X-C motif) ligand 9
Ccl22	0.3	2.6	9.7	NM_009137	Chemokine (C-C motif) ligand 22
Tnfsf14	0.3	0.6	2.1	NM_019418	Tumor necrosis factor (ligand) superfamily, member 14

*The correlation coefficient between TLM and TCM fold change was $R2 = 0.52$ ($p < 0.001$).

Table 2.3. DON-induced down-regulation of inflammatory response genes in translatome (TLM) and transcriptome (TCM).

Symbol	Fold Change TLM/ TCM	TCM	TLM	Gene Bank	Gene Description
Tlr2	1.3	0.54	0.41	NM_011905	Toll-like receptor 2
Cd40	0.8	0.22	0.27	NM_011611	CD40 antigen
Tlr3	0.7	0.50	0.71	NM_126166	Toll-like receptor 3
Il18rap	0.7	0.44	0.66	NM_010553	Interleukin 18 receptor accessory protein
Il7	0.6	0.23	0.38	NM_008371	Interleukin 7
Il18	0.5	0.20	0.38	NM_008360	Interleukin 18
Ccl25	0.5	0.44	0.93	NM_009138	Chemokine (C-C motif) ligand 25
Cxcl10	0.4	0.01	0.02	NM_021274	Chemokine (C-X-C motif) ligand 10
Ltb	0.4	0.04	0.09	NM_008518	Lymphotoxin B
Cxcl11	0.1	0.19	1.30	NM_019494	Chemokine (C-X-C motif) ligand 11
Tlr2	1.3	0.54	0.41	NM_011905	Toll-like receptor 2

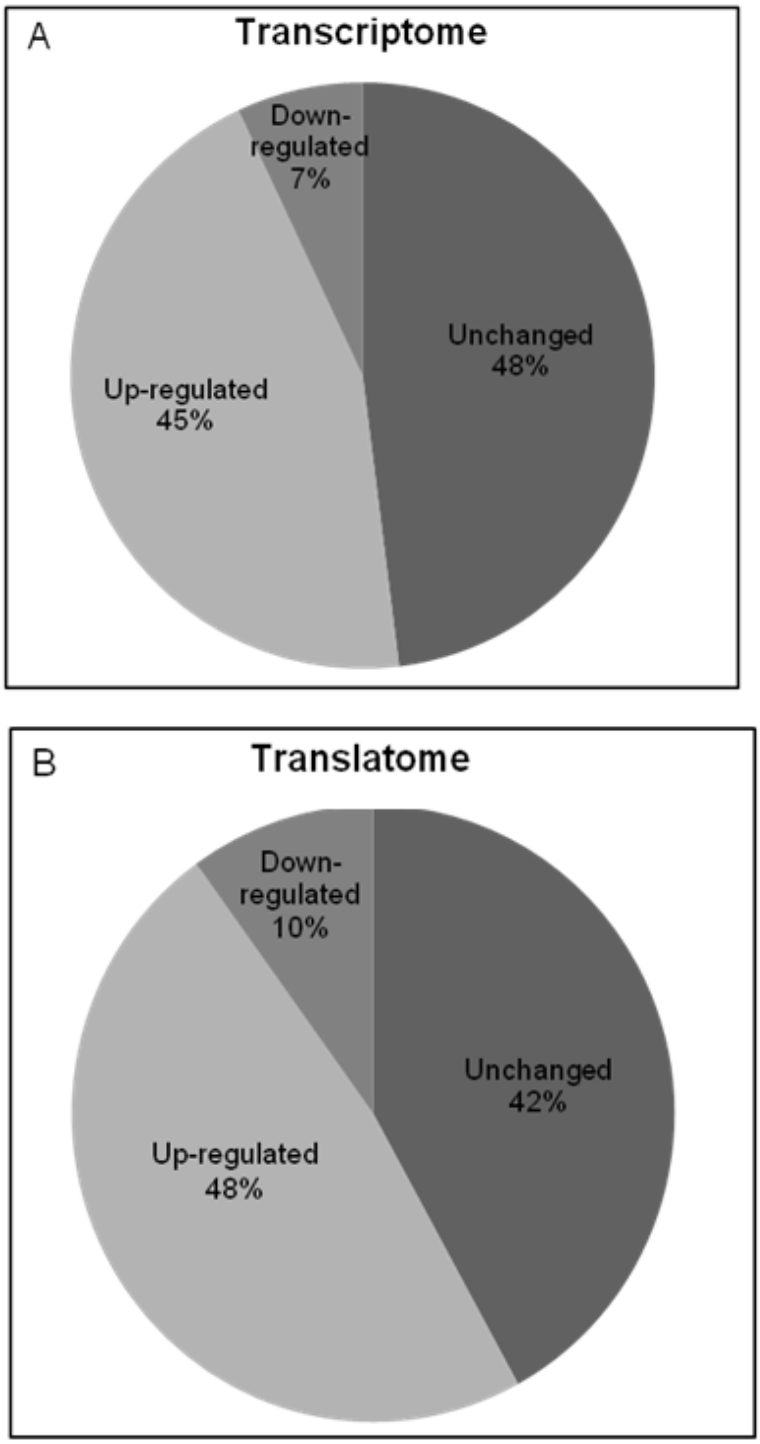

Figure 2.1. Relative numbers of array genes by DON in the transcriptome and translatome. Based on the PCR array data, the percentage of DON-induced up-, down- and unregulated genes were calculated and shown in (A) transcriptome and (B) translatome, respectively, using a two-fold change the threshold for up- and down-regulation.

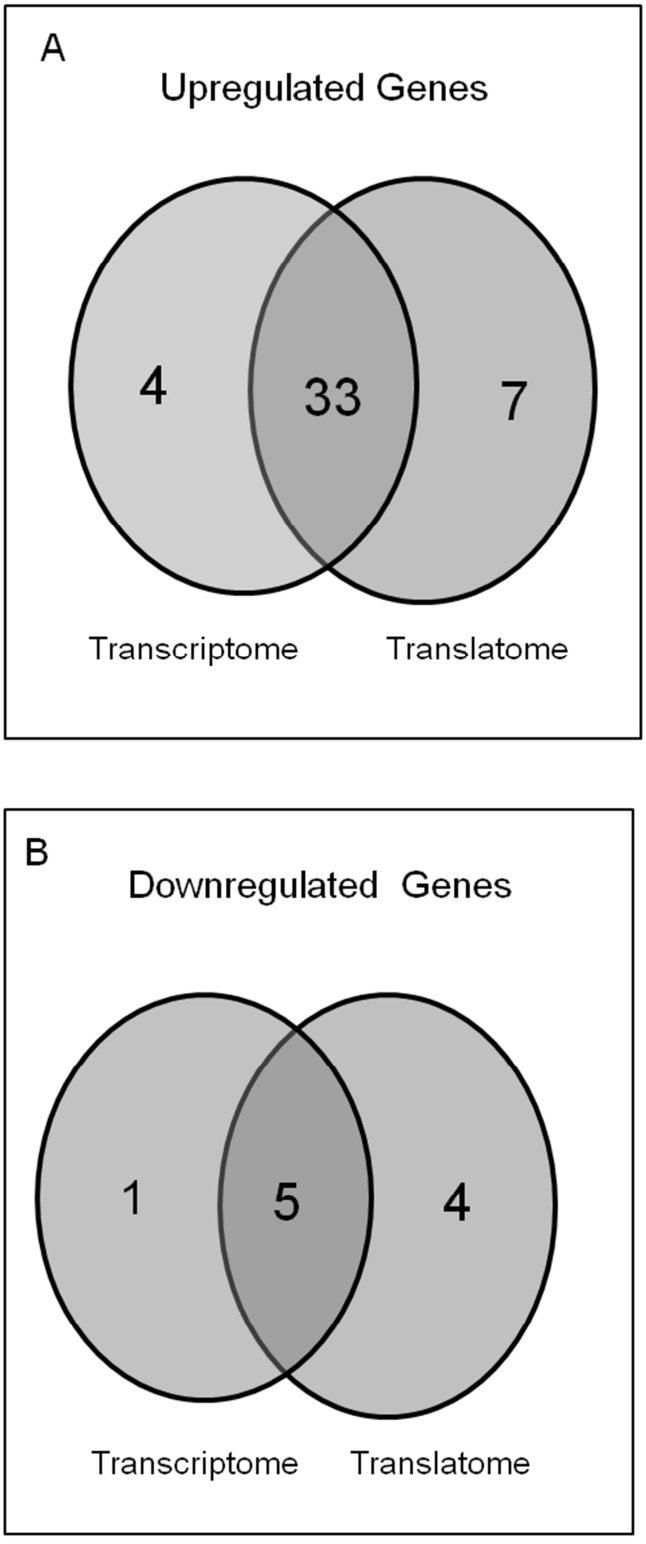

Figure 2.2. Comparison of DON overlapping genes in transcriptome and translatome. Numbers of genes up- and down-regulated by DON in (A) transcriptome and (B) translatome, respectively. Overlapping regions represent the common genes were shared by transcriptome and translatome.

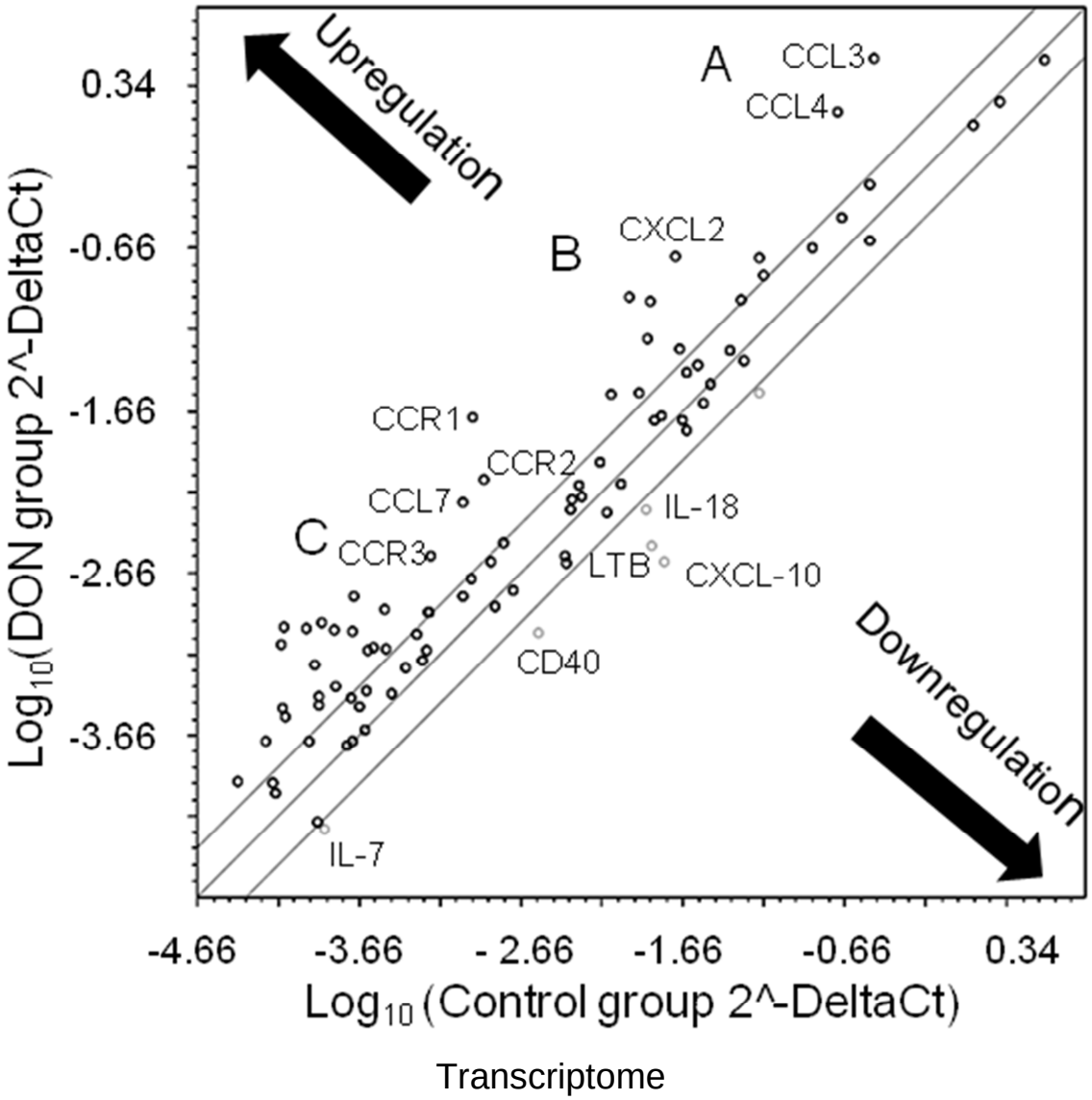

Figure 2.3. Scatter distribution of up- and down-regulated genes in the transcriptome and translatome. Transcriptome and translatome data (DON vs Control) were plotted using SAbiosciences web-based RT² Profiler PCR Array Data Analysis tool and exported. Each dot represents a single gene. The parallel line region indicates two-fold threshold and the black arrows demonstrate the up- or down-regulation of genes. Examples of commonly up-regulated (CCL3, CCL4, CXCL2, CCR1, CCR2, CCR3, and CCL7) and down-regulated genes (LTB, IL-7, IL-18, CXCL10, and CD40) are identified.

Figure 2.3 (cont'd)

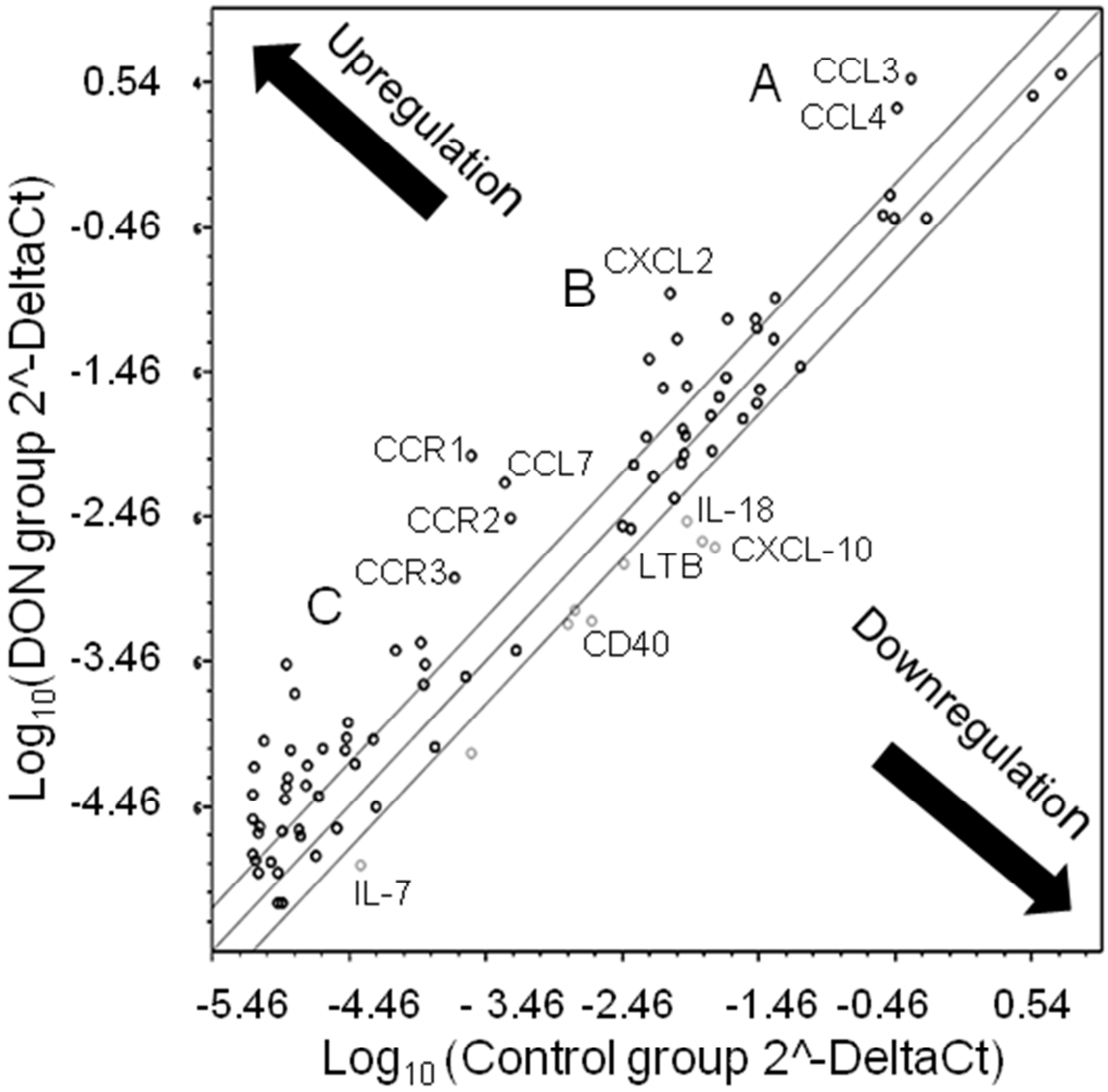

Translatome

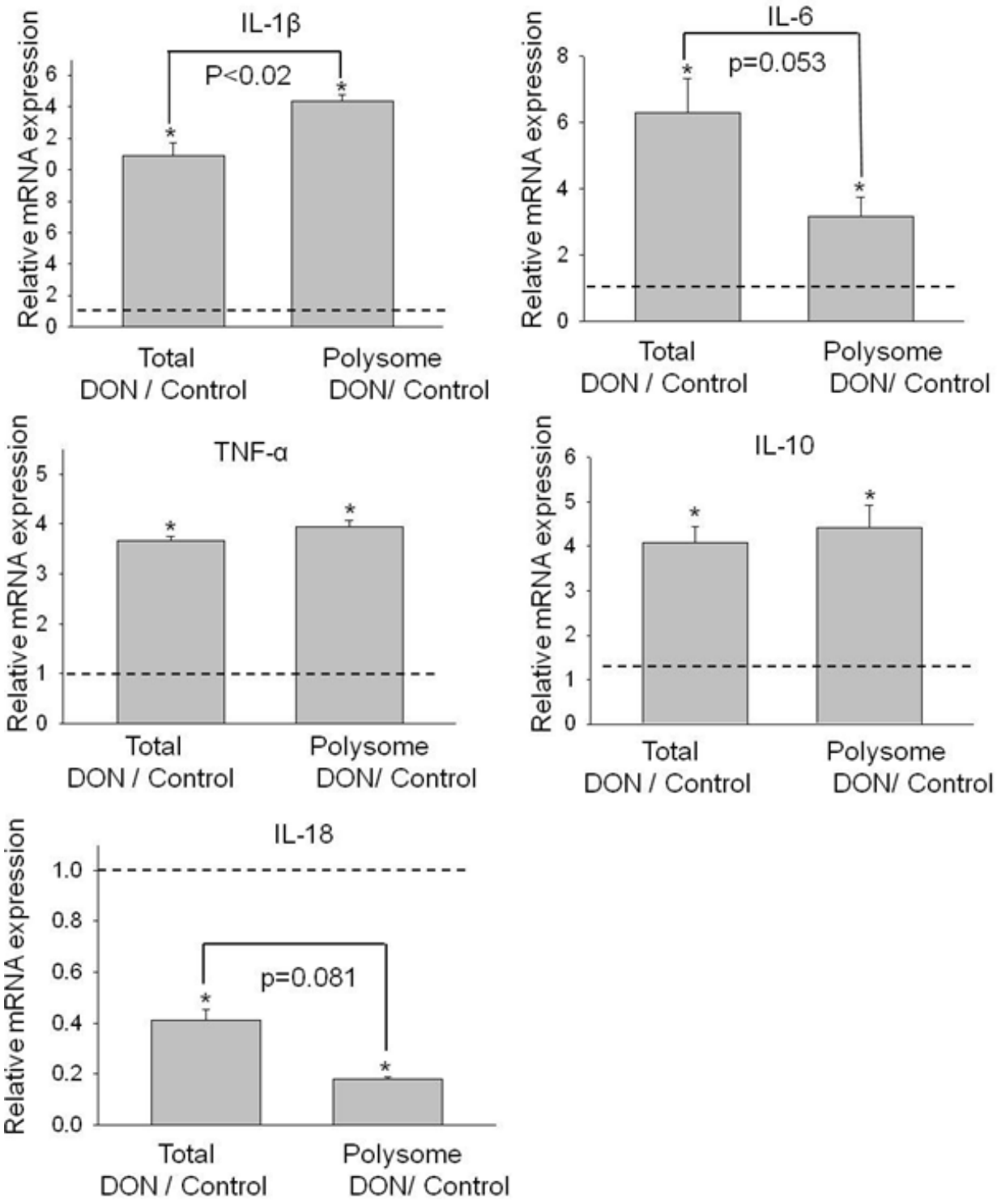

Figure 2.4. PCR verification of cytokine mRNA expression in the transcriptome and translatome. Three independent cell culture experiments were conducted and the transcriptome and translatome analyzed in duplicate were quantified by real-time PCR. The mRNA expression level of each gene was normalized to the GAPDH internal control. Data are mean ± SE of triplicate wells. The dotted line indicates the basal level of gene expression (one-fold) in total and polysome controls. Asterisk indicates induced significant increases in mRNA expression relative to respective controls ($p<0.05$).

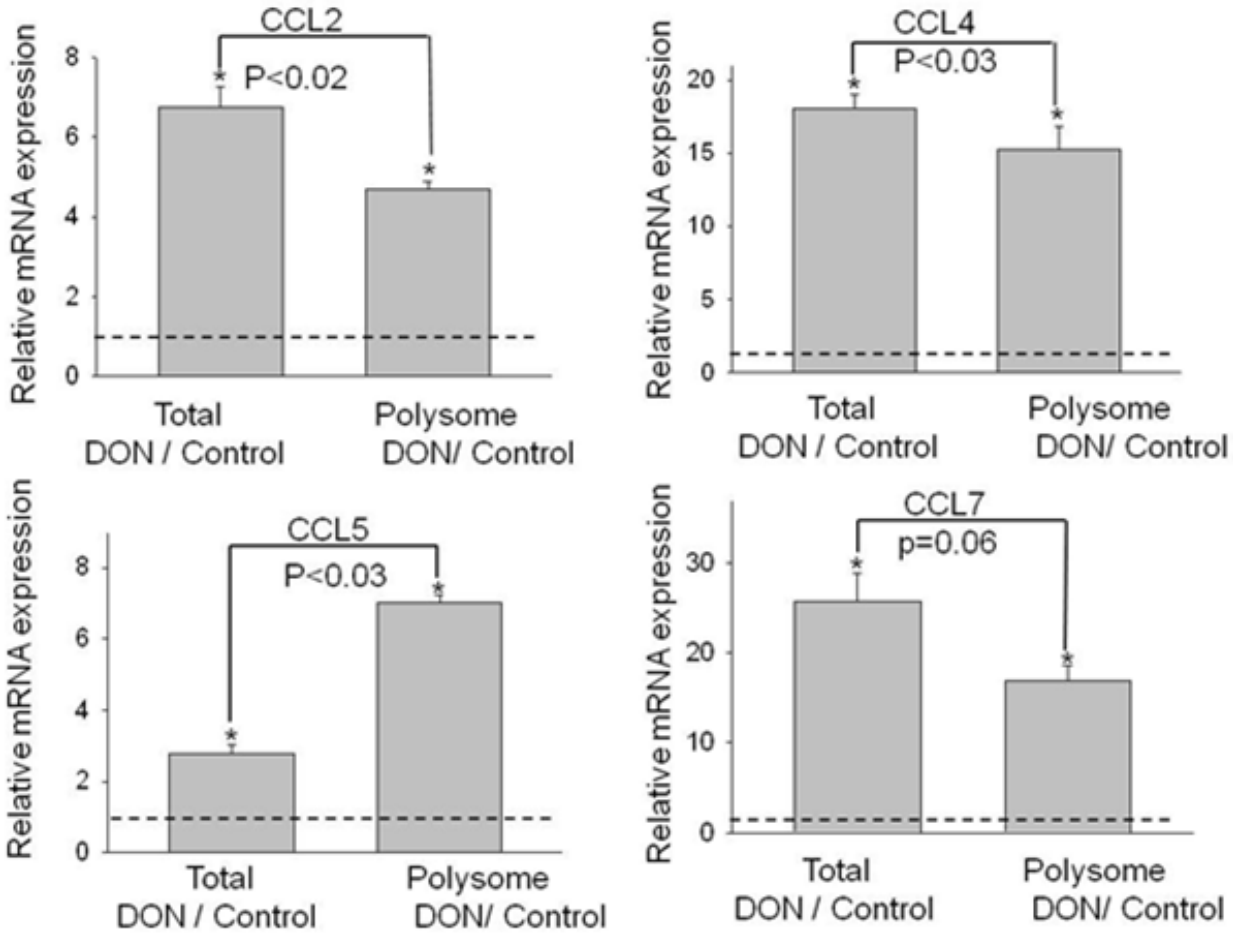

Figure. 2. 5. Real-time PCR verification of chemokines and chemokine receptors expression in transcriptome and translatome. Study was conducted and analyzed as described in Fig. 4 legend.

Figure 2.5 (cont'd)

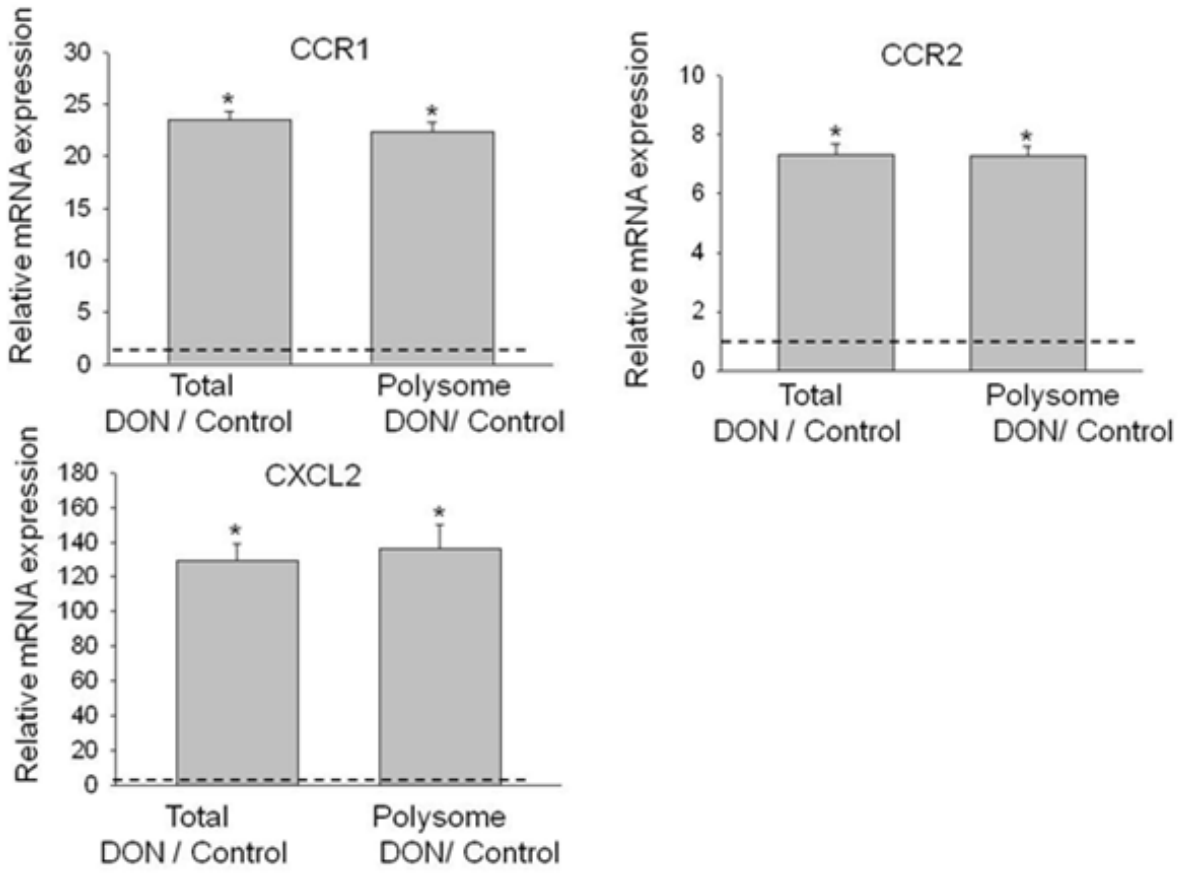

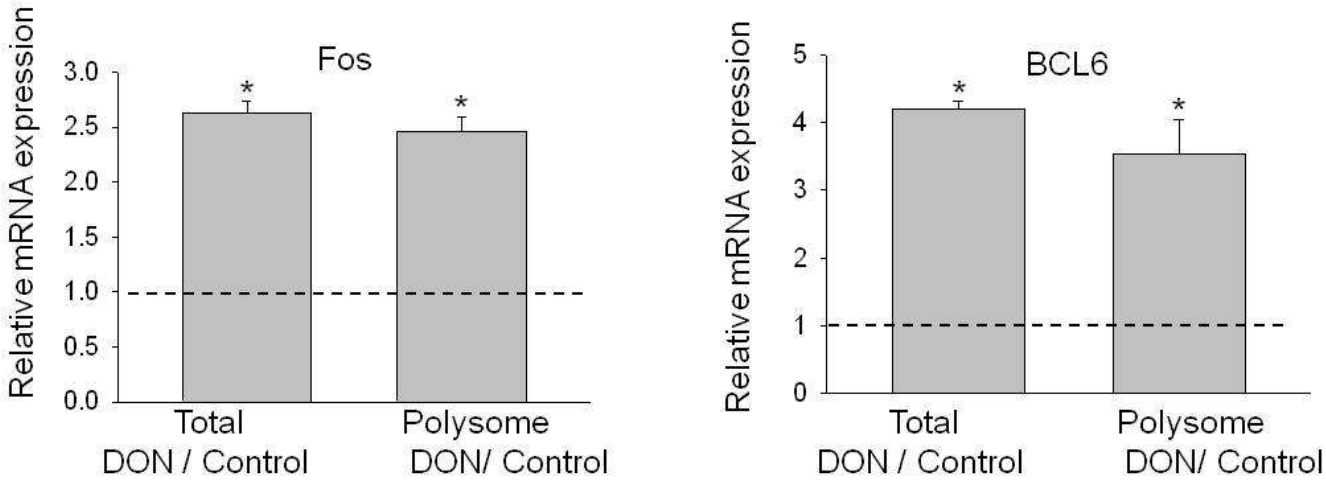

Figure 2. 6. PCR Verification of transcription factor mRNA expression in the transcriptome and translatome. Study was conducted and analyzed as described in Fig. 4 Legend.

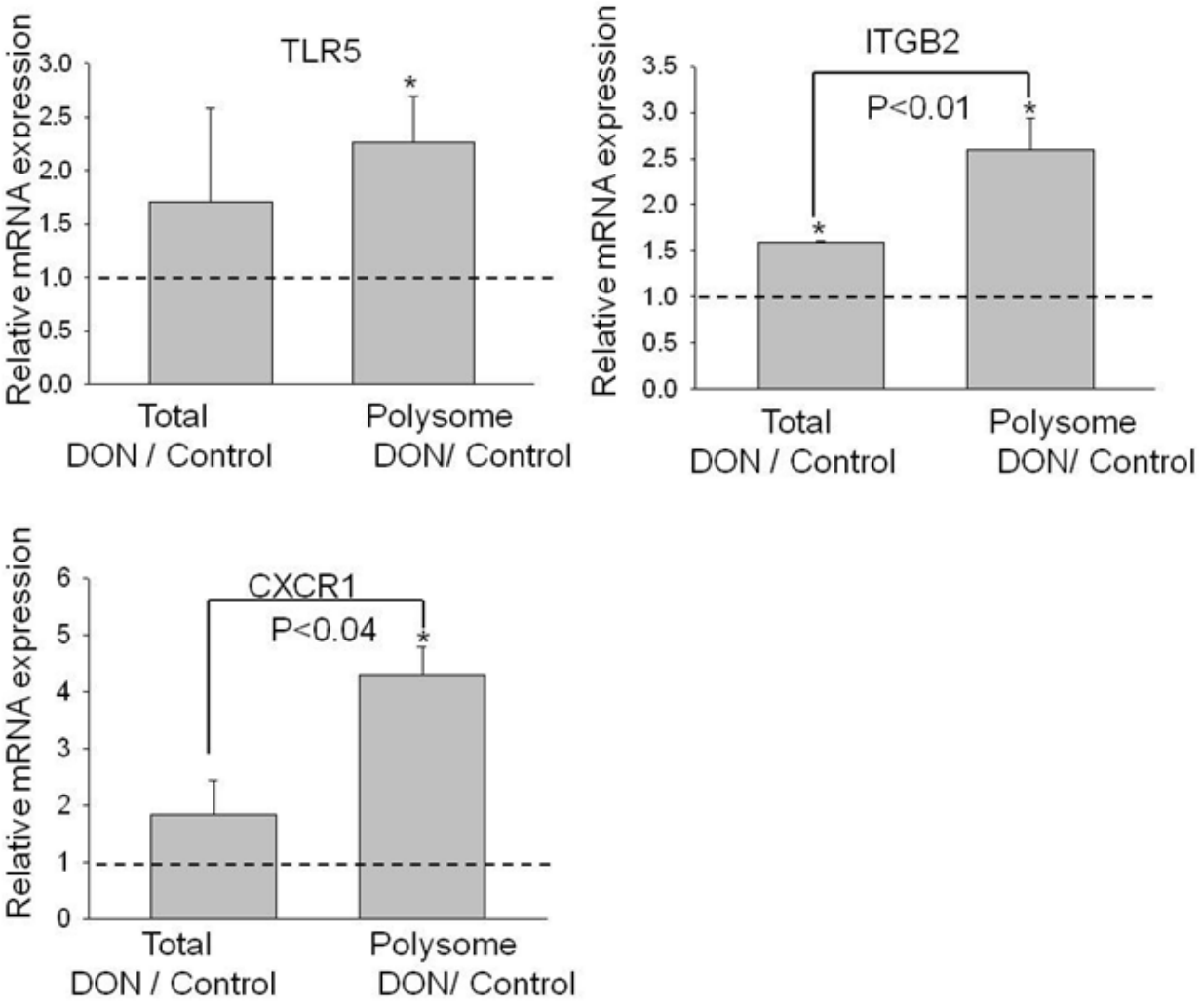

Figure 2.7. PCR verification of translatome-specific mRNA expression. Study was conducted and analyzed as described in Fig. 4 Legend.

per gene were 5.6 and 0.26 in the transcriptome, respectively, and 5.9 and 0.25 in the translatome, respectively. Ratios of translatome/transcriptome, for 73% modulated genes, were between 0.5-2.0 (Table 2.2, 2.3).

Real-time PCR of samples from three additional independent experiments was used to validate modulated expression of selected genes in the polysome and total cellular pools as determined by PCR array analysis. Upregulation of cytokine genes (IL-1β, IL-6, IL-10, IL-18, TNF-α) (Fig. 2.4), chemokine and chemokine receptor genes (CCL2, CCL4, CCL5, CCL7, CXCL2, CCR1, CCR2) (Fig. 2.5), and transcription factors (Fos, BCL6) (Fig. 2.6) were confirmed in both the transcriptome and translatome. For some genes (IL-1β, CCL2, CCL4, CCL5, CXCR1, ITGB2), significant differeneces in the translatome and transcriptome were observed. Down-regulation of IL-18 (Fig. 2.4) was again observed in both populations. Three genes (TLR5, CXCR1 and ITGB2) identified in the array to be selectively upregulated in translatome but not in transcriptome were also verified by real-time PCR (Fig. 2.7). Taken together, these data suggest that while upregulation of inflammation-related genes following DON treatment occurred primarily through selective transcription, moderate translational regulation was also evident.

DISCUSSION

While DON-induced gene expression has been previously investigated relative to the total cellular mRNA pool, this is the first attempt to identify and measure the polysomal mRNAs to profile genes being actively translated following toxin exposure. Given DON's capacity to target innate immune function and induce inflammation-associated genes, we employed a cloned macrophage model and a focused PCR array. Although previous studies indicate that 250 ng/ml of DON partially inhibits translation in RAW 264.7 cells(Zhou *et al.*, 2003b), this did not appear to significantly skew the profile of genes being translated. Comparison between the transcriptome and translatome indicated the most genes in the two pools showed similar changes by DON, suggesting the translation to a large extent closely reflected the total cellular pool of mRNAs. Nevertheless, a small number of genes appear to be regulated at the level of translation.

The profile of genes (cytokine, chemokine, receptor, transcription factor and inflammation) in the translatome and transcriptome provides additional new insight into the immunotoxicological mechanisms of DON. DON-induced up-regulation of IL-1β, IL-6 and TNF-α as observed here is highly consistent with previous findings (Wong *et al.*, 1998; Zhou *et al.*, 1998; Wong *et al.*, 2001). IL-6 can act as both a pro-inflammatory and anti-inflammatory cytokine and it also stimulates the synthesis of interleukin 1 receptor antagonist (IL-1rn) and IL-10 (Borish and Steinke, 2003; Petersen and Pedersen, 2005), the up-regulation of which were also found in this study. IL-1rn can non-functionally bind to the same receptor as IL-1 and IL-10 inhibits production of IL-1β, IL-6, IL-12, CXCL8 and TNF-α in monocyte/macrophage (Commins *et al.*, 2010). Taken together, the DON-induced up-regulation of IL receptor (IL-1r1) and IL-1, and mutual

induction of TNF and IL-1 may be negatively regulated by IL-1rn, IL-6 and IL-10. In total, these responses are consistent with tempering an inflammatory response to an appropriate level that would minimize physiological damage to tissue.

The observation that the CC chemokine family was markedly upregulated upon DON exposure is important because this family of small molecules directs the receptor-mediated trafficking of leukocytes. The CC chemokines control both recruitment of effector leukocytes to target sites of infection and the migration of cells during normal processes of tissue maintenance or development (Borish and Steinke, 2003; Moser *et al.*, 2004). CCL2 and CCL7, which were previously reported to be upregulated in spleens of DON-exposed mice (Kinser *et al.*, 2004; Kinser *et al.*, 2005), are potent chemoattractants that direct monocytes/macrophages to inflammatory sites by regulating the expression of adhesion molecules and cytokines in these cells(Jiang *et al.*, 1992; Maddaluno *et al.*, 2011). Our data, for the first time, also show that DON upregulated CCL3 and CCL4, both of which have potent chemotactic activities for monocytes and T cells (Hasegawa *et al.*, 1999). It is notable that receptors for these chemokines were also up-regulated in the transcriptome and translatome (CCR1, CCR2 and CXCR2). Elevated expression of chemokines and their receptors strongly suggest that DON exposure modulates leukocyte chemotaxis and might contribute to an aberrant systemic inflammatory response in exposed animals.

Two transcription factors, Fos and BCL6, were also observed here to be up-regulated by DON in the transcriptome and translatome. Fos heterodimerizes with other subunits to form activator protein-1 (AP-1) transcriptional factor complex and regulates gene expression in response to various stimuli, including cytokines, stress, and

bacterial and viral infections (Hess *et al.*, 2004). Increased AP-1 binding to the promoter region has been observed in DON-exposed RAW 264.7 cells(Wong *et al.*, 2002). Similarly, binding activity of AP-1 is elevated upon DON treatment in mouse spleen, which precedes the up-regulation of inflammatory cytokine expression (Zhou *et al.*, 2003a; Kinser *et al.*, 2004). BCL6 first identified in the present study as being upregulated by DON, is a zinc-finger transcription factor that represses transcription in a sequence-specific manner and modulates inflammation (Barish *et al.*, 2010) by cistronic antagonism of NF-kB, a transcription factor that is also activated by DON (Zhou *et al.*, 2003a; Gray and Pestka, 2007). BCL6 was also reported to repress transcription of IL-18 (Takeda *et al.*, 2003; Yu *et al.*, 2005), the down-regulation of which was observed here in the PCR array and confirmed by real-time PCR. BCL6 also regulates the gene transcription of CCL2 and CCL7, and also CCL1, CCL8, CCL11 and CCL12, known target genes of BCL6 in macrophage that have been found to be negatively regulated by BCL6 which attenuates inflammation (Toney *et al.*, 2000; Seto *et al.*, 2011), suggesting BCL6 might be an important negative coordinator of DON-induced immunostimulatory events.

Other genes with significant immunological functions were also identified in this study. DON induced the upregulation of C4b and C3ar1, components of the complement system, which are important players in host defense and enhancement of phagocytosis (Ogundele, 2001). C3ar1, is also reported to be upregulated by DON (Chung *et al.*, 2003b). C-reactive protein (Crp)(Carroll, 2004), an acute phase protein that rises in response to inflammation and activates the complement system, was

upregulated by DON. Overall upregulation of C4b, C3ar1 and Crp indicate involvement of the complement system in DON-induced inflammatory response.

A critical question remains as to how DON might mediate translational regulation of the small subset of genes model here. In the global context, translation is regulated at multiple levels, some of which can be impacted by DON. Mammalian target of rapamycin complex 1 (mTORC1), activated by PI3K via Akt or directly by ERK1/2, promotes phosphorylation/activation of p70 S6 kinases (p70S6Ks) that phosphorylate the small ribosomal subunit protein S6 (Rps6), a process indicated to promote translation (Ma and Blenis, 2009). PI3K-Akt pathway also increase the global initiation rate of translation by promoting phosphorylation of 4E-BP1 and subsequent release of eIF4e to bind to the 7-methylGTP cap of mRNAs and increase the rate of initiation (Ma and Blenis, 2009). Alternatively, p90 ribosomal S6 kinases (p90RSKs), activated by ERK1/2, also phosphorylate eIF4b and eEF2k (Ma and Blenis, 2009). On the contrary, PKR, PERK, GCN2 and HRI suppress global translation by coordinating the phosphorylation of eIF2α. DON is known to concurrently activate the translation-promoting pathway members Akt, ERK1/2 and p90RSK, and the translation-inhibitory PKR (Zhou *et al.*, 2003a; Zhou *et al.*, 2003b). Fine-tuning of the balance between these counteracting pathways might account in part for the concurrent selective translation and translation inhibition observed in this study.

Besides global regulation, translation of specific messages could be modulated on the individual level. For example, translation of GCN4 is activated in response to amino acid deprivation—a condition that generally represses translation—by a mechanism that involves short upstream open reading frames (uORFs) (Hinnebusch,

1997). In addition, translation of specific messages can also be controlled by specific RNA-binding proteins (RBPs) (Gebauer and Hentze, 2004), many of which interact with functionally related groups of mRNAs, illustrating the elaborate regulation on level of translation. microRNAs can also precisely regulate specific gene expression by imperfectly binding to the 3'-UTR of target mRNA. The stalled translation complex could be degraded or relocalized to stress granule for future use (Leung and Sharp, 2010). At the concentrations used here DON can modulate the profile of miRNAs in macrophage at 3 and 6 h, thus suggesting a possible regulation of inflammatory response genes (He and Pestka, 2010). In our study, we specifically examined the correlation between transcriptome and translatome for genes related to innate immunity and identified several genes that are specifically regulated by DON. But further investigation will be needed to elucidate the regulatory elements.

Taken together, DON potently induced translation of various cytokine, chemokine, receptor and transcription factor genes associated with inflammation. While most of this upregulation corresponding to increased transcription, some genes also appeared to be additionally regulated at the translational level. This study deliberately employed focused PCR array with a relatively limited number of genes (84) associated with the inflammatory response and autoimmunity. It will be of interest in the future to compare translatome and transcriptome profiles at a genome-wide level to determine if expression of other genes are regulated similarly to inflammation associated genes. A further limitation here was the use of single time point, which might skew understanding of the expression profile of inflammatory genes. It is thus not possible to discriminate inflammatory genes responding primarily from DON exposure from those affected in

secondary fashion by the upregulation of potent modulatory cytokines and chemokines. Thus, future studies should employ multiple time points. Finally it will be important to confirm that polysome-associated mRNAs are indeed translated to complete proteins using immunoblot or proteomic methods.

CHAPTER 3

Mechanisms of Ribosomal RNA (rRNA) Cleavage by the Trichothecene Deoxynivalenol

This chapter has been published in Toxicological Sciences (2012).

He, K., Zhou, H.R., Pestka, J.J., 2012. Targets and Intracellular Signaling Mechanisms for Deoxynivalenol-Induced Ribosomal RNA Cleavage. Toxicol Sci.2012, 127(2):382-90

ABSTRACT

The mechanisms by which the trichothecene mycotoxin deoxynivalenol (DON), induces ribosomal RNA (rRNA) cleavage were investigated in the RAW 264.7 murine macrophage model. Capillary electrophoresis indicated that DON at concentrations as low as 200 ng/ml evoked rRNA cleavage after 6 h and that 1000 ng/ml caused cleavage within 2 h. Northern blot analysis revealed that DON exposure induced six rRNA cleavage fragments from 28S rRNA and five fragments from 18S rRNA. Neither transfection of the RNase L activator 2′-5′-oligoadenylate (2-5A) into RAW 264.7 cells, nor incubation of 2-5A with recombinant RNase L and purified ribosome under cell-free conditions caused rRNA cleavage, suggesting that increased expression of this enzyme was not solely responsible for rRNA cleavage. When selective kinase inhibitors were used to identify potential upstream signals, inhibition of RNA activated protein kinase (PKR) (C-16), hematopoietic cell kinase (Hck) (PP1) and p38 suppressed rRNA cleavage, while inhibition of JNK and ERK had no effect. Additionally, the p53 inhibitors pifithrin-α and pifithrin-μ as well as the pan caspase inhibitor Z-VAD-FMK suppressed rRNA fragmentation. DON activated caspase 3/8/9, indicating potential involvement of both extrinsic and intrinsic apoptotic pathways. Concurrent apoptosis was confirmed by acridine orange/ethidium bromide (AO/EB) staining and flow cytometry. Taken together, DON-induced rRNA cleavage is likely to be closely linked to apoptosis activation and appears to involve the sequential activation of PKR/Hck→p38→p53→caspase 8/9→caspase 3. Satratoxin G (SG), anisomycin and ricin also induced rRNA cleavage profiles identical to DON, suggesting that ribotoxins share a conserved rRNA cleavage mechanism.

INTRODUCTION

The trichothecenes, a group of sesquiterpenoid mycotoxins produced by *Fusarium* that contaminate wheat, barley and corn globally (Pestka, 2010a), are problematic because of their resistance to degradation during processing and their potential to adversely affect human and animal health. Among the over 200 trichothecenes discovered to date, deoxynivalenol (DON) is most frequently encountered in food and human exposure to this toxin has been well-documented in biomarker studies (Amuzie *et al.*, 2008; Turner *et al.*, 2008a; Amuzie and Pestka, 2010). One of the principal targets of DON is the innate immune system, with low doses causing immunostimulatory effects, and high doses causing immunosuppression (Pestka, 2010b).

At the mechanistic level, DON has been shown in vivo and in vitro to activate mitogen-activated protein kinases (MAPKs), including p38, JNK and ERK (Shifrin and Anderson, 1999; Zhou *et al.*, 2003a), which mediate upregulation of proinflammatory cytokine and chemokine expression as well as apoptosis (Moon and Pestka, 2002; Chung *et al.*, 2003b; Islam *et al.*, 2006). Notably, DON concentration-dependently induces competing survival (ERK/AKT/p90Rsk/Bad) and apoptotic (p38/p53/Bax/mitochondria/caspase-3) pathways in the macrophage (Zhou *et al.*, 2005a). Accordingly, MAPK activation is critical to both stimulation and suppression of the innate immune system.

Two upstream signal transducers that have been identified to be upstream of DON-induced MAPK activation are the double-stranded RNA- (dsRNA)-activated protein kinase (PKR) (Zhou *et al.*, 2003b) and hematopoietic cell kinase (Hck) (Zhou *et*

al., 2005b). PKR is a widely-distributed constitutively-expressed serine/threonine protein kinase that can be activated by dsRNA, interferon, proinflammatory stimuli, cytokines and oxidative stress (Williams, 2001; Garcia *et al.*, 2006). PKR also activates p53, p38, JNK, NF-κB, signal transducer and activator of transcription (STAT) and interferon regulatory factor-1 (IRF-1) (Williams, 1999). Hck, a member of Src kinase family, is expressed specifically in myelomonocytic cell lineages and transduces extracellular signals that regulate proliferation, differentiation and migration (Ernst *et al.*, 2002; Tsygankov, 2003). Both PKR and Hck are activated prior to the MAPKs and their respective inhibitors suppress downstream MAPK activation (Zhou *et al.*, 2003b; Zhou *et al.*, 2005b). Although crosstalk between PKR and Hck is not clearly understood, PKR is required for Hck interaction with the ribosome in the human monocyte U937 cell line (Bae *et al.*, 2010).

A further prominent consequence of DON exposure in macrophages is the induction of rRNA cleavage, which has been suggested to result from upregulated RNase expression, most notably RNase L (Li and Pestka, 2008). Oligonucleotide extension experiments revealed that DON, and another trichothecene, T-2 toxin, as well as ricin induce rRNA cleavage in the peptidyltransferase center and at at least two other cleavage sites (A3560 and A4045) on 28S rRNA (Li and Pestka, 2008). Because of limitations imposed by RNA hairpin structures on this oligonucleotide extension technique, the full extent of rRNA cleavage has not yet been fully elucidated. Ribosome inactivating proteins (RIPs), such as ricin, are well-known to cleave rRNA via a highly specific mechanism that involves N-glycosidase-mediated adenine depurination at highly conserved sarcin/ricin (S/R) loop (Endo and Tsurugi, 1986; Hartley and Lord,

2004b). However, the trichothecenes are low molecular weight chemicals and are devoid of inherent enzyme activities(Li and Pestka, 2008). To date, induction of rRNA cleavage by chemicals or viruses have been linked to either RNase L-dependent or apoptosis-associated mechanisms (Banerjee *et al.*, 2000; Naito *et al.*, 2009). In this study, we employed the RAW 264.7 murine macrophage cell model to determine the relative roles of RNase L and apoptosis in DON-induced rRNA cleavage. The results demonstrate that DON promotes cleavage of 18S RNA and 28S rRNA into at least five and six fragments, respectively. PKR, Hck, p38, p53 and caspases mediated DON-induced rRNA cleavage, whereas RNase L did not appear to be the primary driver of the response. Three other translational inhibitors, satratoxin G, anisomycin and ricin evoked comparable rRNA cleavage to DON, suggesting a common mechanism might exist for other ribotoxins.

MATERIALS AND METHODS

Chemicals. DON, anisomycin, PKR inhibitor C-16 and Hck inhibitor PP1 were purchased from Sigma-Aldrich (St. Louis, MO). Ricin was obtained from Vector Labs Inc. (Burlingame, CA). Satratoxin G (SG) was purified as described previously(Islam *et al.*, 2009). The p38 inhibitor SB 203580, JNK inhibitor SP600125, ERK inhibitor PD 98059, RNase L Activator, p53 inhibitor pifithrin-α and pifithrin-μ were purchased from EMD Chemicals Inc. (Gibbstown, NJ). Pan caspase inhibitor Z-VAD-FMK was supplied by BD Pharmingen (San Diego, CA). [γ-^{32}P]ATP was purchased from PerkinElmer (Shelton, CT). All other chemicals and media components were obtained from Sigma-Aldrich, except where noted.

Macrophage cell culture. RAW 264.7 cell (ATCC, Rockville, MD), a mouse macrophage cell line, was cultured in Dulbecco's modified Eagle's medium (DMEM) supplemented with 10% (v/v) heat-inactivated fetal bovine serum (Atlanta Biologicals, Lawrenceville, GA), streptomycin (100 μg/ml) and penicillin (100 U/ml) at 37^{o}C in a humidified incubator with 5% CO_2. Macrophage cell number and viability were assessed by trypan blue dye exclusion using a hematocytometer. Prior to exposure of toxins (DON, SG, anisomycin and ricin) or inhibitors, cells (2.5 x 10^{6}) were seeded and cultured in 100 mm tissue culture plates for 24 h to achieve approximately 80% confluency.

RNA purification and quality analysis*.* RNAs were extracted by TRIZOL (Invitrogen, Carlsbad, CA) following the manufacturer's protocol and their concentrations were measured using a Nanodrop reader (Thermo Fisher, Wilmington,

DE). Integrity of RNA (300 ng/µl) was assessed by capillary electrophoresis using an Agilent 2100 Bioanalyzer with a Nano Chip (Agilent, Santa Clara, CA) according to manufacturer's instructions.

Northern blot analysis. Northern blot analysis was performed by modifying a previously described procedure (Li and Pestka, 2008). Briefly, probes (Table 1) were labeled with γ-^{32}P by DNA 5' end-labeling system (Promega, Madison, WI) and purified by Micro-Bio-Spin6 chromatography column (Bio-Rad, Hercules, CA). Label incorporation was measured using a TopCount NXT (PerkinElmer, Shelton, CT). Total RNA (10 µg/lane) was separated on a 1.2% (w/v) formaldehyde denaturing agarose gel and transferred to a Biodyne membrane (Pall Gelman Laboratory, Ann Arbor, MI). After UV crosslinking (Stratagene, Cedar Creek, TX), membranes containing immobilized RNA were prehybridized for 1 h at 68 °C and then incubated with [γ-^{32}P]-labeled probes **(**1x10^{6} CPM/ml) in Quickhyb solution (Stratagene, Cedar Creek, TX) containing 200 µg /ml of herring sperm DNA at 68℃ for 2 h. Blots were washed twice with 2x SSC containing 0.1% (w/v) SDS at room temperature and once for 15 min with 0.1 x SSC containing 0.1% (w/v) SDS at 50°C. The membranes were assembled with the Hyblot autoradiography film (Denville, Metuchen, NJ) into an X-ray exposure cassette and the film was developed after 24 h.

Ribosome Preparation*.* Ribosomes were purified as previously described with modifications (Naito *et al.*, 2009). RAW 264.7 cells (1 x 10^{7}) were washed twice with ice-cold phosphate-buffered saline (PBS) and lysed in 1 ml polysome extraction buffer (0.3 mM NaCl, 15 mM Tris–HCl, pH 7.4, 15 mM $MgCl_2$, DEPC-treated water, protease inhibitor). Homogenates were centrifuged for 15 min at 16,000 x g and supernatants

Table 3.1. 18S and 28S rRNA probes for Northern blot analysis of rRNA cleavage

Probe Sequences	Positions in 18s and 28s rRNA
28s probe 1:ACCCGGCGTTCGGTTCAT	1,690-1,707
28s probe 2:AAAGGACGGGGGGTCTCCCCGG	2,732–2,753
28s probe 3:GGGTTGGACCCGCCGCCCCGGAG	2,877–2,899
28s probe 4:GCGGGCCTTCGCGATGCTTTGTT-3	3,304–3,326
28s probe 5:ACCCAGAAGCAGGTCGTCTACGAATGGTTTAGCGCCAG	4,605–4,642
18s probe 1:GCACCAGACTTGCCCTCC	598–615
18s probe 2: GAATAAC GCCGCCGCATC-3	1,100–1,117
18s probe 3: CGGA CATCTAAGGG CATCACAG	1,493–1,514

NCBI access numbers for 28S and 18S rRNA sequences are NR_003279 and NR_003278, respectively.

(0.9 ml) were layered onto a cushion of 9 ml 1 M sucrose with protease inhibitor, 15 mM Tris–HCl, pH 7.4, 15 mM $MgCl_2$, 200,000 x g for 3 h at 4℃. The resultant ribosomal pellets were resuspended in 200 µl ribosome resuspension buffer (0.25 M sucrose, 25 mM Tris–HCl, pH 7.4, 10 mM $MgCl_2$, and 100 mM KCl, 1 mM DTT, in DEPC-treated water). The ribosome solutions were centrifuged for 10 min at 16,000 x g to remove insoluble materials and stored in aliquots at -80℃.

RNase L studies. Recombinant purified human RNase L (1.37 mg/ml), fluorescence resonance energy transfer (FRET) assay probe (200 µM) and 2-5A (1 mM) were prepared and employed as described previously with some modifications (Thakur *et al.*, 2005). For in vitro activity assays, RNase L (14 ng/µl) was preincubated in 5 µM 2-5A in 25 µl cleavage buffer (25 mM Tris-HCl, pH 7.4, 1 mM KCl, 10 mM $MgCl_2$, 0.05 mM ATP, pH 7.4, and 7 mM mercaptoethanol) on ice for 30 min. FRET probe (0.5 µM), purified rRNA (1 µg) or purified ribosome containing 1 µg rRNA in 25µl cleavage buffer were added and incubated for 90 min (22 ℃), 5 min (30 ℃), and 120 min (30 ℃), respectively. Fluorescence intensity of FRET probe incubation mixture was determined by Bio-Tek Synergy HT multi-mode microplate reader using 485 nm and 535 nm as excitation and emission wavelengths, respectively. rRNA and ribosome reaction mixtures were diluted 10-fold with 100 mM Tris–HCl (pH 8.0), 100 mM NaCl, 1 mM EDTA, and RNA was extracted with phenol. The aqueous phase was reextracted and cleavage products were measured by capillary electrophoresis as described above.

Transfection method. 2-5A was transfected into RAW 264.7 cells using Lipofectamine 2000 (Invitrogen, Carlsbad, CA) according to the manufacturer's protocol. Briefly, RAW 264.7 cells (2 ml/well) were seeded in 6-well plates and cultured for 24 h

to achieve about 80% confluency. For each well, dilute 2-5A in 250 µl of Dulbecco's modified Eagle's medium (DMEM) without serum to 50 µM. Dilute 10 µl Lipofectamine 2000 in 250 µl of DMEM, mix gently and incubate for 5 minutes at room temperature. After the 5 minute incubation, combine the diluted 2-5A with the diluted Lipofectamine 2000, mix gently and incubate for 20 minutes at room temperature. Add the 500 µl of 2-5A-Lipofectamine 2000 complexes to each well and the transfected RAW 264.7 cells were cultured at 37℃ in a CO_2 incubator for 6 h. Then RNA was purified and analyzed by capillary electrophoresis as described above.

Immunoblotting. Western analyses were conducted using primary antibodies specific for murine forms of total/cleaved caspase-9 (Catalog No. 9504), cleaved caspase 3 (Asp 175), total caspase 8 (Catalog No. 4927) and cleaved caspase 8 (Asp387) (Cell Signaling, Beverly, MA). Mouse β-actin antibody (Sigma) was also used to verify equal loading. Cells were washed twice with ice-cold phosphate-buffered saline (PBS), lysed in boiling lysis buffer (1% [w/v] SDS, 1 mM sodium ortho-vanadate and 10 mM Tris, pH 7.4), boiled for 5 min and sonicated briefly, the resultant lysate centrifuged at 12,000 × **g** for 10 min at 4℃ and protein concentration measured with a BCA Protein Assay Kit (Fisher, Pittsburgh, PA). Total cellular proteins (40 µg) were separated on BioRad precast 4-20% polyacrylamide gels (BioRad, Hercules, CA) and transferred to a polyvinylidene difluoride (PVDF) membrane (Amersham, Arlington Heights, IL). After incubating with blocking buffer (Li-Cor, Lincoln, NE) for 1 h at 25 ℃, membranes were incubated with murine and/or rabbit primary antibodies (1:1000 dilution in Li-Cor blocking buffer) to immobilized proteins of interest overnight at 4℃. Blots were washed three times of 10 min with Tris-Buffered Saline and Tween 20 (TBST) (50 mM Tris-HCl,

150 mM NaCl, 0.1% Tween 20, pH 7.5), and then incubated with secondary IRDye 680 goat anti-rabbit and/or IRDye 800CW goat anti-mouse IgG antibodies (Li-Cor) (1:2000 dilution in Li-Cor blocking buffer) for 1 h at 25℃. After washing three times, infrared fluorescence from these two antibody conjugates were simultaneously measured using a Li-Cor Odyssey Infrared Imaging System (Lincoln, Nebraska).

Apoptosis measurement by acridine orange/ethidium bromide (AO/EB) staining. AO/EB staining was performed using a previously described procedure (Muppidi *et al.*, 2004). Slides were cleaned and sterilized by UV light, placed into 100-mm tissue culture plates and cultured with RAW 264.7 cells (2.5×10^6) for 24 h to achieve approximately 80% confluency. RAW 264.7 cells were treated with DON (1000 ng/ml) for 6 h and the slides were stained for 2 min with 100 µg/ml acridine orange and 100 µg/ml ethidium bromide in PBS. The slides were washed twice with cold PBS, then covered with coverslip and examined at 400 x under Nikon fluorescence microscope equipped with a wide-band FITC filter. Cells (≥200) were classified based on their nuclear morphology (bright chromatin, highly condensed or fragmented nuclei) in to four categories: viable normal (VN), viable apoptotic (VA), nonviable apoptotic (NVA), nonviable necrotic (NVN). The apoptotic index was calculated as follows: (VA+NVA) / (VN+VA+NVN+NVA) x100.

Apoptosis measurement by flow cytometry. RAW 264.7 cells were treated with vehicle PBS or DON (1000ng/ ml) for 6h. Total DON-treated cells and adherent DON-treated cells were collected separately. After washing twice with cold PBS, Annexin staining was performed according to the manufacturer's protocol (BD bioscience). Briefly, cells were resuspended to 1x binding buffer at a concentration of

$2.5x10^6$ cells/ml, and 100 µl of the cell suspension was transferred to FACS tubes. Cells were incubated with 5 µl of Annexin V and PI for 15 min at room temperature in dark. Finally, samples were resuspended to 400ul volume with binding buffer, acquired on the Accuri C6 (BD Accuri Cytometers, Ann Arbor, MI) and analyzed using FlowJo software (Tree Star, Ashland, OR). Live Raw 264.7 cells were gated using FSC vs SSC.

Statistics. Data were analyzed by t-test using Sigma Stat 3.11 (Jandel Scientific, San Rafael, CA). Data sets were considered significantly different when $p<0.05$.

RESULTS

DON induces rRNA cleavage

The capacity of DON to induce rRNA cleavage in RAW 264.7 macrophages was assessed by denaturing gel electrophoresis (Fig. 3.1A) and capillary electrophoresis (Fig. 3.1B, C). Distinct 18S, 28S rRNA bands were evident in both control and DON-treated RAW 264.7 cells, whereas at least 5 additional rRNA fragment bands were detected in DON-treated cells (Fig. 3.1C). Based on its high resolution and reproducibility as compared to conventional electrophoresis, capillary electrophoresis was employed to monitor cleavage in subsequent experiments.

When the kinetics of DON-induced rRNA cleavage were measured, the toxin (1000 ng/ml) was found as early as 2 h to cause rRNA cleavage that was very robust by 6 h (Fig. 2A). Cleavage at 6 h was concentration-dependent with 200 ng/ml of DON evoking modest rRNA cleavage as compared with more marked rRNA cleavage induced by 1000 ng/ml of DON (Fig. 3.2B). Incubation with DON at 1000 ng/ml for 6 h was therefore employed for subsequent mechanistic studies.

DON induces 28S and 18S rRNA cleavage

Northern analyses using ^{32}P-labeled oligonucleotide probes (Table 3.1) for 18S and 28S rRNAs were performed to identify and map sites of rRNA cleavage. Incubation with five probes complementary to 28S rRNA revealed six fragments (*a*-*f*) with sizes approximating 4000, 3200, 2800, 1500, 1000, 500 nts (Fig. 3.3A). Fragments *b, c, d, e* from 28S rRNA were consistent with those observed by us previously (Li and Pestka, 2008). Two other fragments (*a* and *f*) were identified possibly from the use of additional

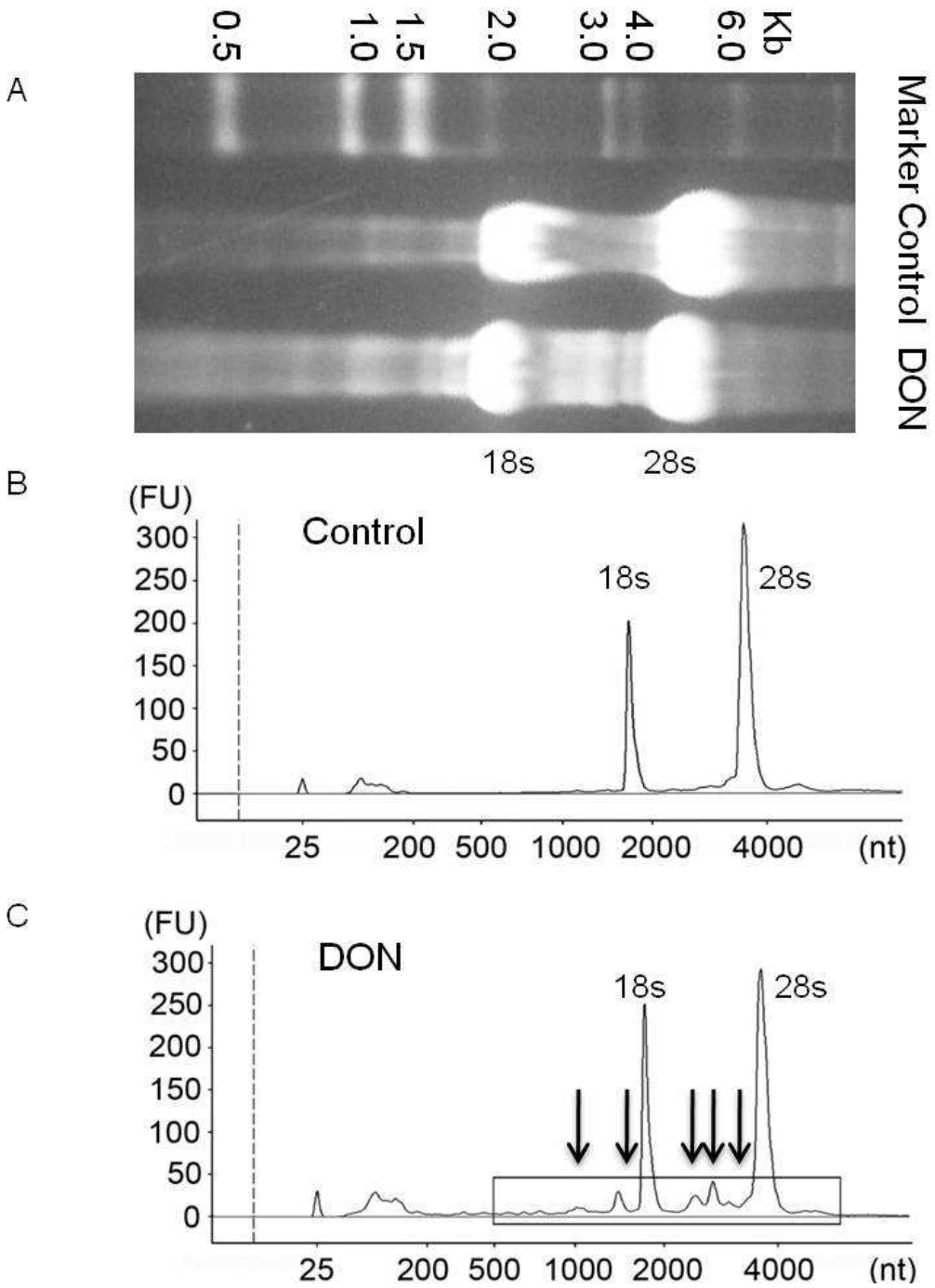

Figure 3.1. Detection of DON-induced rRNA cleavage in RAW 264.7 by agarose gel and capillary electrophoresis. Cells were treated with or without 1000 ng/ml DON for 6 h. RNAs were purified and analyzed either (A) on 1.2% formaldehyde denaturing agarose gel (10 µg) or (B and C) by capillary electrophoresis (300 ng). The X-axis indicates the size of the fragments in nucleotide (nts) and the Y-axis indicates relative peak intensity in fluorescence units (FU). The two major peaks represent 18S rRNA (~2000 nts) and 28S rRNA (~4000 nts). Arrows designate three significant cleavage peaks between 28S and 18S rRNA and two peaks below 18S rRNA. Rectangle in C indicates chart region to be shown in subsequent figures.

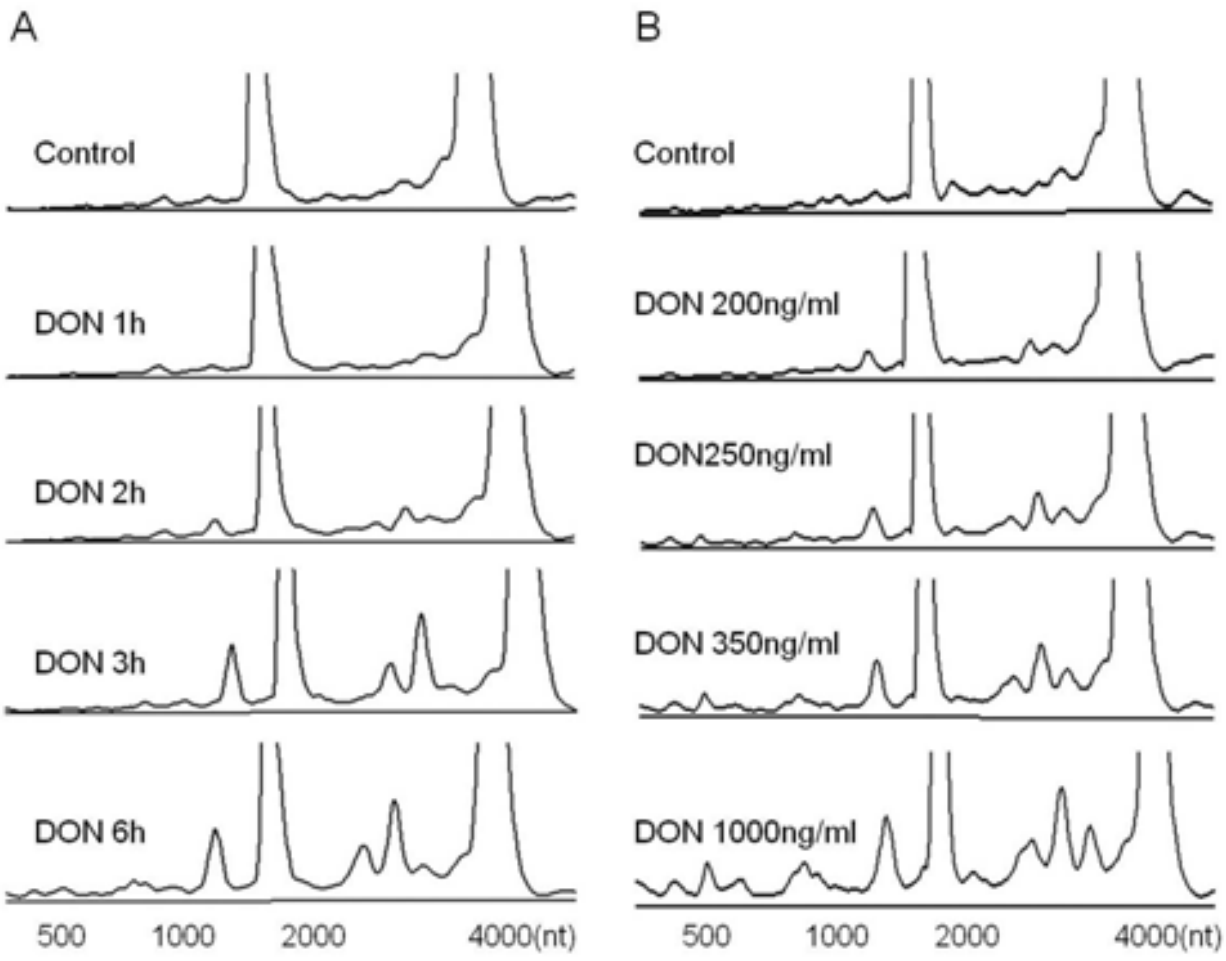

Figure 3.2. Kinetics and concentration dependence of DON-induced rRNA cleavage in RAW 264.7. (A) Cells were treated with 1000 ng/ml DON at intervals and total RNA were analyzed for cleavage by capillary electrophoresis. (B) RAW 264.7 cells were treated with indicated concentrations of DON for 6 h and total RNAs were purified and analyzed by capillary electrophoresis. Only the regions between 500 to 4000 nts are shown.

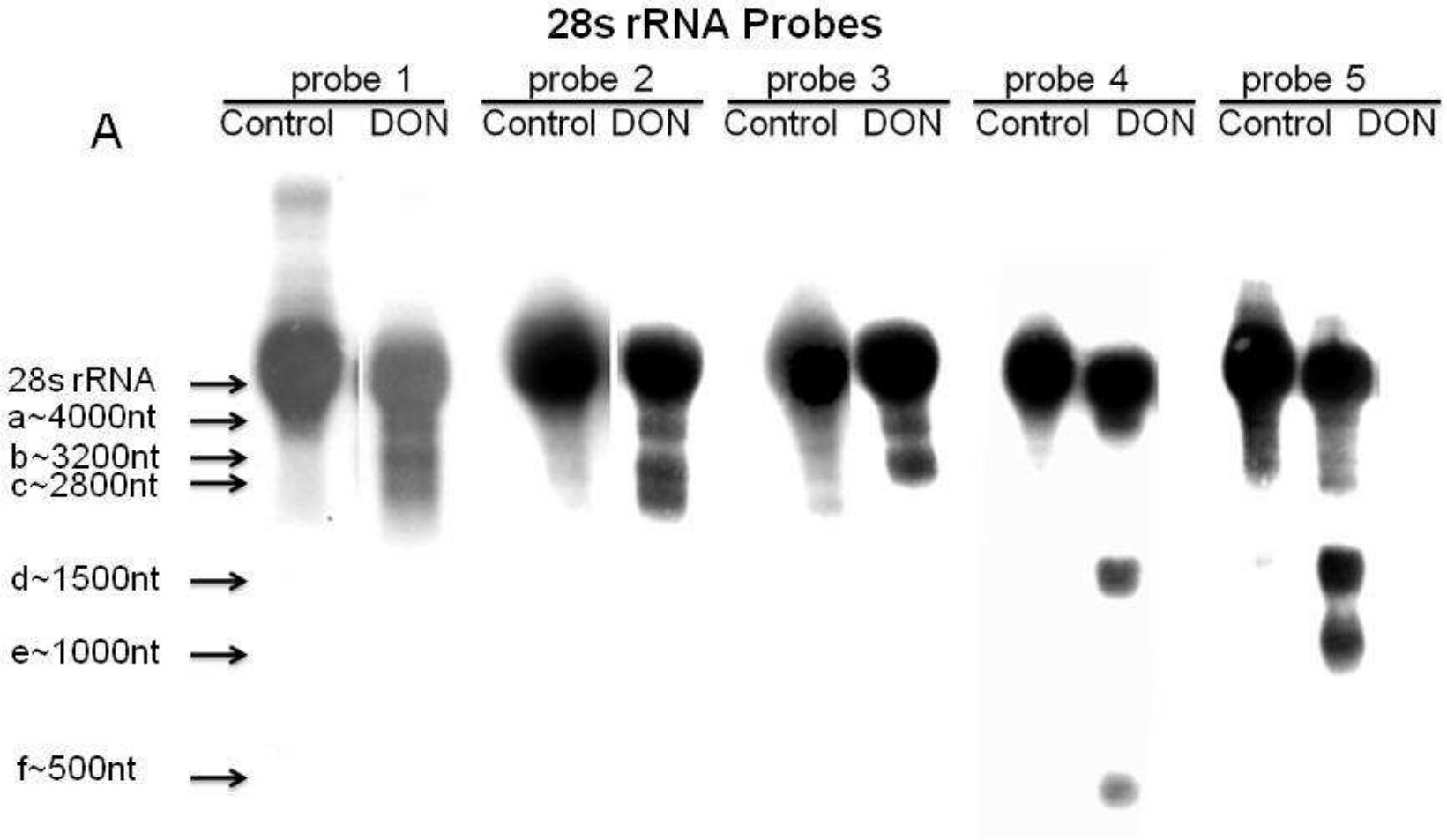

Figure 3.3. Proposed 28S rRNA cleavage sites in RAW 264.7 based on Northern analysis. (A) Five probes complementary to 28S rRNA were hybridized to RNAs from RAW 264.7 cells treated with vehicle or DON (1000 ng/ml) for 6 h. Arrows indicate fragments from 28S rRNA identified by Northern analysis and their corresponding sizes (nts). Results are representative of three separate experiments. (B) Depiction of proposed 28S rRNA cleavage pattern. Fragments with same symbol (* and ‡) are likely to originate from the same intact 28S rRNA.

Figure 3.3 (cont'd)

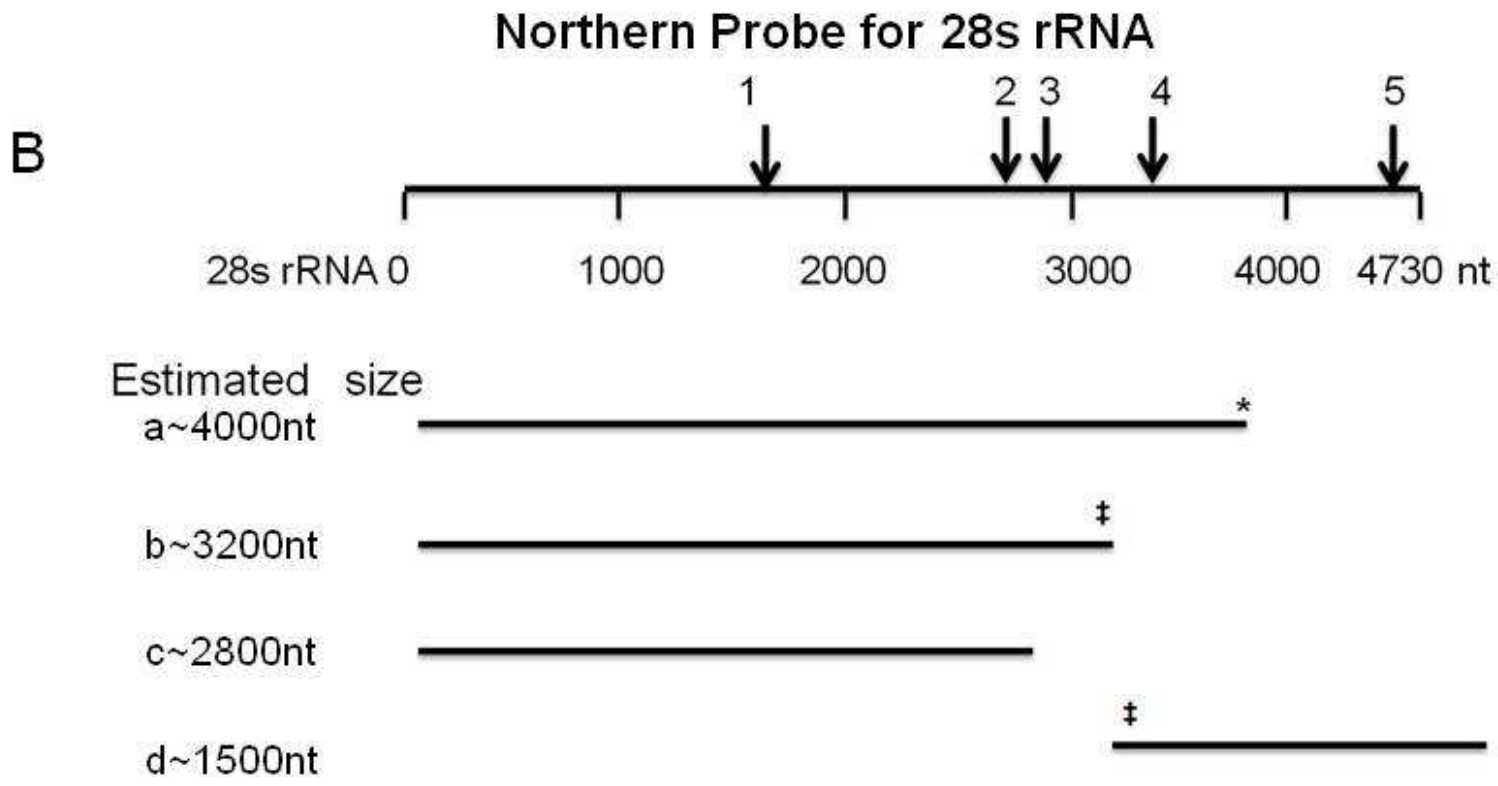

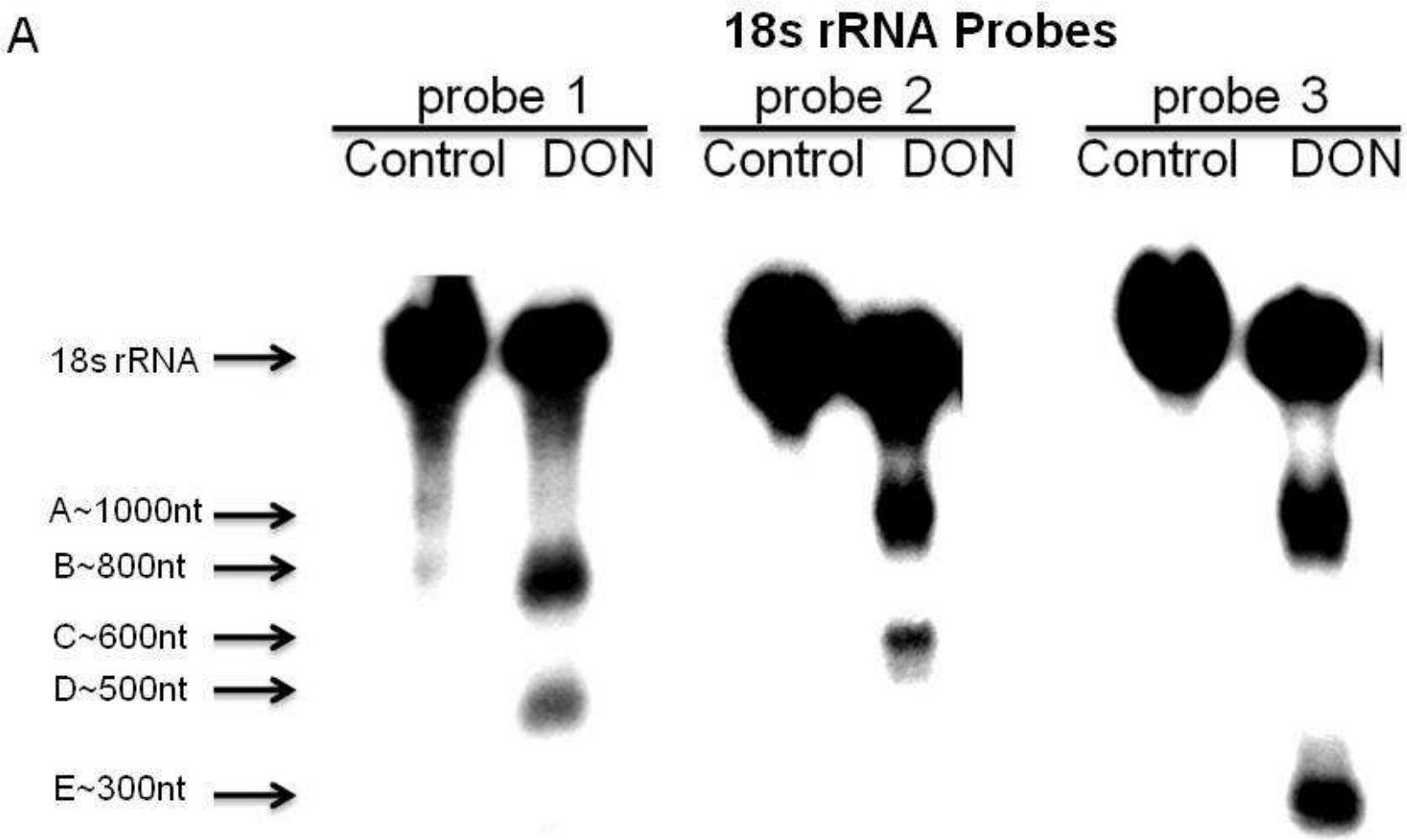

Figure 3.4. Proposed 18S rRNA cleavage sites in RAW 264.7 based on Northern analysis. (A) Three probes complementary to 18S rRNA were hybridized to RNAs from RAW 264.7 cells treated with vehicle or DON (1000 ng/ml) for 6 h. Arrows indicate fragments from 18S rRNA identified by Northern analysis and their corresponding sizes (nts). Results are representative of three separate experiments. (B) Depiction of proposed cleavage pattern for 18S rRNA. Fragments with same symbol (* and ‡) are likely to originate from the same intact 18S rRNA.

Figure 3.4 (cont'd)

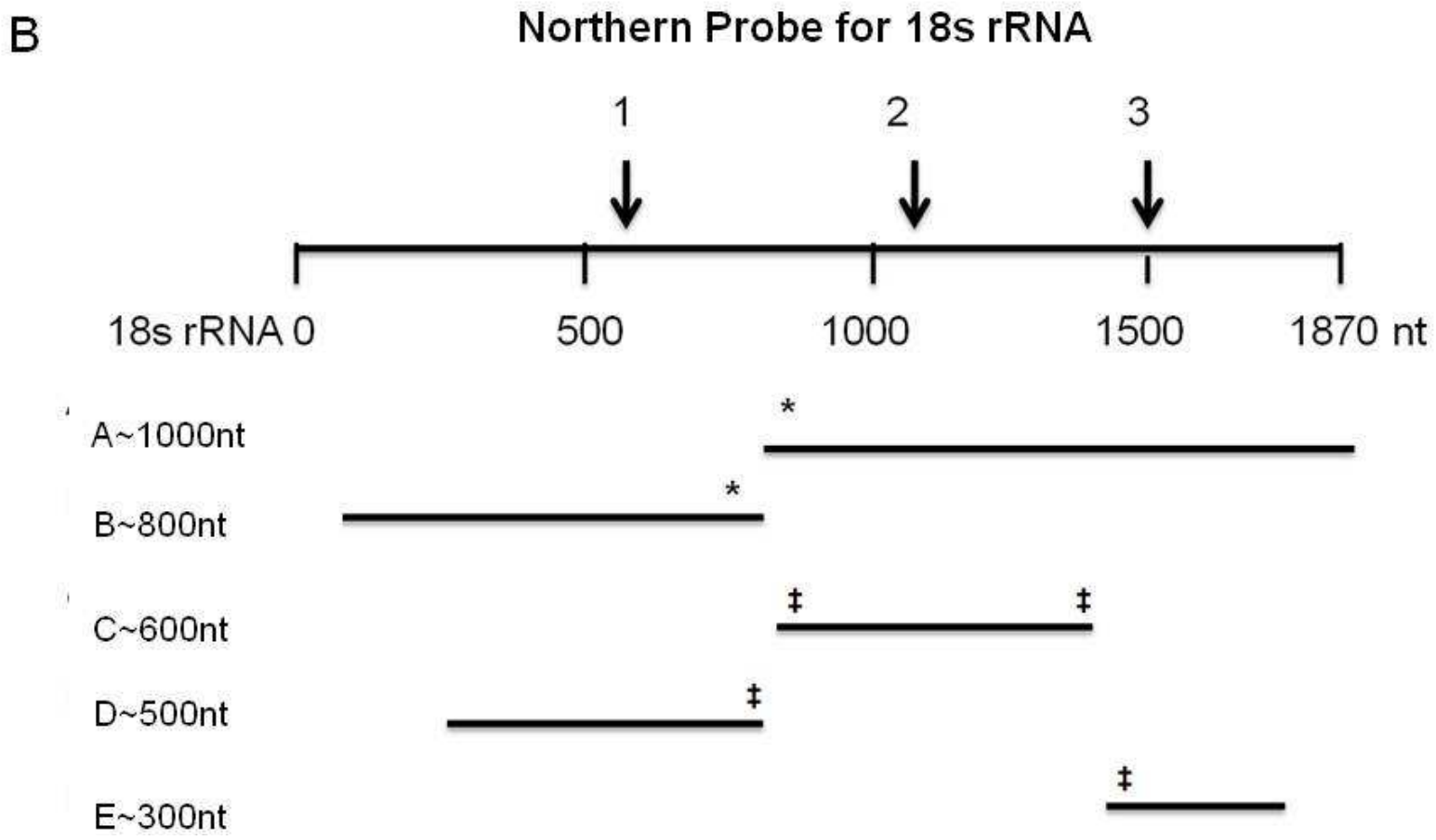

probes labeled with [γ-^{32}P]. Based on rRNA fragment sizes, position of [γ-^{32}P]-labeled probes and Northern blotting, putative cleavage sites of 28S rRNA were deduced (Fig. 3.3B). DON appeared to cleave 28S rRNA into one of two pairs of fragments, *a*+*e* (approximately 5000 nts) and *b*+*d* (approximately 4700 nts). Fragment *c* was likely to be a product of the subsequent degradation of *a* or *b*.

Hybridization with three probes complementary to 18S rRNA identified five fragments (*A*-*E*) with approximate sizes of 1000, 800, 600, 500, 300 nts (Fig. 3.4 A). Fragments *A*-*E* from 18S rRNA included two previously identified DON-induced 18S rRNA cleavage fragments (~1000, ~600nts) (Li and Pestka, 2008). The putative 18S rRNA cleavage pattern suggested that fragment *A* (approximately 1000 nts) and *B* (approximately 800 nts) may assemble into an intact 18S rRNA, while the remaining fragments (*C, D* and *E,* approximately 600, 500 and 300 nts, respectively) arose from further secondary cleavage of the two primary fragments (Fig. 3.4B).

RNase L activation is insufficient to cleave rRNA

We previously observed that, upon DON exposure, RNase L mRNA and protein expression were upregulated and this corresponded with increased RNase activity (Li and Pestka, 2008). A cell-free assay employing a FRET probe was performed to determine whether purified rRNA or purified ribosomes are degraded during incubation with RNase L with or without its natural activator 2-5A. FRET probes are chemically synthesized short RNAs containing a fluorophore and a quencher, that when cleaved emit a fluorescence signal. Significantly higher fluorescence was detected in the samples containing FRET probe, recombinant RNase L and 2-5A as compared to

FRET probe and RNase L only (Fig. 3.5A), confirming that 2-5A and recombinant RNase L were both active. In the presence of RNase L and 2-5A, purified rRNA was markedly degraded in 5 min (Fig. 3.5B). The degradation was random without specific cleavage sites being evident. In contrast, incubation with RNase L and 2-5A did not evoke rRNA cleavage in purified ribosomes for up to 120 min (Fig. 3.5C). Similarly, this incubation mixture supplemented with DON (1000 ng/ml) did not cause rRNA cleavage (data not shown). Taken together, these *in vitro* data suggest that activated RNase L is unlikely to directly cleave rRNA in the intact ribosome in the macrophage. To further assess the role of RNase L in rRNA cleavage, the natural RNase L activator 2-5A (5 µM) or another commercial RNase L Activator (RLA) (100 µM) were transfected into RAW 264.7 cells and rRNA integrity was monitored over time. No rRNA cleavage was evident up to 6 h (Fig. 3.5D), again suggesting RNase L activation per se did not cause rRNA cleavage in viable cells.

DON-induced apoptosis is concurrent with rRNA cleavage

AO/EB staining of adherent RAW 264.7 cells revealed that DON exposure (1000 ng/ml, 6 h) induced significant apoptosis concurrent with rRNA degradation (Fig. 3.6A). Since RAW 264.7 cells attach to the bottom of the cell culture plate under normal physiological conditions but detach during apoptosis, flow cytometry was additionally employed to measure apoptosis in adherent and suspended cells following DON treatment (Fig. 3.6B). Both adherent and total populations contained markedly higher annexin V positive cells (early apoptotic) (60% and 78%, respectively) than the control total cells (31%). Similarly, the percentage of annexin V/PI double positive cells (late

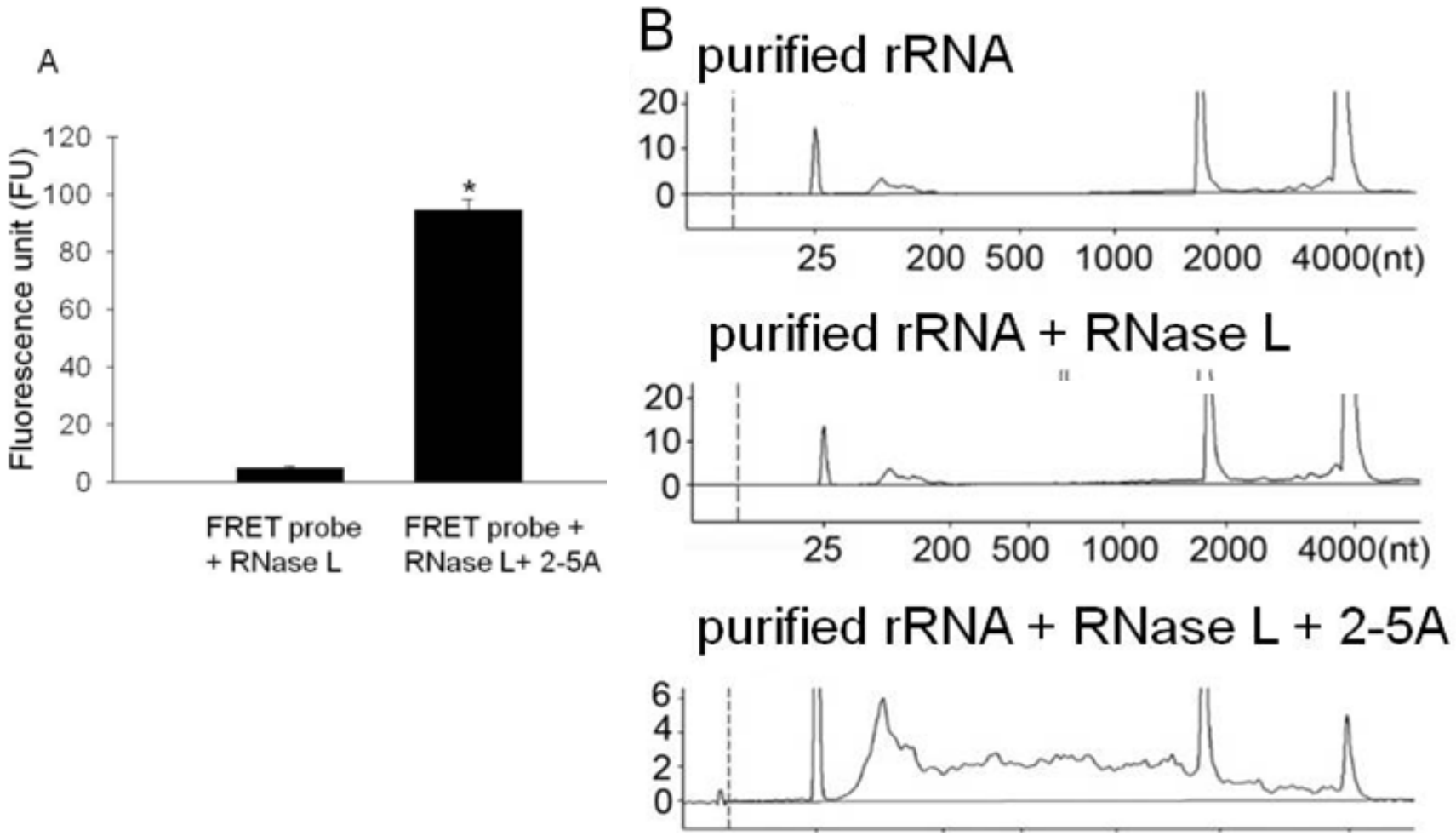

Figure 3. 5. Activated RNase L does not induce rRNA cleavage in intact ribosomes or in RAW 264.7. (A) Verification of 2-5A activity. FRET probes were incubated with RNase L in the presence or absence of 2-5A for 90 min and fluorescence intensity was measured Asterisk indicates statistically significant differences in FRET probe fluorescence intensity as compared to non 2-5A control ($p < 0.05$) by t-test.. (B) Purified rRNA (1 µg) or (C) corresponding whole ribosome were incubated with RNase L with or without 2-5A for 5 and 120 min, respectively, and subjected to capillary electrophoresis. (D) 2-5A did not induce rRNA cleavage in RAW 264.7 cells. Cells were transfected with 5 µM 2-5A or 100 µM RNase L activators for 6 h and total RNAs were purified and analyzed by capillary electrophoresis.

Figure 3.5 (cont'd)

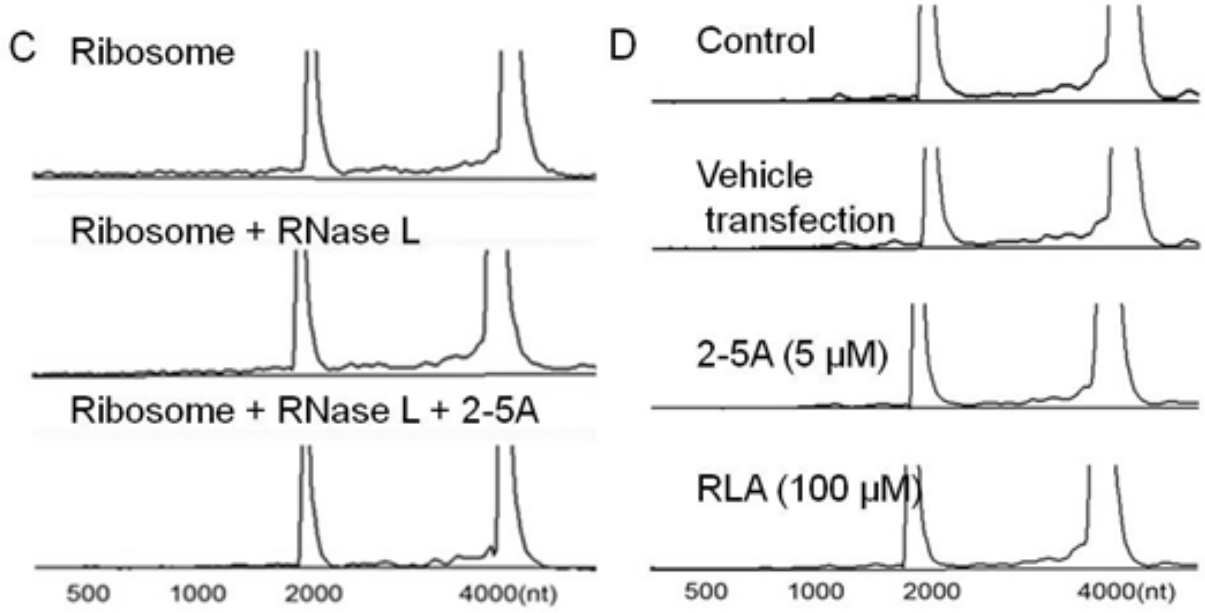

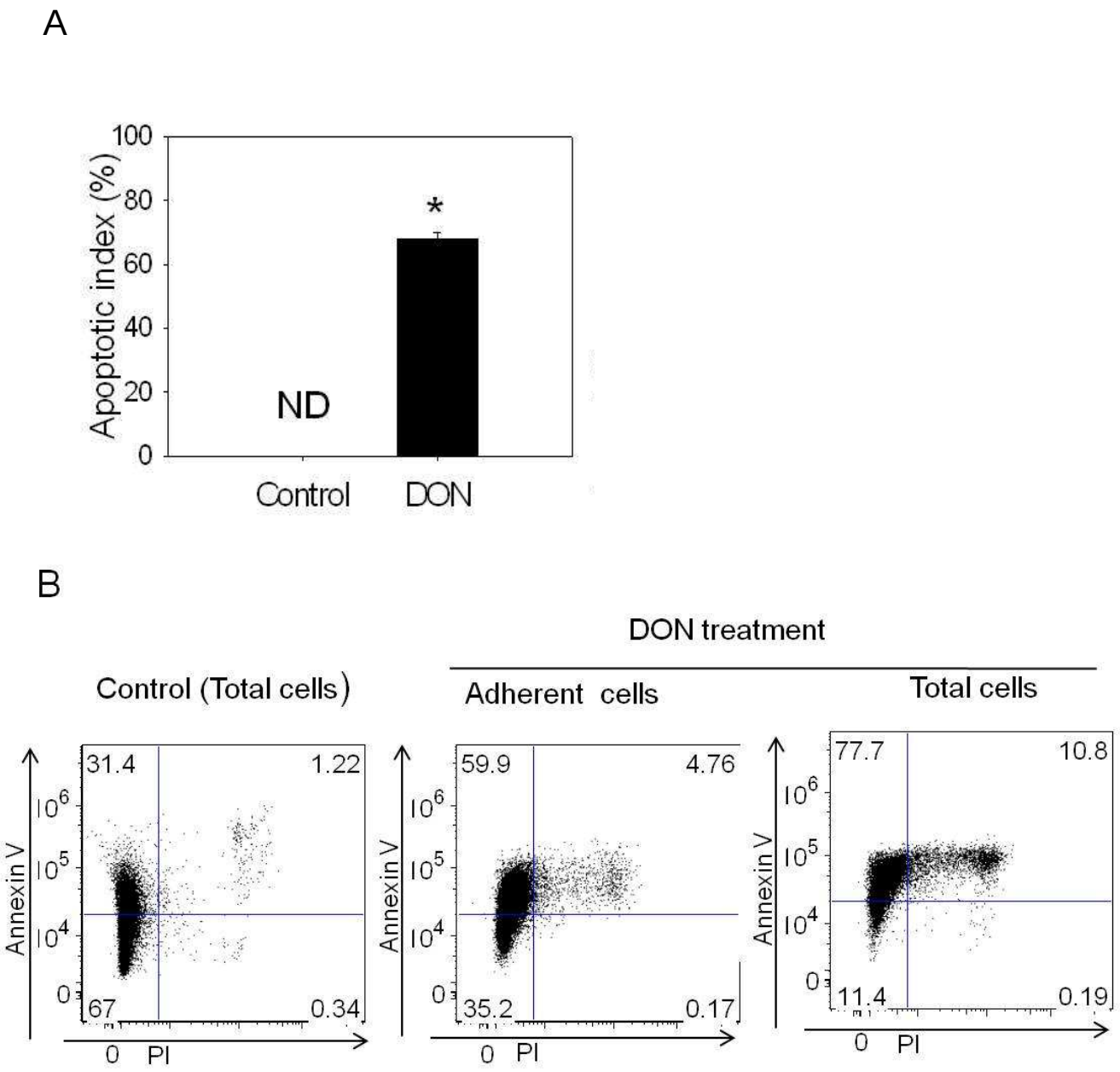

Figure 3. 6. DON exposure induces apoptosis in RAW 264.7. Cells were treated with DON (1000 ng/ml) for 6 h. (A) Acridine orange/ethidium bromide staining (AO/EB) was used to calculate apoptotic index in adherent cells. ND indicates non-detectable. Asterisk indicates statistically significant differences in cell apoptosis as compared to control ($p < 0.05$). (B) Flow cytometry with annexin V/propidium iodide (PI) was used to compare apoptosis in control and DON-treated adherent cells and total cells.

apoptotic) were much higher in adherent (4.8%) and total (10.8%) populations than of the control (1.2%).

DON-induced rRNA cleavage requires PKR, Hck, p38, p53 and caspase activation

Since DON-induced apoptosis involves activation of PKR, Hck and mitogen-activated protein kinases (Zhou *et al.*, 2003b; Zhou *et al.*, 2005b), the role of these kinases in rRNA cleavage was determined using selective inhibitors. Both the PKR inhibitor C-16 (0.1 and 0.3 µM) (Fig. 3.7A) and Hck inhibitor PP1 (5 and 25 µM) (Fig. 3.7B) were found to concentration-dependently suppress DON-induced rRNA cleavage. While the p38 inhibitor (SB 203580; 1 and 5 µM) also inhibited DON-induced rRNA cleavage concentration-dependently (Fig. 3.7C), inhibitors for JNK (SP600125; 0.2, 1 and 5 µM) and ERK (PO 98059; 20 and 100 µM) did not (data not shown) show an inhibitory effect. Thus PKR, Hck and p38 appeared to be key upstream elements for DON-induced rRNA cleavage.

It was previously shown that p38 mediates the sequential activation of p53 and caspase 3 to induce apoptosis in RAW 264.7 cells (Zhou *et al.*, 2005a). Suppression of DON-induced rRNA cleavage was observed both for pifithrin-α (80 and 100 µM) (Fig. 3.7D), which can reversibly inhibit p53-dependent transactivation of p53-responsive genes and apoptosis and for pifithrin-µ (10 and 25 µM) (Fig. 3.7E), which blocks p53 interaction with Bcl-2 family proteins and selectively inhibits p53 translocation to mitochondria. The caspase inhibitor Z-VAD-FMK also caused concentration-dependent

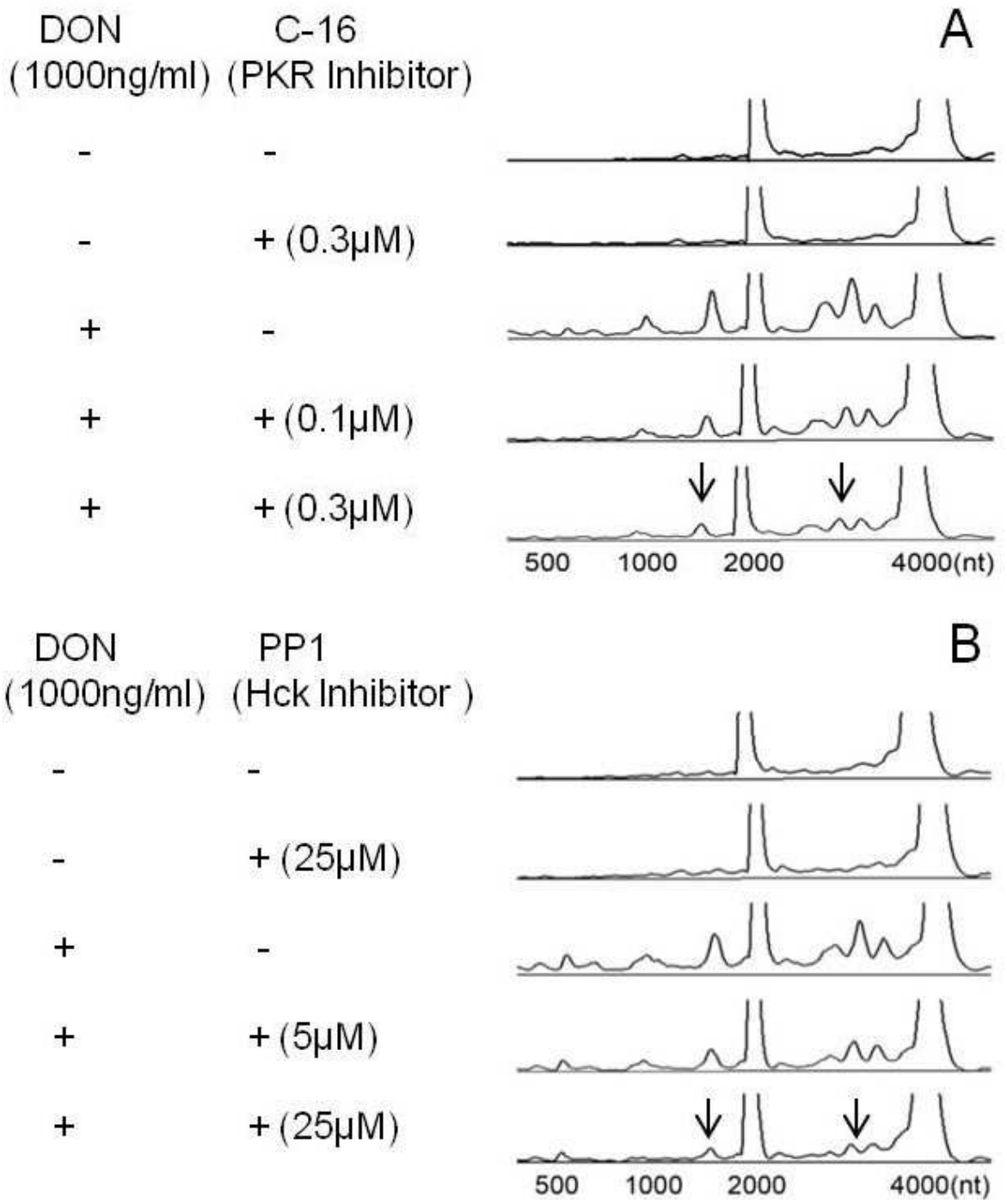

Figure 3.7. DON-induced rRNA cleavage in RAW 264.7 involves PKR, Hck, p38, p53 andcaspases. Cells were pre-incubated with (A) C-16 (0.1 or 0.3 μM), (B) PP1 (5 or 25 μM), (C) SB-203580 (1 or 5 μM), (D) Pifithrin-α (80 or 100 μM), (E) Pifithrin-μ (10 or 25 μM) or (F) Z-VAD-FMK (50 or 100 μM) for 1 h and then with DON (1000 ng/ml) for 6 h. RNAs were purified and analyzed by capillary electrophoresis. Results are representative of three separate experiments. Arrows indicate that fragmentation to major cleavage peaks is suppressed by inhibitor.

Figure 3.7 (cont'd)

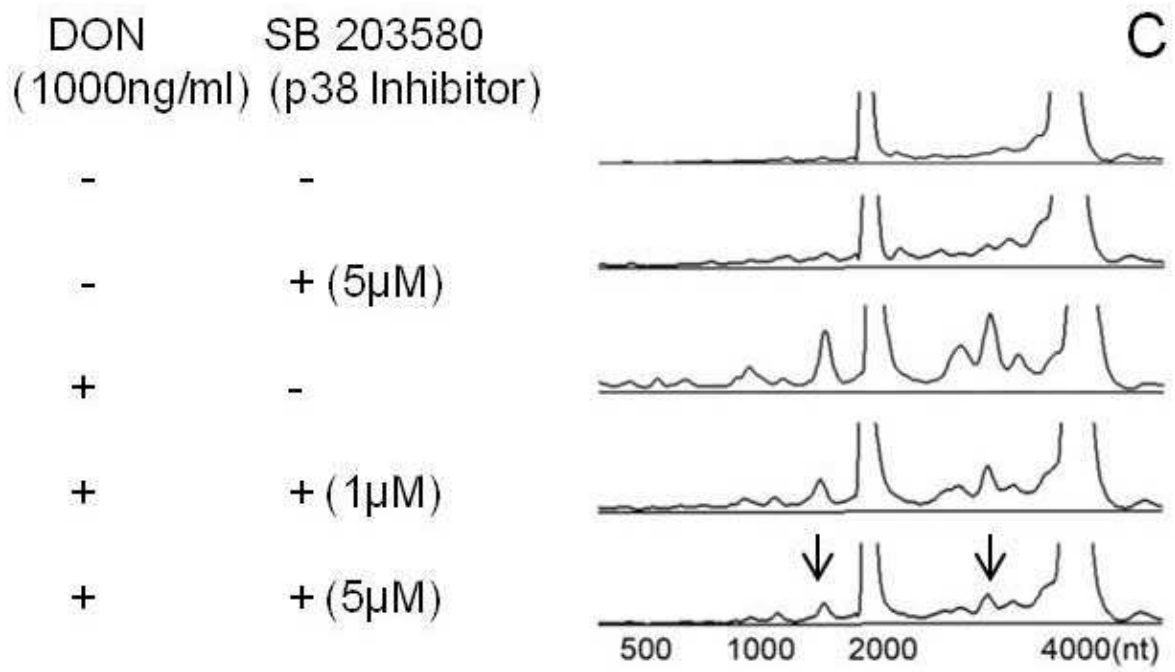

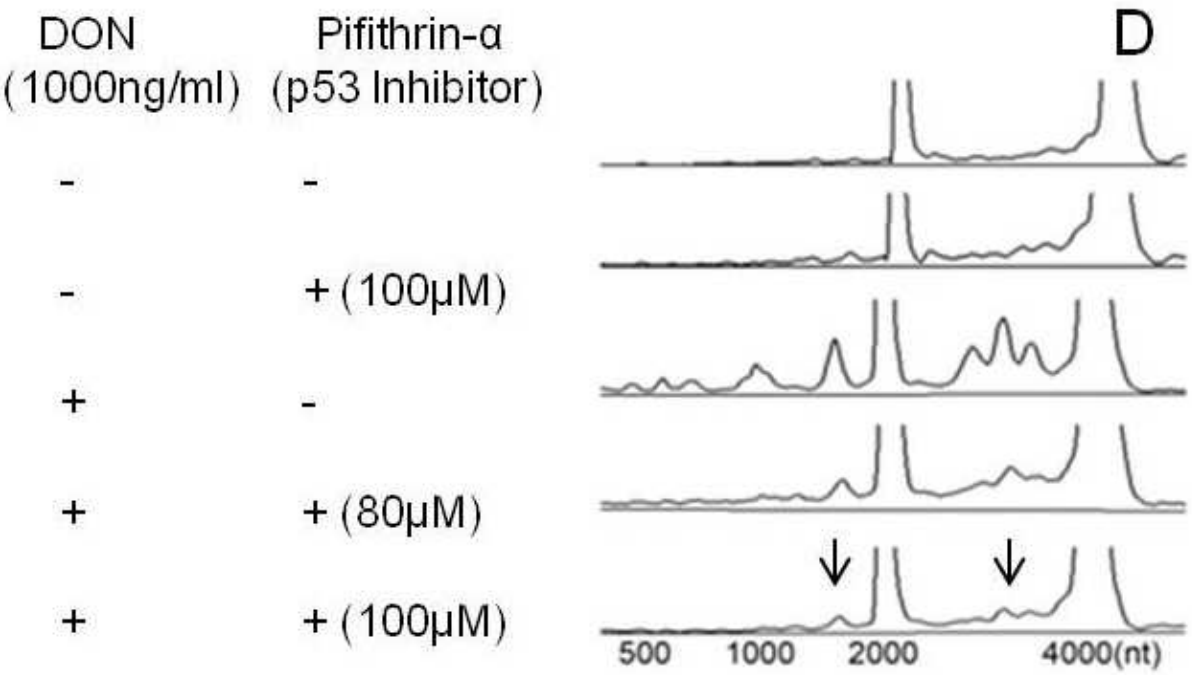

Figure 3.7 (cont'd)

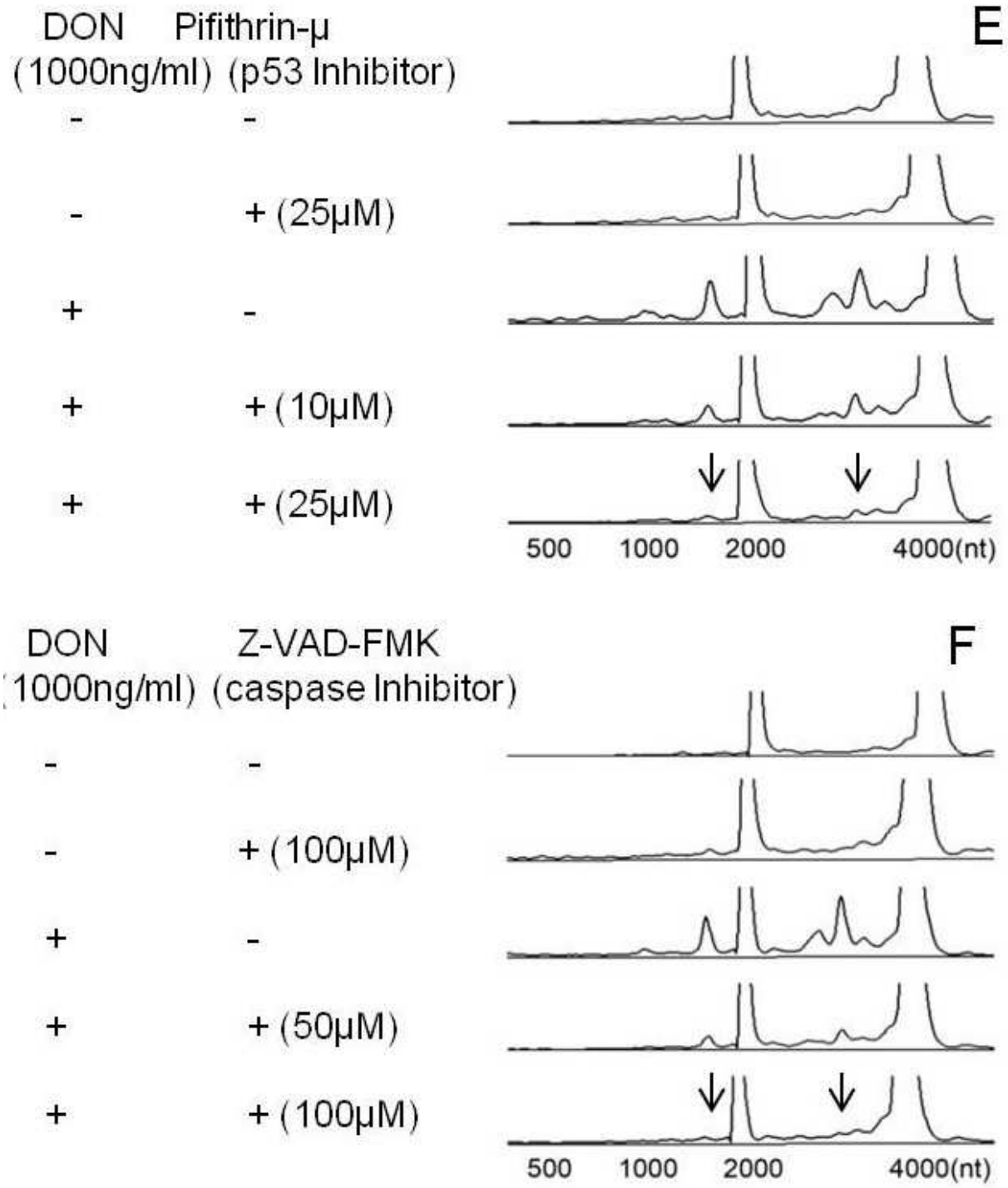

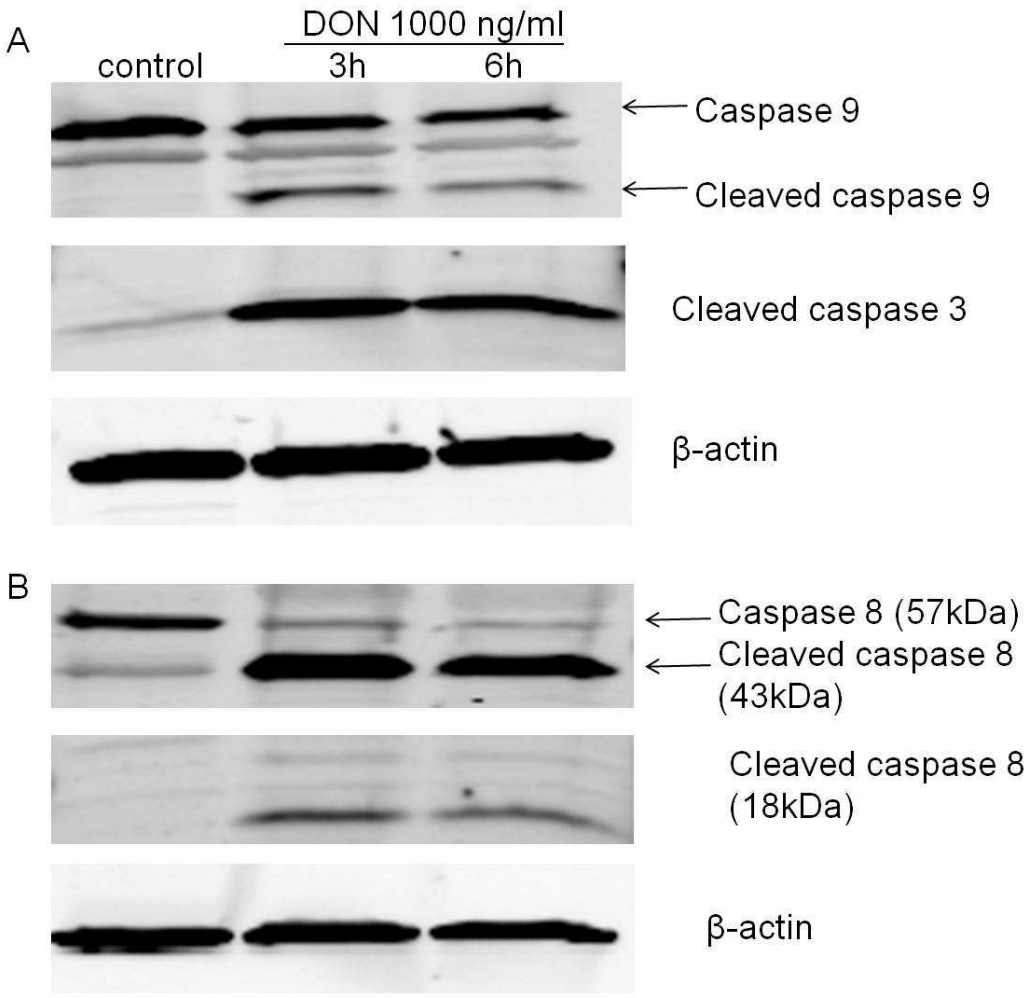

Figure 3.8. DON induces cleavage of caspase 3, 8 and 9 in RAW 264.7. Cells were treated with DON (1000 ng/ml) for 3 and 6 h. Western blotting was used to detect (A) caspase 9, cleaved caspase 9 and cleaved caspase 3 and (B) caspase 8 and cleaved caspase 8. β-actin was used as loading control. Data are representative of three separate experiments.

inhibition of DON-induced rRNA cleavage (Fig. 3.7F). Accordingly, both p53 and caspase activation are additional upstream elements in the signaling pathway leading to DON-induced rRNA cleavage.

Extrinsic and intrinsic apoptotic pathways activate caspase 3 through caspase 8 and caspase 9, respectively. To discern the contribution of these two pathways, RAW 264.7 cells were treated with DON for 3 and 6 h and the presence of cleaved caspase 8, 9 and 3 was determined by Western analysis. Cleavage of caspase 9, 3 and 8 was observed (Fig. 8A, B), suggesting that extrinsic and intrinsic pathways were involved in DON-induced apoptosis.

Satratoxin G (SG), anisomycin and ricin but not LPS evoke rRNA cleavages

Since DON is a translational inhibitor and causes rRNA cleavage indirectly, we questioned whether this might be a common effect for other ribotoxins. Cells are incubated with SG and anisomycin, which can freely diffuse through the cell membrane, and ricin, a ribosome inactivating protein which can enter the cells by endocytosis and retrograde translocation to ER and cytosol. Unlike SG and anisomycin that directly bind to the ribosome to inhibit translation, ricin possesses inherent RNA N-glycosidase activity to depurinate RNA. Although these toxins have different mechanisms to inhibit translation, SG, anisomycin and ricin induced a similar apoptosis-mediated cleavage profile to DON (Fig.3.9), suggesting that ribotoxins must share a conserved mechanism to cause rRNA cleavage. Lipopolysaccharide (LPS), a major component of the outer membrane of Gram-negative bacteria that can activate macrophages via the TLR4 receptor, did not affect rRNA integrity indicating that the macrophage activation per se was insufficient to induce RNA cleavage.

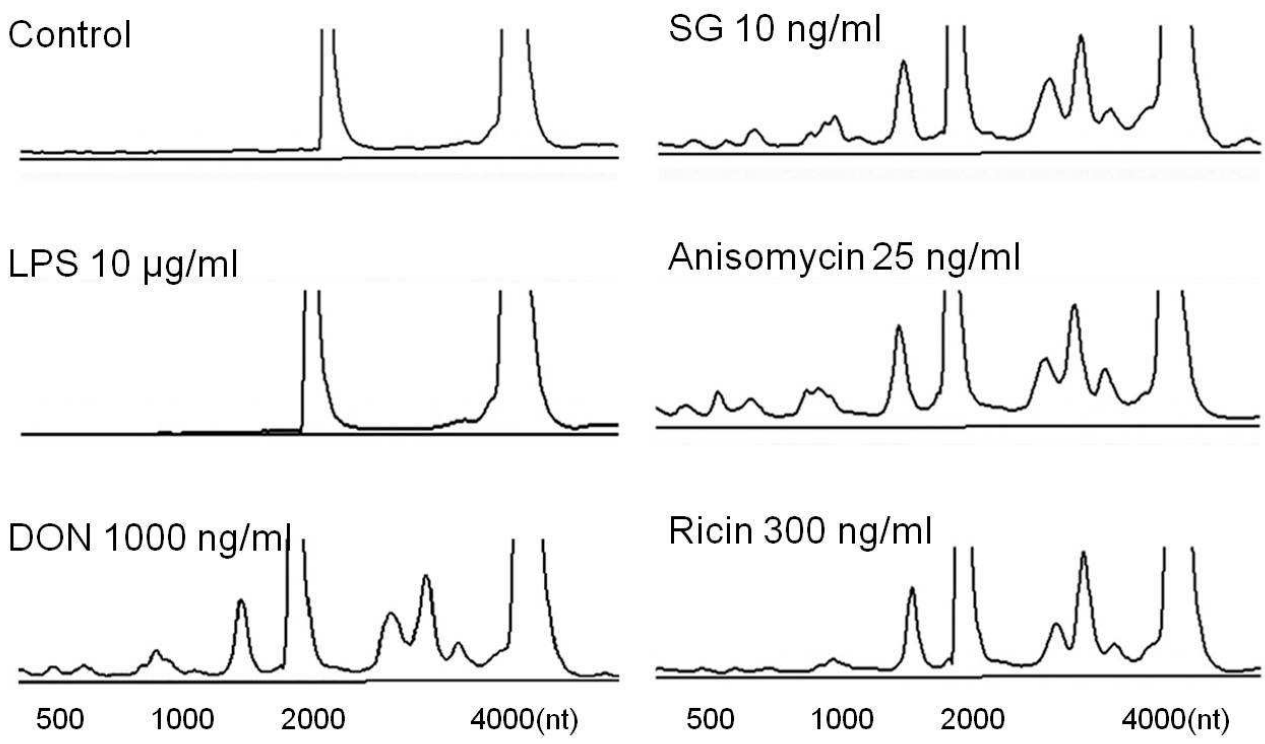

Figure 3.9. Satratoxin G (SG), anisomycin and ricin but not LPS induce rRNA cleavage patterns identical to DON in RAW 264.7. Cells were treated with DON (1000 ng/ml), SG (10 ng/ml), anisomycin (25 ng/ml) ricin (300 ng/ml) and LPS (10 µg/ml), for 6 h. RNAs were purified and analyzed by capillary electrophoresis. Results are representative of three separate experiments.

DISCUSSION

Understanding how DON induces rRNA degradation in the mononuclear phagocyte will provide insight into the mechanisms by which DON and other ribotoxins exert immunotoxicity. The results presented here indicate for the first time that DON-induced rRNA cleavage is closely linked to apoptosis in the macrophage. This is supported by the observation that rRNA cleavage was inhibited by pifithrin-α, which reversibly inhibits p53-dependent transactivation of p53-responsive genes and apoptosis, as well as by pifithrin-μ, which blocks p53 interaction with Bcl-2 family proteins and selectively inhibits p53 translocation to mitochondria. We have previously demonstrated that DON induces translocation of BAX (a member of Bcl-2 family) to mitochondria and release of cytochrome c leading to apoptosis (Zhou *et al.*, 2005a). Furthermore, DON-induced rRNA cleavage was completely suppressed by the pan caspase inhibitor Z-VAD-FMK, indicating that activation of caspases was a prerequisite of rRNA cleavage. Notably, DON activated caspase 8 and 9, both of which can activate caspase 3 to induce apoptosis, suggesting the involvement of both extrinsic and intrinsic apoptotic pathways, respectively, in rRNA cleavage.

28S rRNA in higher eukaryotes contains twelve conserved but variable divergent domains (D1-D12), originating from evolutionary large-scale length and diversity expansions (Michot *et al.*, 1984). Although the functions of D domains are not clearly understood, D2 and D8 have higher divergency rates than other domains (Houge *et al.*, 1995). Mouse 28S rRNA cleavage sites have been mapped within D2 (approximately 400-1140 nts) and/or D8 domains (approximately 2700-3280 nts) (Houge *et al.*, 1993; Houge *et al.*, 1995; Houge and Doskeland, 1996; Naito *et al.*, 2009). Apoptosis-

associated cleavage pathways were previously reported to target D2 and D8 followed by secondary cleavage in other domains. As demonstrated here, DON-induced rRNA cleavage fragments (*b, c, d* and *f*) were from within D8 while other cleavage sites (*a* and *e*) were most likely being within D10 (approximately 3785-3822 nts) (Michot *et al.*, 1984) rather than canonical D2. It might be speculated that DON binds to the ribosome rendering D2 inaccessible to RNase whereas D10 is more exposed to the enzyme. But this requires further investigation.

RNase L, a latent endonuclease widely-expressed in most tissues, can mediate inhibition of protein synthesis, apoptosis induction and antiviral activity (Stark *et al.*, 1998). Although RNase L is activated by stress-inducing reagents such as H_2O_2, the only known natural direct activator is 2-5A, a product of oligoadenylate synthetase (OAS) (Pandey *et al.*, 2004; Liang *et al.*, 2006). Upon binding to 2-5A, RNase L is activated by dimerization and possibly inhibits protein synthesis via the degradation of both mRNA and 28S rRNA (Clemens and Vaquero, 1978; Wreschner *et al.*, 1981). We have previously reported that upregulated expression of RNase L and possibly other RNases in DON-treated RAW 264.7 cells occur concurrently with rRNA degradation(Li and Pestka, 2008). Here we show that transfection of 2-5A and RNase L activator (RLA) into RAW 264.7 cells did not induce rRNA cleavage. Although RNase L readily cleaved both FRET probe and purified rRNA in the presence of 2-5A under cell-free conditions, it did not degrade rRNA in purified whole ribosomes in this system. Thus increased RNase L activity alone was not likely to be sufficient to induce rRNA cleavage observed in RAW 264.7.

Caspases are independently activated via the intrinsic pathway through caspase-9 or the extrinsic pathway through caspase-8 and can play important roles in inflammation and cell death(Fuentes-Prior and Salvesen, 2004). Caspases mediate degradation of several ribosomal components including eIF2α, eIF3/p35, eIF4B, eIF4G family (Clemens *et al.*, 2000) and these enzymes might make previously unexposed rRNA accessible to endogenous RNases or induced RNases resulting in the limited specific cleavage observed here. Notably, previous 2-5A-induced rRNA cleavage was found in caspase-containing cell-free systems(Wreschner *et al.*, 1981) or a post-mitochondria supernatant(Silverman *et al.*, 1982), while our RNase L in vitro assay only employed 2-5A, RNase L and purified ribosomes, suggesting the prerequisite of caspase in rRNA cleavage.

The observation that p38 but not JNK mediated DON-induced rRNA cleavage is consistent with our previous findings on the centrality of p38 in the cell fate decision in DON exposure (Zhou *et al.*, 2005a). Our findings further demonstrate that PKR and Hck mediate DON-induced rRNA cleavage. Although crosstalk between PKR and Hck is still not completely understood, these kinases are well-established upstream mediators of DON-induced p38 activation (Zhou *et al.*, 2003b; Zhou *et al.*, 2005b). In addition, the 40S ribosome subunit-associated PKR, Hck and p38 are activated upon DON exposure (Bae *et al.*, 2010).

We have previously proposed that rRNA cleavage might yield a double-stranded hairpin fragments capable of activating ribosome-associated PKR (Li and Pestka, 2008). The data presented here do not fully support this hypothesis. First, PKR and Hck are activated by DON within minutes (Zhou *et al.*, 2003b; Zhou *et al.*, 2005b), whereas

DON-induced rRNA cleavage was detectable only after 2 h and required relatively high DON concentrations. Second, suppression of DON-induced rRNA cleavage by PKR, Hck and p38 inhibitors (Fig. 7) suggests that their activation is an upstream rather than downstream event. We therefore propose an alternative, damage-associated molecular pattern (DAMP) model in which DON treatment rapidly disrupts the conformation of rRNA yielding accessible hairpin loops at the surface of ribosome. These exposed loops activate PKR or other double-stranded RNA binding kinases, initiating a stress response which ultimately leads to apoptosis and rRNA cleavage.

It was notable that other ribotoxins also induced a cleavage profile identical to DON, which suggests the existence of a conserved mechanism. Interestingly, ricin, which possesses N-glycosidase enzymatic activity for 28S rRNA depurination, induced the same cleavage profile as the much smaller translational inhibitors DON, SG and anisomycin. Possibly, in all four cases, toxin-mediated ribosome damage activated a canonical apoptosis-associated rRNA cleavage pathway. While the consequences of toxin-induced rRNA cleavage are not yet resolved, it might be a routine event that facilitates homeostatic regulation of protein synthesis shutdown during apoptosis (Degen *et al.*, 2000).

Taken together, DON induced rRNA cleavage involving sequential PKR/Hck, p38, p53 and caspase activation. This is depicted in Fig. 3.10. Future work should focus on mechanism of DON-induced rRNA target sites that mediate PKR activation, identification of the executing RNases and determinant of whether induction of rRNA cleavage by other ribotoxins is similarly associated with apoptosis and shares the same signaling pathway.

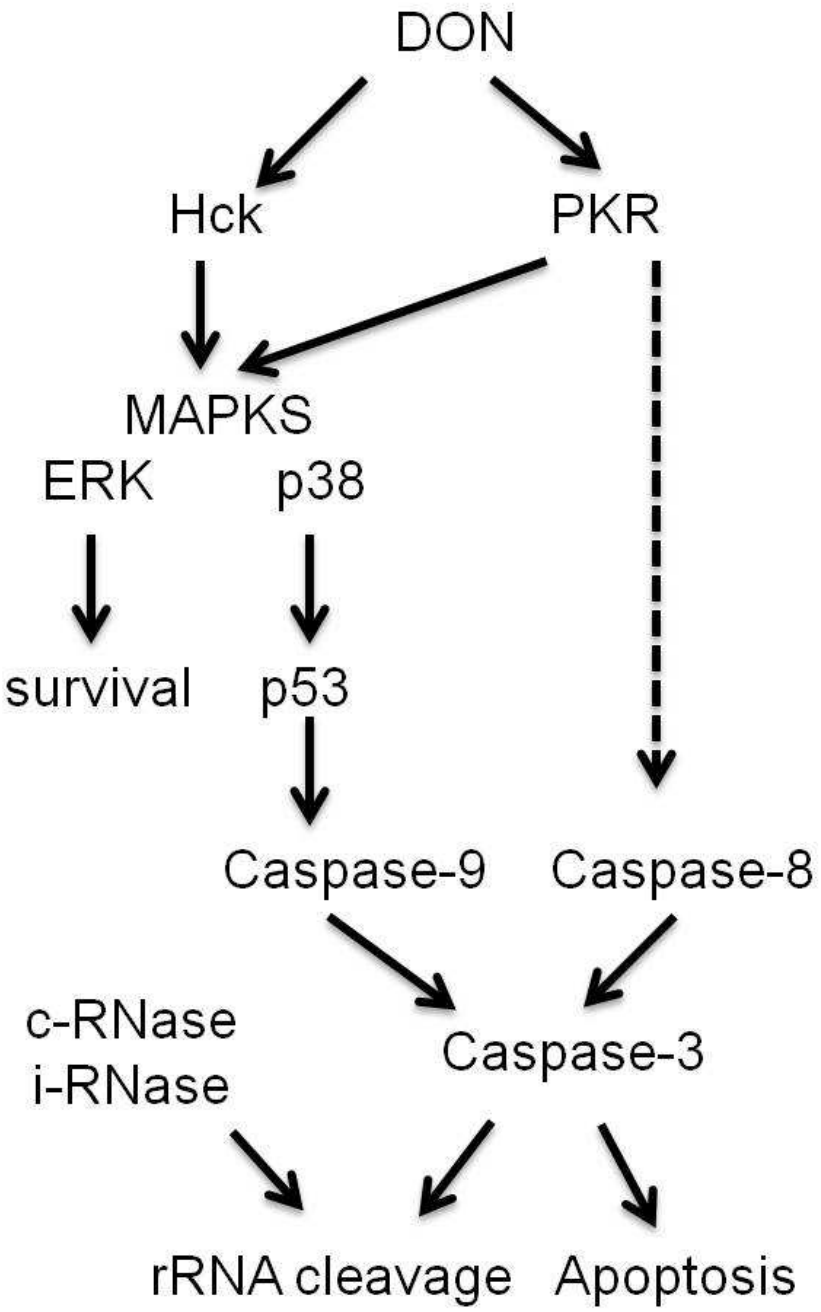

Figure 3.10. Model for DON-induced rRNA cleavage. Figure depicts putative signaling pathways for induction of rRNA cleavage by DON. DON sequentially activates PKR/Hck, p38, p53 and caspase 9/3 leading to apoptosis-associated rRNA cleavage. Caspase 8 might also be concurrently activated by PKR further contributing to caspase 3-mediated apoptosis-associated rRNA cleavage. Note both constitutive (c) and inducible (i) RNases might contribute to the cleavage of rRNA exposed by caspase action.

CHAPTER 4

Mechanisms for Ribotoxin-induced Ribosomal RNA Cleavage

This chapter has been published in Toxicology and Applied Pharmacology (2012). He, K., Zhou, H.R., Pestka, J.J., 2012. Mechanisms for ribotoxin-induced ribosomal RNA cleavage. Toxicol Appl Pharmacol. 2012 Nov 15; 265(1):10-8.

ABSTRACT

The trichothecene mycotoxin deoxynivalenol (DON), a known small molecule translational inhibitor, has been previously demonstrated to induce ribosomal RNA (rRNA) cleavage in RAW 264.7 macrophages through p38-directed activation of caspases. Here we determined the role of this pathway in rRNA cleavage induced by other ribotoxic agents in the murine macrophage model. Capillary electrophoresis indicated that DON and anisomycin (≥25 ng/ml), the type D macrocylic trichothecene satratoxin G (SG) (≥10 ng/ml) and ribosome-inactivating protein ricin (≥300 ng/ml) induced rRNA cleavage within 6 h. Like DON, anisomycin strongly activated p38, JNK and ERK1/2 within 30 min. In contrast, SG and ricin induced maximal p38, JNK and ERK2 phosphorylation only after more prolonged incubation (2 to 6 h). Inhibition of p38 but not JNK and ERK1/2 inhibited anisomycin induced rRNA degradation, whereas none of those inhibitors affected SG- and ricin-induced rRNA fragmentation. Selective inhibition of two kinases known to be upstream of DON-induced p38 activation, double-stranded RNA activated kinase (PKR) and hematopoietic cell kinase (Hck), suppressed induction of rRNA cleavage by anisomycin but not by SG and ricin. The p53 inhibitor pifithrin-μ (25 μM) and pan caspase inhibitor Z-VAD-FMK (100 μM) suppressed the rRNA cleavage induced by anisomycin, SG and ricin, indicating that they shared a conserved downstream pathway. Activation of caspase 8, 9 and 3 concurring with apoptosis suggested the parallel involvement of both extrinsic and intrinsic pathways of programmed cell death. Furthermore, inhibition of p53 suppressed anisomycin-, SG-, ricin- and DON-induced cleavage of caspase 8, suggesting that p53 is upstream of caspase 8 activation. Notably, pan inhibitor for cathepsins, a family of cysteine

proteases in lysosome, also suppressed anisomycin-, SG-, ricin- and DON-induced rRNA cleavage, indicating release of cathepsins was critical to induction of rRNA cleavage for all four ribotoxins. When specific inhibitors for cathepsin L and B, two cysteine cathepsins active at cytosolic neutral pH, were tested, only the former impaired rRNA cleavage. Taken together, all four ribotoxins induced apoptosis-associated rRNA cleavage via activation of cathepsin and p53→caspase 8/9→caspase 3, the activation of which by DON and anisomycin involved p38 whereas SG and ricin activated p53 by an alternative mechanism.

INTRODUCTION

A number of natural toxins interfere with translation and initiate a “ribotoxic stress response”, which has been linked to both activation of mitogen-activated protein kinases (MAPKs) and aberrant regulation of gene expression and apoptosis (Iordanov *et al.*, 1997; Laskin *et al.*, 2002; Bunyard *et al.*, 2003; Xia *et al.*, 2007). Specific ribotoxins, such as the trichothecene mycotoxins, are low-molecular-weight compounds that directly bind to the ribosome and inhibit translation. Other ribotoxins, such as ricin and Shiga toxin are ribosome-inactivating proteins (RIPs).

Trichothecenes and anisomycin have been proposed to interact with the peptidyl transferase center on 28S rRNA and activate many kinases (Iordanov *et al.*, 1997; Pestka, 2010a). The former are a family of secondary sesquiterpenoid mycotoxin metabolites (>200), which are divided into four types (A, B, C, D) based on group differences on the conserved sesquiterpene backbone with a 9,10-double bond and a 12,13-epoxide(Kimura *et al.*, 2007). The type B trichothecene deoxynivalenol (DON), a frequent contaminant in cereal products worldwide that exerts adverse effects on human and animals, has been extensively studied with regard to its ability to induce RSR(Pestka, 2010a). Another type D trichothecene satratoxin G (SG) is detected in indoor environments as an airborne *Stachybotrys* mycotoxin and can cause damp building-related illness (DBRI) (Pestka, 2008). Anisomycin is an antibiotic produced by *Streptomyces* and proposed to freely diffuse through cell membrane and inhibit translation by binding to the peptidyl transferase center (PTC) (Grollman, 1967; Iordanov *et al.*, 1997).

Ribosome-inactivating proteins are divided into two types based on the composition of the peptide: type 1 RIPs consist of a single peptide (A-chain) and type 2 RIPs are composed of two peptides (A- and B-chain). The A-chain of RIPs contains a RNA N-glycosidase domain that specifically cleaves adenine from the highly conserved sarcin/ricin (S/R) loop on eukaryotic 28S rRNA, while B-chain can bind to the cell surface and mediate the entrance of whole RIPs into the cell by endocytosis (Hartley and Lord, 2004a). Ricin is a type 2 RIP found in castor beans. After entering the cells by endocytosis, ricin undergoes vesicular retrograde transport from early endosomes to the trans-Golgi network (TGN) and reaches the lumen of the ER, where A-chain is released and translocates into the cytosol to depurinate 28S rRNA(Olsnes, 2004), which has been proposed as one sensor for ribotoxic stress (Iordanov *et al.*, 1997). Additionally, ricin causes two cleavage sites on 28S rRNA at A3560 and A4045 (Li and Pestka, 2008), but the mechanism is largely unknown.

It is intriguing that the small molecules anisomycin, SG, and DON, which are devoid of N-glycosidase enzymatic activity, induce an identical rRNA cleavage profile as the RIP ricin(He *et al.*, 2012), suggesting that ribotoxins share a common mechanism for mediating apoptosis-associated rRNA cleavage. To test this hypothesis, we compared the signaling pathway of DON-, anisomycin-, SG- and ricin-induced rRNA cleavage in the RAW 264.7 murine macrophage cell model. Our data show that DON and anisomycin rapidly activated p38, JNK and ERK1/2 whereas SG and ricin activated these MAPKs more slowly and to a less extent. Although activating different upstream signaling pathways, each of these ribotoxins induced apoptosis-associated rRNA cleavage through both extrinsic and intrinsic apoptotic pathways, mediated by

sequential activation of p53 and caspases. Those observations supported the involvement of lysosome-derived cathepsin L in apoptosis-associated rRNA cleavage.

MATERIALS AND METHODS

Chemicals. DON, anisomycin, PKR inhibitor C16 and Hck inhibitor PP1 were purchased from Sigma-Aldrich (St. Louis, MO). Ricin was obtained from Vector Labs Inc. (Burlingame, CA). Satratoxin G (SG) was purified as described previously(Islam *et al.*, 2009). The p38 inhibitor SB203580, JNK inhibitor SP600125, ERK inhibitor PD98059, p53 inhibitor pifithrin-μ, pan cathepsin inhibitor and cathepsin B and L inhibitors were purchased from EMD Chemicals Inc. (Gibbstown, NJ). Pan caspase inhibitor Z-VAD-FMK was supplied by BD Pharmingen (San Diego, CA). All other chemicals and medium components were obtained from Sigma-Aldrich, except where noted.

Macrophage cell culture. RAW 264.7 (ATCC, Rockville, MD), a mouse macrophage cell line, was cultured in Dulbecco's modified Eagle's medium (DMEM) supplemented with 10% (v/v) heat-inactivated fetal bovine serum (Atlanta Biologicals, Lawrenceville, GA), streptomycin (100 μg/ml) and penicillin (100 U/ml) at 37^{o}C in a humidified atmosphere with 5% CO_2. Macrophage cell number and viability were assessed by trypan blue dye exclusion using a hematocytometer. Cells (2.5 x 10^6) were seeded and cultured in 100-mm tissue culture plates for 24 h to achieve approximately 80% confluency prior to treatments of toxins (anisomycin, SG, ricin and DON) or inhibitors,.

RNA purification and cleavage analysis*.* RNAs were extracted by TRIZOL (Invitrogen, Carlsbad, CA) following manufacturer's protocol and their concentrations measured using a Nanodrop reader (Thermo Fisher, Wilmington, DE). The cleavage of rRNA (300 ng/μl) was analyzed by capillary electrophoresis using an Agilent 2100

Bioanalyzer with a Nanochip (Agilent, Santa Clara, CA) following the manufacture's instruction.

Immunoblotting. Western analyses were conducted using primary antibodies specific for murine forms of total/cleaved caspase-9, cleaved caspase 3 (Asp175), total caspase 8 and cleaved caspase 8 (Asp387), total and phosphorylated p38, JNK and ERK1/2 (Cell Signaling, Beverly, MA). Mouse β-actin antibody (Sigma) was to confirm loading. Cells were washed twice with ice-cold phosphate-buffered saline (PBS), lysed in boiling lysis buffer (1% [w/v] sodium dodecylsulfate, 1 mM sodium ortho-vanadate and 10 mM Tris, pH 7.4), boiled for 5 min and sonicated briefly; the lysate was centrifuged at 12,000 × **g** for 10 min at 4 ℃. Protein in the resultant supernatant was measured with a BCA protein assay kit (Fisher, Pittsburgh, PA). Total cellular proteins (40 µg) were separated on BioRad precast 4-20% polyacrylamide gel (BioRad, Hercules, CA) and transferred to a polyvinylidene difluoride (PVDF) membrane (Amersham, Arlington Heights, IL). After incubating with blocking buffer (Li-Cor, Lincoln, NE) for 1 h at 25 ℃, membranes were incubated with murine and/or rabbit primary antibodies (1:1000 dilution in Li-Cor blocking buffer) to immobilized proteins of interest overnight at 4 ℃. After washing three times with Tris-Buffered Saline and Tween 20 (TBST) for 10 min each, blots were incubated with secondary IRDye 680 goat anti-rabbit and/or IRDye 800 goat anti-mouse IgG antibodies (Li-Cor) (1:2000 dilution in fresh Li-Cor blocking buffer) for 1 h at 25 ℃. After washing three times, infrared fluorescence from these two antibody conjugates were simultaneously measured using a Li-Cor Odyssey Infrared Imaging System.

Morphometric measurement of apoptosis following Acridine orange/ethidium bromide (AO/EB) staining was performed using a previously described (Muppidi *et al.*, 2004) with modifications. Briefly, slides were cleaned, sterilized by UV light, added to 100-mm tissue culture plates and then seeded with RAW 264.7 cells (2.5×10^6) for 24 h to achieve approximately 80% confluency. Cells were then treated with anisomycin (25 ng/ml), SG (10 ng/ml), or ricin (500 ng/ml) for 6 h and the slides with attached cells stained for 2 min in dye mixture consisting of 100 µg/ml acridine orange and 100 µg/ml ethidium bromide in PBS. After washed twice with cold PBS, slides were covered with coverslip and examined at 400x under Nikon fluorescence microscope equipped with a wide-band FITC filter. Cells (>200) were classified based on their nuclear morphology (bright chromatin, highly condensed or fragmented nuclei) in to four categories: viable normal (VN), viable apoptosis (VA), nonviable apoptosis (NVA), nonviable necrosis (NVN) and at least 200 cells were counted. The apoptotic index was calculated as follows: (VA+NVA) / (VN+VA+NVN+NVA) x100.

Statistics. Data were analyzed by one-way ANOVA using Tukey's test using Sigma Stat 3.11(Jandel Scientific, San Rafael, CA). Data sets were considered significantly different when $p < 0.05$.

RESULTS

Anisomycin, SG, and ricin induce rRNA cleavage

Exposure of RAW 264.7 cells for 6 h to anisomycin, SG and ricin induced rRNA cleavage at concentrations as low as 10 ng/ml, 4 ng/ml and 50 ng/ml, respectively (Fig. 4.1 A, B, and C). In a follow-up kinetic study, anisomycin (25 ng/ml), SG (10 ng/ml) and ricin (300 ng/ml) were found to induce significant rRNA cleavage beginning at 3 h, 4 h, 5 h, respectively (Fig.4.2 A, B, C). These latter concentrations were selected for subsequent mechanistic studies.

Anisomycin-induced MAPK activation temporally differs from that for SG and ricin.

The capacities of the aforementioned ribotoxins to induce MAPK activation were compared to that of DON. While anisomycin induced robust phosphorylation of p38 at 30 min comparable to that for DON and through all 6 h, SG- and ricin-activated p38 was detected at 1 h, which was maximal at 2 h and lasted 6 h, (Fig. 4.3 A). Anisomycin also activated JNK and ERK1/2 at 30 min which was attenuated after 2 h. In contrast, SG and ricin activated JNK at ≥2 h (Fig. 4.3 B) as well as induced modest phosphorylation of ERK2 (Fig. 4.3 C). When activation of p38, JNK and ERK by anisomycin, SG and ricin at 30 min were compared to that of DON, only anisomycin showed a similar activation pattern.

PKR, Hck and p38 inhibition suppresses induction of cleavage by anisomycin but not SG and ricin.

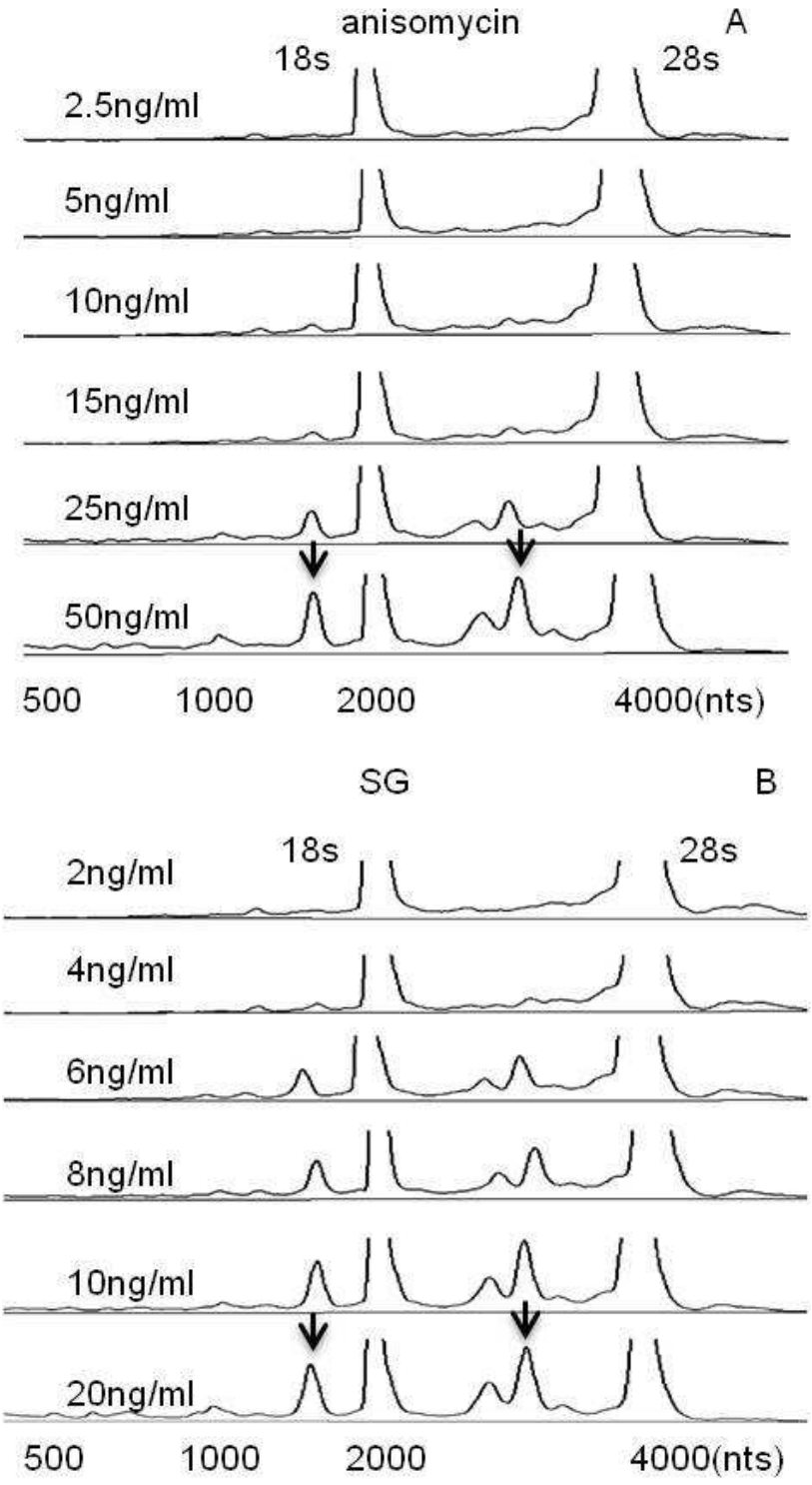

Figure 4.1. Concentration dependence of anisomycin-, SG- and ricin-induced rRNA cleavage. RAW 264.7 cells were treated with indicated concentrations of (A) anisomycin, (B) SG and (C) ricin, respectively, for 6 h and total RNA was analyzed by capillary electrophoresis. The peaks of 18S and 28S rRNAs were labeled and only the regions between 500 to 4000 nts are shown. The Y-axis fluorescence unit (FU) cutoff is 50.

Figure 4.1 (cont'd)

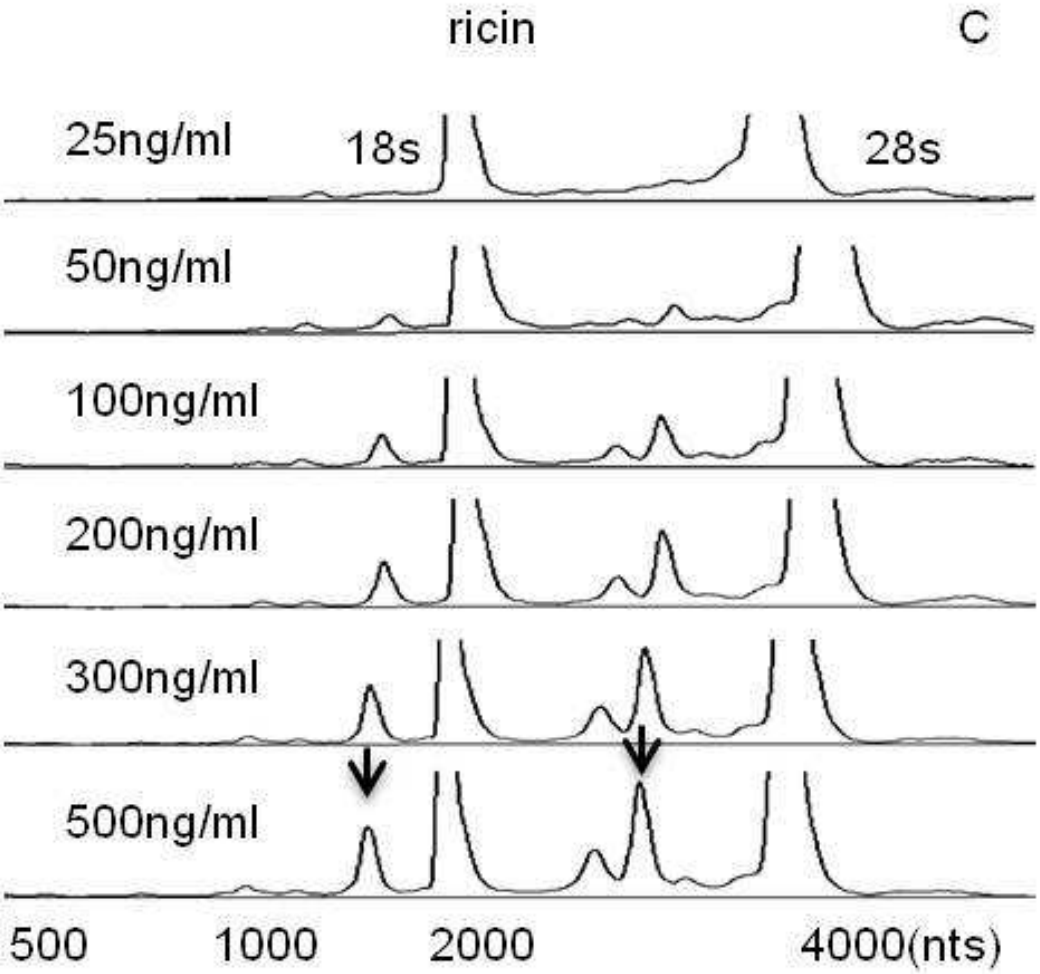

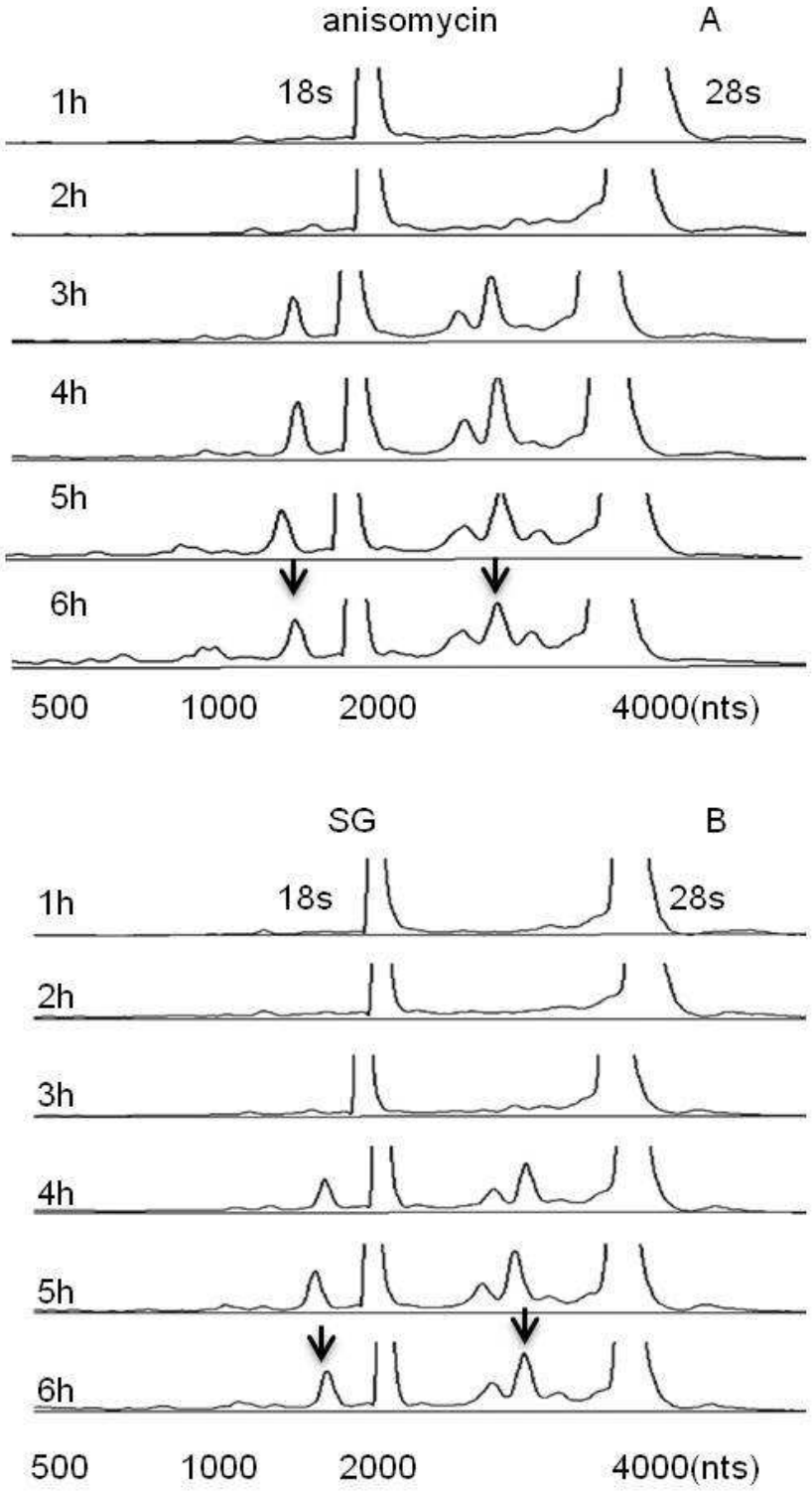

Figure 4.2. Kinetics of anisomycin-, SG- and ricin-induced rRNA cleavage. RAW 264.7 cells were treated with (A) anisomycin (25 ng/ml), (B) SG (10 ng/ml) and (C) ricin (300 ng/ml), respectively, for indicated times. RNA cleavage was analyzed for cleavage by capillary electrophoresis as reported in Fig. 1 legend.

Figure 4.2 (cont'd)

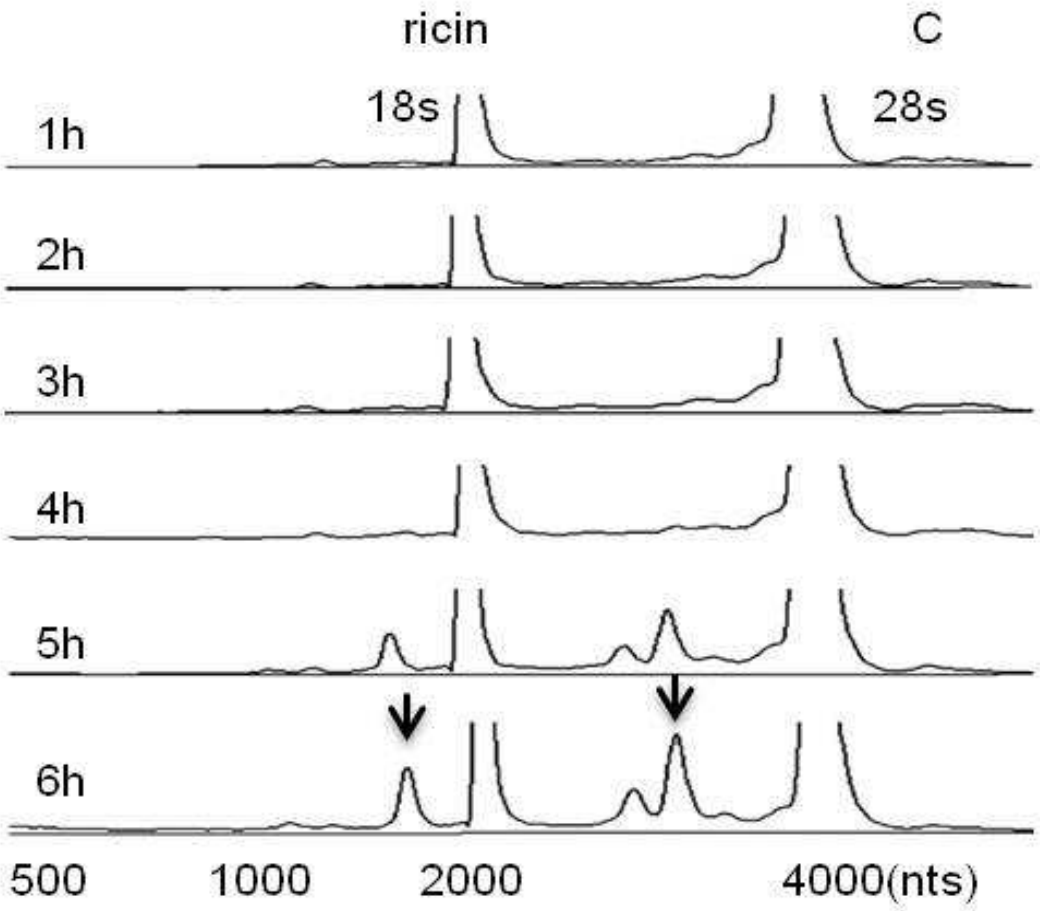

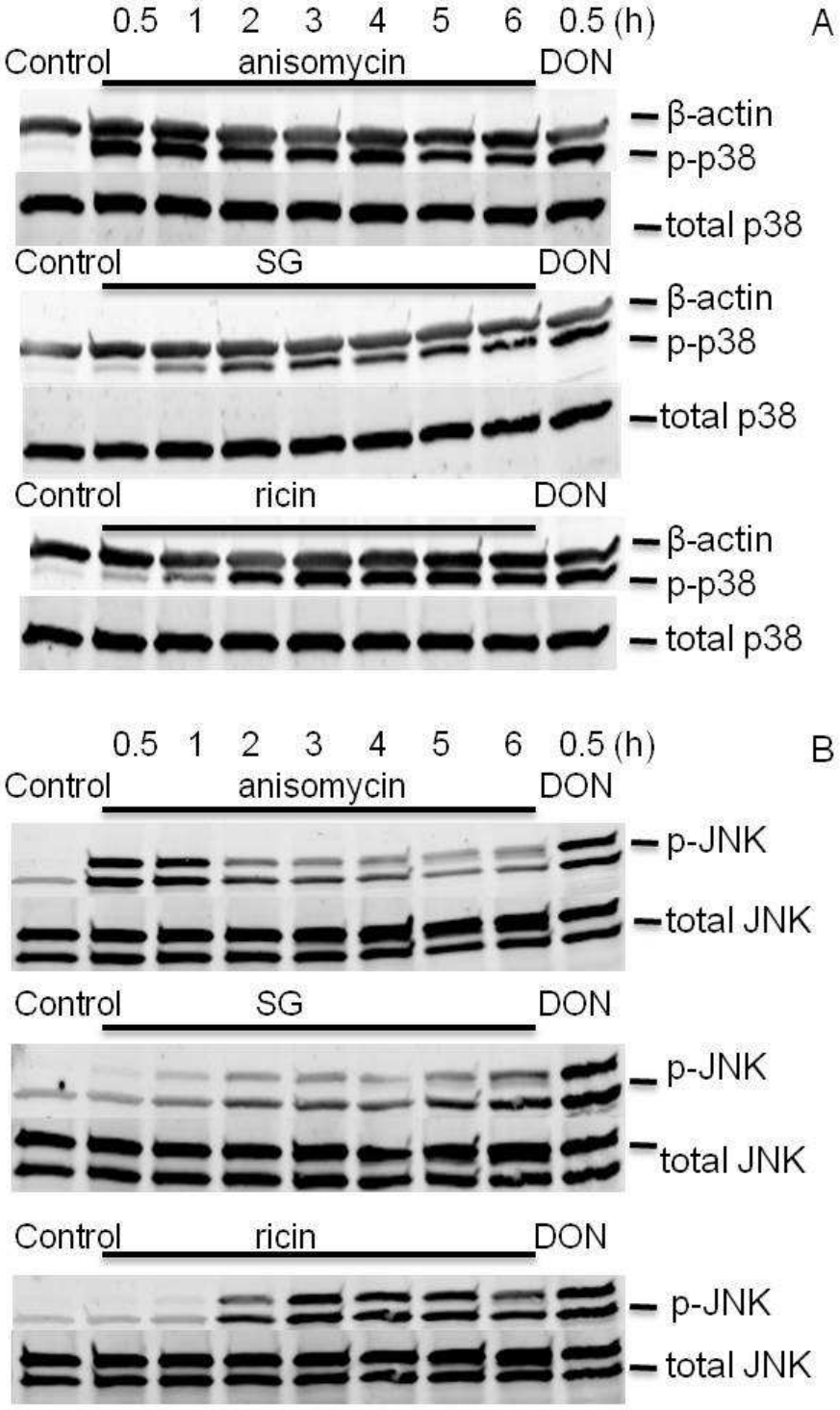

Figure 4.3. Anisomycin, SG and ricin differentially activate p38, JNK and ERK. Cells were treated with anisomycin (25 ng/ml), SG (10 ng/ml) and ricin (300 ng/ml) for 0.5, 1, 2, 3, 4, 5 and 6 h, and DON (1000 ng/ml) for 0.5 h, respectively. The cells were then lysed and subjected to Western blotting analysis with total and phosphorylated (A) p38, (B) JNK and (C) ERK antibodies. β-actin was also stained as a loading control (A).

Figure 4.3 (cont'd)

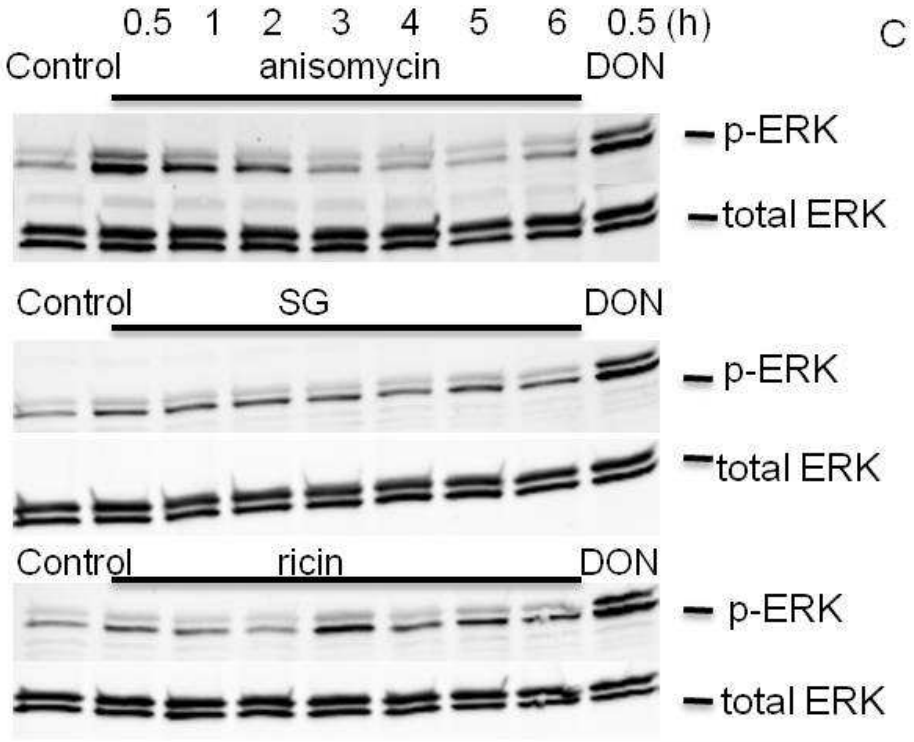

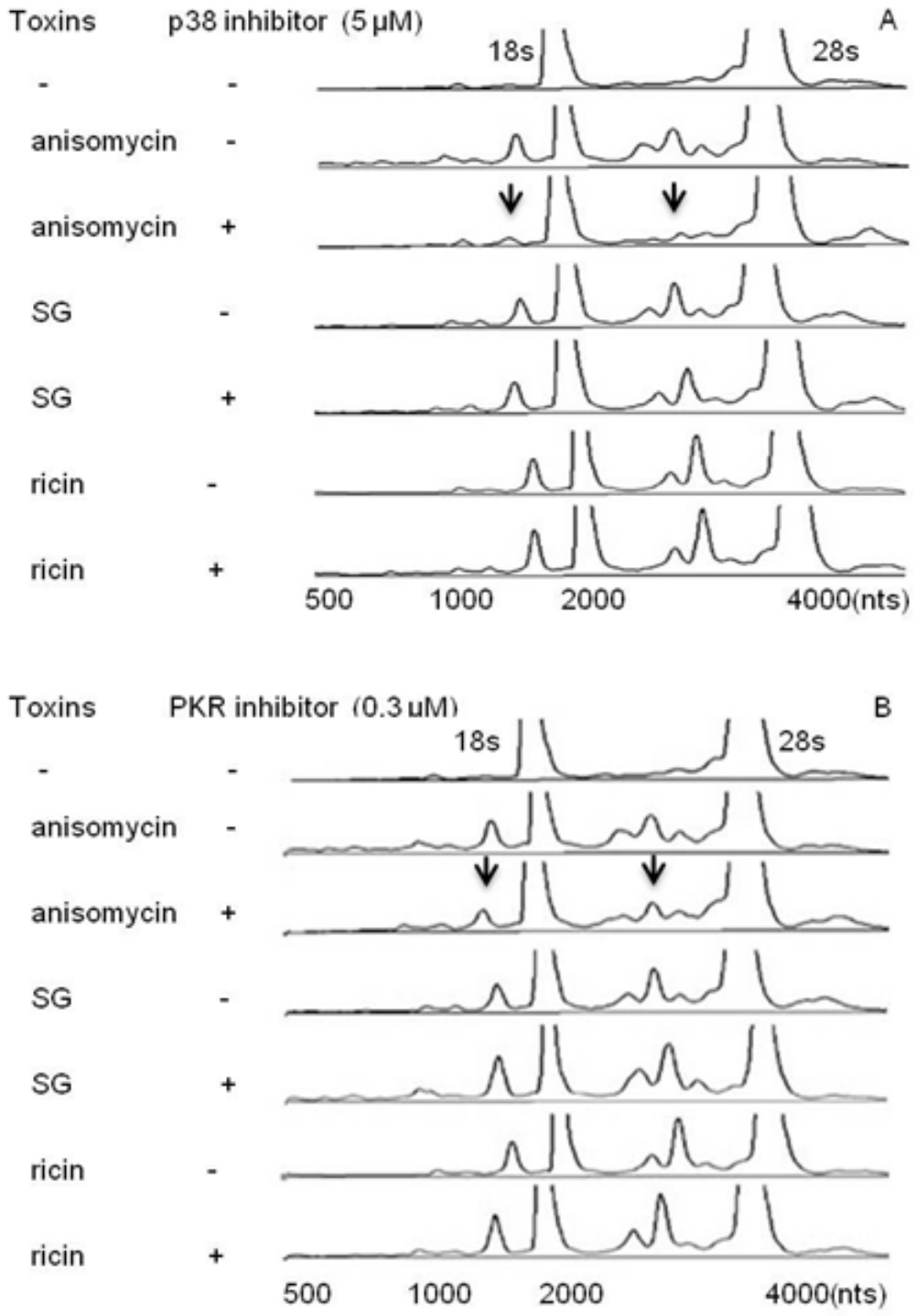

Figure 4.4. Anisomycin, but not SG and ricin, induce rRNA cleavage through p38, PKR and Hck. Cells were pre-treated with (A) SB-203580 (5 μM), (B) C-16 (0.3 μM) or (C) PP1 (25 μM) for 1 h before anisomycin (25 ng/ml), SG (10 ng/ml) and ricin (300 ng/ml) treatment for 6 h, respectively. RNAs were purified and analyzed by capillary electrophoresis as described in Fig. 1 legend. Results are representative of three separate experiments. Arrows indicate that fragmentation to major cleavage peaks are suppressed by inhibitors.

Figure 4.4 (cont'd)

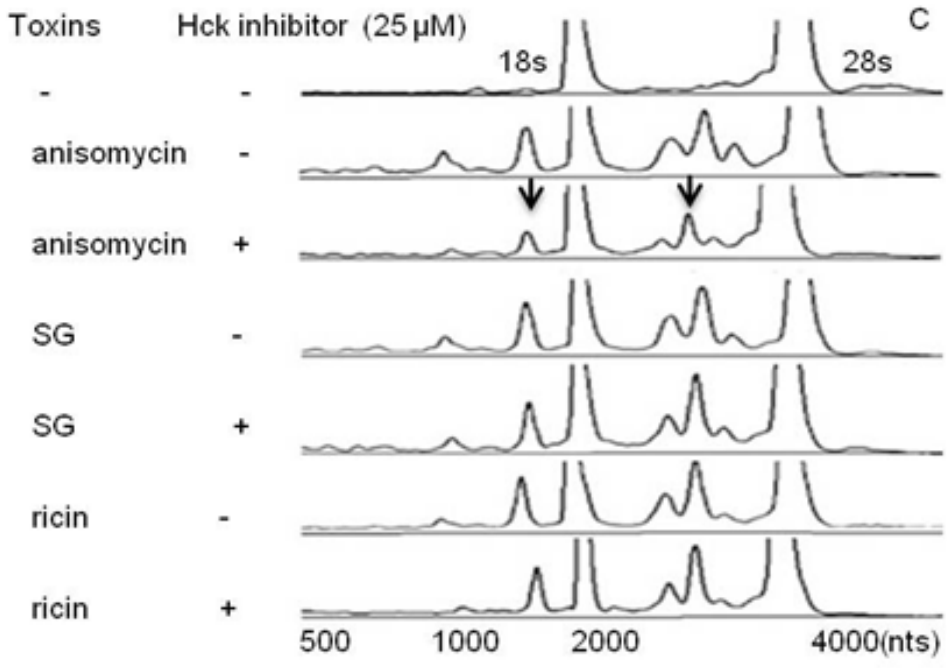

As has been described previously for DON(He *et al.*, 2012), pharmacological inhibition of p38 (5 µM, Fig. 4.4 A), suppressed anisomycin-induced rRNA cleavage, but this inhibitor did not block SG- or ricin-induced rRNA cleavage. Like DON, JNK and ERK inhibitors did not have any inhibitory effects on anisomycin-, SG- and ricin-induced rRNA cleavage (data not shown). Both PKR and Hck have been previously shown to be upstream of DON-induced p38 activation and required for rRNA cleavage(He *et al.*, 2012). Similar to DON, inhibition of these kinases blocked rRNA cleavage induction by anisomycin but not by SG and ricin (Fig. 4.4 B, C). The data suggested that anisomycin shared the same signaling pathway to DON, but SG and ricin might activate other signaling molecules to mediate rRNA cleavage.

p53 and pan caspase inhibitor inhibit SG-, anisomycin- and ricin-induced rRNA cleavage.

As observed in prior studies of DON(He *et al.*, 2012), the p53 inhibitor pifithrin-µ and the broad spectrum caspase inhibitor Z-VAD-FMK markedly inhibited anisomycin-, SG- and ricin-induced rRNA cleavage (Fig. 5 A, B). Thus anisomycin, SG and ricin appeard to share a conserved downstream pathway with DON involving p53 and caspases to induce rRNA cleavage.

Anisomycin, SG and ricin induce apoptosis through extrinsic and intrinsic pathways

DON-induced rRNA cleavage was previously associated with apoptosis(He *et al.*, 2012), AO/EB staining revealed that, likewise, anisomycin, SG and ricin induced

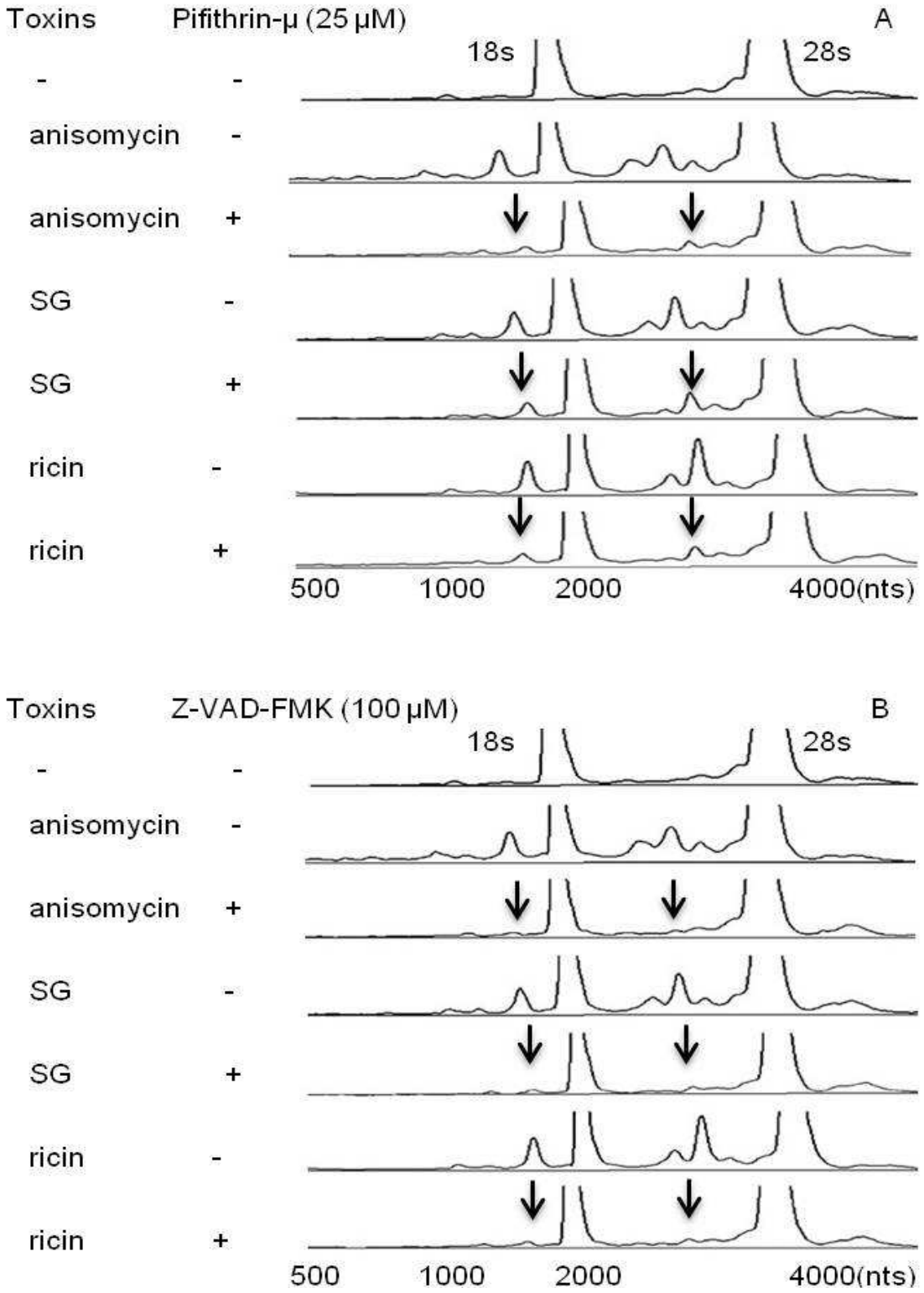

Figure 4.5. Anisomycin-, SG- and ricin-induced rRNA cleavage involves p53 and caspase. Cells were pre-treated with (A) pifithrin-μ (25 μM) or (B) Z-VAD-FMK (100 μM) for 1 h before SG (10 ng/ml), anisomycin (25 ng/ml) and ricin (300 ng/ml) exposure for 6 h, respectively. RNAs were analyzed by capillary electrophoresis as described in Fig. 1 legend.

markedly apoptosis concurrently with rRNA cleavage at 6 h (Fig. 4.6). Apoptosis can be via extrinsic and intrinsic pathways, which activate caspase 3 through caspase 8 and caspase 9, respectively. DON and anisomycin strongly activated caspase 9/3/8 at 3 h, which were attenuated at 6 h (Fig. 4.7 A, B). On the contrary, SG and ricin evoked more caspase 9/3/8 cleavage at 6 h than 3 h (Fig. 4.7 A, B). These data were consistent with time course studies of four toxins, in which DON and anisomycin caused rRNA cleavage at 2 to 3 h, whereas SG and ricin induced cleavage at 4 h, 5 h, respectively.

p53 inhibitor inhibits caspase 8 activation by all four toxins but p38 inhibitor only suppresses DON- and anisomycin-activated caspase 8.

Inhibition of p53 markedly suppressed anisomycin-, SG-, ricin- and DON-induced rRNA cleavage, suggesting a critical role for p53 in induction of rRNA cleavage. Suppression of p53 completely inhibited the cleavage of 18 KDa subunit (p18) upon exposure of four toxins respectively (Fig. 4.8, A, B, C, D), which forms active caspase with 12 KDa subunits (p10) (Zhao *et al.*, 2010). p38 inhibition only suppressed anisomycin- and DON-induced caspase 8 activation (Fig. 4.8 A, D), which is consistent with previous data that p38 only mediated DON- and anisomycin-induced rRNA cleavage but not that of SG and ricin(Fig. 4.4 A).

Lysosomal cathepsins, especially cathepsin L are involved in anisomycin, SG, ricin and DON induced apoptosis-associated rRNA cleavage

Lysosome membrane permeabilization (LMP) and subsequent cathepsin release are believed to contribute to caspase-dependent apoptosis through the cleavage of BID

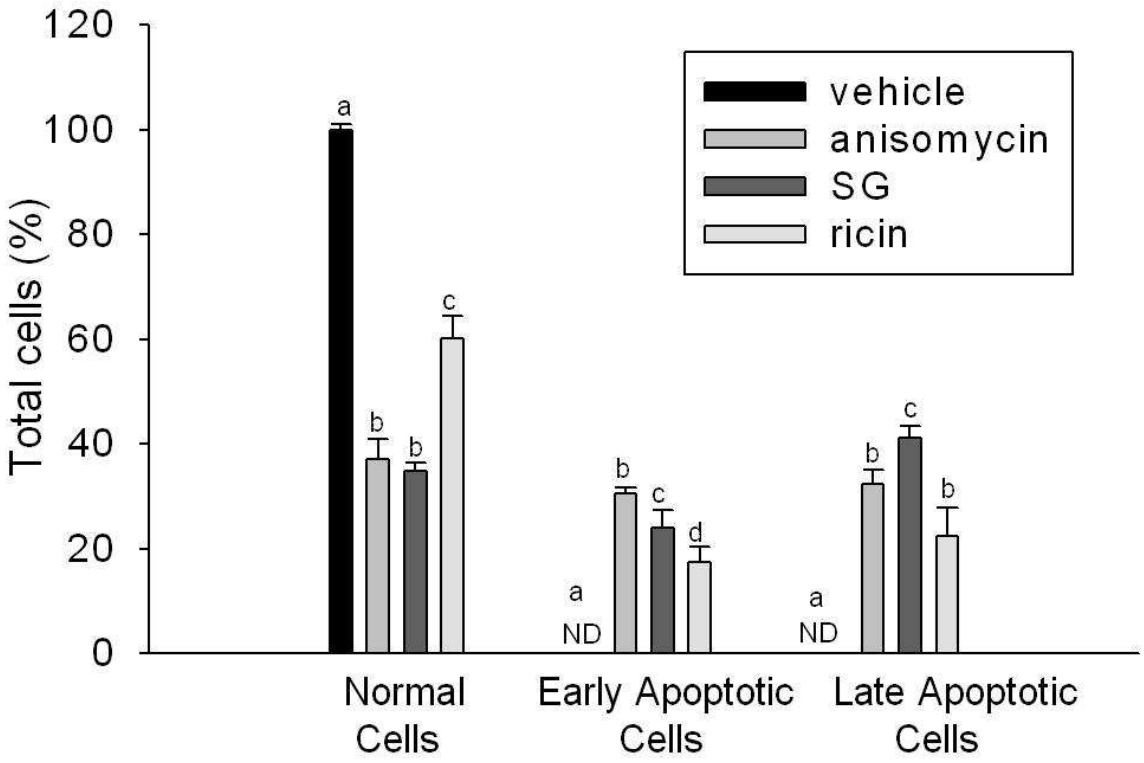

Figure 4.6. Anisomycin, SG and ricin induce apoptosis in RAW 264.7 cells. Cells were treated with anisomycin (25 ng/ml), SG (10 ng/ml) and ricin (300 ng/ml) for 6 h, respectively. Acridine orange/ethidium bromide staining (AO/EB) was used to calculate percentage of normal, early and late apoptotic adherent cells. A one-way ANOVA using Tukey's test was employed to assess significant differences ($p < 0.05$) in control and anisomycin-, SG- and ricin-treated RAW 264.7 macrophages in normal, early apoptotic and late apoptotic cells, respectively. Data are mean ± SE of triplicate wells. ND indicates non-detectable. Bars with different letters differ ($p<0.5$).

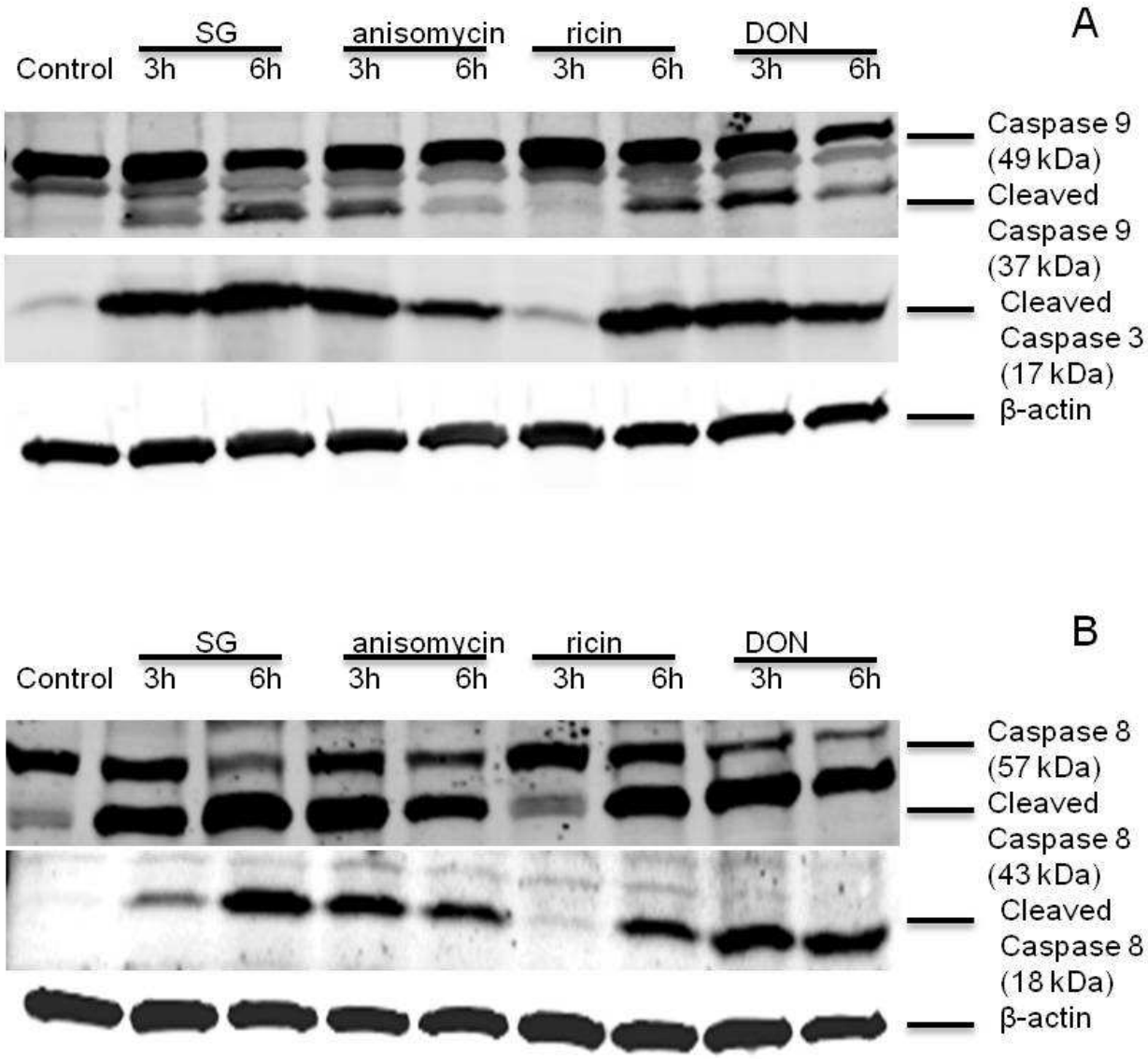

Figure 4.7. Anisomycin, SG, ricin and DON activate caspases 8, 9 and 3. Cells were treated with SG (10 ng/ml), anisomycin (25 ng/ml), ricin (300 ng/ml) and DON (1000 ng/ml) for 3 and 6 h, respectively. Cells were lysed and subjected to Western blot analysis with (A) total and cleaved caspase 9 and cleaved caspase 3 antibodies or (B) total and cleaved caspase 8 antibodies. β-actin was also stained as loading control and this is shown at the bottom of each panel (A, B).

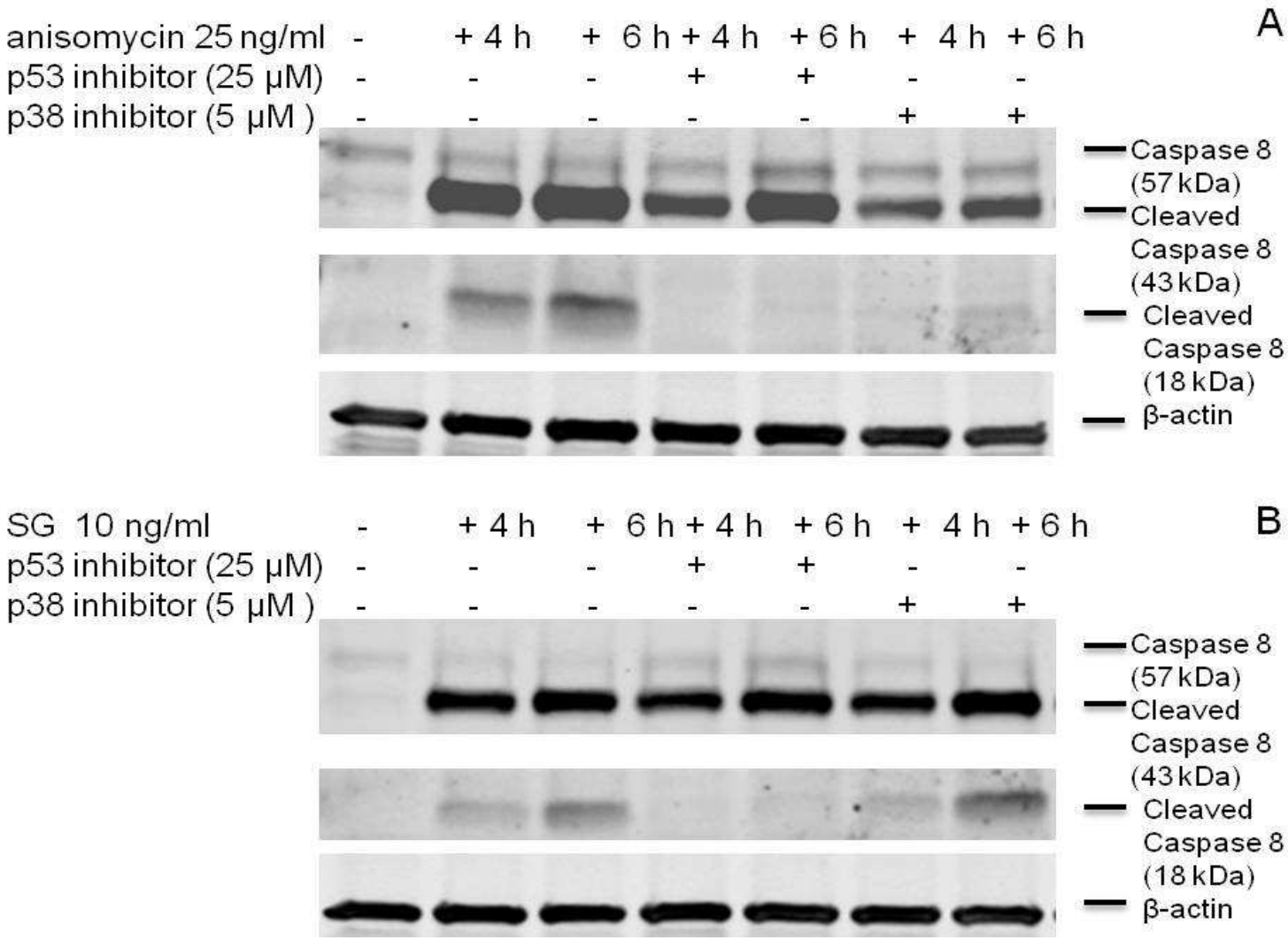

Figure 4.8. p38 inhibition suppresses only DON- and anisomycin-induced caspase 8 activation but p53 inhibition inhibits caspase 8 activation by all four toxins. Cells were pretreated with vehicle, p53 inhibitor pifithrin-μ (25 μM) or p38 inhibitor SB-203580 (5 μM) for 1 h prior to treatment of (A) anisomycin (25 ng/ml), (B) SG (10 ng/ml), (C) ricin (300 ng/ml) and (D) DON (1000 ng/ml) for 4 and 6 h, respectively. Cells were lysed and subjected to Western blotting with total and cleaved caspase 8. β-actin was also stained as loading control and shown at the bottom (A, B, C, D).

Figure 4.8 (cont'd)

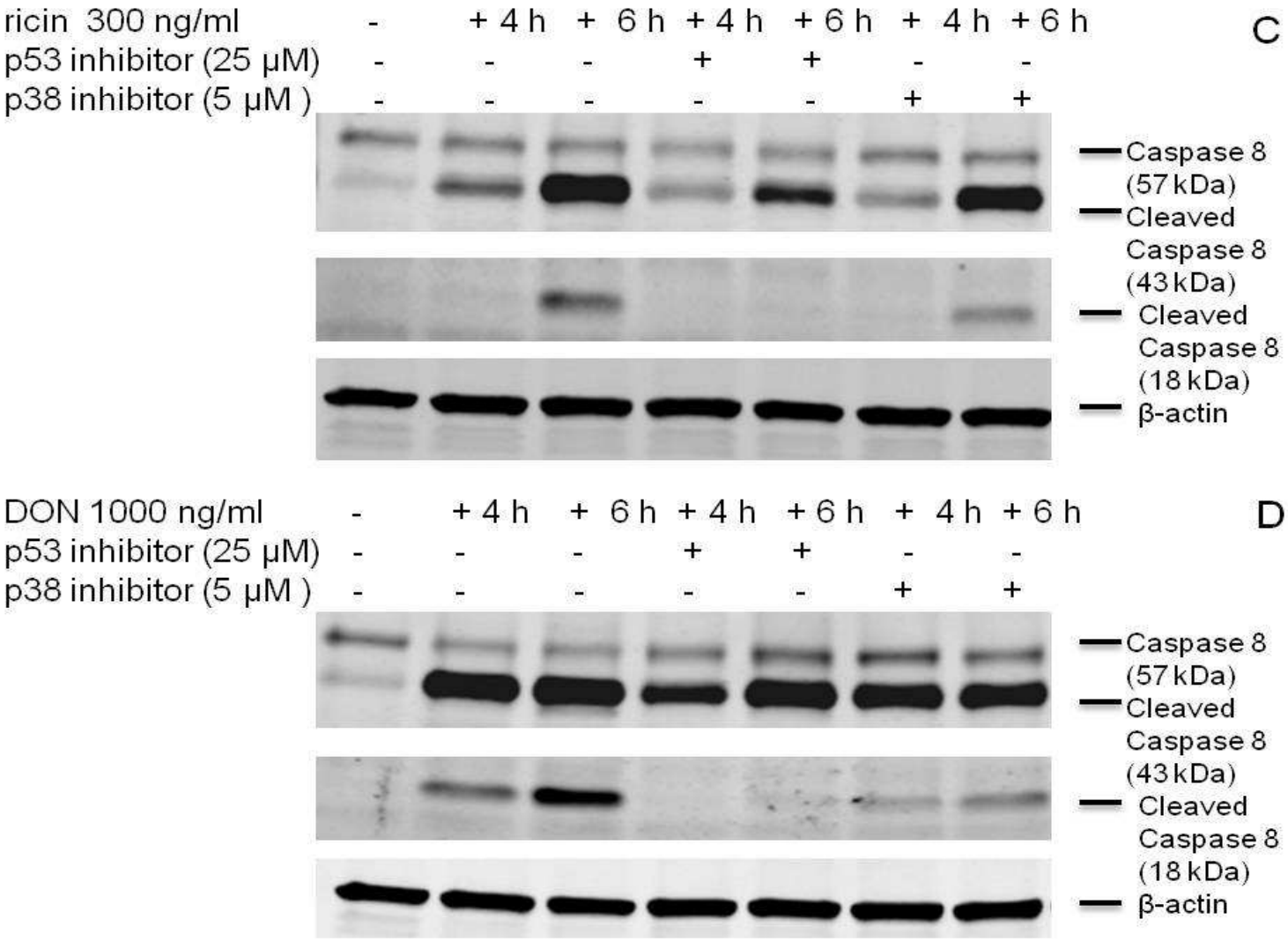

and proapoptotic Bcl-2 homologues (Droga-Mazovec *et al.*, 2008). A pan cathepsin inhibitor was found significantly to inhibit anisomycin-, SG-, ricin- and DON-induced rRNA cleavage (Fig. 4.9). Since cathepsin B and L derived from lysosomes are the most active cysteine cathepsins under neutral cytosolic pH (Boya and Kroemer, 2008), specific inhibitors for them were used to identify the executive cathespin. Cathepsin L inhibition significantly suppressed anisomycin-, SG-, ricin- and DON-induced rRNA cleavage (Fig. 4.9), while cathepsin B inhibitor had no inhibitory effect (data not shown). Thus, in addition to cathepsin L's known executive action during apoptosis, its activation also appears to be critical for rRNA cleavage.

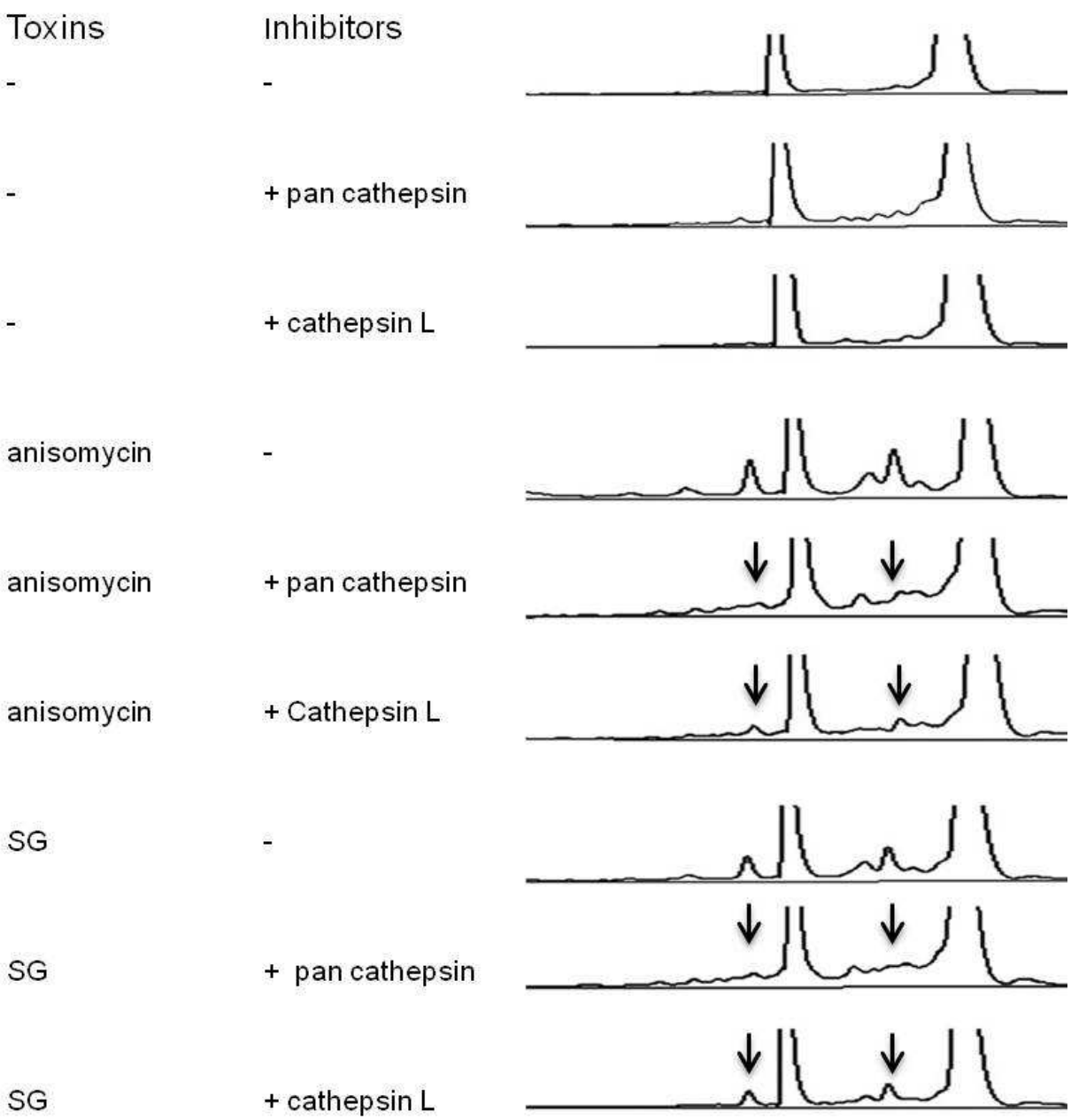

Figure 4.9. Cathepsin L is involved in anisomycin-, SG-, ricin- and DON-induced rRNA cleavage. Cells were pretreated with vehicle, pan cathepsin inhibitor (40 µM) or cathepsin L inhibitor (20 µM) for 1 h followed by anisomycin (25 ng/ml), SG (10 ng/ml), ricin (300 ng/ml) and DON (1000 ng/ml) exposure for 6 h, respectively. RNAs were analyzed by capillary electrophoresis as described in Fig. 1 legend. The results are representative of three separate experiments. Arrows indicate that fragmentation to major cleavage peaks is suppressed by inhibitors.

Figure 4.9 (cont'd)

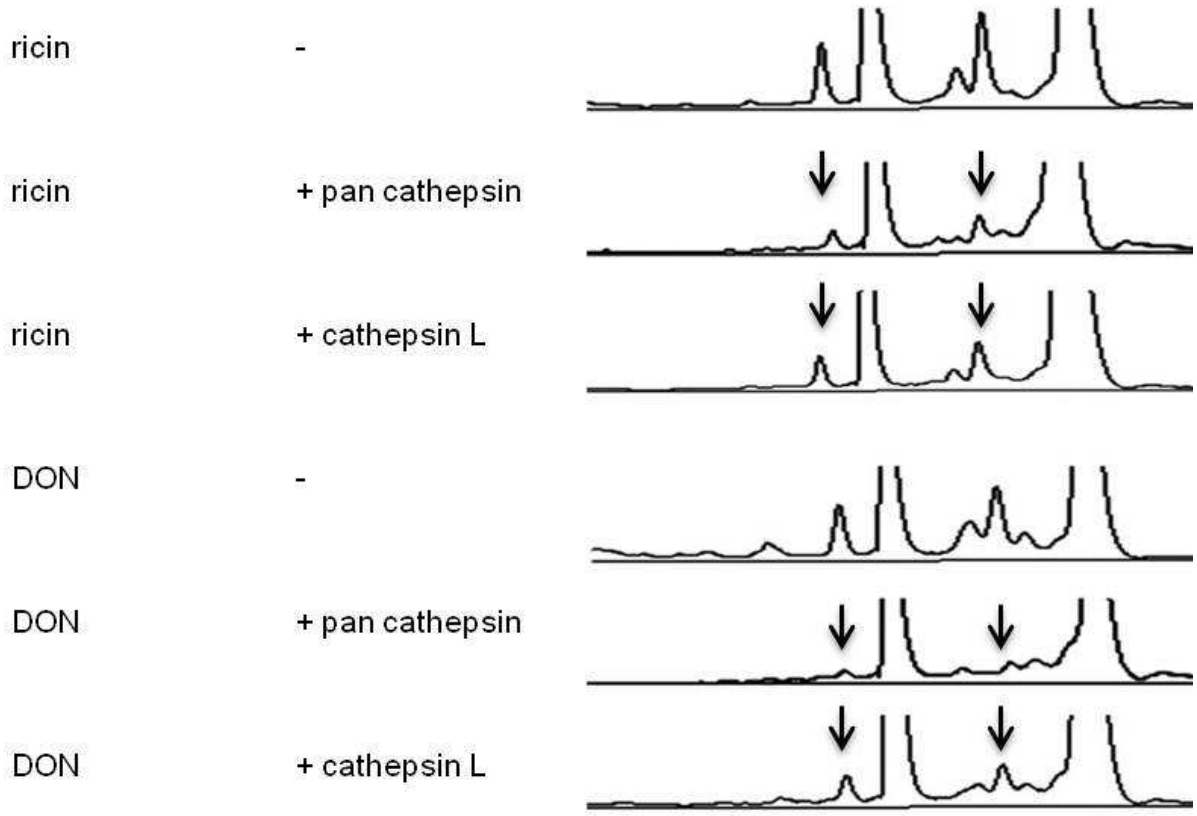

DISCUSSION

The results described here and in a previous study (He *et al.*, 2012) demonstrate that four ribotoxins DON, anisomycin, SG and ricin, although different in structure and activity, induce apoptosis-associated rRNA cleavage. Anisomycin triggered rRNA cleavage through the PKR/Hck-mediated extrinsic and intrinsic apoptotic pathways. In contrast, SG and ricin evoked rRNA cleavage via activation of p53 and caspase 8/9/3. These findings are consistent with the rapid induction of MAPK activation by DON and anisomycin, in contrast to the slower and weaker activation of MAPKs induced by SG and ricin. Notably, pan cathepsin and cathepsin L inhibitors markedly inhibited DON-, anisomycin-, SG- and ricin-induced rRNA cleavage. Taken together, ribotoxins appear to induce apoptosis and rRNA cleavage through conserved activation of p53 and caspases involving cathepsins, especially cathepsin L, but differed with respect to the roles of MAPKs (Fig. 10).

Apoptosis is mediated by intrinsic and extrinsic apoptotic pathways. The intrinsic pathway is characterized by mitochondrial dysfunction, release of apoptotic activators and sequential activation of casapase 9 and 3(Chandra *et al.*, 2004). Our data showed that anisomycin, SG and ricin can cause the cleavage of caspase 9, indicating they all activate intrinsic pathway. The extrinsic pathway is mediated by death receptors, the binding of ligands to which will recruit the procaspase 8 to the death-inducing signaling complex (DISC) via the interaction with FADD(von Roretz and Gallouzi, 2010). Inactive procaspase 8 is activated by sequential cleavage at Asp374/384 and Asp216, releasing small and large subunits (p10 and p18), which assemble into an active heterotetramer caspase 8 (Zhao *et al.*, 2010). We demonstrate here that DON, anisomycin, SG and

ricin all caused cleavage of procaspase 8 and generated an active p18 subunit, and this process was completely suppressed by p53 inhibitor. This result is consistent with previous studies that p53 upregulates caspase 8 expression (Ehrhardt *et al.*, 2008) and mediates caspase 8 activation in both transcription-dependent and -independent manners (Ding *et al.*, 2000; Yao *et al.*, 2007). In addition, p53 also induces cell apoptosis through cytochrome c release and caspase 9 activation (Soengas *et al.*, 1999; Schuler and Green, 2001; Zhou *et al.*, 2005a). As determined previously, p53 plays a pivotal role in caspase activation and induction of rRNA cleavage. Our data showed that inhibitors for p53 or caspases similarly inhibit these toxin-induced apoptosis-associated rRNA cleavage (Fig. 4.5), suggesting they are the conserved mediators for ribotoxin-induced rRNA cleavage.

It has been suggested that ribotoxins that share same binding sites on rRNA may initiate identical signal transduction (Iordanov *et al.*, 1997). Anisomycin and DON are small molecules that are proposed to freely diffuse through the cell membrane and bind to the peptidyl transferase center (PTC) on 28S rRNA (Iordanov *et al.*, 1997; Shifrin and Anderson, 1999), expecting to activate same signaling pathways. DON-induced in vivo and in vitro activation of PKR, Hck, p38, JNK and ERK has been well-documented(Pestka, 2010a) and subsequently signaling competing apoptotic (p38/p53/Bax/mitochondria/caspase-3) and survival (ERK/AKT/p90Rsk/Bad) signals in the macrophages(Zhou *et al.*, 2005a). Anisomycin rapidly activated MAPKs within 30 min (Fig. 4.3 A, B, C) as observed for DON and PKR, Hck and p38 inhibition suppressed anisomycin-induced rRNA cleavage, suggesting DON and anisomycin bind to the same site at the PTC of 28S rRNA and activate the identical signaling pathway.

Previous studies on anisomycin- and ricin-induced ribotoxic stress suggest that JNK activation is the hallmark response to translational inhibition or 28S rRNA depurination (Iordanov *et al.*, 1997; Ouyang *et al.*, 2005). Our data showed that a JNK inhibitor did not suppress anisomycin- and ricin-induced rRNA cleavage in RAW 264.7 macrophage but a p38 inhibitor did impair anisomycin/DON-induced rRNA cleavage, suggesting that ribotoxic stress induces multiple signaling pathways and evokes different biological effects, respectively. Furthermore, p38, but not JNK, appears to play a central role in mediation of small-PTC-binding-thranslation-inhibitor induced cell death and apoptosis-associated rRNA cleavage, representing by DON and anisomycin.

Ricin possesses N-glycosidase activity and inhibits translation by depurinating the 28S rRNA to induce apoptosis. Although the signaling pathway between depurination and apoptosis is not fully understood, it is generally accepted that inhibition of protein synthesis by RIPs triggers a mitochondrial stress response followed by loss of mitochondrial membrane potential (MMP), rapid release of cytochrome c and activation of caspase-9(Narayanan *et al.*, 2005). Consistent with that notion, our data showed that ricin-induced apoptosis-associated rRNA cleavage was mediated by p53 and caspase 8/9/3.

Lysosomes are acidic (pH ≤5), highly dynamic single-membrane bound organelles that contain hydrolytic enzymes to degrade intracellular macromolecules. Our findings suggest that lysosome-derived cathepsin L was a key protease in the rRNA cleavage induction. Cathepsins are the best characterized proteases in lysosome and include cysteine, serine (A and G) and aspartate cathespins(D and E)(Johansson *et al.*, 2010). In response to a variety of stress stimuli, prerequisite lysosomal

membrane permeabilization (LMP) and release of cathepsins into cytosol, especially cathepsin B, L and D which remain active at neutral cytosolic pH, promote apoptosis (Boya and Kroemer, 2008). LMP is suggested to be upstream of mitochondrial membrane permeabilization (MMP)(Terman *et al.*, 2006; Droga-Mazovec *et al.*, 2008). Active cathepsins are released upon LMP and cleave various protein substrates such as the intrinsic and extrinsic pathway linker pro-apoptotic BID and anti-apoptotic BCL-2 molecules (BCL-2, BCL-XL and MCL-1) leading to MMP, the central event in the intrinsic apoptotic pathway regulating the release of cytochrome c(Repnik and Turk, 2010). LMP-induced MMP is also proposed to contribute to LMP in an amplifying loop(Terman *et al.*, 2006).

LPM can be induced by a range of distinct agents and molecules, such as ROS, p53 and lysosomotropic agents(Boya and Kroemer, 2008). Anisomycin-, SG-, ricin- and DON-induced apoptosis-associated rRNA cleavage was suppressed by inhibitors of cathepsins and p53, suggesting that p53 might mediate ribotoxin-induced LMP and cathepsin release. p53 has been found to induce LMP in transcription-independent fashions (Johansson *et al.*, 2010). After being phosphorylated at Ser15, p53 translocates to the lysosome membrane and directly triggers LMP (Li *et al.*, 2007). Increased association of phospho-p53 (ser15) with lysosome not only destabilize lysosomal membrane but also concurrently increases the cytosolic cathepsin L activity(Fogarty *et al.*, 2010). Consistent with this model, pan cathepsins and cathepsin L inhibitors suppressed anisomycin-, SG-, ricin- and DON-induced rRNA cleavage. We speculated that p53 coordinates LMP- and MMP-dependent apoptotic pathways, as

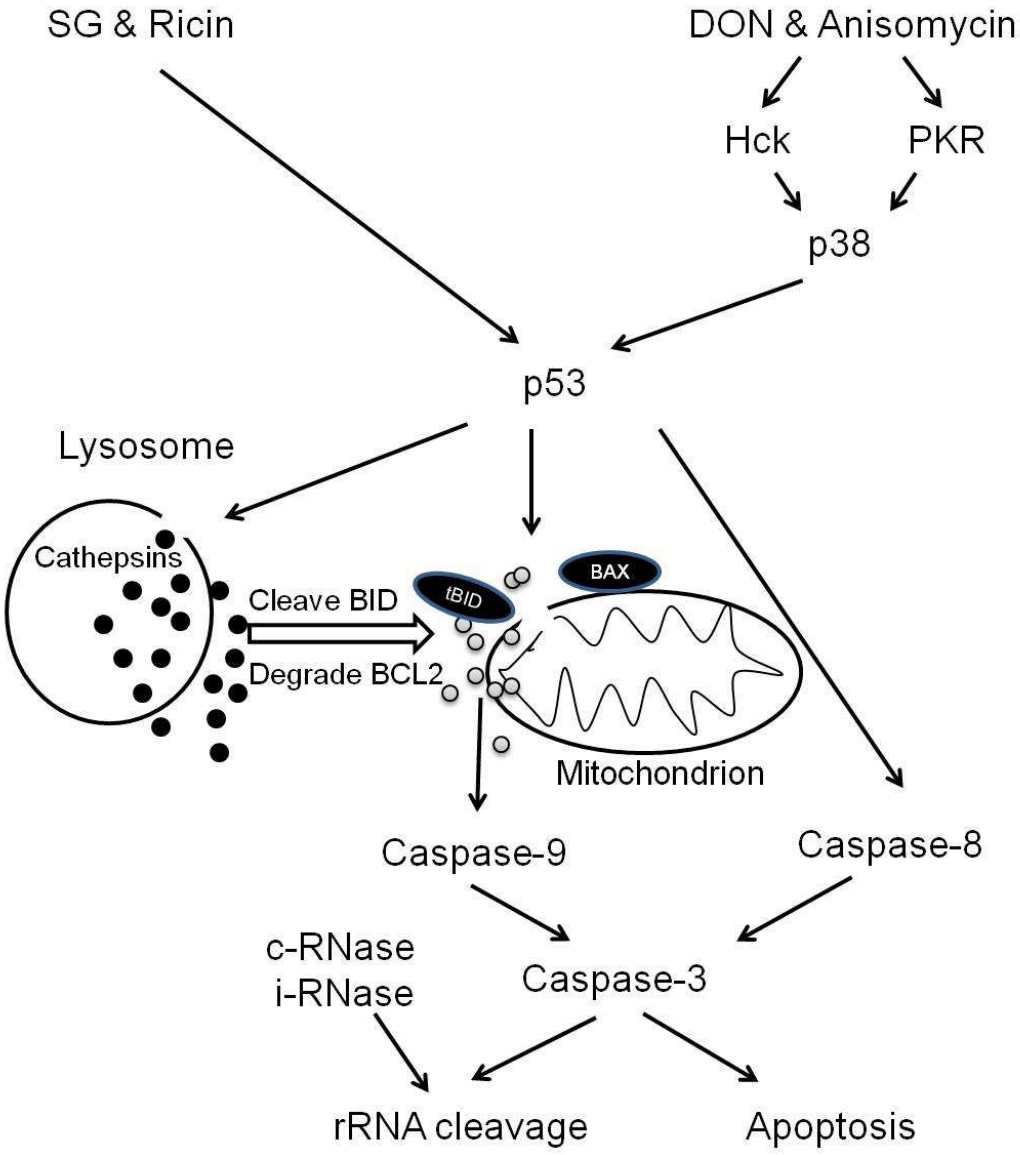

Figure 4.10. Model for ribotoxin-induced rRNA cleavage model in RAW 264.7 cells. Picture depicts putative signaling pathways for induction of rRNA cleavage by DON, anisomycin, SG and ricin. DON and anisomycin sequentially activate PKR/Hck, p38, p53 and caspases leading to apoptosis-associate rRNA cleavage, while SG and ricin activate p53 and caspases by an alternative mechanism. Cathepsin L seems released from lysosome and promotes DON-, anisomycin-, SG- and ricin-induced apoptosis and rRNA cleavage. Both constitutive (c) and inducible (i) RNases might contribute to the ribotoxin-induced cleavage of rRNA exposed by caspase action. Black and gray circles represent cathepsins and cytochrome c, respectively.

well as associated rRNA cleavage, However, the exact details of p53-mediated LMP and the crosstalk between LMP and MMP remain to be determined.

The results presented here and previously demonstrate that anisomycin, SG, ricin and DON caused apoptosis-associated rRNA cleavage via a conserved downstream signaling pathway (Fig. 4.10). DON- and anisomycin-induced rRNA cleavage requires prior sequential activation of PKR/Hck, p38, p53 and caspases, while SG and ricin activated p53 and caspases but this did not involve PKR, Hck and p38. Notably, lysosome and cathepsin L are also involved in mediation of ribotoxin-induced rRNA cleavage. Future work should focus on clarifying (1) the mechanisms by which lysosome membrane integrity is disrupted leading to release of cathepsins, (2) the role of cathepsin L in induction of apoptosis and rRNA cleavage, (3) crosstalk between lysosome-dependent and caspase-dependent apoptotic pathways and indentifying the executing RNases specifically cleaving rRNA, (4) the upstream signaling pathways by which SG and ricin activate p53. Ultimately, in vivo studies of the ribotoxin-induced apoptosis-associated rRNA cleavage are needed to establish the systemic biological significance of rRNA cleavage.

CHAPTER 5

Summary and future research

Low-molecular-weight (e.g. DON, anisomycin) and protein (e.g. ricin) ribotoxins are proposed to bind to or damage the 3'-end of 28S rRNA, respectively, to trigger the ribotoxic stress response. DON is a ribotoxin that commonly contaminates cereal-based foods and has the potential to adversely affect humans and animals. At low doses, DON partially inhibits translation, induces PKR-mediated MAPK activation and upregulates mRNA stability of proinflammatory genes. However, the relationship between DON-modulated transcription and translation of inflammatory genes is unclear. In contrast, high doses of DON cause immunosuppression by evoking apoptosis and rRNA cleavage. DON and ricin both induce common ribosomal RNA cleavage at A3560 and A4045 on 28S rRNA in RAW 264.7 macrophages. However, mechanisms of rRNA cleavage are not understood.

The first major finding in this thesis is that while DON-altered translation of inflammation-associated genes was predominantly driven by selective transcription, a small subset of these genes might further be regulated at the translational level. By comparing DON-induced changes in profiles of polysome-associated mRNA transcripts (translatome) to total cellular mRNA transcripts (transcriptome) in the RAW 264.7 murine macrophage model (Chapter 2), we demonstrated DON induced robust expression changes in inflammatory response genes including cytokines, cytokine receptors, chemokines, chemokine receptors, and transcription factors, which were remarkably similar in translatome and transcriptome. Over 70 percent of DON-regulated genes in the translatome and transcriptome overlapped. When expression changes of a total of 17 selected cytokine, chemokine, receptor, transcription factor and inflammatory response genes in the polysome and cellular mRNA pools were confirmed by real-time

PCR in a follow-up study, coordinate regulation of the translatome and transcriptome was evident. However, modest differences in expression of some genes were again detectable, indicating that translational regulation exists in DON-modulated expression of inflammatory response proteins.

Second, we demonstrated that DON-induced rRNA cleavage involves the sequential activation of PKR/Hck/p38/p53/caspase 8/9/3, which is associated with apoptosis (Chapter 3). In addition, Northern blot analysis revealed that DON exposure induced six rRNA cleavage fragments from 28S rRNA and five fragments from 18S rRNA, indicating that both 28S and 18S rRNAs are ribotoxic stress sensors. Interestingly, anisomycin, SG and ricin also induced specific rRNA cleavage profiles identical to those of DON (Chapter 4). In contrast, DON- and anisomycin activated p53 by an upstream PKR/Hck/p38 while SG and ricin activated p53 by an alternative mechanism. Further studies found that cathepsins, especially cathepsin L, are also involved in ribotoxin-induced rRNA cleavage. Taken together, all four ribotoxins induced cathepsin-involved apoptosis-associated rRNA cleavage via conserved downstream pathway p53→caspase 8/9→caspase 3 mediated by different upstream pathways. Future studies should focus on identification of executive RNase. Although the mRNA and protein level of RNase L are regulated upon DON exposure(Li and Pestka, 2008), the *in vivo* transfection of RNase L activator, 2-5A, and *in vitro* incubation of RNase L, 2-5A with purified ribosomes did not induce rRNA cleavage. It is possible that another RNase other than RNase L is the executive RNase. To narrow down the scope of potential candidates, exact rRNA cleavage sites may be identified by purification of rRNA fragment followed by cDNA synthesis and rapid amplification of cDNA ends

(RACE). Based on the sequence of cleavage sites, we can filter the RNases processing the enzymatic activity to cause the specific cleavage. An alternative possibility is that RNase L may cooperate with caspases to evoke rRNA cleavage, which could damage the ribosome at specific region and render rRNA to RNase. To test this hypothesis, ribosomes could be pre-incubated with active caspases with and without DON followed by addition of activated RNase L or other candidate RNase. In addition, the roles of the lysosome and cathepsin L in ribotoxin-induced apoptosis-associated rRNA cleavage could be investigated.

APPENDICES

Appendix A

Role of Double-stranded RNA-Activated Protein Kinase (PKR) in Ribotoxic Stress Response

ABSTRACT

A number of natural fungal, bacterial and plant toxins are capable of targeting the ribosome and activating the mitogen-activated protein kinases via a process called the ribotoxic stress response (RSR). Although double-stranded RNA-activated protein kinase (PKR) has been identified to be an upstream mediator of RSR, how it initiates signaling via the ribosome is poorly understood. The purpose of this study was to develop a cell-free model for ribotoxin-induced PKR activation and use it to explore the role of ribosomal RNA in the activation process. Exposure of Hela cells to the ribotoxin deoxynivalenol (DON), a trichothecene mycotoxin, activated p38 and JNK within 5 and 15 min respectively, both of which were suppressed by the PKR inhibitor 2-AP. Using Hela lysate preparations as a cell-free model, DON, anisomycin and ricin were found to concentration-dependently induce robust autophosphorylation of PKR which could be blocked by selective PKR inhibitors. When time course of ribotoxin-induced phosphorylation of PKR and its substrate eIF2α were studied, DON (250 ng/ml) rapidly induced PKR activation within 5 min and robust activation of eIF2α at 15 min. In contrast, anisomycin (20 ng/ml) and ricin (20 ng/ml) induced phosphorylation of PKR at 30 min and eIF2α activation at 30 and 60 min, respectively. Ribotoxin treatment for 30 min did not impact RNA integrity, suggesting PKR activation did not require rRNA cleavage. RNA immunoprecipitation (RIP) was conducted with PKR-specific antibody on vehicle and DON-treated Hela extracts and sequences of recovered rRNAs were determined by Illumina cloning. Based on the number and types of clones isolated, sequences fell into three categories: (1) common (shared and equivalent in vehicle and DON-treated samples) (e.g. 28S-C1: 2790-2960 nts, 28S-C2: 3590-3970 nts and 18S-

C1: 80-350 nts); (2) inducible common (shared between groups but elevated in DON-treated sample) (e.g. 28S-IC1: 0-430 nts, 28S-IC2: 2370-2620 nts and 18S-IC1: 820-930 nts); (3) unique to DON-treated sample (e.g. 28S-U1:1816-1873 nts, 28S-U2:4049-4132 nts and 18S-U1:668-699 nts). An RNase protection assay was devised to compare relative amounts of these sequences in RIP preparations from the control and treated groups. In a preliminary experiment, two unique (28S-U2 and 18S-U1) and one inducible common sequences were found to be equivalent in RIP RNA from control and DON-treated Hela lysate by RNase protection assay. Further quantitative analyses are on the way for these sequences. Taken together, PKR appears to associate with both 18S and 28S rRNA prior to and during activation by DON, anisomycin and ricin in an rRNA cleavage-independent manner.

INTRODUCTION

Several natural ribosome-targeting toxins exist that are capable of activating MAPKs via a process termed the “ribotoxic stress response (RSR)” (Iordanov et al., 1997). As initially proposed, damage to 28S rRNA perturbs the 3′-end of the large 28S ribosomal RNA, which functions in aminoacyl-tRNA binding, peptidyltransferase activity, and ribosomal translocation, resulting in activation of p38, JNK and ERK1/2 and subsequent upregulation of gene expression.

Ribotoxins can be either low molecular weight or proteins. Low-molecular-weight ribotoxins, such as the trichothecene mycotoxins and the antibiotic anisomycin, bind directly to the ribosome and inhibit protein synthesis. Several trichothecenes including T-2 toxin, nivalenol and deoxynivalenol (DON), produced by *Fusarium*, were found to trigger marked RSR and activate JNK and p38 (Shifrin and Anderson, 1999; Yang *et al.*, 2000). Consistent with the notion that inhibitors sharing common binding sites initiate identical signaling pathways, the peptidyl transferase center (PTC)-binding antibiotic anisomycin also strongly activates JNK and p38 (Xiong et al., 2006).

Ribosome-inactivating proteins (RIPs), a different class of ribotoxins, contain an RNA N-glycosidase domain that specifically cleaves a conserved adenine off the eukaryotic 28S rRNA. Ricin from castor bean is a prototypic Type 2 RIP. It specifically targets a adenine nucleoside residue in the “Sarcin/Ricin loop” on eukaryotic rRNA (Endo and Tsurugi, 1986) in cell-free conditions. Ricin causes cleavage at two additional sites on 28S rRNA at A3560 and A4045 in the RAW 264.7 model (Li and Pestka, 2008). Ricin potently activates JNK and SEK1/MKK4 to induce the expression of the immediate-early genes c-fos and c-jun(Iordanov et al., 1997). Furthermore, ricin

induces robust JNK-mediated activation of NF-κB at 6 h, knockdown of which by siRNA results in decreased mRNA level of various pro-inflammatory genes including CXCL1, CCL2, IL-8, IL-1b and TNF- α, suggesting ricin-induced expression of these genes is downstream event of RSR (Wong *et al.*, 2007b). In addition, ricin induces expression of IL-1β by sequentially activating MAPKs and NF-κB, which upregulate expression of pro-IL-1β that is converted to mature IL-1β via the Nalp3 inflammasome(Jandhyala et al., 2012).

Double-stranded RNA protein kinase (PKR) has been proposed to be a critical upstream mediator of RSR based on initial studies in the RAW 264.7 macrophage(Zhou *et al.*, 2003b). PKR is a widely-distributed constitutively-expressed serine/threonine protein kinase that can be activated by dsRNA, interferon, proinflammatory stimuli, cytokines and oxidative stress(Williams, 2001; Garcia et al., 2006) and has diverse functions including controlling cell growth, tumor suppressing, apoptosis, and antiviral infection(Koromilas et al., 1992; Lengyel, 1993; Chu et al., 1999). PKR contains two double-stranded RNA binding domains (DSBDs) and one kinase domain whose activity is autoinhibited by DSBD in an intramolecular manner. After binding to dsRNA, PKR is activated by dimerization and autophosphorylation. Activated PKR phosphorylates eIF2α at serine 51, therefore increasing its affinity for the GTP exchange factor eIF-2β and resulting in translation inhibition (Sudhakar et al., 2000). Additionally, PKR activates various factors including signal transducers and activator of transcription (STAT), interferon regulatory factor1 (IRF-1), p53, JNK, p38 and NF-κB(Verma et al., 1995; Williams, 1999; Williams, 2001) and regulates the expression of proinflammatory genes. In RAW 264.7 macrophages treated with DON, PKR is activated within 5 min as

evidenced by its autophosphorylation and the phosphorylation of its downstream substrate eIF2α(Zhou *et al.*, 2003b). DON-induced MAPK activation is suppressed by the PKR inhibitors, 2-aminopurine (2-AP) and adenine. When human a U-937 monocyte cell line is transfected with PKR antisense RNA, there are significantly reduced MAPK responses to DON treatment. In addition, PKR inhibition also suppresses the DON-induced expression of cytokines and chemokines, including TNF-α, MIP-2(Pestka *et al.*, 2004), IL-8(Gray and Pestka, 2007) and IL-6(Shi and Pestka, 2009). Pretreatment of PKR inhibitors also suppress, ricin and Shiga toxin-induced IL-8 expression(Gray and Pestka, 2007). Furthermore, DON, anisomycin, and emetine induce DNA fragmentation and activated caspase-3 in human macrophages but not in PKR-deficient cells, suggesting PKR is required for apoptosis induction by translational inhibitors(Zhou *et al.*, 2003b).

Within mammalian cells, PKR associates with 60S ribosomal subunits via its two double-stranded RNA binding domains (DRBDs) and kinase domain(Wu *et al.*, 1998; Kumar *et al.*, 1999). Overexpression of the ribosomal large subunit protein L18 (RPL18) cause it to interact with DRBDs of PKR, apparently inhibiting autophosphorylation of PKR and PKR-mediated eIF2α in vitro by competing with dsRNA and reversing dsRNA binding to PKR (Kumar et al., 1999). Deletions or residue substitutions in the DRBD sequences block its interaction with both dsRNA and RPL18.

PKR has also been found to have a novel role in forming a functional complex by direct binding to p38 and/or Akt, which permits PKR to effectively regulate their inhibition/activation (Alisi et al., 2008). Rapid ribosomal association and/or activation of PKR, Hck, p38 and ERK have also been observed in DON-treated macrophages (Bae

et al., 2010). Our lab has further found that DON recruits p38 to the ribosome in normal but not in PKR-deficient macrophages, again suggesting that PKR is required for DON-induced p38 activation (Bae *et al.*, 2010). Taken together, PKR appears to sense ribotoxins and/or translational inhibition and be activated to trigger downstream signaling pathways.

The mechanism by which PKR is activated by DON and other ribotoxins is unknown. Here, we hypothesized that PKRs are associated with rRNA and activated upon ribotoxin exposure. We employed the Hela-based cell-free translation system and found that DON, anisomycin and ricin exposure dose-dependently induced rapid and robust phosphorylation of PKR and its substrate eIF2α, which did not temporally correlate with rRNA cleavage. RNA immunoprecipitation (RIP) and RNase protection assay results suggested that PKR bound to both 18S and 28S rRNA, which might enable it to “sense” small perturbations in rRNA tertiary structure leading to kinase activation.

MATERIALS AND METHODS

Hela cell culture. Hela cells (ATCC, Rockville, MD) were cultured in ATCC-formulated Dulbecco's modified Eagle's medium (DMEM) supplemented with 10% (v/v) fetal bovine serum (Atlanta Biologicals, Lawrenceville, GA), streptomycin (100 μg/ml) and penicillin (100 U/ml) at 37 ^{o}C in a humidified atmosphere with 5% CO_2. The cell number and viability were assessed by trypan blue dye exclusion using a hematocytometer. Prior to DON exposure, cells (2.5 x 10^6/plate) were seeded and cultured in 100-mm tissue culture plates for 24 h to achieve approximately 80% confluency.

Hela lysate. A human *in vitro* protein expression kit containing Hela extract was purchased from Thermo Scientific (Wilmington, DE). The Hela lysate contains necessary cellular components for protein synthesis including ribosome, tRNA, initiation, elongation and termination factors. Upon arrival, the lysate was aliquoted and stored at -80 ℃.

Kinase assay. DON-, anisomycin- and ricin-induced PKR phosphorylation of PKR and its substrate eIF2α was determined in Hela cell-free system by kinase assay. The kinase incubation mixtures (50 μl) typically contained 50 μg Hela lysate, 15 mM HEPES-KOH, pH 7.4, 5 mM Mg(OAc), 20 mM KCl, 1 mM DTT, 1 x Halt protease phosphatase inhibitor cocktail (Thermo Scientific), 1 mM EDTA and 0.1 mM ATP. Selected concentrations of toxins with or without inhibitors 2-AP and C16 were added to kinase assay mixture, respectively. Poly (IC) at 100 ng/ml was used as positive control. After incubation at 30 ℃ for 20 min, the reactions were stopped by Laemmli SDS sample buffer (Bio-Rad, Hercules, CA) and analyzed by Western Blot.

Western analysis. Proteins were separated on 4-20% Mini-Protean TGX Precast Gel (Bio-Rad) and then proteins transferred to an Immobilon-FL membrane (Millipore, Billerica, MA). After incubating with blocking buffer (Li-Cor, Lincoln, NE) for 1 h at 25 ℃, membranes were incubated with mouse monoclonal anti-PKR antibody (Santa Cruz) (1:1000 dilution in Li-Cor blocking buffer); rabbit polyclonal anti-PKR (pT451) phospho-specific antibody (Invitrogen, Carlsbad, CA) (1:1000 dilution in Li-Cor blocking buffer); mouse monoclonal anti-eIF2α (Cell Signaling, Beverly, MA) (1:1000 dilution in Li-Cor blocking buffer); rabbit polyclonal anti-phospho-eIF2 (Ser51) antibody (Cell Signaling) (1:1000 dilution in Li-Cor blocking buffer) overnight at 4 ℃, respectively. Blots were washed three times of 10 min with Tris-Buffered Saline and Tween 20 (TBST) (50 mM Tris-HCl, 150 mM NaCl, 0.1% Tween 20, pH 7.5), and then incubated with secondary IRDye 680 goat anti-rabbit and/or IRDye 800CW goat anti-mouse IgG antibodies (Li-Cor) (1:3000 dilution in Li-Cor blocking buffer) for 1 h at 25 ℃. After washing three times, infrared fluorescence from these two antibody conjugates were simultaneously measured using a Li-Cor Odyssey Infrared Imaging System (Lincoln, Nebraska).

Immunoprecipitation of rRNA-PKR complex. PKR immunoprecipitation was performed using RNA ChIP Kit from Active Motif (Carlsbad, CA), following the manufacturer's instructions with modifications. Briefly, Hela lysate containing ribosomes as well as PKR in kinase buffer supplemented with 0.1 mM ATP were incubated with vehicle or 250 ng/ml of DON at 30 ℃ for 20 min. Rea ction mixtures were fixed in 1% formaldehyde for 10 min at RT. After adding glycine stop-fix solution provided in the kit for 5 min at RT, the fixed ribosome-PKR complexes were pelleted on a 10% sucrose cushion (10% sucrose, 15 mM Tris pH7.4, 50 mM KCl, 10 mM MgCl2, 1 mM DTT, 1 x

Halt protease and phosphatase inhibitor cocktail, 1 mM EDTA) by ultracentrifuge with a Sorvall TH641 rotor (Thermo Fisher Scientific, Asheville, NC) at 200,000 x g for 3 h at 4 ℃. The pellets were then resuspended in shearing buffer (provided in the kit) and sheared by a 60 Sonic Dismembrator (Fisher Scientific, Pittsburg, PA) with optimized shearing conditions of power 40%, 5 pulses of 20 seconds each with a 30 sec rest on ice between each pulse. The resultant RNA from that treatment was primarily between 100-500 nucleotides based on capillary electrophoresis.

Immunoprecipitation was conducted by adding rabbit polyclonal anti PKR (K-17) antibody (Santa Cruz, CA) (2 µg/100 µl IP reaction) to sheared rRNA-PKR complex, as well as protein G magnetic beads, RNase inhibitor and protease inhibitors cocktail provided in the Kit, and incubated overnight at 4 ℃. After washing with RNA-ChIP wash buffers, the IP complexes were eluted with provided elution buffer and then collected by Magnet. The supernatant containing PKR-bound rRNA fragments were then digested by adding 5 µl proteinase K (provided in the kit) at 42 ℃ for 1 h and reversed cross-linking by incubation at 65 ℃ for 1.5 h. The specific PKR-bound rRNA fragments were extracted by TRI reagent solution from Ambion (Carlsbad, CA) and BPC (1-bromo-3-chloropropane) phase separation reagent from Molecular Research Center Inc. (Cincinnati, OH) according to the manufacturer's protocol. rRNA concentrations were measured using a Nanodrop reader (Thermo Fisher, Wilmington, DE). Fragmentation of rRNA was assessed by capillary electrophoresis using an Agilent 2100 Bioanalyzer with a Nano Chip (Agilent, Santa Clara, CA) according to manufacturer's instruction.

Cloning and sequencing of PKR associated rRNA fragments. Purified immunoprecipitated rRNA was cloned at the Genomics Core of Michigan State

University Research Technology Support Facility using the methods previously described (Illumina Inc. San Diego, CA). Briefly, the rRNA fragments were first treated with antarctic phosphatase (New England Biolabs) and subsequently T4 polynucleotide kinase (Illumina Inc.). Specific 5' (5'-GUUCAGAGUUCUACAGUCCCAC ACGAUC-3') and 3' (5rApp/ATCTCGTATGCCGTCTTCTGCTTG/3ddC) adapters were then ligated onto the RNA fragments, respectively, and the resulting molecules were reverse transcribed using a primer complementary to the 3' adapter (CAAGCAGAAGACGGCATACGA). The cDNA was then amplified by PCR using forward primer: GAAGCAGAAGACGGCATACGA and reverse primer: AATGATACCGCGACCAC CGACAGGTTCAGAGTTCTACAGTCCGA. The resulting double-stranded DNA was cloned into pCR2.1 vector (Invitrogen) and transformed into chemically competent One-Shot TOP10 cells (Invitrogen). After shaking at 37 ℃, 250 rpm, for 1 h, the cells were spread on LB plate with 100 µg/ ml Ampicillin and cultured at 37 ℃ overnight. Transformed single colonies were selected and sequenced using the M13 forward primer and Applied Biosystems BigDye terminator v3.1 chemistry on an Applied Biosystems 3730xl sequencer. The resulting sequences were then aligned to human 18S (NCBI Reference Sequence: NR-003286.2) and 28S (NCBI Reference Sequence: NR_003287.2) ribosomal RNA genes.

RNase protection assay. RNase protection assay was performed using RPA III™ Ribonuclease Protection Assay Kit (Invitrogen) following the manufacturer's instructions. Briefly, 500 ng RIP RNA and 500 pg ^{32}P labeled probe (Table 5.1) were precipitated by 70% ethanol, resuspended in 10 µl hybridization buffer, denatured at 95 ℃ for 5 min and incubated overnight at 42 ℃. Then 150 µl RNase A/T1 solution

(1:100 dilution in RNase digestion III buffer) were added and incubated at 37 ℃ for 30 min followed by adding 225 µl RNase Inactivation/precipitation III solution. Tubes were vortex, centrifuged briefly and stored at -80℃ for 30 min. RNA were precipitated by centrifugation at 19,000 x g for 15 min, resuspended in 10 µl RNA loading buffer and denatured at 95 ℃ for 5 min. The resultant RNA was separate on 15% Urea-PAGE. The gels were assembled with the Hyblot autoradiography film (Denville, Metuchen, NJ) into an X-ray exposure cassette and the film was developed after 24 h.

Table 1 Table A.1 Probes for RNase protection assay.

Probes	Sequence	Length
28s-U1	1821-CACTAGGCACTCGCATTCCACGCCCGGCTCCAC-1843	33
28s-U2	4074-GCCAGAAGCGAGAGCCCCTCGGGGCTCGCCCCCCCGCCTCACC GGGTCAG-4123	50
28s-IC1	369-CGCCCTCTTGAACTCTCTCTTCAAAGTTCTTTTCAACTTTCCCTTAC-414	47
28s-IC2	2387-CCCATGTTCAACTGCTGTTCACATGGAACCCTTCTCCACTTCGGCC TTC-2437	49
18s-U1	673-GCCCGCTCCCAAGATCCAACTACGAGC-699	27
18s-IC1	1029-CCGACTTTCGTTCTACGACGGTATCTGATCGTCTTCGAACCTC-1072	43
28s-NC	896-TGCCGGGGGGGGCTGTAACACTCGGGGGGGGTTTC-929	34
18s-NC	1812-GAAACCTTGTTACGACTTTTACTTCCTCTA-1841	30

RESULTS

DON induces PKR-mediated activation of p38 and JNK in Hela cells.

The suitability of using Hela cells to study ribotoxic stress was initially assessed. Western blotting revealed that DON at 500 ng/ml induced robust phosphorylation of p38 in 5 min, which was maximal at 15 min and lasted up to 2 h (Fig. A.1A). DON also transiently induced phosphorylation of JNK at 15 and 30 min (Fig. A.1B). The PKR inhibitor 2-AP concentration-dependently suppressed the activation of p38 (Fig. A.2A) and of JNK (Fig. A.2B). These data were consistent with DON-induced PKR-mediated p38 activation in RAW 264.7 cells(Zhou *et al.*, 2003b), suggesting that Hela cells are a viable model to study DON-induced PKR activation and RSR.

DON induces PKR activation in Hela cell-free system

Activation of PKR induces autophosphorylation and phosphorylation of eIF2α at serine 51 (Sudhakar et al., 2000). The effects of DON on PKR activity were evaluated in Hela cell-free system. Using the PKR activator poly (IC) as a positive control, it induced robust PKR activation at 100 ng/ml, while ATP, the phosho-group donor, also induced basal level PKR autophosphorylation at 0.1 mM (Fig. A.3). DON dose-dependently induced PKR phosphorylation in Hela lysates, the activation of which was markedly suppressed by the PKR inhibitors 2-AP (2 mM) and C-16 (2 µM) (Fig. A.3). When the kinetics of PKR and eIF2α activation were measured, DON at 250 ng/ml was found to transiently activate PKR as early as 5 min, and this was attenuated at 15 min (Fig. A.4). Similarly, eIF2α was phosphorylated at 5 min, which was maximal at 15 min (Fig. A.4). These data suggested that the Hela extract assay mixture contained necessary functional components for DON-induced PKR activation under cell-free conditions.

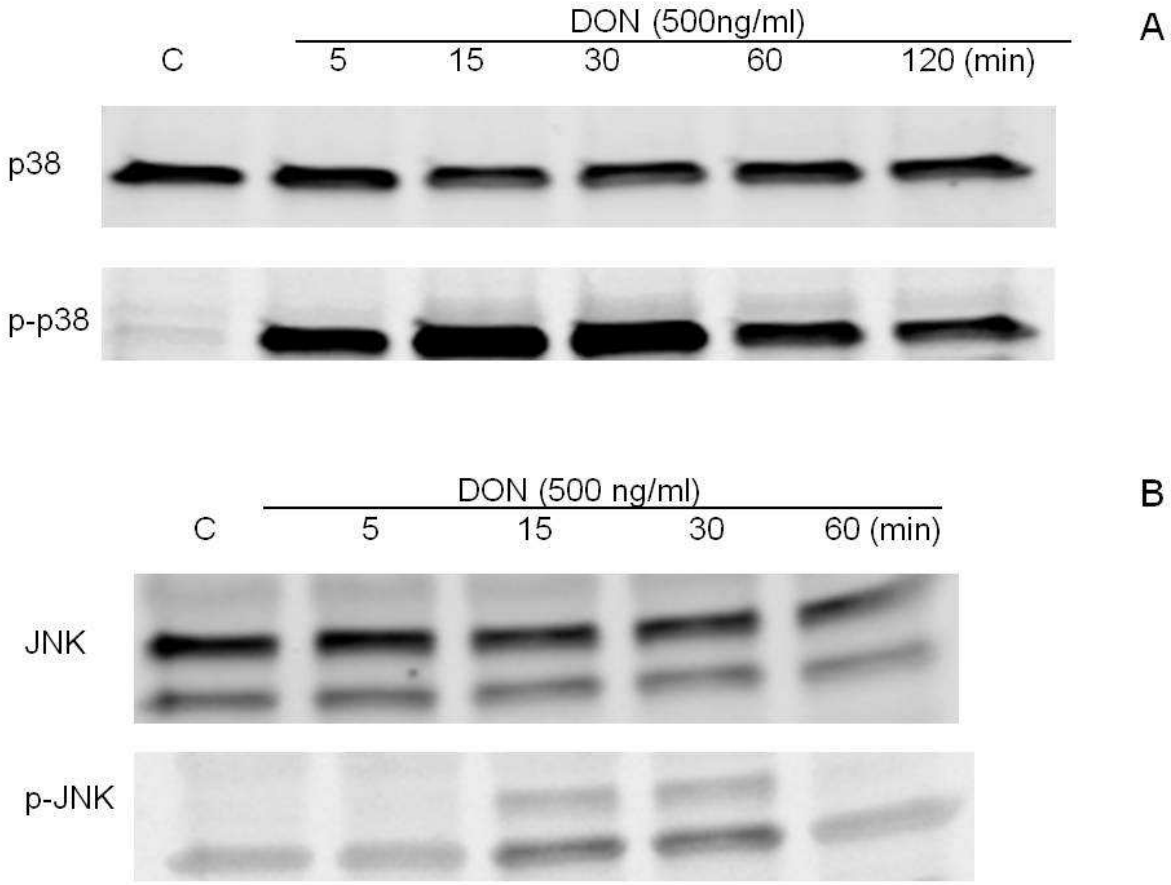

Figure A.1. DON induces phosphorylation of p38 and JNK in Hela cells. Hela cells were treated with 500 ng/ml of DON for 0, 5, 15, 30, 60, 120 min followed by cell lysis and Western blot analysis with total and phosphorylated (A) p38 and (B) JNK.

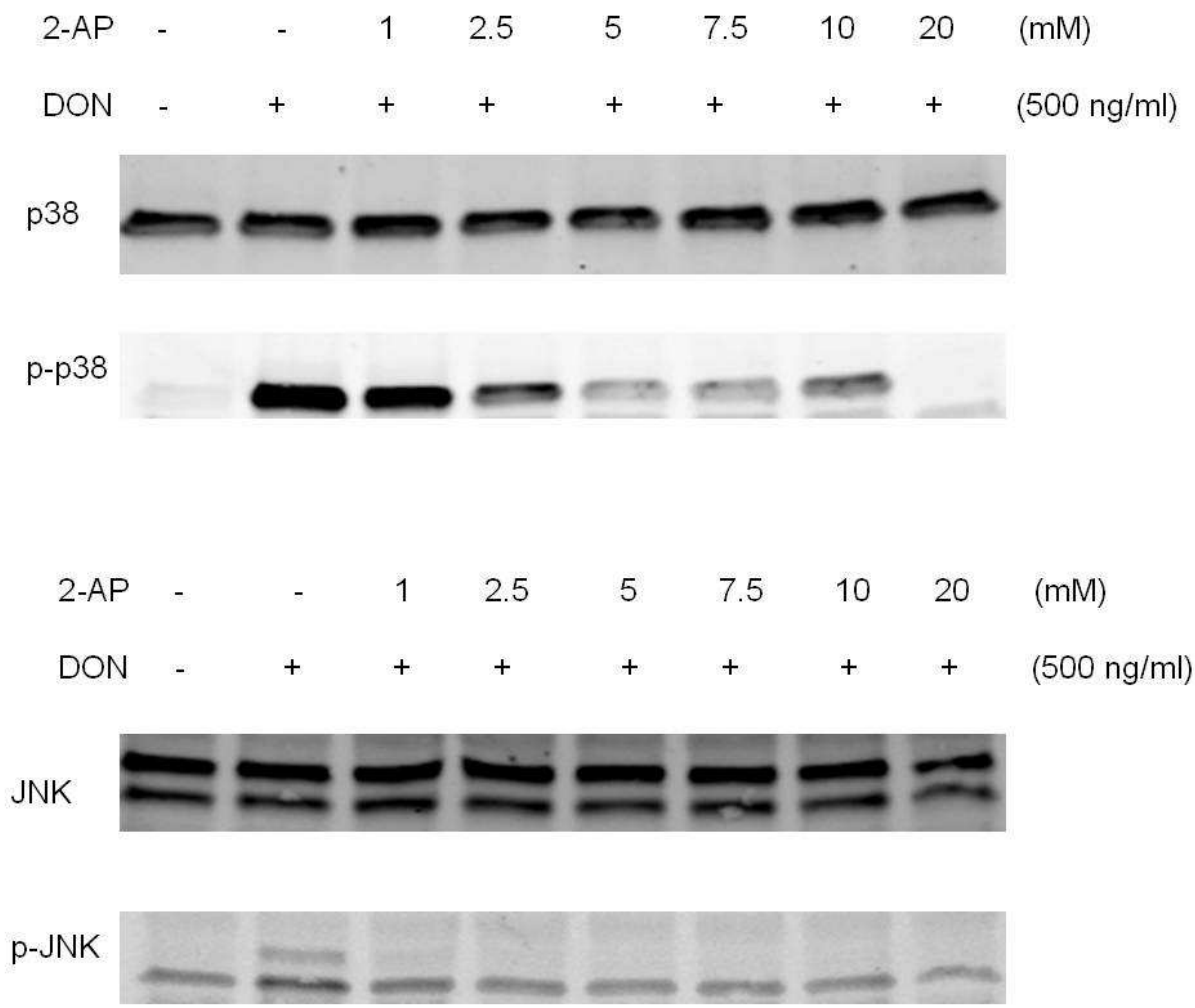

Figure A.2. DON-induced p38 and JNK phosphorylation can be dose-dependently suppressed by the PKR inhibitor 2AP in Hela cells. Hela cells were pretreated with the PKR inhibitor 2-AP at 1, 2.5, 5, 7.5, 10, 20 mM for 1 h followed by 500 ng/ml DON exposure for 15 min and subjected to Western blot analysis for total and phosphorylated (A) p38 and (B) JNK.

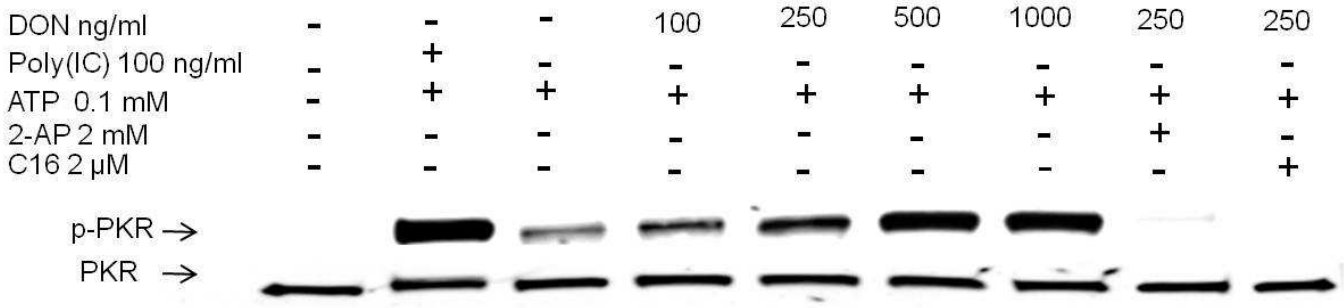

Figure A.3. DON induces PKR phosphorylation in a Hela-based cell-free system. Selected concentrations of DON (100, 250, 1000 ng/ml), 100 ng/ml Poly (IC) and the PKR inhibitors, 2-AP (2mM) and C16 (2 µM), were added into kinase assay buffer, respectively, and incubated for 20 min at 30 ℃ followed by Western ana lysis with PKR and p-PKR antibodies.

Anisomycin and ricin induce PKR activation in the Hela cell-free system

The effects of anisomycin, a low-molecular-weight antibiotic translational inhibitor, on PKR activation and activity were also evaluated in Hela cell-free system. Anisomycin dose-dependently induced phosphorylation of PKR (Fig. A.5), which was markedly suppressed by the PKR inhibitor 2-AP (2 mM) and C16 (2 μM). When the kinetics of PKR activation and its substrate eIF2α were measured, anisomycin at 20 ng/ml was found to markedly activate PKR at 30 min (Fig. A.6). Subsequent phosphorylation of eIF2α was detected at 30 and 60 min respectively (Fig. A.6).

The effect of ricin on the activation of PKR and eIF2α was also determined in the cell-free system. Ricin induced activation of PKR in a concentration-dependent manner beginning at 10 ng/ml. The PKR inhibitors 2-AP and C16 were found to suppress ricin-induced PKR activation (Fig. A.7). When activation of PKR and eIF2α was measured at 5, 15, 30 and 60 min respectively, ricin induced phosphorylation of PKR at 30 min and eIF2α at 60 min (Fig. A.8).

PKR is activated in the absence of obvious rRNA cleavage.

DON has been previously found to induce six cleavage fragments from 28S rRNA and five fragments from 18S(He et al., 2012). It was speculated that the resulting rRNA fragments might fold into a double-stranded structure that would be capable of activating PKR. The kinetics of rRNA cleavage were therefore measured in Hela assay mixtures by incubating with 250 ng/ml DON at 30 ℃ for 30 min. Capillary electrophoresis result showed that the rRNA integrity from DON-treated Hela extract was identical to that of the control (Fig. A.9A). Similarly, anisomycin (20 ng/ml) (Fig. A.9B) and ricin (20 ng/ml) (Fig. A.9C) exposure did not induce rRNA cleavage. These

data suggested that PKR activation is not preceded by rRNA cleavage.

PKR selectively associates with rRNA.

RNA immunoprecipitation (RIP) with PKR-specific antibody was performed to compare PKR-associated rRNA fragments from control and DON-treated Hela extract. Slightly, more PKR-associated sequences were recovered from DON-treated (79 pieces) extract than control (51 pieces) extracts. To better distinguish the sequences, we divided them into three categories: (1) common (shared and equivalent in vehicle and DON-treated samples); (2) inducible common (shared between groups but elevated in DON-treated sample); (3) unique to DON-treated sample. Locations of common sequences were: 28S-C1: 2790-2960 nts, 28S-C2: 3590-3970 nts and 18S-C1: 80-350 nts. The locations of inducible common were 28S-IC1: 0-430 nts, 28S-IC2: 2370-2620 nts and 18S-IC1: 820-930 nts. The locations of unique sequences were: 28S-U1:1816-1873 nts, 28S-U2:4049-4132 nts and 18S-U1:668-699 nts (Fig. A.10).

RNase protection assay of 18S-U1, 28S-U2 and 28S-IC1 sequences.

RNase protection assays were performed to verify PKR-associated sequences (18S-U1, 28S-U2 and 28S-U3) in control and DON-treated RIP RNA using specific probes (Table. 10). However, 18S-U1 and 28S-U2 were both detected in control and DON-treated Hela lysate. In addition, 28S-IC3 was also found in control and DON-treated RIP RNA with similar intensity. These data suggested that PKR was associated with similar rRNA profiles under normal physiological conditions and toxin exposure (Fig. A.11).

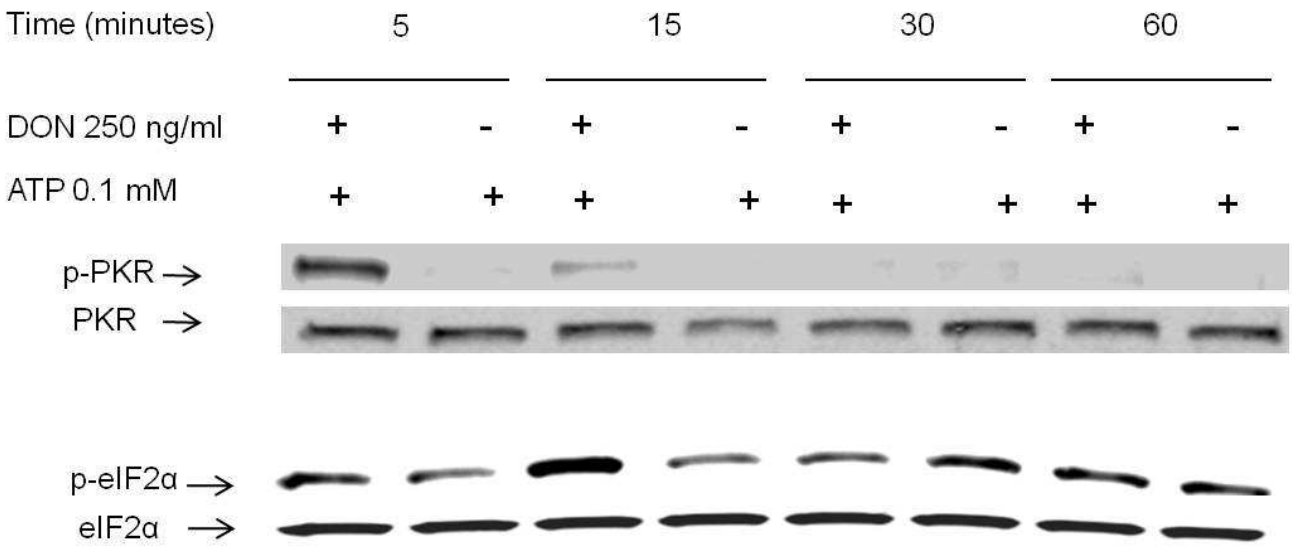

Figure A.4. DON-induced PKR activation is transient. Kinase assays with 250 ng/ml DON were performed for 5, 15, 30 and 60 min respectively and subjected to Western blot analysis with PKR, p-PKR and eIF2α, p-eIF2α antibodies, respectively.

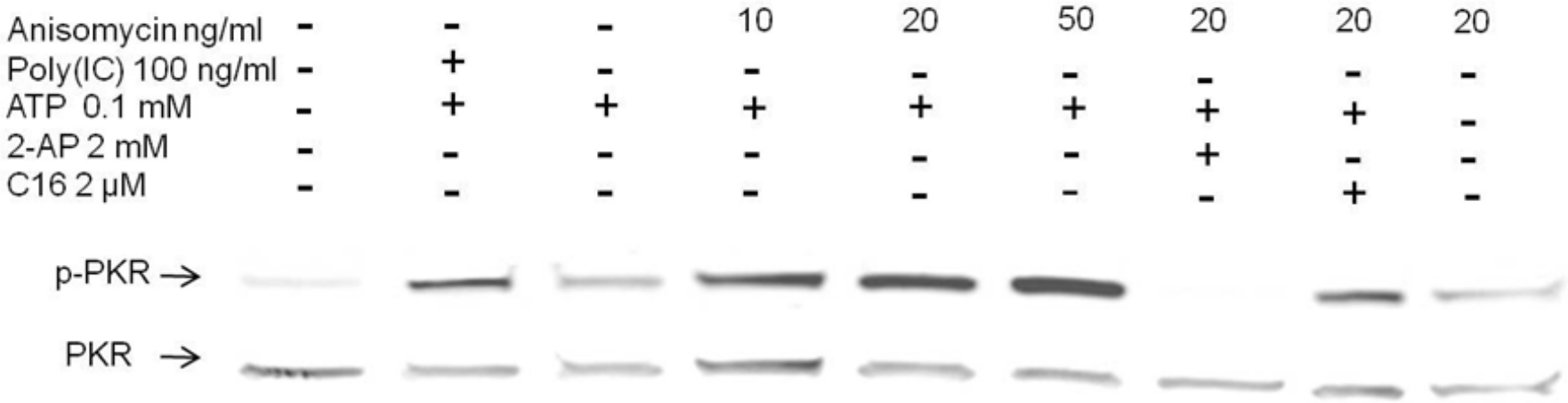

Figure A.5. Anisomycin induces PKR phosphorylation in Hela cell-free system. Selected concentrations of anisomycin (10, 20, 50 ng/ml), 100 ng/ml Poly (IC) and PKR inhibitors, 2AP (2 mM) and C16 (2 µM), were added into kinase assay buffer, respectively, and incubated for 20 min at 30 ℃ followed by Western blot analysis with PKR and p-PKR antibodies.

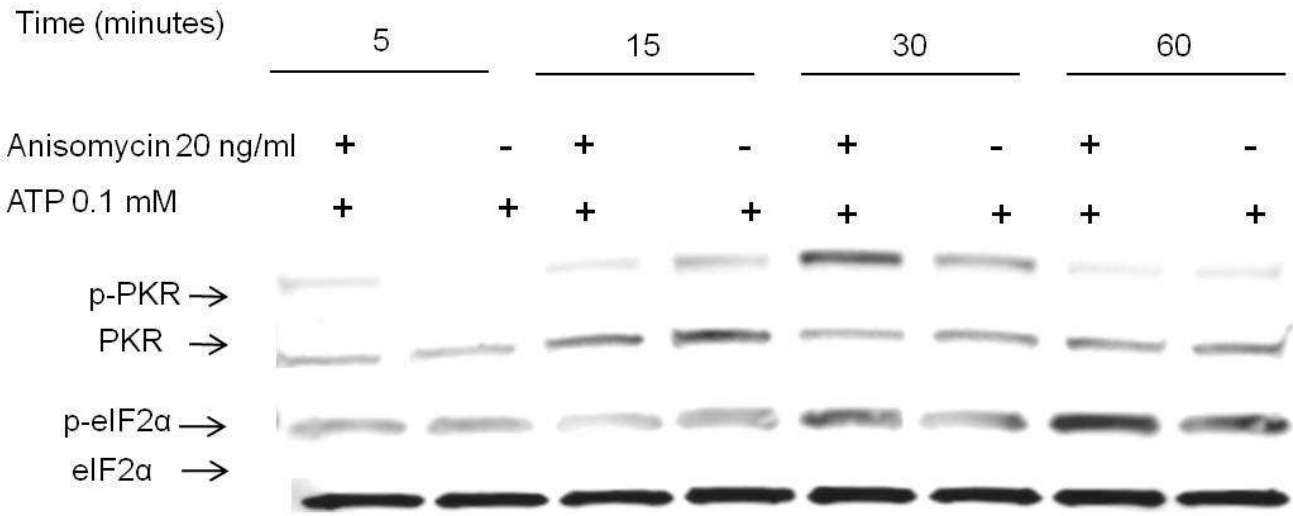

Figure A.6. Anisomycin-induced PKR phosphorylation is transient. Kinase assays with 20 ng/ml anisomycin were performed for 5, 15, 30 and 60 min respectively and subjected to Western blot analysis with PKR, p-PKR and eIF2α, p-eIF2α antibodies, respectively.

Figure A.7. Ricin induces PKR phosphorylation in a Hela cell-free system. Selected concentrations of ricin (10, 20, 50 ng/ml), the PKR inhibitors 2-AP and C16, and 100 ng/ml poly (IC) were added into kinase assay buffer, respectively, and incubated for 20 min at 30 ℃ followed by Western blot analysis with PKR and p-PKR antibodies.

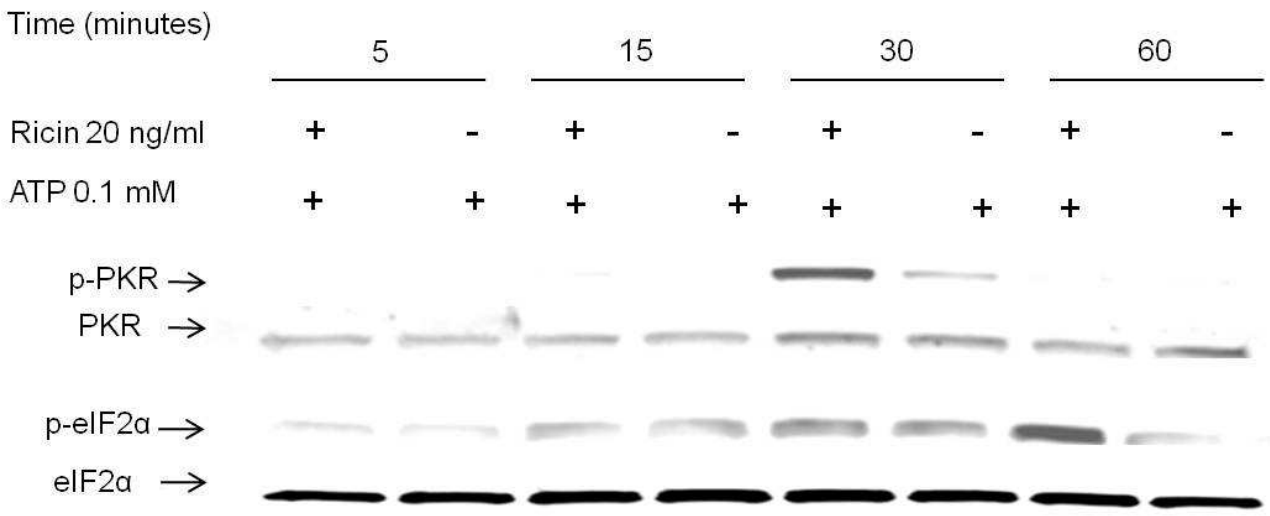

Figure A.8. Ricin-induced PKR activation is transient. Kinase assays with 20 ng/ml ricin were performed for 5, 15, 30 and 60 min respectively and subjected to Western blotting analysis with PKR, p-PKR and eIF2α, p-eIF2α antibodies, respectively.

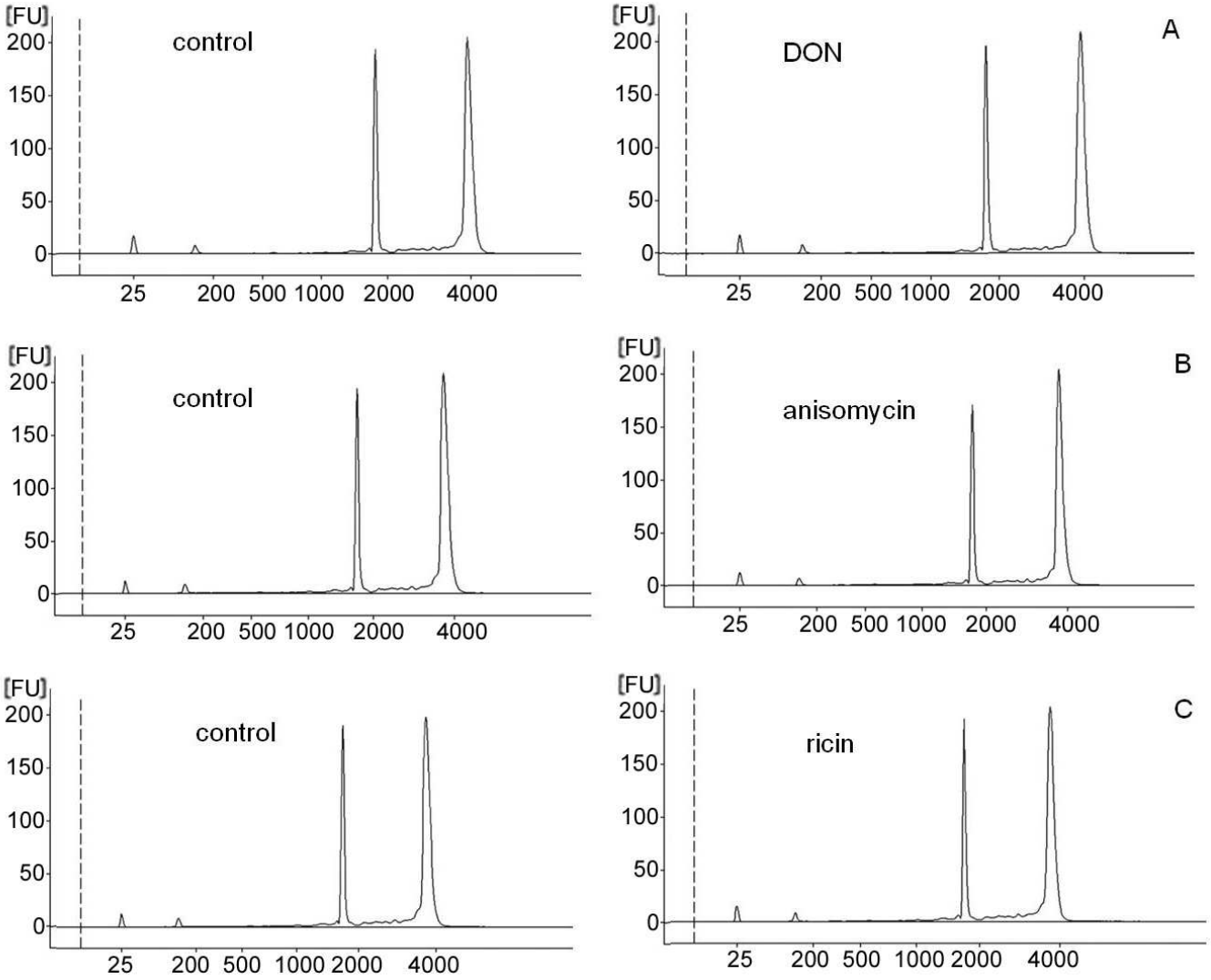

Figure A.9. Comparison of DON-treated and control rRNA profiles in a kinase assay. Aliquots (50 µl) of Hela cell lysate (50 µg) were supplemented with kinase assay buffer and incubated with (A) DON (250 ng/ml), (B) anisomycin (20 ng/ml) and (C) ricin (20 ng/ml) as well as vehicle for 30 min at 30 ℃ followed by RNA purification and capillary electrophoresis. The X-axis indicates fragment size of nucleotides and the Y-axis indicates the fluorescence intensity.

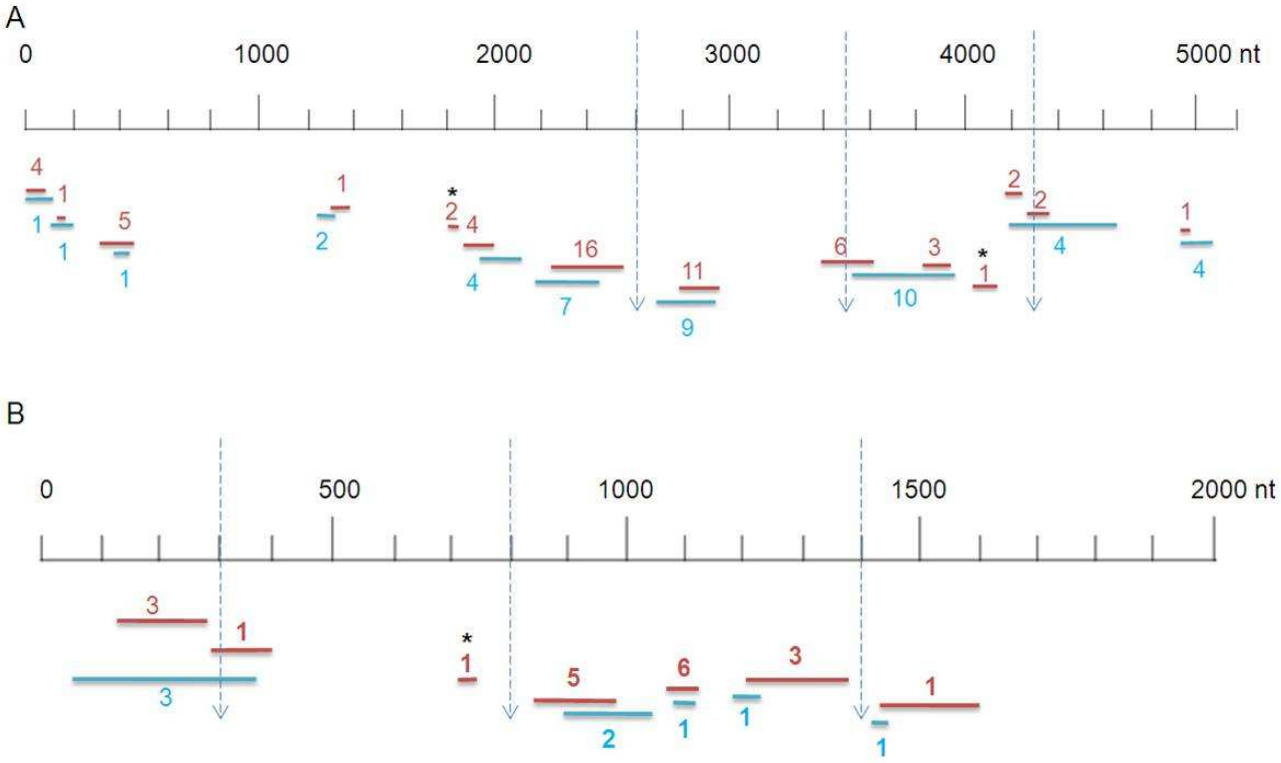

Figure A.10. Distribution of RIP-identified PKR-associated sequences. Purified immunoprecipitated PKR-associated rRNAs were cloned and sequenced. These sequences were aligned to human (A) 28S (NCBI Reference Sequence: NR-003286.2) and (B) 18S (NCBI Reference Sequence: NR_003287.2) ribosomal RNA genes and their relative sizes and locations were shown. The upper and lower lines indicate the PKR-associated sequences identified from DON-treated and control, respectively. The numbers indicates the number of sequences identified in that region. The asterisk presents the PKR-associated rRNA identified in DON-treated Hela cell extract. The dotted lines designate the estimated DON-induced rRNA cleavage sites.

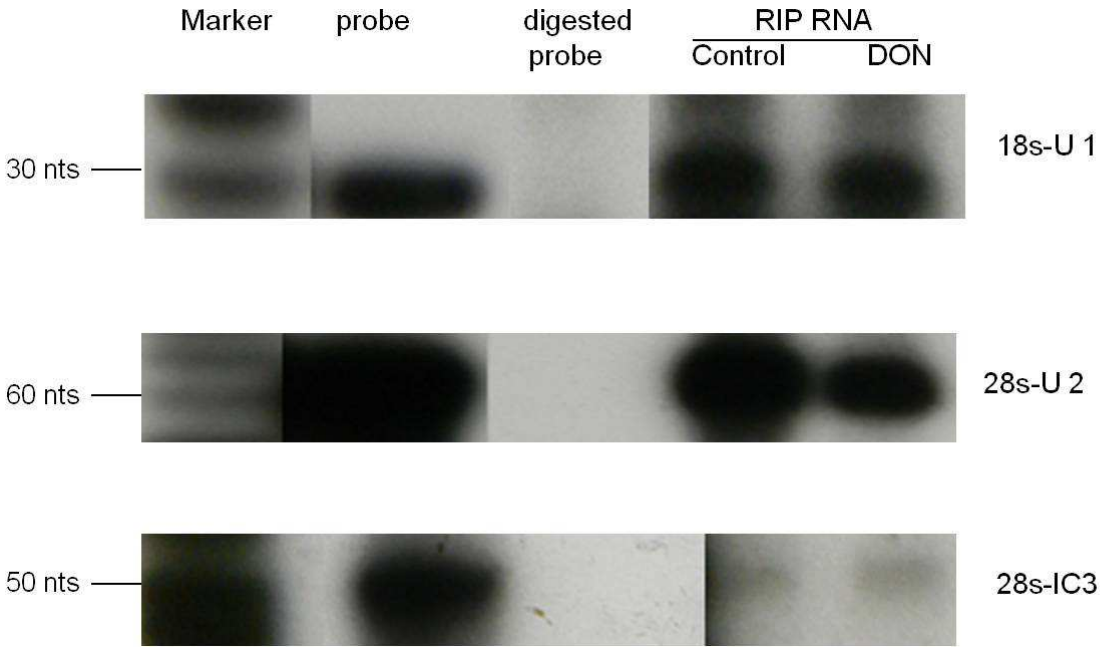

Figure A.11 RNase protection assay of 18S-U1, 28S-U2 and 28S-IC1 in RIP RNA. RNase protection assays were performed with p32 labeled probe (A) 18S-U1 (B) 28S-U2 and (C) 28S-IC1 and 500 ng RIP RNA from control and DON-treated Hela extract, respectively. The resultant RNAs were denatured and separated by 15% Urea-PAGE and subjected to autoradiophotography for 24 h.

DISCUSSION

The results presented here are the first to describe a cell-free model for ribotoxic stress. Consistent with PKR-mediated p38 activation in RAW 264.7 and U937 cells(Zhou *et al.*, 2003b), DON-induced p38 and JNK activation in Hela cells were also dose-dependently suppressed by the PKR inhibitor 2-AP (Fig. A.2), indicating a high similarity of DON-induced RSR in both cell models. The extract employed is a propietary cell-free translational system produced from Hela cells by removing cell debris, nuclei, mitochondria, lipids, DNA and mRNA. Since the phosphorylation of PKR and eIF2α were detected upon DON treatment in this system, it contains all the components necessary for PKR activation.

The Hela cell-free model possesses several advantages over cell culture to study the relationship between rRNA and PKR activation. First, nuclear and cytoplasmic RNA may form dsRNA that could activate PKR. Hela cells contain 2 to 5 percent dsRNA in native heterogeneous nuclear ribonucleoproteins (Calvet and Pederson, 1977; Fedoroff *et al.*, 1977), which could potentially translocate to cytoplasm and activate PKR upon toxin treatment. In addition, cytoplasmic poly(A)-rich RNA reportedly to activates PKR *in vitro* and *in vivo*(Li and Petryshyn, 1991). IFN-γ mRNA has been found to activate PKR (Ben-Asouli *et al.*, 2002; Toroney and Bevilacqua, 2009). Therefore, removal of nucleus and mRNA prevents interferences of these dsRNA with PKR activation. Second, the ribotoxin can react with ribosome quickly without crossing the cell membrane. Ricin is a toxic protein that enters the cell by retrograde transport from early endosomes to the trans-Golgi network (TGN), the lumen of the ER and finally cytoplasm (Olsnes, 2004), where signaling pathways such as ER stress may be initiated. The Hela cell-free

system contains no cell membrane therefore enables ricin to interact with the ribosome when added to the kinase assay mixture. Third, cell-free system is convenient for RNA immunoprecipitation. The PKR-ribosome complex can be fixed immediately after incubation with toxin without cell lysis, a process that might disrupt PKR interaction with the ribosome. Taken together, the Hela cell extract provides a unique and simple model to study the interaction of PKR and the ribosome.

Two mechanisms for ribotoxin-induced PKR activation have been previously proposed. The first is that ribotoxin exposure causes rRNA fragmentation, which exposes sections of dsrRNA capable of activating PKR (Li and Pestka, 2008). The second is that ribotoxin binding alters tertiary structure of ribosome to activate PKR. The first possibility is supported by our previous observations that DON induces 18s and 28s rRNA cleavage in RAW 264.7 macrophages (Li and Pestka, 2008). The data presented here showed that PKR can be activated within 5 min whereas rRNA cleavage was not evident for up to 30 min. These results suggest that the second possibility is more likely.

Previous studies using biochemical fractionation and immunofluorescent staining found that majority (approximate 80 percent) of PKR in mammalian cells is associated with ribosome (Jeffrey *et al.*, 1995; Zhu *et al.*, 1997). Although human PKR expressed in yeast mainly localizes to 40S subunits(Zhu *et al.*, 1997), a similar study in mammalian cells suggested that the kinase primarily associates with the 60S subunit via its dsRNA binding domains (DRBDs) (Zhu *et al.*, 1997; Wu *et al.*, 1998). Since DRBDs could bind dsRNA in a sequence-independent manner (Garcia *et al.*, 2006), rRNA that possesses complex hairpins has been proposed to be a potential activator of PKR (Zhu *et al.*, 1997). Consistent with this notion, the RIP experiment identified 51

PKR-associated sequences from the control Hela lysate, which overlapped with those sequences identified from DON-treated Hela lysate, suggesting that PKRs might associate with similar rRNA sequences in the presence and absence of toxin. Since a limited number of clones were sequenced, ostensibly “unique” low abundance sequences might have been identified only in DON-treated samples simply by chance. The sensitive RNase protection assay enabled relative quantitation of these associated sequences. The results of the preliminary experiment suggest these sequences could be detected similarly in treated and control assay mixture, indicating they might not be unique to DON treatment.

Based on the published secondary structure of 28S and 18S rRNA(Gorski et al., 1987) (Demeshkina et al., 2000), PKR-associated common, inducible common and unique sequences were all composed of or parts of dsrRNA hairpins. It has been previously established that PKR needs to bind to dsRNA longer than 30 nts for its dimerization and auto-phosphorylation(Manche *et al.*, 1992), but Toroney and Bevilacqua found that PKR could compete with the ribosome to bind to IFN-γ mRNA, in which four adjoining short helixes together form a dsRNA complex approximate 33 nucleotides(Toroney and Bevilacqua, 2009), suggesting the potential activation of PKR by spatially adjacent complexed short rRNAs. In addition, previous studies suggested that ribosome-associated PKR is monomer(Langland and Jacobs, 1992). Therefore, PKR may be associated with rRNA in a monomeric form, which dimerizes and autophosphorylates when ribotoxin exposure alters or disrupts the secondary structure of rRNA (Fig. A.12). Further investigation is needed to completely elucidate the specifc mechanisms involved.

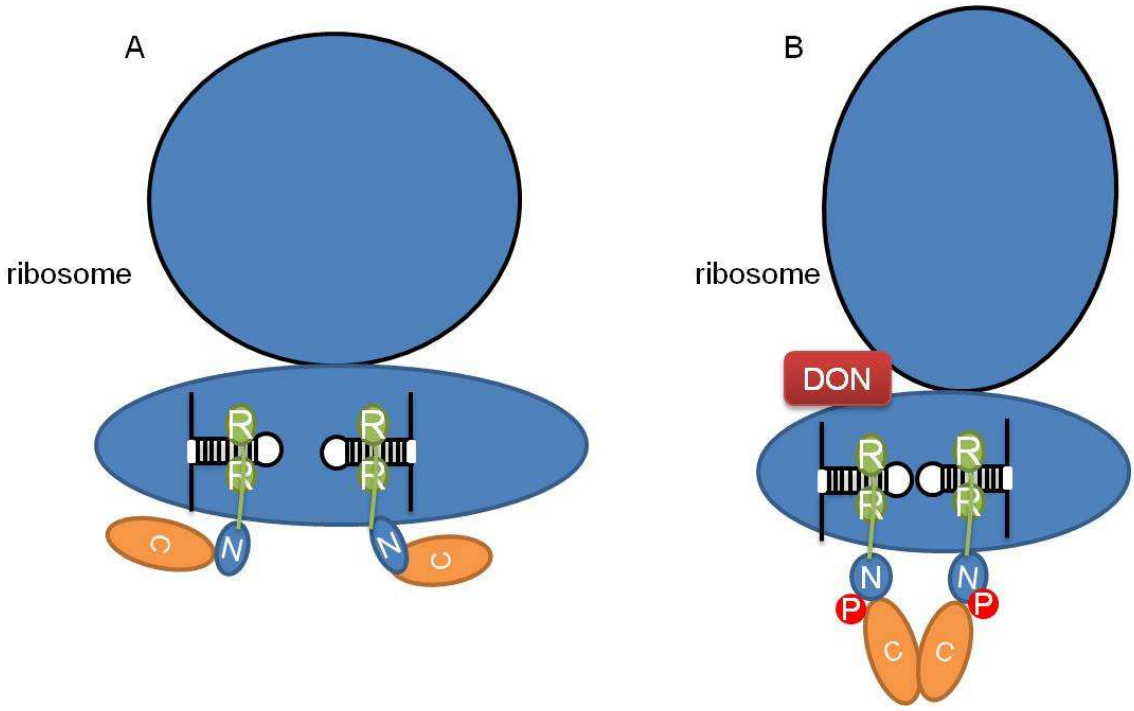

Figure A.12. Proposed model for DON-induced activation of ribosome-associated PKR. PKRs are associated with 18S and 28S rRNA under physiological conditions. DON exposure alters the tertiary structure of rRNA and enables dimerization and autophosphorylation of PKR monomers.

Previously, DON has been found to induce rRNA cleavage at sites located at 2800, 3200 and 4000 nts in mouse 28S and 300, 800, 1400 nts in mouse 18S rRNA(He *et al.*, 2012). It was proposed that these rRNAs might be accessed and specifically cleaved by RNase because of DON-imposed changes to the ribosome conformation (He *et al.*, 2012). The estimated corresponding cleavage sites on human rRNAs (Fig. A.10) showed that, with the excepting sequence 28S-IC1, the sequences overlapped or were close to the estimated rRNA cleavage sites. Therefore, these data suggest that DON might induce a conformational change to expose rRNA commonly accessible to PKR and RNase, and render the rRNA to subsequent cleavage in an apoptosis-directed manner.

It is notable that both DON and anisomycin, small molecule translational inhibitors that directly bind to the 28S rRNA petidyltransferase center (PTC) (Shifrin and Anderson, 1999), and the Type II RIP ricin which processes N-glycosidase enzymatic activity to depurinate 28S rRNA (Iordanov et al., 1997), all induced phosphorylation of PKR and eIF2α in Hela cell-free system. Ricin has been reported to influence the spatial structure of domain II and V of the ribosomal RNA and specifically affects the interaction of eEF-2 and eEF-1 with the ribosome(Larsson et al., 2002), suggesting the conformational changes may be also critical to its toxicity. In addition, primer extension studies revealed that DON and ricin targeted two sites, A3560 and A4045, located in the mouse 28S rRNA peptidyl transferase center, specifically within the central loop region of domain V (Li and Pestka, 2008). Thus DON and ricin could possibly induce identical conformational changes, especially in domain V, leading to the activation of PKR.

Previous studies aiming to identify the ribotoxin-resistant ribosome revealed that site-directed mutagenesis at amino acid 255 of RPL3 changed from tryptophan (W) to cysteine (C) confered the resistance of yeast and plants to DON, anisomycin and the type I RIP Pokeweed antiviral protein (PAP)(Fried and Warner, 1981; Harris and Gleddie, 2001; Afshar *et al.*, 2007). *S. cerevisiae* that contained the mutated RPL3 at C255 treated with anisomycin showed the same growth rate as wild-type yeast without toxin exposure(Kobayashi *et al.*, 2006). PAP, a Type 1 RIP, has been shown to bind to RPL3 in wild-type yeasts and subsequently to depurinate the α-sarcin/ricin loop of rRNA(Hudak *et al.*, 1999). Although PAP is still associated with ribosome in truncated RPL3 expressing yeast, the cells were resistant to PAP and trichothecene mycotoxin DON (Di and Tumer, 2005). These data suggest that, although the target of ribotoxin is PTC of rRNA, RPL3 must be an essential component of this interaction. In addition, the large subunit ribosomal protein L18 negatively regulates activity of PKR by competing with its DRBD for dsRNA, (Kumar et al., 1999), suggesting the activation of PKR requires involvement and coordination of RPL3, RPL18 and rRNA. Further investigation is needed to full elucidate their interaction.

DON, anisomycin and ricin dose-dependently induced marked phosphorylation of PKR at 20 min in Hela cell-free system, suggesting that PKR may be a universal sensor of ribotoxic stress. Notably, treatment of these toxins for 30 min did not induce rRNA cleavage, suggesting PKR activation did not require rRNA cleavage. RNA immunoprecipitation (RIP) and RNase protection assay results suggested that PKR bound to both 18S and 28S rRNA, which might enable it to “sense” small perturbations in rRNA tertiary structure leading to kinase activation.

Taken together, the findings of this study are consistent with a model whereby ribotoxins activate PKR by altering the tertiary structure of 18S and 28S rRNA, a process that does not require rRNA cleavage. Future work should determine if these sequences identified by clone sequencing are really associated with PKR by other approaches, such as a RNase protection assay and real-time PCR. Additionally, RIP using an isotype control antibody should also be performed to determine whether these sequences are specifically immunoprecipitated by PKR antibody. Since the ribosome and rRNA are proposed to undergo a conformational change upon toxin-exposure, which is critical to PKR activation, chemical probing of ribotoxin-bound ribosome could be conducted to elucidate this process. As a follow-up, a photo-crosslinking approach may be used to confirm the interaction of PKR with rRNA and/or ribosomal proteins. To fill the gap in our understanding of RSR, investigation on the dynamics of ribotoxin-induced conformational change of rRNA and ribosome, and mobilization of signaling molecules are also needed to fully elucidate the mechanism by which PKR is activated to mediate the downstream signaling pathways.

Appendix B

Construction and Expression of FLAG-tagged Ribosomal Proteins in HEK 293T and Hela Cells

ABSTRACT

The trichothecene mycotoxin deoxynivalenol (DON), a known small molecule translational inhibitor that directly binds to ribosome, has been previously demonstrated to activate MAPKs via PKR and Hck and mediate the downstream up-regulation of pro-inflammatory genes. However, this process is not fully understood. To better understand DON-induced mobilization of signaling molecules and altered mRNA translational profile, specific affinity purification of ribosome and associated molecules are critically needed. Here we test our hypothesis that fusion protein of N- and C-terminal FLAG-tagged mouse ribosomal proteins are able to incorporate into and immunoprecipitate ribosomes in human cells. Our data showed that six plasmids expressing N- and C-terminally FLAG-tagged recombinant ribosomal proteins (RPL18, 23a and RPS6) were successfully expressed in HEK 293T. Furthermore, most of these recombinant proteins were able to incorporate into ribosome, which was used to immunoprecipitate ribosome in HEK 293T cells. Because HEK 293T cells do not secret cytokines, alternative cytokine-secreting Hela cells were tested on DON-induced activation of MAPKs. DON induced rapid activation of p38 and JNK in Hela cells at 5 and 15 min, respectively, which were dose-dependently suppressed by pretreatment of PKR inhibitor 2AP, suggesting Hela cell may be used as a novel model to study DON-induced ribotoxic stress response. Successful expression of all six plasmids was also confirmed in Hela cells. Three recombinant proteins, N-FLAG RPL18, 23a and C-FLAG RPL23a, were able to incorporate into ribosome at 24 h post-transfection.

INTRODUCTION

Deoxynivalenol (DON), a trichothecene produced by *Fusarium,* is a ubiquitously contaminant in cereal grains and its adverse effects on human and animals have been well-documented (Pestka and Smolinski, 2005; Pestka, 2008). Primary targets of this ribotoxic mycotoxin are monocytes and macrophages of the innate immune system, in which DON directly binds to ribosome and inhibit translation. Both in vitro and in vivo studies have demonstrated that DON induces phosphorylation of mitogen-activated protein kinases (MAPKs) which drive upregulated expression of mRNAs and proteins for inflammation-related genes such as the cytokines, chemokines and cyclooxygenase-2 (COX-2) (Shifrin and Anderson, 1999; Moon and Pestka, 2002; Chung *et al.*, 2003b; Zhou *et al.*, 2003a; Islam *et al.*, 2006). This process is termed the "ribotoxic stress response" (RSR) (Iordanov *et al.*, 1997). To date, two kinases, the double-stranded RNA- (dsRNA)-activated protein kinase (PKR) and hematopoietic cell kinase (Hck) (Zhou *et al.*, 2003b; Zhou *et al.*, 2005b), have been found be activated earlier than MAPKs and their inhibitors block MAPK activation or downstream events in macrophage, indicating they are possible upstream mediators of RSR.

The ribosome, the cellular target of DON, is also a potential scaffold for many kinases. Remarkably, sequence analysis of ribosomal proteins revealed that ribosome contains putative docking sites for various kinases, such as PKR, Hck, ERK, PDK1, AKT, P70, RSK1(Pestka, 2008). PKR, the known upstream mediator of RSR, is found to be associated with ribosome via the double-stranded RNA binding domains (DRBD) sequence, deletions or residue substitutions in which block its association with ribosome(Zhu *et al.*, 1997). Furthermore, the ribosomal large subunit protein L18

negatively regulates activity of PKR by competing the DRBD with dsRNA and reversing dsRNA binding to PKR (Kumar *et al.*, 1999). In addition, PKR forms a functional complex by direct binding the p38 and/or Akt, which permits PKR to timely regulate the inhibition/activation of p38 and Akt(Alisi *et al.*, 2008). Furthermore, DON recruits p38 to the ribosome in murine peritoneal macrophages but not in PKR-deficient cells, suggesting the PKR activation may be required for DON-induced p38 activation(Bae *et al.*, 2010). Extremely rapid association and/or activation of PKR, Hck, p38 and ERK are detectable in ribosome of DON-treated macrophages. Earliest activation of kinases (1–3 min) is detected in the monosome fraction, and later in the polysome fraction (3–5 min). Thus the ribosome appears to function as a scaffold to kinases, allowing their mobilization and rapid sequential activation.

It is critical to understand how DON mediates signaling molecule mobilization and kinase activation. Specific isolation of ribosome-associated proteins and mRNAs is a fundamental prerequisite to achieve this goal. Although conventional sucrose gradient fractionation has been used to isolate ribosome-associated proteins (Kuhn *et al.*, 2001; Bae *et al.*, 2010), it is a non-specific approach for separating cellular complex and based solely on molecular weight. In addition, this analysis requires a large amount of starting biological material, and thus cannot be routinely performed on samples of limited quantity(Inada *et al.*, 2002). Alternatively, affinity purification of ribosome is a promising method to specifically pull down ribosome and associated molecules. One-step affinity purification of ribosome from budding yeast was successfully performed with C-terminally FLAG-tagged RPL25p resulting in co-purification of mRNAs, large subunit, monosome, polysome and ribosome-associated proteins; This approach led to

the identification of two novel proteins, Mpt4p and Asc1p (Inada *et al.*, 2002). A His6-FLAG dual epitope tag at the N-terminal of RPL18 is constructed in *Arabidopsis* and used to isolate ribosome-associated mRNAs(Zanetti *et al.*, 2005). Whole-genome profiling using DNA microarray reveals that, on average, 62% of total mRNAs are associated with the epitope-tagged polysomal complexes(Zanetti *et al.*, 2005), suggesting it is a valuable tool for the quantification of mRNAs present in translation complexes in plant cells. Furthermore, this FLAG-tagged RPL18 was later used in *Arabidopsis* to profile mRNAs from ribosome complexes, termed translatome, and identify differentially expressed mRNAs in 21 cell populations under hypoxia stress, providing insight on specific gene expression at the cell-, region-, and organ-specific levels(Mustroph *et al.*, 2009).

Affinity purification was also creatively used in animal. A RiboTag mouse line was created, which carries an RPL22 allele with a floxed wild-type C-terminal exon followed by an identical C-terminal exon that has three copies of the hemagglutinin (HA) epitope inserted before the stop codon(Sanz *et al.*, 2009). When the RiboTag mouse is crossed to a cell-type-specific Cre recombinase-expressing mouse, Cre recombinase activates the expression of epitope-tagged ribosomal protein RPL22HA, which is incorporated into actively translating polyribosomes and used to immunoprecipitate polysomes-associated mRNA transcripts from specific cell types.

To better understand DON-induced mobilization of signaling molecules and altered mRNA translational profile, we constructed N- and C-terminal FLAG-tagged mouse large subunit ribosomal protein 18, 23a (homologue of yeast RPL25p) and small subunit ribosomal protein S6, all of which are reported to be on the surface of

ribosome(Marion and Marion, 1987; Marion and Marion, 1988). All these proteins were expressed and incorporated into ribosome in HEK 293T cells. Further immunoprecipitation with anti-FLAG antibody revealed that, except C-FLAG-RPL18, the other recombinant recombinant ribosomal proteins were concurrently detected with RPL7, indicating the successful ribosome pulldown. However, HEK 293T cells are not ideal molel for RSR study, we used Hela cell as a alternate. Notably, DON induced robust activation of p38 and JNK in Hela cells, which were dose-dependently suppressed by pretreatment of PKR inhibitor 2AP, suggesting Hela cell might be applicable to study RSR. While expression of all six plasmids were successfully confirmed in Hela cells, only three recombinant proteins, N-FLAG RPL18, 23a and C-FLAG RPL23a, were able to incorporate into ribosome at 24 h post-transfection. With further optimization to improve the expression of these plasmids, this approach might serve as a powerful tool to study the DON-induced signaling mobilization and translatome.

MATERIALS AND METHODS

Bacterial strains, enzymes and plasmids. E. coli DH5-α (Invitrogen, Carlsbad, CA) was used for plasmid propagation. Plasmid 15234 and Plasmid 13824 (Addgene, Cambridge, MA) were modified pcDNA 3.1 vectors with N- and C-terminal FLAG-coding sequences on the backbone, respectively, and used for construction of FLAG-tagged ribosomal proteins. After confirmation by sequencing, the FLAG-tagged RPs were re-cloned to another eukaryotic expressing vector pmCitrine-N1, a gift from Dr. Joel Swanson at University of Michigan. Restriction enzymes EcoR I, Xho I, Bam H1 Sac II and Sma I were purchased from New England Biolabs (Ipswich, MA), Pfu polymerase was purchased from Stratagen (Amsterdam, The Netherlands) and T4 ligase was from Promega (Madison, WI).

Cloning of FLAG-tagged RPL18, 23a and RPS6 at N- and C-terminal. Total RNA was extracted from RAW 264.7 cells using the RNeasy mini kit (Qiagen, Valencia, CA) and reverse-transcribed into cDNA using an oligo-dT primer (Invitrogen). The PCR amplification of RPL18, 23a and RPS 6 were performed in a 50 µl reaction volume: 5 µl of 10 x reaction buffer, 50 ng template cDNA, forward/reverse primer 1 µl (10 µM), dNTP mix 1 µl (10 mM), Pfu DNA polymerase 2.5 U and nuclease-free H2O up to 50µl. Primers for construction of N-FLAG (Table. B.1) proteins were used, respectively. PCR was run at step 1: 95 ℃, 1 min, step 2: 95 ℃, 30 s econds, 56 ℃, 1 min, 68 ℃ for 2 min (go to step 2 repeat 35 cycles), step 3: 72 ℃ 10 mi n, hold at 4 ℃. PCR products were purified by PCR product purification kit (Qiagen, Valencia, CA). Then the PCR products and plasmids (Adgene Cat.15234 and 13824) were treated with restriction enzyme EcoR I and Xho I for N-FLAG or EcoR I and Bam H1 for C-FLAG construction,

respectively. The digested PCR products and vectors were incubated with T4 ligase at 4℃ overnight, transformed into competent E. coli DH5 -α cells and cultured overnight on solid Luria-Bertani (LB) plate containing ampicillin (100 μg/ml). Positive clones were sequenced from both ends to confirm the constructions were correct in frame.

These FLAG-tagged ribosomal proteins were re-cloned to pmCitrine-N1 using the method described above but with different primers and restriction enzymes. The primers for N-FLAG (Table. B.2) ribosomal proteins were used respectively. In addition, restriction enzyme Sac II and Sma I were used individually for N-FLAG and C-FLAG constructions. After sequencing, the plasmids were propagated, purified by Endofree plasmid purification kit (Qiagen, Valencia, CA), diluted to 1 μg/μl and stored at -20 ℃.

Cell culture. Both HEK 293T and Hela cells (ATCC, Rockville, MD) were cultured in ATCC-formulated Dulbecco's modified Eagle's medium (DMEM) supplemented with 10% (v/v) fetal bovine serum (Atlanta Biologicals, Lawrenceville, GA), streptomycin (100 μg/ml) and penicillin (100 U/ml) at 37 ^{o}C in a humidified atmosphere with 5% CO_2. The cell number and viability were assessed by trypan blue dye exclusion using a hematocytometer. Prior to transfection or DON exposure, cells (2.5 x 10^6/plate) were seeded and cultured in 100-mm tissue culture plates for 24 h to achieve approximately 80% confluency.

Ribosome pelleting by sucrose cushion. For polysome isolation, cells were washed twice with ice-cold phosphate-buffered saline (PBS) and lysed in 500 μl ice-cold polysome extraction buffer (PEB) (50 mM KCl, 10 mM $MgCl_2$, 15 mM Tris–HCl (pH 7.4), 1% (v/v) Triton X-100, 0.1 mg/ml cycloheximide and 0.5 mg/ml heparin)(Bae *et al.*, 2009). Sucrose solution (34.2%, w/v) were prepared prior to use by dissolving sucrose

Table B.1. PCR primers for cloning N- and C-FLAG ribosome proteins.

N- FLAG RPL18 forward	5'- TTGAATTCGCATGGGTGTTGACATTCGCC-3'
N-FLAG RPL18 reverse	5'-TTCTCGAG TTAGTTTTTGTAGCCTCTGCTGG-3'
N- FLAG RPL23a forward	5'-AAGAATTCGC ATGGCGCCGAAAGCGAAG-3'
N- FLAG RPL23a reverse	5'-TACTCGAG TTAGATGATCCCAATCTTGTTGGC-3'
N-FLAG RPS6 forward	5'-CAGAATTCGC ATGAAGCTGAACATCTCCTTCCC-3'
N-FLAG RPS6 reverse	5'-GCCTCGAG TCATTTTTGACTGGACTCAGACTTAG-3'
C- FLAG RPL18 forward	5'-CAGGATCC ATGGGTGTTGACATTCGCC-3'
C-FLAG RPL18 reverse	5'-GCGAATTC TAAGTTTTTGTAGCCTCTGCTGG-3'
C- FLAG RPL23a forward	5'-TAGGATCCATGGCGCCGAAAGCGAAG-3'
C- FLAG RPL23a reverse	5'-CCGAATTCTAAGATGATCCCAATCTTGTTGGC-3'
C-FLAG RPS6 forward	5'- CTGGATCCATGAAGCTGAACATCTCCTTCCC-3'
C-FLAG RPS6 reverse	5'-CTGAATTC TAATTTTTGACTGGACTCAGACTTAG-3'

Table B.2. PCR primers for recloning N- and C-FLAG ribosome proteins to pmCitrine-N1.

N- FLAG Common forward	5'-TTCCGCGGATGGACTACAAGGACGACGATG-3'
N-FLAG RPL18 reverse	5'-TTCCCGGGTTAGTTTTTGTAGCCTCTGCTGG-3'
N- FLAG RPL23a reverse	5'-TACCCGGGTTAGATGATCCCAATCTTGTTGGC-3
N- FLAG RPS6 reverse:	5'-TTCCCGGGTCATTTTTGACTGGACTCAGACTTAG-3'
C-FLAG RPL18 forward	5'-AACCGCGG ATGGGTGTTGACATTCGCC-3'
C-FLAG RPL23a forward	5'-AACCGCGG ATGGCGCCGAAAGCGAAG-3'
C-FLAG RPS6 forward	5'-ATCCGCGG ATGAAGCTGAACATCTCCTTCCC-3'
C-FLAG Common reverse	5'-TTCCCGGG TAGAAGGCACAGTCGAGG-3'

into RNase-free water with 50 mM KCl, 15 mM Tris–HCl (pH 7.4), 10 mM $MgCl_2$, 0.1 mg/ml cycloheximide and protease inhibitor. Cell lysates were centrifuged at 16,000 × g, 4 ℃, for 15 min to remove nuclei, mitoc hondria and cell debris. The resultant clear supernatant was layered on a 9 ml sucrose cushion and centrifuged at 200,000 × g, 4 ℃ for 3 h in Sorvall TH-641 rotor. The resultant pellet was washed with cold PEB buffer, resuspended in boiling SDS lysis buffer (1% [w/v] SDS, 1 mM sodium ortho-vanadate and 10 mM Tris, pH 7.4) and subjected to Western analysis.

Transfection method. Plasmids were transfected into HEK 293 T or Hela cells using Lipofectamine 2000 (Invitrogen, Carlsbad, CA) according to the manufacturer's protocol. Briefly, cells (2 ml/well) were seeded in 6-well plates and cultured for 24 h to achieve about 80% confluency. For each well, dilute plasmids (2 µg) and Lipofectamine 2000 in 250 µl Dulbecco's modified Eagle's medium (DMEM), respectively, mix gently and incubate for 5 minutes at room temperature. After the 5 minute incubation, combine the diluted plasmid with Lipofectamine 2000, mix gently and incubate for 20 minutes at room temperature. Add the 500 µl of plasmid-Lipofectamine 2000 complexes to each well and the transfected cells were cultured at 37℃ in a CO2 incubator for 24 h. The cells were lysed in boiling SDS lysis buffer (1% [w/v] SDS, 1 mM sodium ortho-vanadate and 10 mM Tris, pH 7.4) and subjected to Western analysis.

Western analysis. Western was conducted using primary antibodies specific for murine forms of total p38 (Catalog No. 9216), phosphorylated p38 (Catalog No. 9212), total JNK (Catalog No. 9258) and phosphorylated JNK (Catalog No. 9255) from Cell Signaling (Beverly, MA), and RPL7 (Catalog No. A300-741A) and RPS6 (Catalog No. A300-557A) from Bethyl Laboratory Inc. (Montgomery, TX). Cells were washed twice

with ice-cold phosphate-buffered saline (PBS), lysed in boiling SDS lysis buffer (1% [w/v] SDS, 1 mM sodium ortho-vanadate and 10 mM Tris, pH 7.4), boiled for 5 min and sonicated briefly, the resultant lysate centrifuged at 12,000 × g for 10 min at 4℃ and protein concentration measured with a BCA Protein Assay Kit (Fisher, Pittsburgh, PA). Total cellular proteins (40 µg) were separated on BioRad precast 4-20% polyacrylamide gels (BioRad, Hercules, CA) and transferred to a polyvinylidene difluoride (PVDF) membrane (Amersham, Arlington Heights, IL). After incubating with blocking buffer (Li-Cor, Lincoln, NE) for 1 h at 25 ℃, membranes were incubated with murine and/or rabbit primary antibodies (1:1000 dilution in Li-Cor blocking buffer) to immobilized proteins of interest overnight at 4℃. Blots were washed three times of 10 min with Tris-Buffered Saline and Tween 20 (TBST) (50 mM Tris-HCl, 150 mM NaCl, 0.1% Tween 20, pH 7.5), and then incubated with secondary IRDye 680 goat anti-rabbit and/or IRDye 800CW goat anti-mouse IgG antibodies (Li-Cor) (1:2000 dilution in Li-Cor blocking buffer) for 1 h at 25℃. After washing three times, infrared fluorescence from these two antibody conjugates were simultaneously measured using a Li-Cor Odyssey Infrared Imaging System (Lincoln, Nebraska).

Immunoprecipitation: Protein A agarose beads (25 µl) were washed once with 1 ml HNTG buffer (20 mM HEPES pH 7.5,150 mM NaCl, 0.1 % Triton X-100, 10% glycerol) and centrifuged at 6000 × g, 1 min at 4℃. Then the supernatant was removed. The resultant protein A agarose bead pellet was resuspended in 25 µl HNTG buffer, added 1 µl anti-FLAG antibody (Sigma–Aldrich) and incubated for 0.5 h at room temperature. The cells were lysed in 400 µl lysis buffer (50 mM HEPES pH 7.5, 150 mM NaCl, 1.5 mM $MgCl_2$, 1 mM EGTA, 10 % glycerol, 1% Triton X-100) and centrifuged at

12,000 × g for 10 min at 4℃. Clarified cell lysates (300 µl) were incubated with 25 µl of FLAG antibody-bounded Protein A agarose beads for 90 min at 4 ℃ and the immunoprecipitates were washed two times with HNTG buffer.

RESULTS

Expression, incorporation, and immunoprecipitation of FLAG-tagged ribosomal proteins in HEK 293T cells

We constructed six plasmids expressing recombinant ribosomal proteins (RPL18, RPL23a and RPS6) tagged with FLAG at N- and C-end, which were confirmed by sequencing (data not shown). Since RAW 264.7 cells did not efficiently express exogenous plasmids so we tested whether the FLAG-tagged ribosomal proteins could be expressed in frame in HEK 293T cells, which have been modified to efficiently express exogenous plasmids. After transfection for 24 h, the FLAG-tagged ribosomal proteins were detected in both cell lysates and ribosome pellet (Fig. B.1A) by Western, indicating the recombinant proteins were expressed very well and successfully incorporated into the ribosome. In addition, except C-FLAG-RPL18, the other recombinant ribosomal proteins were concurrently detected with RPL7 after immunoprecipitation, indicating the whole ribosome can be successfully pulled down by anti-FLAG antibody (Fig. B.1B).

DON-induced activation of p38 and JNK can be dose-dependently suppressed by PKR inhibitor 2AP in Hela cells.

The RSR is characterized by the activation of mitogen-activated protein kinases (MAPKs) and subsequent upregulation of gene expression (Iordanov *et al.*, 1997). As a

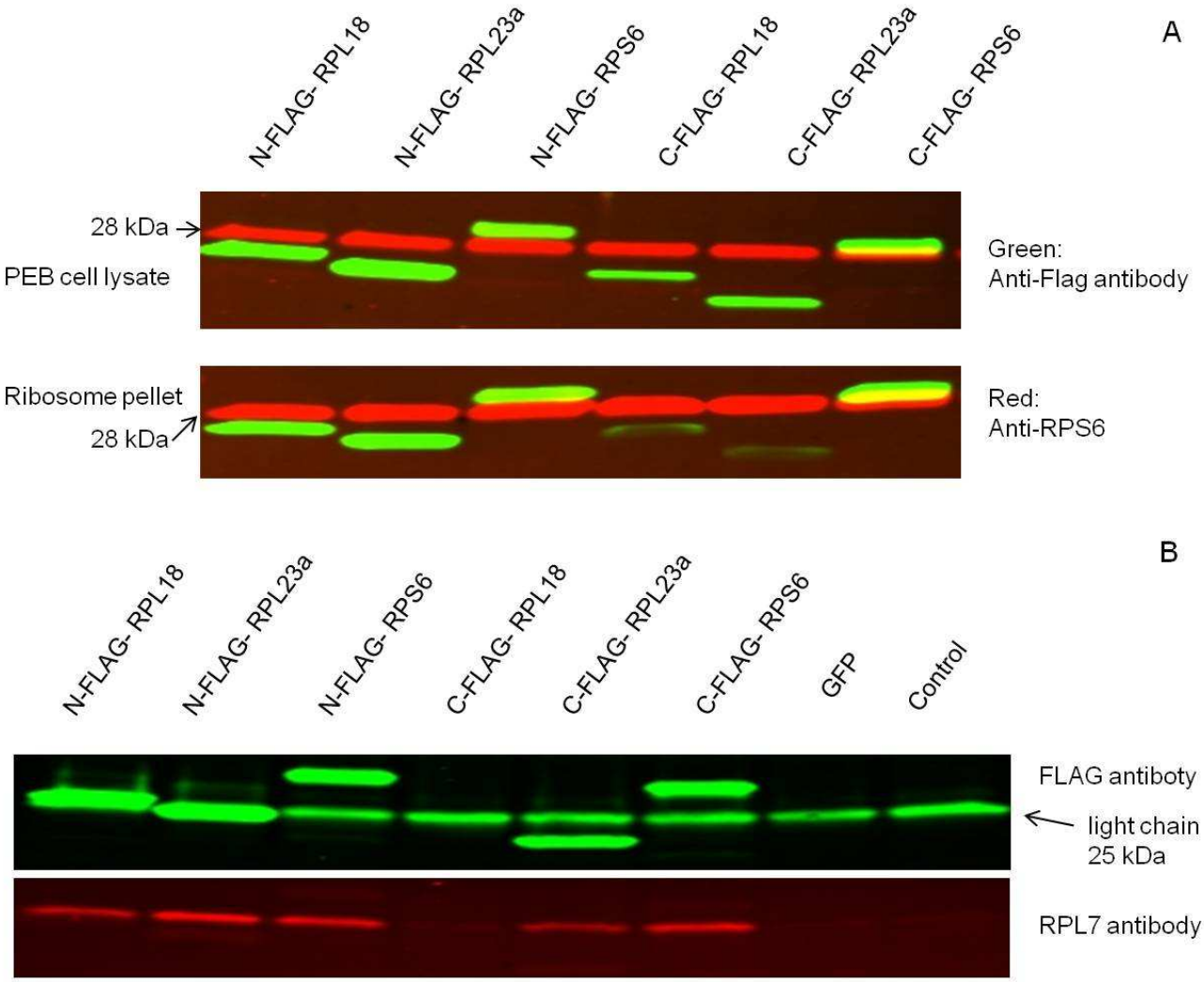

Figure B.1. FLAG-tagged ribosomal proteins are expressed in HEK 293T cells, incorporated into ribosome and immonuprecipitated ribosome. HEK 293T cells were transfected with 2 µg plasmids expressing FLAG-tagged ribosome proteins, respectively, and incubated for 24 h. Then the cells were lysed by PEB buffer followed by ribosome pelleting through 1 M sucrose cushion and subjected to Western analysis with mouse anti-FLAG (green) and rabbit anti-RPS6 anti-bodies (red) Alternatively, (B) immunoprecipitation was performed with anti-FLAG antibody conjugated to beads and subjected to Western blotting with anti-FLAG (green) and anti-RPL7 (red) antibodies. The green bands lower than the RPL7 indicated IgG light chain.

well-studied RSR inducer, DON rapidly activates p38, JNK and ERK and upregulates numerous inflammation-related genes in RAW 264.7 cells(Pestka, 2008). However, RAW 264.7 is not a good model to express exogenous plasmids. Therefore, we sought to substitute another cell line for macrophage model. Ongoing studies in our lab using Hela cell-free system have found that DON, ricin and anisomycin activate PKR and subsequently phoshorylates of eIF2α, Hela cell seems to be a outstanding candidate. Similar to RAW 264.7 cells, Hela cells also secrete cytokines including IL-1β, IL-6, TNF-α, IL-17, TGF-β1, IL-4, IL-12p35, and IL-15 (Hazelbag *et al.*, 2001; Lazar and Chifiriuc, 2010) and process opposing survival ERK and apoptotic p38 signaling pathway(Fan *et al.*, 2007). Our data showed that DON activated p38 in 5 min and JNK in 15 min (Fig. B. 2 A, B). Consistent with PKR-mediated p38 activation in RAW 264.7 cells(Zhou *et al.*, 2003b), DON-induced p38 and JNK activation were also dose-dependently suppressed by PKR inhibitor 2AP (Fig. B.3), suggesting the high similarity between macrophage and Hela model in DON-induced RSR.

Expression of GFP and FLAG-tagged ribosomal proteins in Hela cells.

To better understand DON-induced kinase mobilization to ribosome and changes of translational mRNA profile, we could express and immuneprecipitate the whole ribosome and the associated kinases and mRNA. The prerequisite for these studies is to express the FLAG-tagged ribosomal proteins in Hela cells. The expression of FLAG-tagged ribosomal proteins (Fig. B.4A) were detected in Hela cells at 24 h post-transfection. Further ribosome pelleting data revealed that all three N-FLAG RPL18, 23a and C-FLAG RPL23a were able to incorporate into ribosome at the same time (Fig. B.4B), suggesting they might be used for ribosome immunoprecipitation.

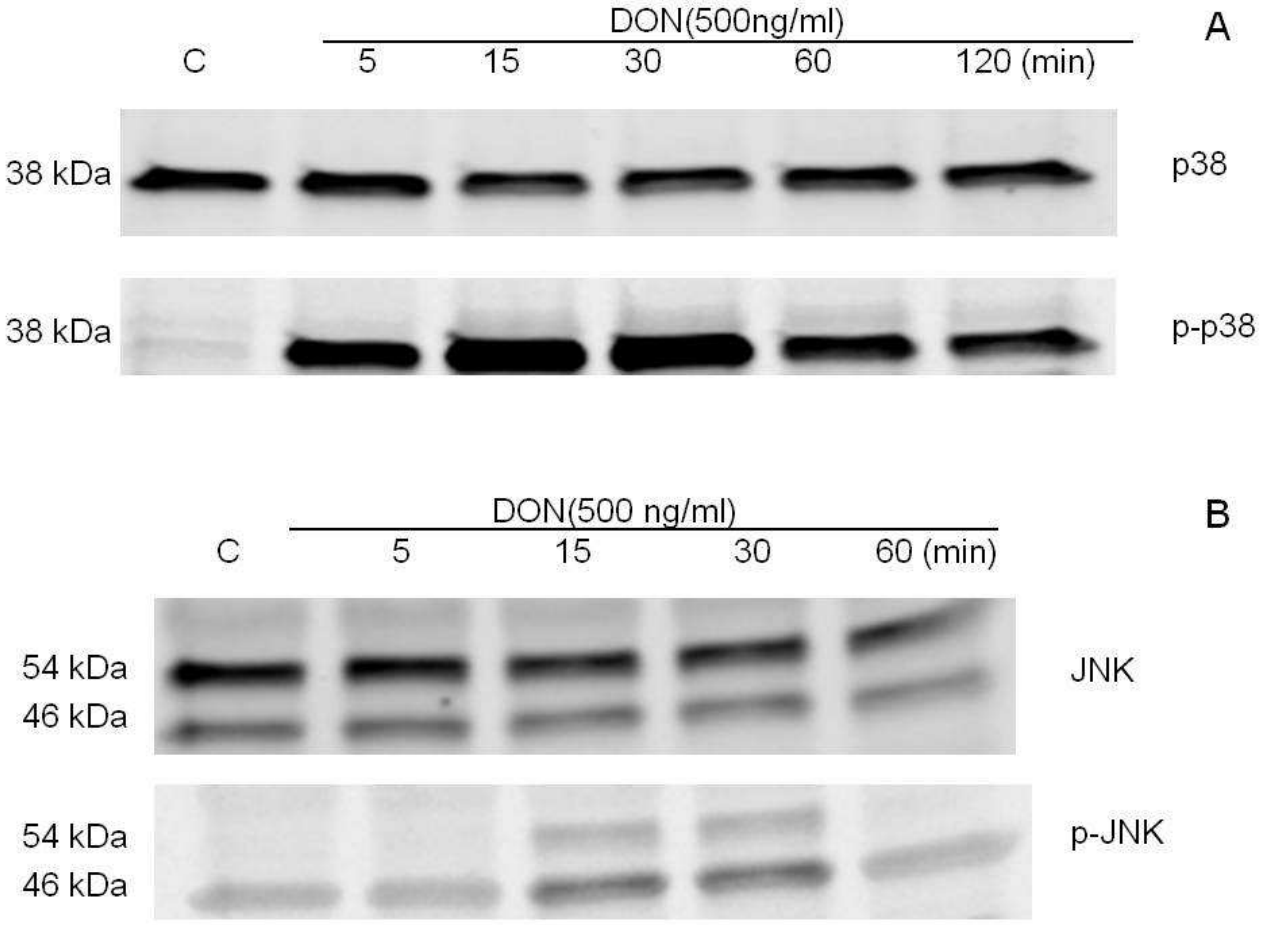

Figure B.2. DON induces phosphorylation of p38 and JNK in Hela cells. Hela cells were treated with 500 ng/ml of DON for 0, 5, 15, 30, 60, 120 min followed by cell lysis and Western blot analysis with total and phosphorylated (A) p38 and (B) JNK.

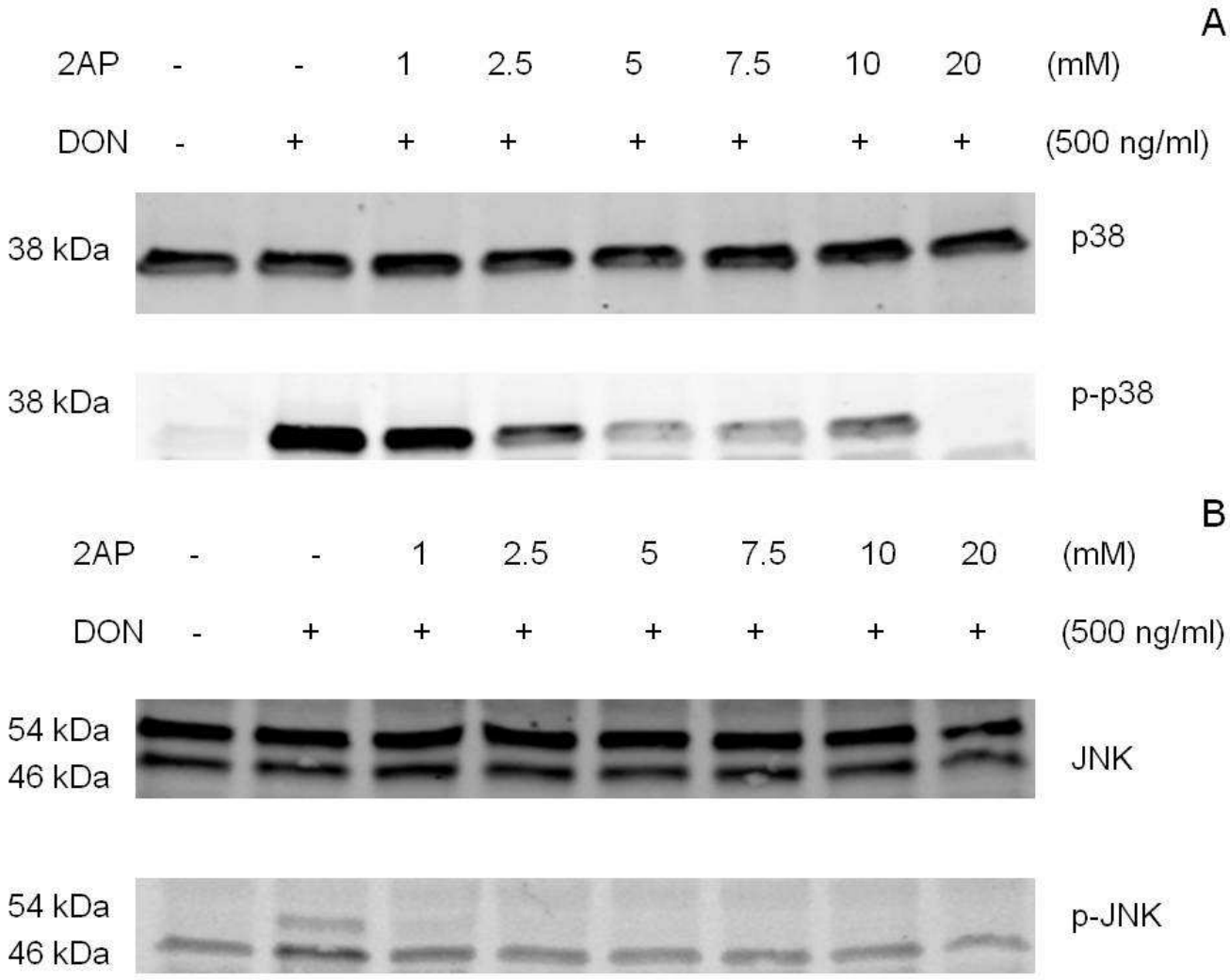

Figure B.3. DON-induced p38 and JNK phosphorylation can be dose-dependently suppressed by PKR inhibitor 2AP in Hela cells. The Hela cells were pretreated with PKR inhibitor 2AP at 1, 2.5, 5, 7.5, 10, 20 mM for 1 h followed by 500 ng/ml DON exposure for 15 min and subject to Western bloting with total and phosphorylated (A) p38 and (B) JNK.

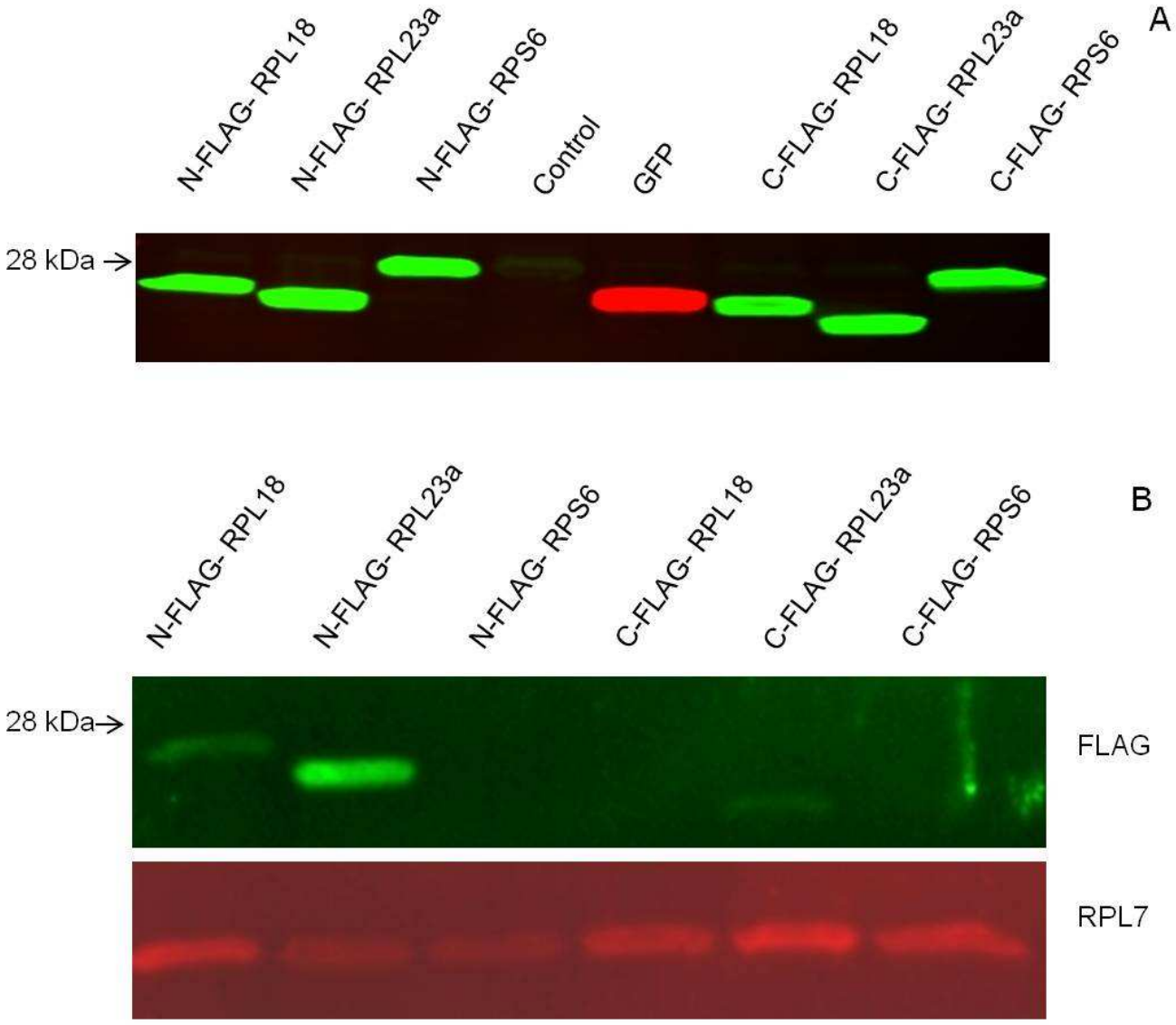

Figure B.4. FLAG-tagged ribosomal proteins are expressed in Hela cells, and incorporated into ribosome. Hela cells were transfected with 2 µg GFP and plasmids expressing FLAG-tagged ribosomal proteins, respectively, incubated for 24 h followed by (A) cell lysis using PEB buffer and (B) ribosome pelleting through 1 M sucrose cushion and Western blot analysis with mouse anti-FLAG (green) and rabbit anti-RPL7 antibodies (red).

DISCUSSION

FLAG-tagged murine ribosomal proteins were developed to express in RAW 264.7 macrophages, our standard model to study DON-induced RSR. However, the RAW 264.7 cells inefficiently express exogenous plasmids transfected with various methods, such as electroporation, Lipofectamine 2000, Lipofectamine LXT, and Fugene HD (data not shown). To test whether the plasmids can be corrected expressed and incorporated into ribosome, which is the prerequisite for affinity purification of ribosome, we needed to find an alternative cell line. Because the eukaryotic ribosome is evolutionarily conserved in structure, we hypothesize that recombinant murine ribosome proteins can also be functionally incorporated into human ribosome and used to immunoprecipitate ribosome. So HEK 293T cells, which were genetically modified to express exogenous plasmids, were chosen and the successful immunoprecipitation of ribosome in HEK 293T verified this hypothesis.

Although the HEK 293T cells efficiently express recombinant ribososomal proteins, they process an obvious disadvantage of not secreting cytokines, which makes it impractical for the study of MAPK-mediated expression of downstream proinflammatory genes in RSR. Hela cells have been reported to secrete cytokines including IL-1β, IL-6, TNF-α, IL-17, TGF-β1, IL-4, IL-12p35, and IL-15 (Hazelbag *et al.*, 2001; Lazar and Chifiriuc, 2010). They are thus potentially an alternative candidate. Interestingly, similar to DON-induced opposing survival ERK and apoptotic p38 signaling pathway in RAW 264.7 cells (Zhou *et al.*, 2005a), Hela cells also process these competing survival and apoptotic pathways (Fan *et al.*, 2007). Consistent with that PKR mediates the activation of p38 in RAW 264.7 cells(Zhou *et al.*, 2003b), DON-

induced p38 and JNK activation were also dose-dependently suppressed by PKR inhibitor 2AP (Fig. B.3), suggesting the Hela cells can be used as a novel model to study DON-induced RSR like RAW 264.7 macrophages.

Ribosome is composed of about 80 ribosomal proteins and rRNAs, and the assembly process is complicated. Since FLAG tag may affect the folding of recombinant ribosomal proteins, which compete with wild-type ribosomal proteins for ribosome assembly, the FLAG tag as well as a short linker were constructed to each ribosomal protein at N- or C-terminal, respectively, to screen for the maximum incorporation. Interestingly, although the N-terminal FLAG constructs have additional 30 amino acids, they have higher efficiency in incorporating into the ribosome than the C-terminal FLAG with additional 13 amino acids, suggesting the C-terminal may be more important in folding and interaction with other ribosomal proteins. Notably, the immunoprecipitation of ribosome in HEK 293T cells showed that N-FLAG RPL18, but not C-FLAG RPL18, successfully pulled down ribosome. Although all the recombinant proteins were expressed very well in Hela cells for 24 h transfection, the ribosome pelleting data did not match those in HEK 293T cells as expected. However, the RPL7 ribosomal marker was not comparable to HEK 293T, suggesting this experiment did not efficiently pull down ribosome. Repeat of ribosome pelleting is need in Hela cells to confirm the incorporation of these FLAG-tagged proteins into ribosome. Alternatively, since only transfection of 2 μg plasmids for 24 h were performed in Hela cells, optimization such as different transfection times, various plasmid concentrations and starting cell density may be needed to determine the optimal conditions for the maximum incorporation rate and immunoprecipitation of ribosome in Hela cells.

The affinity purified ribosome will be a powerful tool for future studies on RSR, selective translation, rRNA cleavage and other ribosome-associated events. For example, there is still a gap in DON treatment and the activation of PKR. DON has been proposed to bind to ribosome and change its confirmation leading to the activation. However, other kinases, for example, direct PKR activator PACT may respond to stress, mobilize to ribosome and activate PKR. With the successful immunoprecipitation of ribosome and associated kinases, we may be able to identify all kinases associated with ribosome in response to toxin exposure and establish the complete signaling map. DON is also found to specifically cleave rRNA at A3560 and A4045 on 28S rRNA(Li and Pestka, 2008) and mRNA and protein level of RNase L are both elevated in this process, suggesting it is the executive RNase. Further studies employing RNase L in vitro assay and transfection of 2-5A, the natural activator of RNase L, do not induce rRNA cleavage, indicating either coordination with capsase is needed or other RNases are the executive RNases (He and Pestka, 2010). Affinity purified ribosomes might be applicable to elucidate the exact mechanism.

Taken together, most of the plasmids are expressed and incorporated into ribosome both in HEK 293T and Hela cells, and there can potentially be used to immunoprecipitate ribosome and facilitate ribosome-related studies in the near future. However, optimization may still be needed to achieve the maximum incorporation rate and optimal efficiency for immunoprecipitation. In addition, the biological activity of FLAG-tagged ribosome should be compared to the wild-type ribosome to make sure they are all actively involved in translation.

Appendix C

Comparison of DON-induced Proinflammatory Genes in Wildtype and PKR Knockout Mice

ABSTRACT

Deoxynivalenol (DON), a trichothecene mycotoxin primarily produced by *Fusarium spp.*, is a translational inhibitor and commonly contaminates cereal-based foods and has the potential to adversely affect humans and animals. At low doses, DON could induce immunostimulatory effects by upregulating expression and stability of various proinflammatory genes both *in vivo* and *in vitro*. Although double-stranded RNA protein kinase (PKR) is the known upstream mediator, its role on the *in vivo* expression of proinflammatory genes has not been investigated. Here we employed PKR knockout mice to test the hypothesis that these mice will show attenuated proinflammatory cytokine expression compared to wildtype controls. PKR knockout and wildtype mice (7 wk) were treated with DON at 5 and 25 mg/kg for 2 h, followed by relative mRNA expression analyses of IL-1β, IL-4, IL-6 and INF-γ in liver, spleen and kidney using realtime PCR. Our data showed that expression of IL-4 was suppressed in liver and spleen at both low and high doses while IL-6 was only attenuated by DON at 5 mg/kg in kidney and spleen. IFN-γ was suppressed in spleen of PKR knockout mice at both doses but IL-1β was only attenuated at 25 mg/kg DON in liver. These data suggested that PKR knockout mice only partially attenuated DON-upregulated expression of proinflammatory genes specifically depending on gene, dose and tissue.

INTRODUCTION

Deoxynivalenol (DON), a trichothecene mycotoxin primarily produced by *Fusarium spp.*, is a translational inhibitor and commonly contaminates cereal-based foods and has the potential to adversely affect humans and animals. The cellular target of DON is the peptidyl transferase region of the ribosome, binding to which by DON interferes with initiation and elongation of translation. In mouse model, orally administered DON (25 mg/kg body weight), is detectable from 5 min to 24 h in plasma, liver, spleen and brain and from 5 min to 8 h in heart and kidney(Pestka *et al.*, 2008a). At low doses, DON induces immunostimulatory effects by upregulating expression of genes including TNF-α, IL-6, MIP-2 and COX-2 in macrophages(Moon and Pestka, 2002; Chung *et al.*, 2003a; Chung *et al.*, 2003b; Jia *et al.*, 2004), IL-8 in monocytes(Gray and Pestka, 2007; Gray *et al.*, 2008) and IL-2 in T cells(Li *et al.*, 1997).

MAPKs play cirtical roles in DON-induced upregulation of proinflammatory cytokine and chemokine expressions. DON has been shown to activate p38, JNK and ERK1/2 in Jurkat T-cell line by triggering “ribotoxic stress response” (RSR) (Shifrin and Anderson, 1999; Pestka *et al.*, 2005). However, only ERKs and p38, but not JNKs, were found to mediate DON-induced COX-2 gene expression in macrophages (Moon and Pestka, 2002). In addition, DON treatment could activate p38 to upregulate IL-8 (Islam *et al.*, 2006) and TNF-α expression by elevating both transcription and mRNA stability (Chung *et al.*, 2003b). Consistent with the in vitro studies, in vivo studies on the activation of MAPKs and transcription factors in mouse spleen confirm that rapid phosphorylation of MAPKs precedes the activation of transcription factors including AP-1, CREB and NF-κB and proinflammatory cytokine mRNA expression(Zhou *et al.*,

2003a).

Double-stranded RNA protein kinase (PKR) is the upstream mediator of RSR first identified in RAW 264.7 macrophage(Zhou *et al.*, 2003b). PKR is a widely-distributed constitutively-expressed serine/threonine protein kinase that can be activated by dsRNA, interferon, proinflammatory stimuli, cytokines and oxidative stress(Williams, 2001; Garcia et al., 2006) and has diverse functions including controlling cell growth, tumor suppressing, apoptosis, and antiviral infection(Koromilas et al., 1992; Lengyel, 1993; Chu et al., 1999). After binding to dsRNA, PKR is activated by dimerization and phosphorylation and phosohorylates eIF-2α at serine 51, which leads to the higher affinity to the GTP exchange factor eIF-2β and results in translation inhibition (Sudhakar et al., 2000). Additionally, PKR also activates various factors including signal transducers and activator of transcription (STAT), interferon regulatory factor1 (IRF-1), p53, JNK, p38 and NF-κB(Verma et al., 1995; Williams, 1999; Williams, 2001) and regulate the expression of proinflammatory genes. In RAW 264.7 macrophages, PKR is activated in 5 minutes by detecting its autophorylation and has been proved to be upstream activator for MAPKs(Zhou *et al.*, 2003b). Human U-937 monocyte cell line transfected with PKR antisense RNA also showed significantly reduced MAPK response to DON treatment. In addition, PKR inhibition also suppresses the DON-induced cytokine and chemokine expressions, including TNF-a, MIP-2 and IL-8(Gray and Pestka, 2007).

Although PKR is found to mediate DON-induced gene expression, but its role in the regulation of *in vivo* cytokine and chemokine expression is largely unknown. Our data presented here showed that PKR knockout mice showed significantly suppressed

expression of IL-4 and IFN-γ in spleen and IL-4 in liver at both 5 and 25 mg/kg DON. Expression of IL-6 in spleen and kidney were also attenuated in PKR knockout mice at 5 mg/kg while IL-1β in liver was only reduced at 25 mg/kg DON. Taken together, PKR knockout mice attenuated the expression of some proinflammatory genes but not all of them, which seems to be in a gene-, dose- and tissue-dependent manner.

MATERIALS AND METHODS

Animals. All animal studies were conducted according to National Institutes of Health guidelines as overseen by the All University Committee on Animal Use and Care at Michigan State University. Young adult (7 wk) female C57BL/6 wildtype or PKR knockout mice (Van Andel, MI) were randomly assigned to experimental groups and acclimated for 1 wk. Mice were housed 3 per cage under a 12 h light/dark cycle, and provided with standard rodent chow and water. Room temperature and relative humidity were maintained between 21 and 24 ℃ and 40–55% humidity, respectively.

PKR knockout mice genotyping. Genomic DNA (gDNA) was extracted from mouse tail clips using the Genomic DNA purification kit (Qiagen, Valencia, CA). PCR were then performed in a 50 µl reaction volume: 5 µl of 10 x reaction buffer, 100 ng template gDNA, forward/reverse primer 1 µl (10 µM), dNTP mix 1 µl (10 mM), Taq DNA polymerase 50 U and nuclease-free water up to 50 µl. Primers for identification of wildtype (forward: AGC CTT TTA TGT GGG TGC TG and reverse: GCA CCA TCC AAC CAA TTT TC) and PKR knockout (forward: CAG CGC ATC GCC TTC TAT C and reverse: GCA CCA TCC AAC CAA TTT TC) mice were used. PCR was programmed as follows: step 1: 95 ℃, 5 min, step 2: 95 ℃, 30 seconds, 56 ℃, 1 min, 60 ℃, 1 min (go to step 2 repeat 35 cycles), step 3: 72 ℃ 10 min, hold at 4 ℃. PCR product were mix with loading dye, separated on 1% agarose gel and stained with ethidium bromide. The expected fragment size for wildtype and PKR knockout are 700 bp and 900 bp, respectively.

Experimental design. The experimental design is shown in Fig. C.1. For each experiment, groups of mice (n = 5) were gavaged with 5 or 25 mg/kg bw DON (Sigma

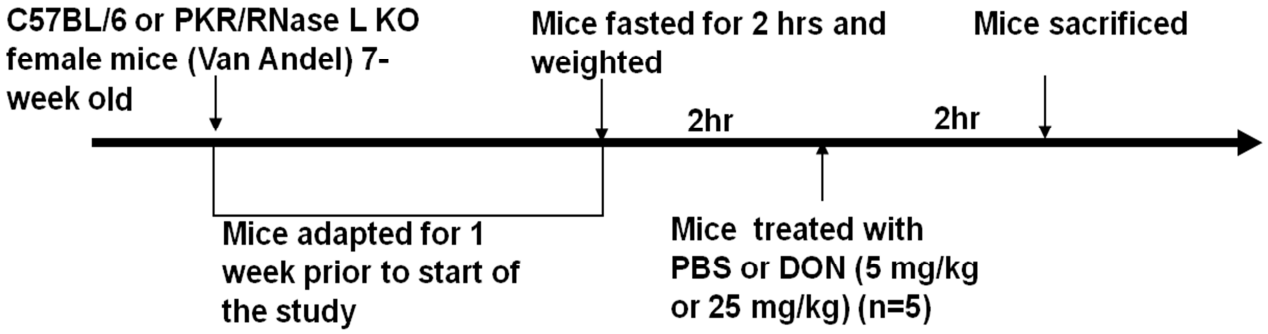

Figure C.1. Experimental design for DON-induced mRNA expression of proinflammatory genes. Mice are acclimated for one week before fasted for 2 h following by oral gavage of vehicle, 5 and 25 mg/kg DON, respectively, which were sacrificed two hours later.

Chemical Co., St. Louis, MO), dissolved in 100 µl of Dulbecco's phosphate buffered saline (PBS) (Sigma–Aldrich, St Louis, MO), using a 22 G intubation needle (Popper and Sons, New Hyde Park, NY). After 2 h, mice were deeply anesthetized by i.p. injection with 0.1 ml of 12% (w/v) sodium pentobarbital in saline. The abdominal cavity was opened. Then cranial half of spleens, lateral lobe of liver and right kidney were collected for total RNA purification.

Realtime PCR for proinflammatory cytokine mRNAs. Excised tissues for PCR analyses were stored in RNAlaterTM (Ambion Inc., Austin, TX) immediately after harvesting. RNA was isolated using Tri Reagent (Molecular Research Center Inc, Cincinnati, OH). Real-time PCR for IL-1β, IL-4, IL-6 and IFN-γ were performed on an ABI PRISM® 7900HT Sequence Detection System, using Taqman One-Step Real-time PCR Master Mix and probes (IL-1β: Mm00434228_m1, IL-4: Mm00445259_m1, IL-6: Mm00446190_m1 and IFN-γ: Mm01168134_m1) according to the manufacturer's protocols (Applied Biosystems, Foster City, NY). Relative quantification of proinflammatory cytokine gene expression was carried out using β2-microglobulin RNA control and an arithmetic formula method (Amuzie et al., 2008).

Statistics. All data were analyzed with SigmaStat v 3.1 (Jandel Scientific, San Rafael,CA) with the criterion for significance set at $p < 0.05$. Two-way ANOVA was used for comparison of multiple groups.

RESULTS

The genotype of PKR knockout and wildtype mice were confirmed by PCR as described in Materials and Methods (data not shown). Relative mRNA expression of proinflammatory cytokines IL-1β, IL-4, IFN-γ and IL-6 in PKR knockout mice were compared to wild-type at 120 min after oral exposure to 5 and 25 mg/kg of DON. In liver, PKR knockout mice showed significantly attenuated expression of IL-4 relative to wildtype controls at both 5 and 25 mg/kg DON (Fig. C.2A), while expression of IL-1β was only reduced at 25 mg/kg DON (Fig. C.2B). In spleen, expression of IFN-γ (Fig. C. 3A), IL-4(Fig. C.3B) and IL-6 (Fig. C.3C) were significantly lowered in PKR knockout mice than wildtype control at 5 mg/kg DON. However, at 25 mg/kg, IL-4 and IFN-γ but not IL-6 also showed suppressed expression in PKR knockout mice. In kidney, only IL-6 (Fig. C.4) was detected to be suppressed in PKR knockout mice at 5 mg/kg but not 25 mg/kg.

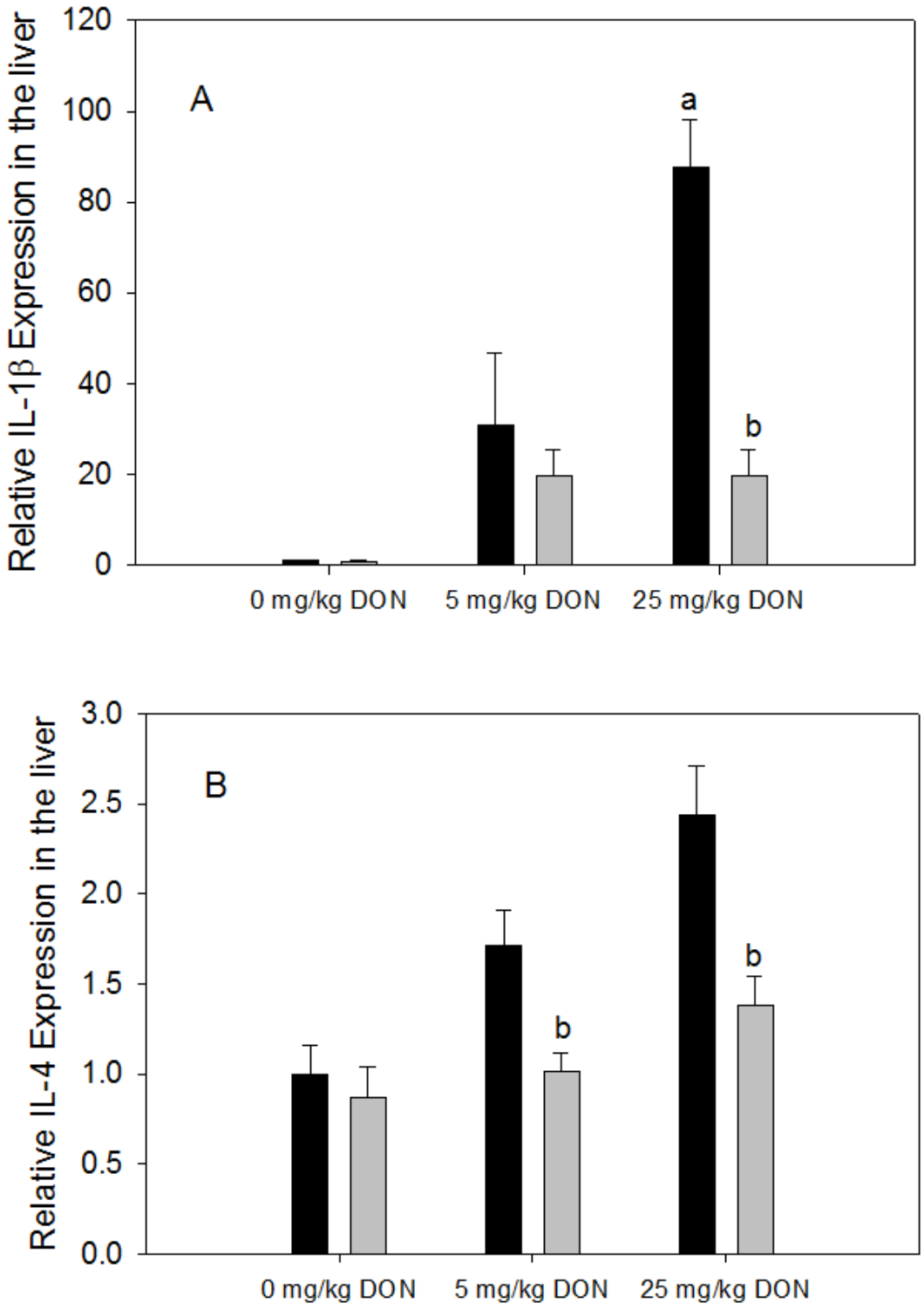

Figure C.2. DON-induced relative mRNA expression of IL-1β and IL-4 in liver. DON-induced changes in proinflammatory cytokine (A) IL-1β and (B) IL-4 mRNA expression in liver of PKR knockout (light bar) and wild-type (dark bar) mice following oral exposure to vehicle, 5 and 25 mg/kg of DON, respectively. Data are mean ± SEM (n = 5). Bars labeled (a) are significantly different from the 5 mg/kg counterparts ($p<0.05$) whereas bars labeled (b) are significantly different from the wild-type at the dose ($p < 0.05$).

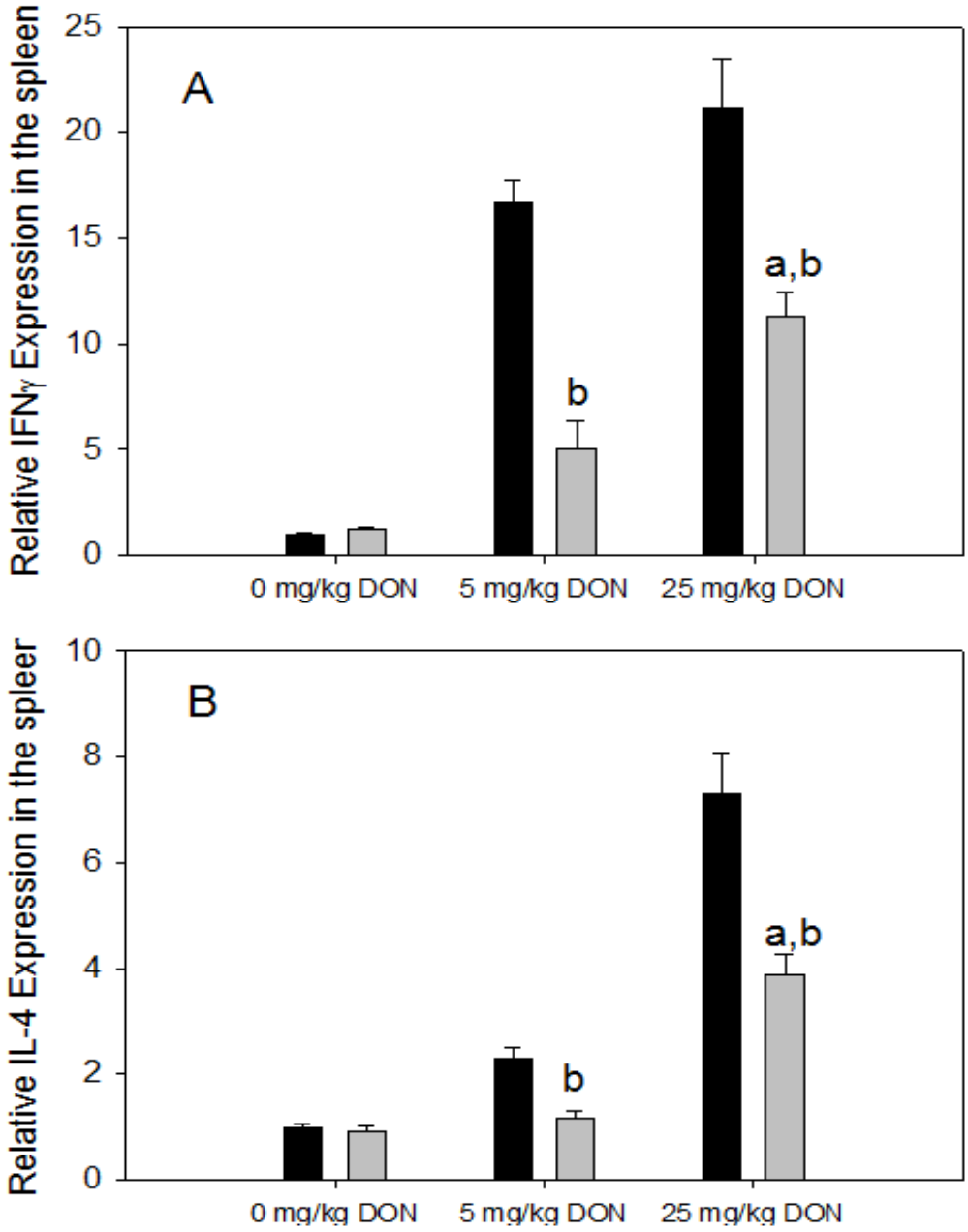

Figure C.3. DON-induced relative mRNA expression of INF-γ, IL-4 and IL-6 in spleen. DON-induced changes in proinflammatory cytokine (A) INF-γ, (B) IL-4 and (C) IL-6 mRNA expression in spleen of PKR knockout (light bar) and wild-type (dark bar) mice following oral exposure to vehicle, 5 and 25 mg/kg of DON, respectively. Data are mean ± SEM (n = 5). Bars labeled (a) are significantly different from the 5 mg/kg counterparts ($p<0.05$) whereas bars labeled (b) are significantly different from the wild-type at the dose ($p < 0.05$).

Figure C.3. (cont'd)

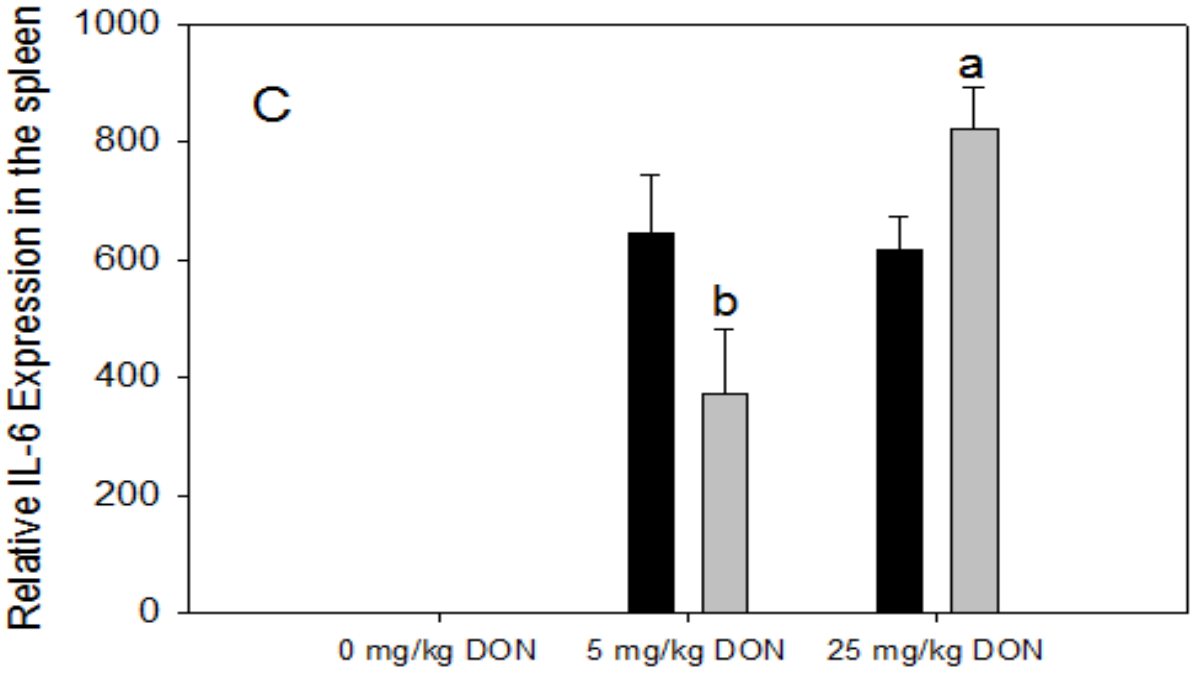

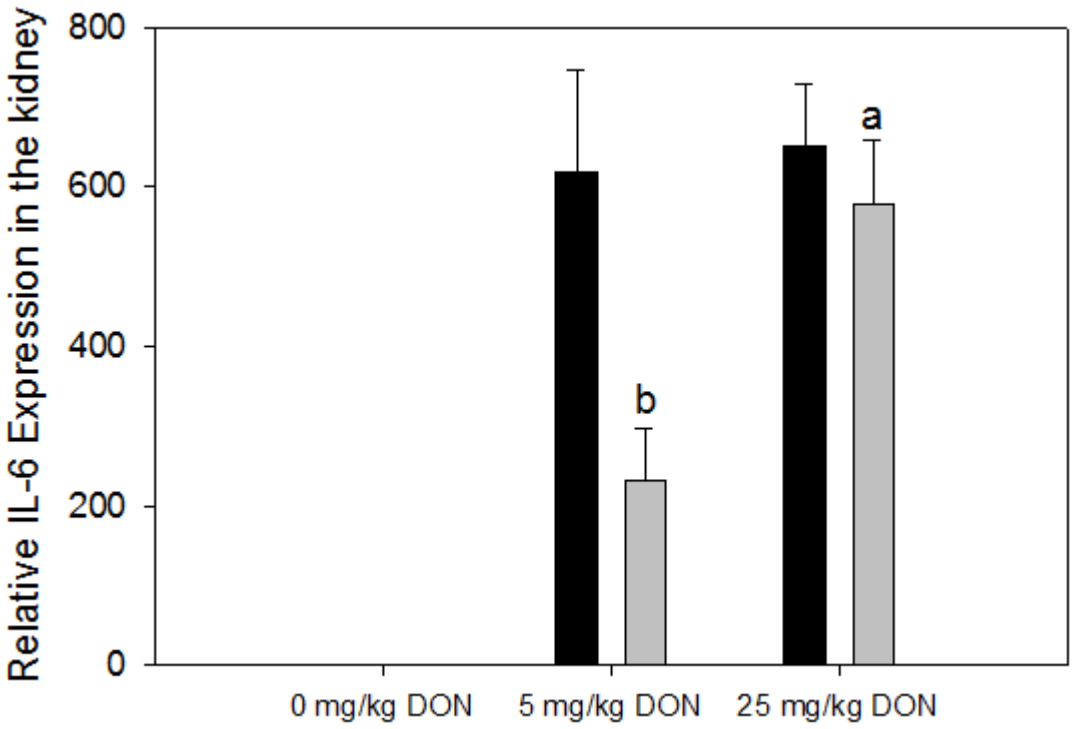

Figure C.4. DON-induced relative mRNA expression of IL-6 in kidney. DON-induced changes in proinflammatory cytokine IL-6 mRNA expression in kidney of PKR knockout (light bar) and wild-type (dark bar) mice following oral exposure to vehicle, 5 and 25 mg/kg of DON, respectively. Data are mean ± SEM (n = 5). Bars labeled (a) are significantly different from the 5 mg/kg counterparts ($p<0.05$) whereas bars labeled (b) are significantly different from the wild-type at the dose ($p < 0.05$).

DISCUSSION

The precise exon-intron organization of the PKR gene has been determined in mouse by sequencing the mouse genomic library, which contains 16 exons and spans about 28 kb(Tanaka and Samuel, 1994). The N-terminal half of PKR mRNA is composed of 8 exons and encodes the RNA binding subdomains, while the C-terminal half is composed of 7 exons and encodes the kinase catalytic subdomains. Basically, Exon 1 and part of exon 2 encode the 5' untranslated region (UTR) of the major (2.4 kb) PKR transcript. Exon 2 includes the AUG translation initiation codon as well as the first 515 amino acids. Exons 3 and 5 encodes the RNA binding motif, respectively. Exon 10 contains the catalytic subdomain. Exon 16 includes the UAG translation termination site and the 3' UTR.

The PKR knockout mice were generated by replacing the wildtype PKR exon 2 and 3 allele with a neomycin-resistant (NEO) gene in an antisense orientation and the upstream mouse sequence (UMS) element which purposely mediates transcription termination. Although substantial levels of mRNA were produced, from which the two disrupted exons were deleted, no PKR fragment was observed by either Western blotting or an autophosphorylation assay, and no kinase activity was detected in *in vitro* assay with eIF-2α as substrate, suggesting the successful establishment of PKR knockout mice(Tanaka and Samuel, 1994). However, another laboratory reported that the 42–44-kDa exon-skipped mouse PKR (ES-PKR) protein was detected in reticulocyte lysates programmed to translate the ES-PKR mRNA from PKR knockout mice(Baltzis *et al.*, 2002). Furthermore, they used antibodies specific to the C terminus of ES-PKR, which was previously unavailable, and demonstrated that ES-PKR is

indeed expressed and contains eIF-2 kinase activity both *in vitro and in vivo*(Baltzis et al., 2002*)*.

Since the protein level of truncated PKR was not determined and the DON-induced signaling pathway leading to PKR activation is not clear, it is hard to compare the role of PKR in different tissues. Although our data showed that PKR knockout mice showed attenuated expression of some proinflammatory genes, the mice with full length PKR knocked out are needed to elucidate the biological function of PKR in DON-induced upregulation of proinflammatory genes.

Appendix D

DON-induced Modulation of MicroRNA Expression in RAW 264.7 Macrophages- A Potential Novel Mechanism for Translational Inhibition.

ABSTRACT

MicroRNAs (miRNAs) are short oligonucleotides that influence various biological processes by binding to the target genes 3'-UTRs thereby facilitating suppression of translation and/or mRNA decay. The objective of this research was to study how the trichothecene mycotoxin deoxynivalenol (DON) influences the endogenous miRNA profile in RAW 264.7 macrophages and predict their potential regulatory roles on ribosomal protein mRNA expression using the miRNA database microCosm. RAW 264.7 cells were treated with 250 ng/ml DON for 2 h and 6 h, and RNA analyzed by RT-PCR array to measure changes in expression of 376 known miRNAs. Clustering analysis revealed that changes in expression of miRNAs was observed both at 2 h and 6 h, but that there were more distinct upregulated miRNAs observed at 6 h. The data showed that 91% of the all ribosomal protein mRNAs could be potentially regulated by miRNAs. The large subunit ribosomal proteins (RPLs) with predicted miRNA upregulation were very similar at 2 and 6 h (90% and 93%, respectively), while those with downregulated miRNAs decreased from 46% at 2 h to 23% at 6 h. The small subunit ribosomal proteins (RPSs) showed a similar trend to RPLs with upregulated miRNA increases from 79% at 2 h to 96.5% at 6 h s and downregulated miRNAs of 48% at 2 h and 27% at 6 h. In addition, DON-induced relative expression of miRNA 155 was confirmed by realtime PCR. The results suggest that downregulation of ribosomal protein mRNAs could conceivably contribute to the known capacity of DON and other trichothecenes to inhibit protein translation.

Table D.1. DON-regulated miRNAs and their predicted targets.

miRNA ID	Relative fold change		predicted ribosomal protein targets
	DON 2h vs Control	DON 6h vs Control	
mmu-miR-1	1.08	4.39	
mmu-miR-100	-38.70	-1.08	RPS21
mmu-miR-124	2.59	1.50	RPL35a gene3/RPS23
mmu-miR-125a-3p	2.86	2.11	RPL35a/ RPL41
mmu-miR-125b-3p	3.18	1.57	RPL31 gene3/ RPL37a gene2/ RPL41
mmu-miR-129-3p	5.50	1.72	RPL7a/ RPL12
mmu-miR-132	2.30	1.69	RPL13a gene2/ RPL15/ RPL21 gene4/ RPL35 gene2/ RPLp1
mmu-miR-133a	1.81	8.09	RPL5/ RPL13a/RPS12
mmu-miR-133b	-2.50	1.01	RPL13a/RPS12
mmu-miR-134	1.78	4.98	RPL7/ RPL23a gene2/gene3/ RPL35a gene5/RPS7
mmu-miR-135b	1.20	3.60	RPS8/ RPS27a
mmu-miR-139-3p	-1.13	10.86	RPL11/ RPL41gene2
mmu-miR-153	2.45	1.40	RPL11 Gene2/ RPL30/RPS21
mmu-miR-155	3.00	5.59	
mmu-miR-184	1.17	-2.21	
mmu-miR-200b*	1.86	2.20	RPL26/RPS4x
mmu-miR-202-3p	2.14	6.30	RPL10/ RPL21 gene2/RPS21
mmu-miR-205	5.85	2.02	RPL12 Gene3/RPS15/RPS26
mmu-miR-208	2.02	2.34	RPL21 gene5/RPL32/ RPL35a gene6
mmu-miR-210	-1.03	3.37	RPL29
mmu-miR-211	14.06	7.15	RPL4/ RPL35a gene3
mmu-miR-212	1.81	8.16	RPL13a/ RPL32/RPSa/ RPS9
mmu-miR-214	1.84	2.63	RPL31/RPS8 gene2/RPS17
mmu-miR-215	-3.18	1.65	RPL4/ RPL23 gene2/RPS8
mmu-miR-216b	1.60	2.82	RPL10a/ RPL21 gene3/ RPL35a gene4/RPS2 gene3
mmu-miR-217	3.75	5.57	RPL27/RPS2 gene2/RPS24
mmu-miR-218	1.13	3.19	RPL6

Table D. 1. (cont'd)

mmu-miR-220	-1.21	3.33	RPL5 Gege/RPL11-RPL11 Gene2/ RPL15/ RPL24/RPL27 gene2/RPL27a/ RPL31 gene2/RPS18
mmu-miR-224	3.50	1.72	Gene3 RPL7a/ RPL35a gene5
mmu-miR-290-5p	-3.56	6.04	RPL13/RPL29 gene2/RPS15/RPS19
mmu-miR-291a-3p	2.06	-1.06	RPL10a/RPL11/RPL27a/ RPL30
mmu-miR-291a-5p	3.51	7.82	RPL12 Gene4/ RPL14/ RPL18a/ RPL35/ RPL37a
mmu-miR-291b-3p	2.86	9.90	RPS26
mmu-miR-292-3p	3.73	1.96	RPL32/RPL35a gene5/RPS3
mmu-miR-294*	5.40	3.85	RPL11/RPLp0
mmu-miR-298	-4.97	-2.68	RPL41/RPS2 gene 2
mmu-miR-300	3.20	1.13	RPL22/ RPL35a gene2/RPS26
mmu-miR-302d	2.06	2.68	RPL11/RPL11 Gene2/RPL27 gene2/RPS3/ RPS5/RPS12/RPS23/RPS28
mmu-miR-31	1.71	3.34	
mmu-miR-32	-2.66	-4.62	
mmu-miR-320	1.44	2.82	RPL23/ RPL35a gene3
mmu-miR-323-5p	2.13	8.96	RPL3/ RPL41
mmu-miR-325	5.18	1.16	RPL5/ RPL41/RPS2 gene4/RPS3
mmu-miR-327	1.25	2.83	
mmu-miR-329	-2.41	-2.02	RPL23/ RPL37a gene2/RPLp0/RPS6/RPS23/ RPS27a
mmu-miR-331-5p	-2.74	1.24	RPL8/ RPL13 gene2/RPLp0//RPS4x
mmu-miR-335-5p	-1.15	3.15	RPL35a gene2/ RPL37/RPS17
mmu-miR-337-3p	3.45	1.31	RPL10a/ RPL13a/ RPL15/RPL26 gene2/RPS13
mmu-miR-337-5p	1.09	2.04	RPL29/RPS gene4
mmu-miR-341	-1.04	2.07	RPS29
mmu-miR-342-5p	1.14	3.04	RPL21 gene2

Table D. 1. (cont'd)

mmu-miR-34b-3p	-2.09	-1.46	RPL31
mmu-miR-363	6.47	2.11	RPL8/RPL11/RPL12 Gene4/ RPL14/ RPL30/RPS2 gene 4
mmu-miR-369-5p	4.51	1.46	RPL35a gene4
mmu-miR-370	-1.90	7.12	RPL11 Gene2/ RPL13a gene2
mmu-miR-375	1.56	9.44	RPLp0
mmu-miR-376a	-2.20	-2.00	
mmu-miR-376b*	2.13	3.32	RPL12 Gene2/ RPL13/ RPL15/RPS28
mmu-miR-376c	5.65	3.04	
mmu-miR-380-3p	2.49	2.17	RPL21 gene2/ RPL35a gene4/RPS21
mmu-miR-384-5p	2.23	3.05	RPL24/RPLp0
mmu-miR-409-5p	-3.79	1.62	RPL11 Gene2/ RPL13 gene2/ RPL31 gene3/ RPL41 gene3/RPS14/RPS23 gene2
mmu-miR-411	1.20	3.41	RPL10a/RPLp0/RPS8 gene2
mmu-miR-423-5p	1.32	2.05	
mmu-miR-448	-2.50	4.39	RPS8/RPS15
mmu-miR-453	2.36	1.24	RPL23/RPS18
mmu-miR-455	3.65	8.75	RPL11/RPL12 Gene4/RPL29/RPLp0/RPS25
mmu-miR-465a-5p	2.27	1.58	RPL21 gene3/ RPL27a
mmu-miR-466d-3p	5.09	1.43	RPL13 Gene2/RPL26
mmu-miR-466f-3p	2.60	1.56	RPL15/ RPL31
mmu-miR-466f-5p	2.95	2.42	RPL10/RPL29/ RPL35a gene3
mmu-miR-467a*	4.96	3.89	
mmu-miR-467e	1.33	6.15	RPL11 Gene2/ RPL13a gene2/ RPL39/ RPL41 gene2
mmu-miR-471	6.49	1.54	RPL35a gene6/ RPL41
mmu-miR-485	3.35	-2.36	
mmu-miR-486	-1.29	28.64	RPL13/ RPL14/ RPL38/RPS5/ RPS7/RPS10/ RPS11/RPS13

Table D. 1. (cont'd)

mmu-miR-487b	2.51	10.62	RPL13a/ RPL22/ RPL31/ RPL41
mmu-miR-488	1.04	2.69	
mmu-miR-490	3.40	2.42	RPL22/ RPL22/ RPL23/ RPLp1/RPS6/RPS12 gene2
mmu-miR-495	2.15	-1.05	RPL8/ RPL34/RPLp0/RPS2/ RPS5/ RPS25/ RPS27a
mmu-miR-496	3.62	4.25	RPL31/RPS4x
mmu-miR-503	1.51	2.88	RPL32/RPS7/RPS17
mmu-miR-504	4.46	4.63	RPL21/ RPL23a/RPS3/RPS14
mmu-miR-541	7.03	3.60	RPL41
mmu-miR-543	8.19	1.11	
mmu-miR-546	3.24	2.88	RPL7a/RPL18/ RPL35a gene6/ RPL37/ RPL41/ RPL41 gene2
mmu-miR-590-3p	5.33	2.03	RPL4/ RPL15 gene2/ RPL22/RPL27/RPL/RPS11
mmu-miR-590-5p	2.24	3.74	RPL31/ RPL32/ RPL37a/RPS11/RPS14
mmu-miR-615-3p	4.27	-1.14	RPL30 gene2/RPS2 gene2
mmu-miR-653	3.55	1.24	RPL39
mmu-miR-654-3p	2.35	2.87	RPL8/RPL18/RPL26 gene2/RPS7
mmu-miR-654-5p	1.04	2.81	RPL18/RPL26/ RPL35/RPS7/ RPS16/RPS17/RPS24
mmu-miR-665	2.42	1.97	RPL11 Gene2
mmu-miR-666-3p	1.89	2.82	RPS15
mmu-miR-667	1.26	12.22	RPL5 Gene 2/RPS8 gene2
mmu-miR-669b	1.50	1.16	
mmu-miR-672	-1.63	2.21	RPS11/RPS27
mmu-miR-675-5p	1.49	3.58	
mmu-miR-676	-1.05	2.77	RPL7a/ RPL30/RPLp0
mmu-miR-678	5.63	3.50	RPL35a gene3
mmu-miR-681	1.37	2.46	RPL21 gene5/ RPL41 gene2/RPS4x
mmu-miR-683	-3.63	-3.39	Gene3 RPL7a/ RPL12/ RPL21 gene3/ RPL35 gene2/RPS18
mmu-miR-684	5.26	-3.46	

Table D. 1. (cont'd)

mmu-miR-686	1.37	24.77	RPL11 Gene2/ RPL12/ RPL28/RPS26
mmu-miR-687	-4.09	-1.34	RPL7a/ RPL13/RPL38/RPSa/RPS8/RPS15
mmu-miR-688	4.44	1.25	RPL11/RPSa/RPS26
mmu-miR-698	2.88	1.74	RPL11/ RPL23a/ RPL37a/RPS10/ RPS21
mmu-miR-699	-1.10	2.65	RPL13a gene2
mmu-miR-702	1.86	4.01	RPL11/ RPL18/ RPL21 gene5
mmu-miR-704	-2.10	-2.91	RPL7a/RPS12/RPS23 gene2
mmu-miR-705	1.43	3.95	
mmu-miR-707	2.49	1.83	RPL10a/RPS13
mmu-miR-711	1.30	2.15	RPL23/RPL27 gene3
mmu-miR-714	1.39	3.23	
mmu-miR-715	-1.02	3.34	RPL5/RPS14
mmu-miR-718	-1.39	18.43	RPS18
mmu-miR-719	-1.33	3.65	RPL11
mmu-miR-720	2.45	2.95	RPL12/ RPL24 gene2
mmu-miR-721	2.31	1.18	RPL28/ RPL35a gene3
mmu-miR-742	-1.03	2.35	RPL26 gene2
mmu-miR-743b-5p	2.09	2.20	RPL27 gene2/RPLp0
mmu-miR-758	-2.03	1.72	RPL18
mmu-miR-759	2.68	22.48	RPL41
mmu-miR-760	-1.12	3.41	RPL35a
mmu-miR-764-3p	2.32	1.18	RPL19/ RPL28/ RPL35a/RPS29
mmu-miR-770-3p	1.61	3.09	RPL18a/ RPL35a/RPS27
mmu-miR-770-5p	1.05	12.50	RPL11/ RPL17/ RPL22/ RPL23/ RPL41 gene3
mmu-miR-802	2.81	-2.90	RPS6/ RPS15a
mmu-miR-804	2.01	2.20	
mmu-miR-871	-1.05	7.42	
mmu-miR-874	1.23	12.67	RPL10a Gene2/ RPL12/ RPL23
mmu-miR-878-3p	3.70	-1.34	RPSa/RPS12
mmu-miR-881*	1.29	3.83	
mmu-miR-882	2.61	4.85	

Table D. 1. (cont'd)

mmu-miR-883a-5p	-4.64	-5.81	RPL15/RPL27/ RPL36/ RPL41/RPS5
mmu-miR-883b-3p	-2.04	3.97	RPL26 /RPL27 gene2/RPS25
mmu-miR-883b-5p	2.09	-1.35	RPL41
mmu-miR-92b	1.20	11.67	

Using 2-fold change as threshod, the up- and down-regulated miRNA were shown in red and green, respectively.

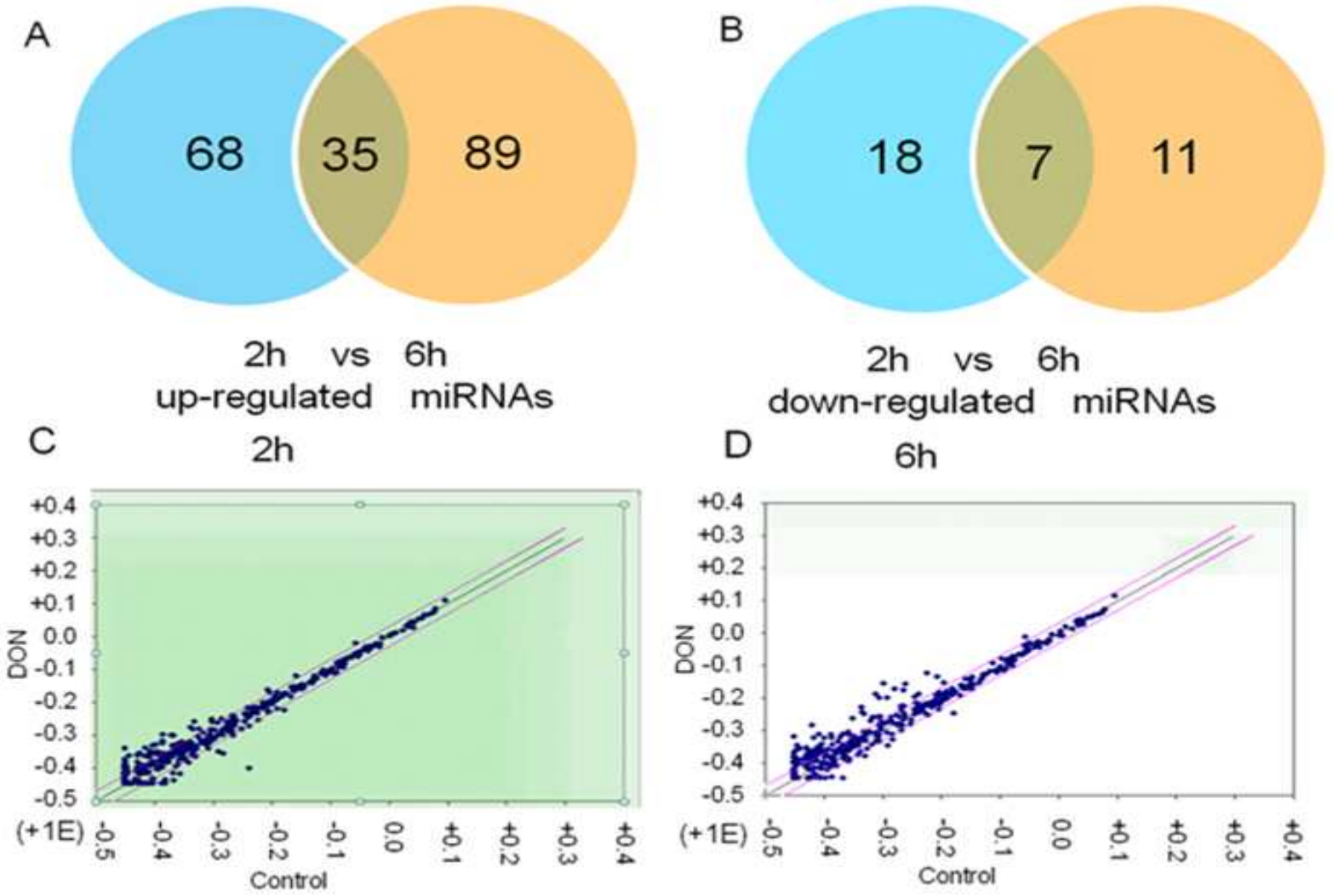

Figure D.1. DON induced miRNA expression change in RAW 264.7 macrophage. Cells were treated with PBS or 250 ng/ml DON for 2 h and 6 h, respectively, followed by cell lysis and miRNA purification. The resultant miRNAs were analyzed by PCR array. The numbers of (A) up- and down-regulated miRNAs using two-fold change threshod were and miRNA profile were summarized in A and B.

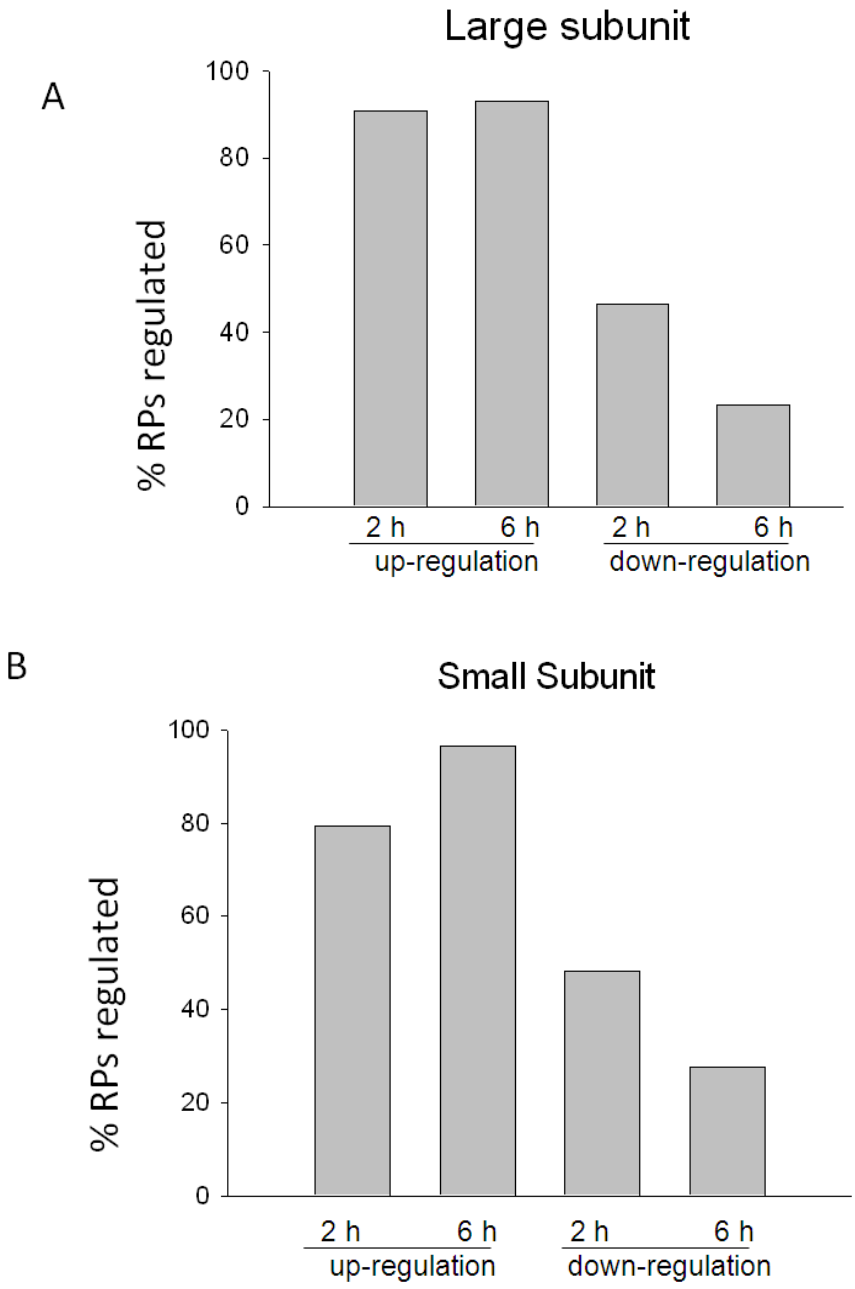

Figure D.2. Percentage of Ribosomal proteins potentially regulated by miRNAs. Ribosomal proteins were searched in online miRNA target prediction software, miBase, for potential regulating miRNAs. The percentage of (A) large and (B) small subunits RPs were calculated and shown.

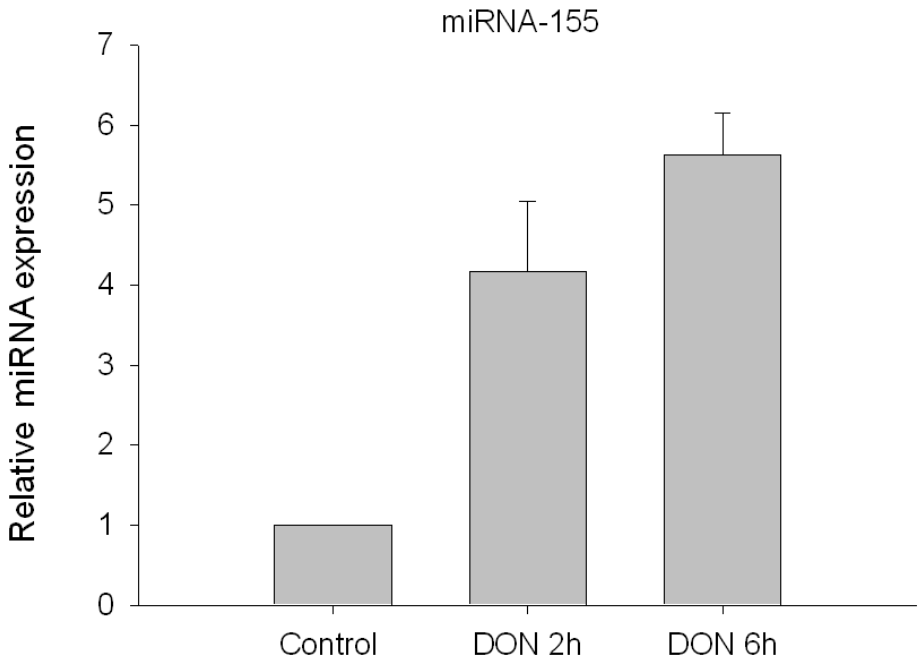

Figure D. 3. DON-induced relative miRNA 155 expression at 2 and 6 h. Three independent cell culture experiments were conducted. Each miRNA sample was analyzed in duplicate and quantified by real-time PCR. Data are mean ± SE of triplicate wells.

REFERENCES

REFERENCES

Abbas, H.K., Mirocha, C.J., Pawlosky, R.J., Pusch, D.J., 1985. Effect of cleaning, milling, and baking on deoxynivalenol in wheat. Appl Environ Microbiol **50**, 482-486.

Afshar, A.S., Mousavi, A., Majd, A., Renu, Adam, G., 2007. Double mutation in tomato ribosomal protein L3 cDNA confers tolerance to deoxynivalenol (DON) in transgenic tobacco. Pak J Biol Sci **10**, 2327-2333.

Alisi, A., Spaziani, A., Anticoli, S., Ghidinelli, M., Balsano, C., 2008. PKR is a novel functional direct player that coordinates skeletal muscle differentiation via p38MAPK/AKT pathways. Cell Signal **20**, 534-542.

Amuzie, C.J., Harkema, J.R., Pestka, J.J., 2008. Tissue distribution and proinflammatory cytokine induction by the trichothecene deoxynivalenol in the mouse: comparison of nasal vs. oral exposure. Toxicology **248**, 39-44.

Amuzie, C.J., Pestka, J.J., 2010. Suppression of insulin-like growth factor acid-labile subunit expression--a novel mechanism for deoxynivalenol-induced growth retardation. Toxicol Sci **113**, 412-421.

Anderson, P.D., 2012. Bioterrorism: toxins as weapons. J Pharm Pract **25**, 121-129.

Bae, H., Gray, J.S., Li, M., Vines, L., Kim, J., Pestka, J.J., 2010. Hematopoietic cell kinase associates with the 40S ribosomal subunit and mediates the ribotoxic stress response to deoxynivalenol in mononuclear phagocytes. Toxicol Sci **115**, 444-452.

Bae, H.K., Shinozuka, J., Islam, Z., Pestka, J.J., 2009. Satratoxin G interaction with 40S and 60S ribosomal subunits precedes apoptosis in the macrophage. Toxicology and Applied Pharmacology **237**, 137-145.

Baltzis, D., Li, S., Koromilas, A.E., 2002. Functional characterization of pkr gene products expressed in cells from mice with a targeted deletion of the N terminus or C terminus domain of PKR. J Biol Chem **277**, 38364-38372.

Banerjee, S., An, S., Zhou, A., Silverman, R.H., Makino, S., 2000. RNase L-independent specific 28S rRNA cleavage in murine coronavirus-infected cells. J Virol **74**, 8793-8802.

Bao, Q., Shi, Y., 2007. Apoptosome: a platform for the activation of initiator caspases. Cell Death Differ **14**, 56-65.

Barish, G.D., Yu, R.T., Karunasiri, M., Ocampo, C.B., Dixon, J., Benner, C., Dent, A.L., Tangirala, R.K., Evans, R.M., 2010. Bcl-6 and NF-kappaB cistromes mediate opposing regulation of the innate immune response. Genes Dev **24**, 2760-2765.

Ben-Asouli, Y., Banai, Y., Pel-Or, Y., Shir, A., Kaempfer, R., 2002. Human interferon-gamma mRNA autoregulates its translation through a pseudoknot that activates the interferon-inducible protein kinase PKR. Cell **108**, 221-232.

Bertolotti, A., Zhang, Y., Hendershot, L.M., Harding, H.P., Ron, D., 2000. Dynamic interaction of BiP and ER stress transducers in the unfolded-protein response. Nat Cell Biol **2**, 326-332.

Bidere, N., Lorenzo, H.K., Carmona, S., Laforge, M., Harper, F., Dumont, C., Senik, A., 2003. Cathepsin D triggers Bax activation, resulting in selective apoptosis-inducing factor (AIF) relocation in T lymphocytes entering the early commitment phase to apoptosis. J Biol Chem **278**, 31401-31411.

Bondy, G.S., Pestka, J.J., 2000. Immunomodulation by fungal toxins. J Toxicol Environ Health B Crit Rev **3**, 109-143.

Borish, L.C., Steinke, J.W., 2003. 2. Cytokines and chemokines. J Allergy Clin Immunol **111**, S460-475.

Boya, P., Kroemer, G., 2008. Lysosomal membrane permeabilization in cell death. Oncogene **27**, 6434-6451.

Bunyard, P., Handley, M., Pollara, G., Rutault, K., Wood, I., Chaudry, M., Alderman, C., Foreman, J., Katz, D.R., Chain, B.M., 2003. Ribotoxic stress activates p38 and JNK kinases and modulates the antigen-presenting activity of dendritic cells. Mol Immunol **39**, 815-827.

Calvet, J.P., Pederson, T., 1977. Secondary structure of heterogeneous nuclear RNA: two classes of double-stranded RNA in native ribonucleoprotein. Proc Natl Acad Sci U S A **74**, 3705-3709.

Calvo, S.E., Pagliarini, D.J., Mootha, V.K., 2009. Upstream open reading frames cause widespread reduction of protein expression and are polymorphic among humans. Proc Natl Acad Sci U S A **106**, 7507-7512.

Carroll, M.C., 2004. The complement system in regulation of adaptive immunity. Nat Immunol **5**, 981-986.

Carter, C.J., Cannon, M., 1977. Structural requirements for the inhibitory action of 12,13-epoxytrichothecenes on protein synthesis in eukaryotes. Biochem J **166**, 399-409.

Chandra, D., Choy, G., Deng, X., Bhatia, B., Daniel, P., Tang, D.G., 2004. Association of active caspase 8 with the mitochondrial membrane during apoptosis: potential roles in cleaving BAP31 and caspase 3 and mediating mitochondrion-endoplasmic reticulum cross talk in etoposide-induced cell death. Mol Cell Biol **24**, 6592-6607.

Chebath, J., Benech, P., Hovanessian, A., Galabru, J., Revel, M., 1987. Four different forms of interferon-induced 2',5'-oligo(A) synthetase identified by immunoblotting in human cells. J Biol Chem **262**, 3852-3857.

Cheeseman, M.T., Tyrer, H.E., Williams, D., Hough, T.A., Pathak, P., Romero, M.R., Hilton, H., Bali, S., Parker, A., Vizor, L., Purnell, T., Vowell, K., Wells, S., Bhutta, M.F., Potter, P.K., Brown, S.D., 2011. HIF-VEGF pathways are critical for chronic otitis media in Junbo and Jeff mouse mutants. PLoS Genet **7**, e1002336.

Choi, H.J., Yang, H., Park, S.H., Moon, Y., 2009. HuR/ELAVL1 RNA binding protein modulates interleukin-8 induction by muco-active ribotoxin deoxynivalenol. Toxicol Appl Pharmacol **240**, 46-54.

Chu, W.M., Ostertag, D., Li, Z.W., Chang, L., Chen, Y., Hu, Y., Williams, B., Perrault, J., Karin, M., 1999. JNK2 and IKKbeta are required for activating the innate response to viral infection. Immunity **11**, 721-731.

Chung, Y.J., Yang, G.H., Islam, Z., Pestka, J.J., 2003a. Up-regulation of macrophage inflammatory protein-2 and complement 3A receptor by the trichothecenes deoxynivalenol and satratoxin G. Toxicology **186**, 51-65.

Chung, Y.J., Zhou, H.R., Pestka, J.J., 2003b. Transcriptional and posttranscriptional roles for p38 mitogen-activated protein kinase in upregulation of TNF-alpha expression by deoxynivalenol (vomitoxin). Toxicol Appl Pharmacol **193**, 188-201.

Clemens, M.J., Bushell, M., Jeffrey, I.W., Pain, V.M., Morley, S.J., 2000. Translation initiation factor modifications and the regulation of protein synthesis in apoptotic cells. Cell Death Differ **7**, 603-615.

Clemens, M.J., Vaquero, C.M., 1978. Inhibition of protein synthesis by double-stranded RNA in reticulocyte lysates: evidence for activation of an endoribonuclease. Biochem Biophys Res Commun **83**, 59-68.

Cobb, M.H., 1999. MAP kinase pathways. Progress in Biophysics and Molecular Biology **71**, 479-500.

Commins, S.P., Borish, L., Steinke, J.W., 2010. Immunologic messenger molecules: cytokines, interferons, and chemokines. J Allergy Clin Immunol **125**, S53-72.

Cory, S., Adams, J.M., 2002. The Bcl2 family: regulators of the cellular life-or-death switch. Nat Rev Cancer **2**, 647-656.

Degen, W.G., Pruijn, G.J., Raats, J.M., van Venrooij, W.J., 2000. Caspase-dependent cleavage of nucleic acids. Cell Death Differ **7**, 616-627.

Demeshkina, N., Repkova, M., Ven'yaminova, A., Graifer, D., Karpova, G., 2000. Nucleotides of 18S rRNA surrounding mRNA codons at the human ribosomal A, P, and E sites: a crosslinking study with mRNA analogs carrying an aryl azide group at either the uracil or the guanine residue. RNA **6**, 1727-1736.

Desagher, S., Osen-Sand, A., Nichols, A., Eskes, R., Montessuit, S., Lauper, S., Maundrell, K., Antonsson, B., Martinou, J.C., 1999. Bid-induced conformational change of Bax is responsible for mitochondrial cytochrome c release during apoptosis. J Cell Biol **144**, 891-901.

Desjardins, A.E., Proctor, R.H., 2007. Molecular biology of Fusarium mycotoxins. Int J Food Microbiol **119**, 47-50.

Di, R., Tumer, N.E., 2005. Expression of a truncated form of ribosomal protein L3 confers resistance to pokeweed antiviral protein and the Fusarium mycotoxin deoxynivalenol. Mol Plant Microbe Interact **18**, 762-770.

Ding, H.F., Lin, Y.L., McGill, G., Juo, P., Zhu, H., Blenis, J., Yuan, J., Fisher, D.E., 2000. Essential role for caspase-8 in transcription-independent apoptosis triggered by p53. J Biol Chem **275**, 38905-38911.

Droga-Mazovec, G., Bojic, L., Petelin, A., Ivanova, S., Romih, R., Repnik, U., Salvesen, G.S., Stoka, V., Turk, V., Turk, B., 2008. Cysteine cathepsins trigger caspase-dependent cell death through cleavage of bid and antiapoptotic Bcl-2 homologues. J Biol Chem **283**, 19140-19150.

Ehrhardt, H., Hacker, S., Wittmann, S., Maurer, M., Borkhardt, A., Toloczko, A., Debatin, K.M., Fulda, S., Jeremias, I., 2008. Cytotoxic drug-induced, p53-mediated upregulation of caspase-8 in tumor cells. Oncogene **27**, 783-793.

Elmore, S., 2007. Apoptosis: a review of programmed cell death. Toxicol Pathol **35**, 495-516.

Endo, Y., Huber, P.W., Wool, I.G., 1983. The ribonuclease activity of the cytotoxin alpha-sarcin. The characteristics of the enzymatic activity of alpha-sarcin with ribosomes and ribonucleic acids as substrates. J Biol Chem **258**, 2662-2667.

Endo, Y., Mitsui, K., Motizuki, M., Tsurugi, K., 1987. The mechanism of action of ricin and related toxic lectins on eukaryotic ribosomes. The site and the characteristics of the modification in 28 S ribosomal RNA caused by the toxins. J Biol Chem **262**, 5908-5912.

Endo, Y., Tsurugi, K., 1986. Mechanism of action of ricin and related toxic lectins on eukaryotic ribosomes. Nucleic Acids Symp Ser, 187-190.

Endo, Y., Tsurugi, K., Yutsudo, T., Takeda, Y., Ogasawara, T., Igarashi, K., 1988. Site of action of a Vero toxin (VT2) from Escherichia coli O157:H7 and of Shiga toxin on eukaryotic ribosomes. RNA N-glycosidase activity of the toxins. Eur J Biochem **171**, 45-50.

Ernst, M., Inglese, M., Scholz, G.M., Harder, K.W., Clay, F.J., Bozinovski, S., Waring, P., Darwiche, R., Kay, T., Sly, P., Collins, R., Turner, D., Hibbs, M.L., Anderson, G.P., Dunn, A.R., 2002. Constitutive activation of the SRC family kinase Hck results in spontaneous pulmonary inflammation and an enhanced innate immune response. J Exp Med **196**, 589-604.

Fan, T.J., Han, L.H., Cong, R.S., Liang, J., 2005. Caspase family proteases and apoptosis. Acta Biochim Biophys Sin (Shanghai) **37**, 719-727.

Fan, Y., Chen, H., Qiao, B., Luo, L., Ma, H., Li, H., Jiang, J., Niu, D., Yin, Z., 2007. Opposing effects of ERK and p38 MAP kinases on HeLa cell apoptosis induced by dipyrithione. Mol Cells **23**, 30-38.

Fedoroff, N., Wellauer, P.K., Wall, R., 1977. Intermolecular duplexes in heterogeneous nuclear RNA from HeLa cells. Cell **10**, 597-610.

Fogarty, M.P., McCormack, R.M., Noonan, J., Murphy, D., Gowran, A., Campbell, V.A., 2010. A role for p53 in the beta-amyloid-mediated regulation of the lysosomal system. Neurobiol Aging **31**, 1774-1786.

Forsell, J.H., Jensen, R., Tai, J.H., Witt, M., Lin, W.S., Pestka, J.J., 1987. Comparison of acute toxicities of deoxynivalenol (vomitoxin) and 15-acetyldeoxynivalenol in the B6C3F1 mouse. Food Chem Toxicol **25**, 155-162.

Fried, H.M., Warner, J.R., 1981. Cloning of yeast gene for trichodermin resistance and ribosomal protein L3. Proc Natl Acad Sci U S A **78**, 238-242.

Fuentes-Prior, P., Salvesen, G.S., 2004. The protein structures that shape caspase activity, specificity, activation and inhibition. Biochem J **384**, 201-232.

Garcia, M.A., Gil, J., Ventoso, I., Guerra, S., Domingo, E., Rivas, C., Esteban, M., 2006. Impact of protein kinase PKR in cell biology: from antiviral to antiproliferative action. Microbiol Mol Biol Rev **70**, 1032-1060.

Gebauer, F., Hentze, M.W., 2004. Molecular mechanisms of translational control. Nat Rev Mol Cell Biol **5**, 827-835.

Goh, K.C., deVeer, M.J., Williams, B.R., 2000. The protein kinase PKR is required for p38 MAPK activation and the innate immune response to bacterial endotoxin. EMBO J **19**, 4292-4297.

Gorski, J.L., Gonzalez, I.L., Schmickel, R.D., 1987. The secondary structure of human 28S rRNA: the structure and evolution of a mosaic rRNA gene. J Mol Evol **24**, 236-251.

Gray, J.S., Bae, H.K., Li, J.C., Lau, A.S., Pestka, J.J., 2008. Double-stranded RNA-activated protein kinase mediates induction of interleukin-8 expression by deoxynivalenol, Shiga toxin 1, and ricin in monocytes. Toxicol Sci **105**, 322-330.

Gray, J.S., Pestka, J.J., 2007. Transcriptional regulation of deoxynivalenol-induced IL-8 expression in human monocytes. Toxicol Sci **99**, 502-511.

Grolleau, A., Bowman, J., Pradet-Balade, B., Puravs, E., Hanash, S., Garcia-Sanz, J.A., Beretta, L., 2002. Global and specific translational control by rapamycin in T cells uncovered by microarrays and proteomics. J Biol Chem **277**, 22175-22184.

Grollman, A.P., 1967. Inhibitors of protein biosynthesis. II. Mode of action of anisomycin. J Biol Chem **242**, 3226-3233.

Gyles, C.L., 2007. Shiga toxin-producing Escherichia coli: an overview. J Anim Sci **85**, E45-62.

Halbeisen, R.E., Gerber, A.P., 2009. Stress-Dependent Coordination of Transcriptome and Translatome in Yeast. PLoS Biol **7**, e105.

Harris, L.J., Gleddie, S.C., 2001. A modified Rpl3 gene from rice confers tolerance of the Fusarium graminearum mycotoxin deoxynivalenol to transgenic tobacco. Physiological and Molecular Plant Pathology **58**, 173-181.

Hartley, M.R., Lord, J.M., 2004a. Cytotoxic ribosome-inactivating lectins from plants. Biochimica et Biophysica Acta (BBA) - Proteins & Proteomics **1701**, 1-14.

Hartley, M.R., Lord, J.M., 2004b. Cytotoxic ribosome-inactivating lectins from plants. Biochim Biophys Acta **1701**, 1-14.

Hasegawa, M., Sato, S., Takehara, K., 1999. Augmented production of chemokines (monocyte chemotactic protein-1 (MCP-1), macrophage inflammatory protein-1alpha (MIP-1alpha) and MIP-1beta) in patients with systemic sclerosis: MCP-1 and MIP-1alpha may be involved in the development of pulmonary fibrosis. Clin Exp Immunol **117**, 159-165.

Hazelbag, S., Fleuren, G.J., Baelde, J.J., Schuuring, E., Kenter, G.G., Gorter, A., 2001. Cytokine profile of cervical cancer cells. Gynecol Oncol **83**, 235-243.

He, K., Pestka, J.J., 2010. Deoxynivalenol-induced modulation of microRNA expression in RAW 264.7 macrophages-A potential novel mechanism for translational inhibition. The Toxicologist (Toxicol Sci) **114 (Suppl)**, 310.

He, K., Zhou, H.R., Pestka, J.J., 2012. Targets and Intracellular Signaling Mechanisms for Deoxynivalenol-Induced Ribosomal RNA Cleavage. Toxicol Sci.

Hess, J., Angel, P., Schorpp-Kistner, M., 2004. AP-1 subunits: quarrel and harmony among siblings. J Cell Sci **117**, 5965-5973.

Hinnebusch, A.G., 1997. Translational regulation of yeast GCN4. A window on factors that control initiator-trna binding to the ribosome. J Biol Chem **272**, 21661-21664.

Hope, R., Aldred, D., Magan, N., 2005. Comparison of environmental profiles for growth and deoxynivalenol production by Fusarium culmorum and F. graminearum on wheat grain. Lett Appl Microbiol **40**, 295-300.

Horrix, C., Raviv, Z., Flescher, E., Voss, C., Berger, M.R., 2011. Plant ribosome-inactivating proteins type II induce the unfolded protein response in human cancer cells. Cell Mol Life Sci **68**, 1269-1281.

Houge, G., Doskeland, S.O., 1996. Divergence towards a dead end? Cleavage of the divergent domains of ribosomal RNA in apoptosis. Experientia **52**, 963-967.

Houge, G., Doskeland, S.O., Boe, R., Lanotte, M., 1993. Selective cleavage of 28S rRNA variable regions V3 and V13 in myeloid leukemia cell apoptosis. FEBS Lett **315**, 16-20.

Houge, G., Robaye, B., Eikhom, T.S., Golstein, J., Mellgren, G., Gjertsen, B.T., Lanotte, M., Doskeland, S.O., 1995. Fine mapping of 28S rRNA sites specifically cleaved in cells undergoing apoptosis. Mol Cell Biol **15**, 2051-2062.

Hudak, K.A., Dinman, J.D., Tumer, N.E., 1999. Pokeweed antiviral protein accesses ribosomes by binding to L3. J Biol Chem **274**, 3859-3864.

Inada, T., Winstall, E., Tarun, S.Z., Jr., Yates, J.R., 3rd, Schieltz, D., Sachs, A.B., 2002. One-step affinity purification of the yeast ribosome and its associated proteins and mRNAs. RNA **8**, 948-958.

Iordanov, M.S., Choi, R.J., Ryabinina, O.P., Dinh, T.H., Bright, R.K., Magun, B.E., 2002. The UV (Ribotoxic) stress response of human keratinocytes involves the unexpected uncoupling of the Ras-extracellular signal-regulated kinase signaling cascade from the activated epidermal growth factor receptor. Mol Cell Biol **22**, 5380-5394.

Iordanov, M.S., Magun, B.E., 1998. Loss of cellular K+ mimics ribotoxic stress. Inhibition of protein synthesis and activation of the stress kinases SEK1/MKK4,

stress-activated protein kinase/c-Jun NH2-terminal kinase 1, and p38/HOG1 by palytoxin. J Biol Chem **273**, 3528-3534.

Iordanov, M.S., Magun, B.E., 1999. Different mechanisms of c-Jun NH(2)-terminal kinase-1 (JNK1) activation by ultraviolet-B radiation and by oxidative stressors. J Biol Chem **274**, 25801-25806.

Iordanov, M.S., Paranjape, J.M., Zhou, A., Wong, J., Williams, B.R., Meurs, E.F., Silverman, R.H., Magun, B.E., 2000. Activation of p38 mitogen-activated protein kinase and c-Jun NH(2)-terminal kinase by double-stranded RNA and encephalomyocarditis virus: involvement of RNase L, protein kinase R, and alternative pathways. Mol Cell Biol **20**, 617-627.

Iordanov, M.S., Pribnow, D., Magun, J.L., Dinh, T.H., Pearson, J.A., Chen, S.L., Magun, B.E., 1997. Ribotoxic stress response: activation of the stress-activated protein kinase JNK1 by inhibitors of the peptidyl transferase reaction and by sequence-specific RNA damage to the alpha-sarcin/ricin loop in the 28S rRNA. Mol Cell Biol **17**, 3373-3381.

Islam, Z., Gray, J.S., Pestka, J.J., 2006. p38 Mitogen-activated protein kinase mediates IL-8 induction by the ribotoxin deoxynivalenol in human monocytes. Toxicol Appl Pharmacol **213**, 235-244.

Islam, Z., Shinozuka, J., Harkema, J.R., Pestka, J.J., 2009. Purification and comparative neurotoxicity of the trichothecenes satratoxin G and roridin L2 from Stachybotrys chartarum. J Toxicol Environ Health A **72**, 1242-1251.

Jandhyala, D.M., Ahluwalia, A., Obrig, T., Thorpe, C.M., 2008. ZAK: a MAP3Kinase that transduces Shiga toxin- and ricin-induced proinflammatory cytokine expression. Cell Microbiol **10**, 1468-1477.

Jandhyala, D.M., Thorpe, C.M., Magun, B., 2012. Ricin and Shiga toxins: effects on host cell signal transduction. Curr Top Microbiol Immunol **357**, 41-65.

Jeffrey, I.W., Kadereit, S., Meurs, E.F., Metzger, T., Bachmann, M., Schwemmle, M., Hovanessian, A.G., Clemens, M.J., 1995. Nuclear localization of the interferon-inducible protein kinase PKR in human cells and transfected mouse cells. Exp Cell Res **218**, 17-27.

Jia, Q., Zhou, H.R., Bennink, M., Pestka, J.J., 2004. Docosahexaenoic acid attenuates mycotoxin-induced immunoglobulin a nephropathy, interleukin-6 transcription, and mitogen-activated protein kinase phosphorylation in mice. J Nutr **134**, 3343-3349.

Jia, Q., Zhou, H.R., Shi, Y., Pestka, J.J., 2006. Docosahexaenoic acid consumption inhibits deoxynivalenol-induced CREB/ATF1 activation and IL-6 gene transcription in mouse macrophages. J Nutr **136**, 366-372.

Jiang, Y., Beller, D.I., Frendl, G., Graves, D.T., 1992. Monocyte chemoattractant protein-1 regulates adhesion molecule expression and cytokine production in human monocytes. J Immunol **148**, 2423-2428.

Johansson, A.C., Appelqvist, H., Nilsson, C., Kagedal, K., Roberg, K., Ollinger, K., 2010. Regulation of apoptosis-associated lysosomal membrane permeabilization. Apoptosis **15**, 527-540.

Johnson, C.R., Jiffar, T., Fischer, U.M., Ruvolo, P.P., Jarvis, W.D., 2003. Requirement for SAPK-JNK signaling in the induction of apoptosis by ribosomal stress in REH lymphoid leukemia cells. Leukemia **17**, 2140-2148.

Kapp, L.D., Lorsch, J.R., 2004. The molecular mechanics of eukaryotic translation. Annu Rev Biochem **73**, 657-704.

Keshet, Y., Seger, R., 2010. The MAP kinase signaling cascades: a system of hundreds of components regulates a diverse array of physiological functions. Methods Mol Biol **661**, 3-38.

Kimura, M., Tokai, T., Takahashi-Ando, N., Ohsato, S., Fujimura, M., 2007. Molecular and genetic studies of fusarium trichothecene biosynthesis: pathways, genes, and evolution. Biosci Biotechnol Biochem **71**, 2105-2123.

King, K.L., Jewell, C.M., Bortner, C.D., Cidlowski, J.A., 2000. 28S ribosome degradation in lymphoid cell apoptosis: evidence for caspase and Bcl-2-dependent and -independent pathways. Cell Death Differ **7**, 994-1001.

Kinser, S., Jia, Q., Li, M., Laughter, A., Cornwell, P., Corton, J.C., Pestka, J., 2004. Gene expression profiling in spleens of deoxynivalenol-exposed mice: immediate early genes as primary targets. J Toxicol Environ Health A **67**, 1423-1441.

Kinser, S., Li, M., Jia, Q., Pestka, J.J., 2005. Truncated deoxynivalenol-induced splenic immediate early gene response in mice consuming (n-3) polyunsaturated fatty acids. The Journal of Nutritional Biochemistry **16**, 88-95.

Kobayashi, Y., Mizunuma, M., Osada, H., Miyakawa, T., 2006. Identification of Saccharomyces cerevisiae ribosomal protein L3 as a target of curvularol, a G1-specific inhibitor of mammalian cells. Biosci Biotechnol Biochem **70**, 2451-2459.

Komar, A.A., Hatzoglou, M., 2011. Cellular IRES-mediated translation: the war of ITAFs in pathophysiological states. Cell Cycle **10**, 229-240.

Komar, A.A., Mazumder, B., Merrick, W.C., 2012. A new framework for understanding IRES-mediated translation. Gene **502**, 75-86.

Koromilas, A.E., Roy, S., Barber, G.N., Katze, M.G., Sonenberg, N., 1992. Malignant transformation by a mutant of the IFN-inducible dsRNA-dependent protein kinase. Science **257**, 1685-1689.

Krishna, M., Narang, H., 2008. The complexity of mitogen-activated protein kinases (MAPKs) made simple. Cell Mol Life Sci **65**, 3525-3544.

Kuhn, K.M., DeRisi, J.L., Brown, P.O., Sarnow, P., 2001. Global and specific translational regulation in the genomic response of Saccharomyces cerevisiae to a rapid transfer from a fermentable to a nonfermentable carbon source. Mol Cell Biol **21**, 916-927.

Kumar, K.U., Srivastava, S.P., Kaufman, R.J., 1999. Double-stranded RNA-activated protein kinase (PKR) is negatively regulated by 60S ribosomal subunit protein L18. Mol Cell Biol **19**, 1116-1125.

Kumar, S., 2007. Caspase function in programmed cell death. Cell Death Differ **14**, 32-43.

Kuny, S., Gaillard, F., Sauve, Y., 2012. Differential gene expression in eyecup and retina of a mouse model of Stargardt-like macular dystrophy (STGD3). Invest Ophthalmol Vis Sci **53**, 664-675.

Lafarga, M., Lerga, A., Andres, M.A., Polanco, J.I., Calle, E., Berciano, M.T., 1997. Apoptosis induced by methylazoxymethanol in developing rat cerebellum: organization of the cell nucleus and its relationship to DNA and rRNA degradation. Cell Tissue Res **289**, 25-38.

Lai, E., Teodoro, T., Volchuk, A., 2007. Endoplasmic reticulum stress: signaling the unfolded protein response. Physiology (Bethesda) **22**, 193-201.

Langland, J.O., Jacobs, B.L., 1992. Cytosolic double-stranded RNA-dependent protein kinase is likely a dimer of partially phosphorylated Mr = 66,000 subunits. J Biol Chem **267**, 10729-10736.

Larsson, S.L., Sloma, M.S., Nygard, O., 2002. Conformational changes in the structure of domains II and V of 28S rRNA in ribosomes treated with the translational inhibitors ricin or alpha-sarcin. Biochim Biophys Acta **1577**, 53-62.

Laskin, J.D., Heck, D.E., Laskin, D.L., 2002. The ribotoxic stress response as a potential mechanism for MAP kinase activation in xenobiotic toxicity. Toxicol Sci **69**, 289-291.

Lazar, V., Chifiriuc, M.C., 2010. Architecture and physiology of microbial biofilms. Roum Arch Microbiol Immunol **69**, 95-107.

Lee, S.Y., Lee, M.S., Cherla, R.P., Tesh, V.L., 2008. Shiga toxin 1 induces apoptosis through the endoplasmic reticulum stress response in human monocytic cells. Cell Microbiol **10**, 770-780.

Lengyel, P., 1993. Tumor-suppressor genes: news about the interferon connection. Proc Natl Acad Sci U S A **90**, 5893-5895.

Leung, A.K., Sharp, P.A., 2010. MicroRNA functions in stress responses. Mol Cell **40**, 205-215.

Li, G., Xiang, Y., Sabapathy, K., Silverman, R.H., 2004. An apoptotic signaling pathway in the interferon antiviral response mediated by RNase L and c-Jun NH2-terminal kinase. J Biol Chem **279**, 1123-1131.

Li, J., Petryshyn, R.A., 1991. Activation of the double-stranded RNA-dependent eIF-2 alpha kinase by cellular RNA from 3T3-F442A cells. Eur J Biochem **195**, 41-48.

Li, M., Pestka, J.J., 2008. Comparative induction of 28S ribosomal RNA cleavage by ricin and the trichothecenes deoxynivalenol and T-2 toxin in the macrophage. Toxicol Sci **105**, 67-78.

Li, N., Zheng, Y., Chen, W., Wang, C., Liu, X., He, W., Xu, H., Cao, X., 2007. Adaptor protein LAPF recruits phosphorylated p53 to lysosomes and triggers lysosomal destabilization in apoptosis. Cancer Res **67**, 11176-11185.

Li, S., Ouyang, Y., Yang, G.H., Pestka, J.J., 2000. Modulation of transcription factor AP-1 activity in murine EL-4 thymoma cells by vomitoxin (deoxynivalenol). Toxicol Appl Pharmacol **163**, 17-25.

Li, S., Ouyang, Y.L., Dong, W., Pestka, J.J., 1997. Superinduction of IL-2 gene expression by vomitoxin (deoxynivalenol) involves increased mRNA stability. Toxicol Appl Pharmacol **147**, 331-342.

Liang, S.L., Quirk, D., Zhou, A., 2006. RNase L: its biological roles and regulation. IUBMB Life **58**, 508-514.

Lindauer, M., Wong, J., Magun, B., 2010. Ricin Toxin Activates the NALP3 Inflammasome. Toxins (Basel) **2**, 1500-1514.

Liu, T.C., Huang, C.J., Chu, Y.C., Wei, C.C., Chou, C.C., Chou, M.Y., Chou, C.K., Yang, J.J., 2000. Cloning and expression of ZAK, a mixed lineage kinase-like protein containing a leucine-zipper and a sterile-alpha motif. Biochem Biophys Res Commun **274**, 811-816.

Ma, X.M., Blenis, J., 2009. Molecular mechanisms of mTOR-mediated translational control. Nat Rev Mol Cell Biol **10**, 307-318.

Maddaluno, M., Di Lauro, M., Di Pascale, A., Santamaria, R., Guglielmotti, A., Grassia, G., Ialenti, A., 2011. Monocyte chemotactic protein-3 induces human coronary smooth muscle cell proliferation. Atherosclerosis **217**, 113-119.

Malhi, H., Kaufman, R.J., 2011. Endoplasmic reticulum stress in liver disease. J Hepatol **54**, 795-809.

Manche, L., Green, S.R., Schmedt, C., Mathews, M.B., 1992. Interactions between double-stranded RNA regulators and the protein kinase DAI. Mol Cell Biol **12**, 5238-5248.

Marion, M.J., Marion, C., 1987. Localization of ribosomal proteins on the surface of mammalian 60S ribosomal subunits by means of immobilized enzymes. Correlation with chemical cross-linking data. Biochem Biophys Res Commun **149**, 1077-1083.

Marion, M.J., Marion, C., 1988. Ribosomal proteins S2, S6, S10, S14, S15 and S25 are localized on the surface of mammalian 40 S subunits and stabilize their conformation. A study with immobilized trypsin. FEBS Lett **232**, 281-285.

Markou, T., Marshall, A.K., Cullingford, T.E., Tham el, L., Sugden, P.H., Clerk, A., 2010. Regulation of the cardiomyocyte transcriptome vs translatome by endothelin-1 and insulin: translational regulation of 5' terminal oligopyrimidine tract (TOP) mRNAs by insulin. BMC Genomics **11**, 343.

McCormick, S.P., Stanley, A.M., Stover, N.A., Alexander, N.J., 2011. Trichothecenes: from simple to complex mycotoxins. Toxins (Basel) **3**, 802-814.

Medenbach, J., Seiler, M., Hentze, M.W., 2011. Translational control via protein-regulated upstream open reading frames. Cell **145**, 902-913.

Meskauskas, A., Petrov, A.N., Dinman, J.D., 2005. Identification of functionally important amino acids of ribosomal protein L3 by saturation mutagenesis. Mol Cell Biol **25**, 10863-10874.

Michot, B., Hassouna, N., Bachellerie, J.P., 1984. Secondary structure of mouse 28S rRNA and general model for the folding of the large rRNA in eukaryotes. Nucleic Acids Res **12**, 4259-4279.

Mikulits, W., Pradet-Balade, B., Habermann, B., Beug, H., Garcia-Sanz, J.A., Mullner, E.W., 2000. Isolation of translationally controlled mRNAs by differential screening. FASEB J **14**, 1641-1652.

Moon, Y., Pestka, J.J., 2002. Vomitoxin-induced cyclooxygenase-2 gene expression in macrophages mediated by activation of ERK and p38 but not JNK mitogen-activated protein kinases. Toxicol Sci **69**, 373-382.

Moon, Y., Uzarski, R., Pestka, J.J., 2003. Relationship of trichothecene structure to COX-2 induction in the macrophage: selective action of type B (8-keto) trichothecenes. J Toxicol Environ Health A **66**, 1967-1983.

Moser, B., Wolf, M., Walz, A., Loetscher, P., 2004. Chemokines: multiple levels of leukocyte migration control. Trends Immunol **25**, 75-84.

Muppidi, J., Porter, M., Siegel, R.M., 2004. Measurement of apoptosis and other forms of cell death. Curr Protoc Immunol **Chapter 3**, Unit 3 17.

Mustroph, A., Bailey-Serres, J., 2010. The Arabidopsis translatome cell-specific mRNA atlas: Mining suberin and cutin lipid monomer biosynthesis genes as an example for data application. Plant Signal Behav **5**, 320-324.

Mustroph, A., Zanetti, M.E., Jang, C.J., Holtan, H.E., Repetti, P.P., Galbraith, D.W., Girke, T., Bailey-Serres, J., 2009. Profiling translatomes of discrete cell populations resolves altered cellular priorities during hypoxia in Arabidopsis. Proc Natl Acad Sci U S A **106**, 18843-18848.

Nadano, D., Sato, T.A., 2000. Caspase-3-dependent and -independent degradation of 28 S ribosomal RNA may be involved in the inhibition of protein synthesis during apoptosis initiated by death receptor engagement. J Biol Chem **275**, 13967-13973.

Naito, T., Yokogawa, T., Takatori, S., Goda, K., Hiramoto, A., Sato, A., Kitade, Y., Sasaki, T., Matsuda, A., Fukushima, M., Wataya, Y., Kim, H.S., 2009. Role of RNase L in apoptosis induced by 1-(3-C-ethynyl-beta-D-ribo-pentofuranosyl)cytosine. Cancer Chemother Pharmacol **63**, 837-850.

Narayanan, S., Surendranath, K., Bora, N., Surolia, A., Karande, A.A., 2005. Ribosome inactivating proteins and apoptosis. FEBS Lett **579**, 1324-1331.

Norbury, C.J., Hickson, I.D., 2001. Cellular responses to DNA damage. Annu Rev Pharmacol Toxicol **41**, 367-401.

Ogundele, M., 2001. Role and significance of the complement system in mucosal immunity: particular reference to the human breast milk complement. Immunol Cell Biol **79**, 1-10.

Olsnes, S., 2004. The history of ricin, abrin and related toxins. Toxicon **44**, 361-370.

Ouyang, D.Y., Wang, Y.Y., Zheng, Y.T., 2005. Activation of c-Jun N-terminal kinases by ribotoxic stresses. Cell Mol Immunol **2**, 419-425.

Ouyang, Y.L., Li, S., Pestka, J.J., 1996. Effects of vomitoxin (deoxynivalenol) on transcription factor NF-kappa B/Rel binding activity in murine EL-4 thymoma and primary CD4+ T cells. Toxicol Appl Pharmacol **140**, 328-336.

Pandey, M., Bajaj, G.D., Rath, P.C., 2004. Induction of the interferon-inducible RNA-degrading enzyme, RNase L, by stress-inducing agents in the human cervical carcinoma cells. RNA Biol **1**, 21-27.

Peraica, M., Radic, B., Lucic, A., Pavlovic, M., 1999. Toxic effects of mycotoxins in humans. Bull World Health Organ **77**, 754-766.

Pestka, J.J., 2008. Mechanisms of deoxynivalenol-induced gene expression and apoptosis. Food Addit Contam **24**, 1-13.

Pestka, J.J., 2010a. Deoxynivalenol-induced proinflammatory gene expression: mechanisms and pathological sequelae. Toxins (Basel) **2**, 1300-1317.

Pestka, J.J., 2010b. Deoxynivalenol: mechanisms of action, human exposure, and toxicological relevance. Arch Toxicol **84**, 663-679.

Pestka, J.J., Islam, Z., Amuzie, C.J., 2008a. Immunochemical assessment of deoxynivalenol tissue distribution following oral exposure in the mouse. Toxicol Lett **178**, 83-87.

Pestka, J.J., Smolinski, A.T., 2005. Deoxynivalenol: toxicology and potential effects on humans. J Toxicol Environ Health B Crit Rev **8**, 39-69.

Pestka, J.J., Uzarski, R.L., Islam, Z., 2005. Induction of apoptosis and cytokine production in the Jurkat human T cells by deoxynivalenol: role of mitogen-activated protein kinases and comparison to other 8-ketotrichothecenes. Toxicology **206**, 207-219.

Pestka, J.J., Yan, D., King, L.E., 1994. Flow cytometric analysis of the effects of in vitro exposure to vomitoxin (deoxynivalenol) on apoptosis in murine T, B and IgA+ cells. Food Chem Toxicol **32**, 1125-1136.

Pestka, J.J., Yike, I., Dearborn, D.G., Ward, M.D., Harkema, J.R., 2008b. Stachybotrys chartarum, trichothecene mycotoxins, and damp building-related illness: new insights into a public health enigma. Toxicol Sci **104**, 4-26.

Pestka, J.J., Zhou, H.R., Moon, Y., Chung, Y.J., 2004. Cellular and molecular mechanisms for immune modulation by deoxynivalenol and other trichothecenes: unraveling a paradox. Toxicol Lett **153**, 61-73.

Petersen, A.M., Pedersen, B.K., 2005. The anti-inflammatory effect of exercise. J Appl Physiol **98**, 1154-1162.

Preiss, T., Baron-Benhamou, J., Ansorge, W., Hentze, M.W., 2003. Homodirectional changes in transcriptome composition and mRNA translation induced by rapamycin and heat shock. Nat Struct Biol **10**, 1039-1047.

Prelusky, D.B., Trenholm, H.L., 1992. Nonaccumulation of Residues in Swine Tissue Following Extended Consumption of Deoxynivalenol-Contaminated Diets. Journal of Food Science **57**, 801-802.

Proud, C.G., 2007. Signalling to translation: how signal transduction pathways control the protein synthetic machinery. Biochem J **403**, 217-234.

Repnik, U., Turk, B., 2010. Lysosomal-mitochondrial cross-talk during cell death. Mitochondrion **10**, 662-669.

Robbana-Barnat, S., Lafarge-Frayssinet, C., Cohen, H., Neish, G.A., Frayssinet, C., 1988. Immunosuppressive properties of deoxynivalenol. Toxicology **48**, 155-166.

Rotter, B.A., Prelusky, D.B., Pestka, J.J., 1996. Toxicology of deoxynivalenol (vomitoxin). J Toxicol Environ Health **48**, 1-34.

Rousseaux, C.G., Schiefer, H.B., Hancock, D.S., 1986. Reproductive and teratological effects of continuous low-level dietary T-2 toxin in female CD-1 mice for two generations. J Appl Toxicol **6**, 179-184.

Samali, A., Gilje, B., Doskeland, S.O., Cotter, T.G., Houge, G., 1997. The ability to cleave 28S ribosomal RNA during apoptosis is a cell-type dependent trait unrelated to DNA fragmentation. Cell Death Differ **4**, 289-293.

Sanz, E., Yang, L., Su, T., Morris, D.R., McKnight, G.S., Amieux, P.S., 2009. Cell-type-specific isolation of ribosome-associated mRNA from complex tissues. Proc Natl Acad Sci U S A **106**, 13939-13944.

Schindler, T., Sicheri, F., Pico, A., Gazit, A., Levitzki, A., Kuriyan, J., 1999. Crystal structure of Hck in complex with a Src family-selective tyrosine kinase inhibitor. Mol Cell **3**, 639-648.

Schuler, M., Green, D.R., 2001. Mechanisms of p53-dependent apoptosis. Biochem Soc Trans **29**, 684-688.

Schultz, L.D., Friesen, J.D., 1983. Nucleotide sequence of the tcml gene (ribosomal protein L3) of Saccharomyces cerevisiae. J Bacteriol **155**, 8-14.

Seto, T., Yoshitake, M., Ogasawara, T., Ikari, J., Sakamoto, A., Hatano, M., Hirata, H., Fukuda, T., Kuriyama, T., Tatsumi, K., Tokuhisa, T., Arima, M., 2011. Bcl6 in pulmonary epithelium coordinately controls the expression of the CC-type

chemokine genes and attenuates allergic airway inflammation. Clin Exp Allergy **41**, 1568-1578.

Shenton, D., Smirnova, J.B., Selley, J.N., Carroll, K., Hubbard, S.J., Pavitt, G.D., Ashe, M.P., Grant, C.M., 2006. Global translational responses to oxidative stress impact upon multiple levels of protein synthesis. J Biol Chem **281**, 29011-29021.

Shi, Y., Pestka, J.J., 2009. Mechanisms for suppression of interleukin-6 expression in peritoneal macrophages from docosahexaenoic acid-fed mice. J Nutr Biochem **20**, 358-368.

Shi, Y., Porter, K., Parameswaran, N., Bae, H.K., Pestka, J.J., 2009. Role of GRP78/BiP degradation and ER stress in deoxynivalenol-induced interleukin-6 upregulation in the macrophage. Toxicol Sci **109**, 247-255.

Shifrin, V.I., Anderson, P., 1999. Trichothecene mycotoxins trigger a ribotoxic stress response that activates c-Jun N-terminal kinase and p38 mitogen-activated protein kinase and induces apoptosis. J Biol Chem **274**, 13985-13992.

Silverman, R.H., Cayley, P.J., Knight, M., Gilbert, C.S., Kerr, I.M., 1982. Control of the ppp(a2'p)nA system in HeLa cells. Effects of interferon and virus infection. Eur J Biochem **124**, 131-138.

Slee, E.A., Adrain, C., Martin, S.J., 2001. Executioner caspase-3, -6, and -7 perform distinct, non-redundant roles during the demolition phase of apoptosis. J Biol Chem **276**, 7320-7326.

Smirnova, J.B., Selley, J.N., Sanchez-Cabo, F., Carroll, K., Eddy, A.A., McCarthy, J.E., Hubbard, S.J., Pavitt, G.D., Grant, C.M., Ashe, M.P., 2005. Global gene expression profiling reveals widespread yet distinctive translational responses to different eukaryotic translation initiation factor 2B-targeting stress pathways. Mol Cell Biol **25**, 9340-9349.

Sobrova, P., Adam, V., Vasatkova, A., Beklova, M., Zeman, L., Kizek, R., 2010. Deoxynivalenol and its toxicity. Interdiscip Toxicol **3**, 94-99.

Soengas, M.S., Alarcon, R.M., Yoshida, H., Giaccia, A.J., Hakem, R., Mak, T.W., Lowe, S.W., 1999. Apaf-1 and caspase-9 in p53-dependent apoptosis and tumor inhibition. Science **284**, 156-159.

Sonenberg, N., Hinnebusch, A.G., 2009. Regulation of translation initiation in eukaryotes: mechanisms and biological targets. Cell **136**, 731-745.

Stark, G.R., Kerr, I.M., Williams, B.R., Silverman, R.H., Schreiber, R.D., 1998. How cells respond to interferons. Annu Rev Biochem **67**, 227-264.

Sudhakar, A., Ramachandran, A., Ghosh, S., Hasnain, S.E., Kaufman, R.J., Ramaiah, K.V., 2000. Phosphorylation of serine 51 in initiation factor 2 alpha (eIF2 alpha) promotes complex formation between eIF2 alpha(P) and eIF2B and causes inhibition in the guanine nucleotide exchange activity of eIF2B. Biochemistry **39**, 12929-12938.

Takeda, K., Kojima, Y., Ikejima, K., Harada, K., Yamashina, S., Okumura, K., Aoyama, T., Frese, S., Ikeda, H., Haynes, N.M., Cretney, E., Yagita, H., Sueyoshi, N., Sato, N., Nakanuma, Y., Smyth, M.J., 2008. Death receptor 5 mediated-apoptosis contributes to cholestatic liver disease. Proc Natl Acad Sci U S A **105**, 10895-10900.

Takeda, N., Arima, M., Tsuruoka, N., Okada, S., Hatano, M., Sakamoto, A., Kohno, Y., Tokuhisa, T., 2003. Bcl6 is a transcriptional repressor for the IL-18 gene. J Immunol **171**, 426-431.

Tanaka, H., Samuel, C.E., 1994. Mechanism of interferon action: structure of the mouse PKR gene encoding the interferon-inducible RNA-dependent protein kinase. Proc Natl Acad Sci U S A **91**, 7995-7999.

Tebaldi, T., Re, A., Viero, G., Pegoretti, I., Passerini, A., Blanzieri, E., Quattrone, A., 2012. Widespread uncoupling between transcriptome and translatome variations after a stimulus in mammalian cells. BMC Genomics **13**, 220.

Terman, A., Gustafsson, B., Brunk, U.T., 2006. The lysosomal-mitochondrial axis theory of postmitotic aging and cell death. Chem Biol Interact **163**, 29-37.

Thakur, C.S., Xu, Z., Wang, Z., Novince, Z., Silverman, R.H., 2005. A convenient and sensitive fluorescence resonance energy transfer assay for RNase L and 2',5' oligoadenylates. Methods Mol Med **116**, 103-113.

Toney, L.M., Cattoretti, G., Graf, J.A., Merghoub, T., Pandolfi, P.P., Dalla-Favera, R., Ye, B.H., Dent, A.L., 2000. BCL-6 regulates chemokine gene transcription in macrophages. Nat Immunol **1**, 214-220.

Toroney, R., Bevilacqua, P.C., 2009. PKR and the ribosome compete for mRNA. Nat Chem Biol **5**, 873-874.

Trigo-Stockli, D.M., 2002. Effect of processing on deoxynivalenol and other trichothecenes. Adv Exp Med Biol **504**, 181-188.

Tsygankov, A.Y., 2003. Non-receptor protein tyrosine kinases. Front Biosci **8**, s595-635.

Turner, P.C., Burley, V.J., Rothwell, J.A., White, K.L., Cade, J.E., Wild, C.P., 2008a. Deoxynivalenol: rationale for development and application of a urinary biomarker. Food Addit Contam Part A Chem Anal Control Expo Risk Assess **25**, 864-871.

Turner, P.C., Burley, V.J., Rothwell, J.A., White, K.L., Cade, J.E., Wild, C.P., 2008b. Dietary wheat reduction decreases the level of urinary deoxynivalenol in UK adults. J Expo Sci Environ Epidemiol **18**, 392-399.

Turner, P.C., Rothwell, J.A., White, K.L., Gong, Y., Cade, J.E., Wild, C.P., 2008c. Urinary deoxynivalenol is correlated with cereal intake in individuals from the United kingdom. Environ Health Perspect **116**, 21-25.

Turner, P.C., White, K.L., Burley, V.J., Hopton, R.P., Rajendram, A., Fisher, J., Cade, J.E., Wild, C.P., 2010. A comparison of deoxynivalenol intake and urinary deoxynivalenol in UK adults. Biomarkers **15**, 553-562.

Ueno, Y., 1984. Toxicological features of T-2 toxin and related trichothecenes. Fundam Appl Toxicol **4**, S124-132.

Ueno, Y., 1985. The toxicology of mycotoxins. Crit Rev Toxicol **14**, 99-132.

Uptain, S.M., Kane, C.M., Chamberlin, M.J., 1997. Basic mechanisms of transcript elongation and its regulation. Annu Rev Biochem **66**, 117-172.

Urano, F., Wang, X., Bertolotti, A., Zhang, Y., Chung, P., Harding, H.P., Ron, D., 2000. Coupling of stress in the ER to activation of JNK protein kinases by transmembrane protein kinase IRE1. Science **287**, 664-666.

Uzarski, R.L., Islam, Z., Pestka, J.J., 2003. Potentiation of trichothecene-induced leukocyte cytotoxicity and apoptosis by TNF-alpha and Fas activation. Chem Biol Interact **146**, 105-119.

Uzarski, R.L., Pestka, J.J., 2003. Comparative susceptibility of B cells with different lineages to cytotoxicity and apoptosis induction by translational inhibitors. J Toxicol Environ Health A **66**, 2105-2118.

Verma, I.M., Stevenson, J.K., Schwarz, E.M., Van Antwerp, D., Miyamoto, S., 1995. Rel/NF-kappa B/I kappa B family: intimate tales of association and dissociation. Genes Dev **9**, 2723-2735.

von Roretz, C., Gallouzi, I.E., 2010. Protein kinase RNA/FADD/caspase-8 pathway mediates the proapoptotic activity of the RNA-binding protein human antigen R (HuR). J Biol Chem **285**, 16806-16813.

Walsh, T.A., Morgan, A.E., Hey, T.D., 1991. Characterization and molecular cloning of a proenzyme form of a ribosome-inactivating protein from maize. Novel mechanism of proenzyme activation by proteolytic removal of a 2.8-kilodalton internal peptide segment. J Biol Chem **266**, 23422-23427.

Wang, X., Mader, M.M., Toth, J.E., Yu, X., Jin, N., Campbell, R.M., Smallwood, J.K., Christe, M.E., Chatterjee, A., Goodson, T., Jr., Vlahos, C.J., Matter, W.F., Bloem, L.J., 2005a. Complete inhibition of anisomycin and UV radiation but not cytokine induced JNK and p38 activation by an aryl-substituted dihydropyrrolopyrazole quinoline and mixed lineage kinase 7 small interfering RNA. J Biol Chem **280**, 19298-19305.

Wang, Z.B., Liu, Y.Q., Cui, Y.F., 2005b. Pathways to caspase activation. Cell Biol Int **29**, 489-496.

Williams, B.R., 1999. PKR; a sentinel kinase for cellular stress. Oncogene **18**, 6112-6120.

Williams, B.R., 2001. Signal integration via PKR. Sci STKE **2001**, re2.

Wong, J., Korcheva, V., Jacoby, D.B., Magun, B., 2007a. Intrapulmonary delivery of ricin at high dosage triggers a systemic inflammatory response and glomerular damage. Am J Pathol **170**, 1497-1510.

Wong, J., Korcheva, V., Jacoby, D.B., Magun, B.E., 2007b. Proinflammatory responses of human airway cells to ricin involve stress-activated protein kinases and NF-kappaB. Am J Physiol Lung Cell Mol Physiol **293**, L1385-1394.

Wong, S., Schwartz, R.C., Pestka, J.J., 2001. Superinduction of TNF-alpha and IL-6 in macrophages by vomitoxin (deoxynivalenol) modulated by mRNA stabilization. Toxicology **161**, 139-149.

Wong, S.S., Zhou, H.R., Marin-Martinez, M.L., Brooks, K., Pestka, J.J., 1998. Modulation of IL-1beta, IL-6 and TNF-alpha secretion and mRNA expression by the trichothecene vomitoxin in the RAW 264.7 murine macrophage cell line. Food Chem Toxicol **36**, 409-419.

Wong, S.S., Zhou, H.R., Pestka, J.J., 2002. Effects of vomitoxin (deoxynivalenol) on the binding of transcription factors AP-1, NF-kappaB, and NF-IL6 in raw 264.7 macrophage cells. J Toxicol Environ Health A **65**, 1161-1180.

Woo, B.H., Lee, J.T., Lee, K.C., 1998. Purification of Sepharose-unbinding ricin from castor beans (Ricinus communis) by hydroxyapatite chromatography. Protein Expr Purif **13**, 150-154.

Wreschner, D.H., James, T.C., Silverman, R.H., Kerr, I.M., 1981. Ribosomal RNA cleavage, nuclease activation and 2-5A(ppp(A2'p)nA) in interferon-treated cells. Nucleic Acids Res **9**, 1571-1581.

Wu, S., Kumar, K.U., Kaufman, R.J., 1998. Identification and requirement of three ribosome binding domains in dsRNA-dependent protein kinase (PKR). Biochemistry **37**, 13816-13826.

Xia, S., Li, Y., Rosen, E.M., Laterra, J., 2007. Ribotoxic stress sensitizes glioblastoma cells to death receptor induced apoptosis: requirements for c-Jun NH2-terminal kinase and Bim. Mol Cancer Res **5**, 783-792.

Xiong, W., Kojic, L.Z., Zhang, L., Prasad, S.S., Douglas, R., Wang, Y., Cynader, M.S., 2006. Anisomycin activates p38 MAP kinase to induce LTD in mouse primary visual cortex. Brain Res **1085**, 68-76.

Yang, G.H., Jarvis, B.B., Chung, Y.J., Pestka, J.J., 2000. Apoptosis induction by the satratoxins and other trichothecene mycotoxins: relationship to ERK, p38 MAPK, and SAPK/JNK activation. Toxicol Appl Pharmacol **164**, 149-160.

Yang, G.H., Pestka, J.J., 2002. Vomitoxin (deoxynivalenol)-mediated inhibition of nuclear protein binding to NRE-A, an IL-2 promoter negative regulatory element, in EL-4 cells. Toxicology **172**, 169-179.

Yang, J.J., 2002. Mixed lineage kinase ZAK utilizing MKK7 and not MKK4 to activate the c-Jun N-terminal kinase and playing a role in the cell arrest. Biochem Biophys Res Commun **297**, 105-110.

Yang, W., Tiffany-Castiglioni, E., Koh, H.C., Son, I.H., 2009. Paraquat activates the IRE1/ASK1/JNK cascade associated with apoptosis in human neuroblastoma SH-SY5Y cells. Toxicol Lett **191**, 203-210.

Yao, Z., Duan, S., Hou, D., Heese, K., Wu, M., 2007. Death effector domain DEDa, a self-cleaved product of caspase-8/Mch5, translocates to the nucleus by binding to ERK1/2 and upregulates procaspase-8 expression via a p53-dependent mechanism. EMBO J **26**, 1068-1080.

Yoshizaw.T, Morooka, N., 1973. DEOXYNIVALENOL AND ITS MONOACETATE - NEW MYCOTOXINS FROM FUSARIUM-ROSEUM AND MOLDY BARLEY. Agricultural and Biological Chemistry **37**, 2933-2934.

Yoshizawa, T., Takeda, H., Ohi, T., 1983. STRUCTURE OF A NOVEL METABOLITE FROM DEOXYNIVALENOL, A TRICHOTHECENE MYCO-TOXIN, IN ANIMALS. Agricultural and Biological Chemistry **47**, 2133-2135.

Yu, R.Y., Wang, X., Pixley, F.J., Yu, J.J., Dent, A.L., Broxmeyer, H.E., Stanley, E.R., Ye, B.H., 2005. BCL-6 negatively regulates macrophage proliferation by suppressing autocrine IL-6 production. Blood **105**, 1777-1784.

Zanetti, M.E., Chang, I.F., Gong, F., Galbraith, D.W., Bailey-Serres, J., 2005. Immunopurification of polyribosomal complexes of Arabidopsis for global analysis of gene expression. Plant Physiol **138**, 624-635.

Zhao, Y., Sui, X., Ren, H., 2010. From procaspase-8 to caspase-8: revisiting structural functions of caspase-8. J Cell Physiol **225**, 316-320.

Zhou, H.R., Harkema, J.R., Hotchkiss, J.A., Yan, D., Roth, R.A., Pestka, J.J., 2000. Lipopolysaccharide and the trichothecene vomitoxin (deoxynivalenol) synergistically induce apoptosis in murine lymphoid organs. Toxicol Sci **53**, 253-263.

Zhou, H.R., Islam, Z., Pestka, J.J., 2003a. Rapid, sequential activation of mitogen-activated protein kinases and transcription factors precedes proinflammatory cytokine mRNA expression in spleens of mice exposed to the trichothecene vomitoxin. Toxicol Sci **72**, 130-142.

Zhou, H.R., Islam, Z., Pestka, J.J., 2005a. Induction of competing apoptotic and survival signaling pathways in the macrophage by the ribotoxic trichothecene deoxynivalenol. Toxicol Sci **87**, 113-122.

Zhou, H.R., Jia, Q., Pestka, J.J., 2005b. Ribotoxic stress response to the trichothecene deoxynivalenol in the macrophage involves the SRC family kinase Hck. Toxicol Sci **85**, 916-926.

Zhou, H.R., Lau, A.S., Pestka, J.J., 2003b. Role of double-stranded RNA-activated protein kinase R (PKR) in deoxynivalenol-induced ribotoxic stress response. Toxicol Sci **74**, 335-344.

Zhou, H.R., Yan, D., Pestka, J.J., 1998. Induction of cytokine gene expression in mice after repeated and subchronic oral exposure to vomitoxin (Deoxynivalenol): differential toxin-induced hyporesponsiveness and recovery. Toxicol Appl Pharmacol **151**, 347-358.

Zhu, S., Romano, P.R., Wek, R.C., 1997. Ribosome targeting of PKR is mediated by two double-stranded RNA-binding domains and facilitates in vivo phosphorylation of eukaryotic initiation factor-2. J Biol Chem **272**, 14434-14441.

Zong, Q., Schummer, M., Hood, L., Morris, D.R., 1999. Messenger RNA translation state: the second dimension of high-throughput expression screening. Proc Natl Acad Sci U S A **96**, 10632-10636.